The Development of Amine-Functionalised Polymeric Stars as Dual-Functional Catalysts for Polyurethane Foam

Marianne S. Rolph

Submitted for the degree of Doctor of Philosophy

Department of Chemistry

November 2016

...For my grandad

Table of Contents

List of Figures, Schemes, and Tables

Figures

Schemes

Tables

Acknowledgments

First and foremost I would like to thank my supervisor Rachel O'Reilly, for giving me the opportunity to work in her group. Thanks for all the support, encouragement and guidance you have given me over the last four years, it has been invaluable and without it none of this would have been possible. I would also like to thank AWE for funding for this PhD, and Colin and Anna for their all their suggestions and support over the course of this project.

Thanks to all of the O'Reilly group members, past and present, for all the help you have offered over the years. Thanks for making my time in the lab more fun, and for all your suggestions and help, without them I know this Thesis would look very different. A special thanks goes to Alice and Anne for making the lab a fun place to work, and for fully embracing the rubbish music on the radio and singing it loudly in the lab with me (sorry to those in the office!). Thanks also to Guillaume for your advice and support, and for putting up with all my bus journey rants. A special thanks to those who have kindly proofread this Thesis: Guillaume, Becky, Anaïs, Lewis and Kay – it would be nothing like it is without your input. I would also like to thank the Dove group, for making life during this PhD a little bit more sociable.

Thanks to my friends who were always happy to suggest a weekend away to catch-up and remind me that there is far more to life than the lab.

Lastly, and by no means least, I would like to thank my family. Whilst I am fairly sure you don't really have much of an idea what I have spent the last four years doing (feel free to read on…), I can't express enough how grateful I am for your support. I must also thank Joe for everything he does. Thanks for all your support and encouragement, thanks for reminding me that the world won't end if something doesn't get done, and thanks for going to your own lab at the weekend to make me feel better about going to mine!

Declaration of Authorship

This thesis is submitted to the University of Warwick in support for the degree of Doctor of Philosophy. It has been composed by myself and has not been submitted in any previous applications for any degree. The work presented (including data generated and data analysis) was carried out by the author, except in the case outlined below:

- The SAXS data in Chapter 2 was obtained and analysed by Dr Anaïs Pitto-Barry (Australian Synchrotron Facility and University of Warwick);
- The foam data in Chapters 2 and 4 was obtained by Dr Anna Markowska (AWE, Aldermaston);
- The particle size analysis of ground polymeric catalysts in Chapter 2 was performed by Dr Anna Markowska (AWE, Aldermaston);
- The TEM images in Chapters 2 and 5 were obtained by Miss Maria Inam (University of Warwick);
- The TEM images in Chapter 3 were obtained by Dr Anaïs Pitto-Barry (University of Warwick);
- The XPS data in Chapter 6 was obtained by Dr Marc Walker and analysed by Dr Marc Walker and Mr Adam Bennett (University of Warwick);
- The starting reagent (S,S'-bisdithiobenzoate) used for the synthesis of the chain transfer agent CPBD was prepared by Dr Daniel Wright.

Publications

1. Blocked Isocyanates: from Analytical and Experimental Considerations to Non-Polyurethane Applications, M.S. Rolph, A.L.J. Markowska, C.N. Warriner, R.K. O'Reilly, ***Polym. Chem.***, 2016, DOI: 10.1039/C6PY01776B.
2. Use of complementary nucleobase-containing synthetic polymers to prepare complex self-assembled morphologies in water, Y. Kang, A. Pitto-Barry, M.S. Rolph, Z.Hua, I. Hands-Portman, N.Kirby and R.K. O'Reilly, ***Polym. Chem.***, *2*016, 7, 2836-2846.

Summary of Thesis

This Thesis explores the synthesis of amine-functionalised polymeric stars synthesised using Reversible Addition-Fragmentation Chain Transfer (RAFT) polymerisation, and their applicability as dual functional catalysts for both the catalysis of polyurethane foam production, and for the deblocking of blocked isocyanates.

Chapter 1 introduces polyurethane chemistry, and provides an in-depth summary of blocked isocyanates. Additionally, it introduces the RAFT polymerisation chemistry utilised for catalyst synthesis within this thesis.

Chapter 2 investigates the use of RAFT polymerisation for the production of non-responsive crosslinked methacrylate polymeric stars. Evaluation of polymeric stars with different structural properties in the polyurethane foam formulation was carried out to assess the protection afforded to the catalytic amine when tethered within the star polymer.

Chapter 3 utilises the RAFT synthesis of analogous acrylate based polymeric stars, the hydrolytic susceptibility of which is able to act as a model to those introduced in Chapter 2. Evaluation of the hydrolytic behaviour allowed for further probing of the effect of structural parameters on the protection of the amine.

Chapter 4 describes the incorporation of responsive crosslinkers to produce stimuli responsive polymeric stars, including the incorporation of a furan-maleimide thermoresponsive crosslinker utilising Diels-Alder chemistry, in addition to a disulphide based crosslinker which is redox responsive.

Chapter 5 explores the incorporation of a diisocyanate based crosslinker with a view towards the production of thermoresponsive polymeric stars using blocked isocyanate chemistries, and therefore minimising the addition of contaminants (*e.g.* other crosslinkers) to the polyurethane formulation.

Chapter 6 discusses the determination of the deblocking temperature of isocyanates in order to understand any trends in the deblocking of both externally and internally blocked isocyanates, as well probing the effect of amines on the deblocking temperature.

In the final Chapter, a summary of the work reported in Chapters 2- 6 is provided, with an outlook towards further applications of the polymeric stars reported in this thesis.

Abbreviations

^2J	Geminal coupling constant
^3J	Vicinal coupling constant
a	Mark-Houwink parameter
AcN	Acetonitrile
AcN-d_3	Deuterated acetonitrile
AIBN	2,2'-azobis(2-methylpropionitrile)
Ar	Aromatic
ATC	Advanced test container
B-H	Active hydrogen-containing blocking group
br	Broad
CPBD	2-cyano-2-propyl benzodithioate
CRP	Controlled Radical Polymerisation
CTA	Chain Transfer Agent
d	Doublet
DA	Diels-Alder
DABCO	1,4-diazabicyclo[2.2.2]octane
DBTL	Dibutyltin dilaurate
dd	Doublet of doublets
DEGDA	Di(ethylene glycol) diacrylate
D_h	Hydrodynamic diameter
DLS	Dynamic Light Scattering
$Đ_M$	Dispersity (Molecular weight distribution, M_w/M_n)
DMAE	2-dimethylaminoethanol
DMAEA	*N,N'*-(dimethylamino)ethyl acrylate
DMAEMA	*N,N'*-(dimethylamino)ethyl methacrylate
DMF	*N,N'*-dimethylformamide
DMF-d_7	Deuterated dimethylformamide
DMSO	Dimethylsulfoxide
DMSO-d_6	Deuterated dimethylsulfoxide
DP	Degree of polymerisation
DSC	Differential Scanning Calorimetry
DSDMA	bis(2-methacryloyl) oxyethyl disulfide
DTT	Dithiothreitol
eq.	Equivalents
Ethylene glycol-d_6	Deuterated ethylene glycol
f	Number of arms (star functionality)
FRP	Free radical polymerisation
FT	Fourier Transform
GC	Gas Chromatography
GO	Graphene oxide
GPC	Gel Permeation Chromatography
H_{12}-MDI	Hydrogenated methylenediphenyl diisocyanate
HDI	Hexamethylene diisocyanate
HEA	2-hydroxyethyl acrylate
HEMA	2-hydroxyethyl methacrylate
IPA	2-propanol
IPDI	Isophorone diisocyanate

IR	Infra-red
IV	Intrinsic viscosity
k_1	Deblocking rate constant
k_{-1}	Recombination rate constant
K_a	Acid dissociation constant
k_{add}	Addition rate constant
k_i	Initiation rate constant
K_m	Michaelis-Menten constant
k_p	Propagation rate constant
k_t	Termination rate constant
LS	Light Scattering
m	Multiplet
m	*meta*
MA	Methyl acrylate
MADIX	Macromolecular Design by Interchange of Xanthates
MDI	Methylenediphenyl diisocyanate
MEKO	Methylethyl ketone oxime
M_n	Number-average molecular weight
M_v	Viscosity-average molecular weight
MW	Viscosity-average molecular weight
MWCO	Molecular weight cut-off
NMR	Nuclear Magnetic Resonance
Nu	Nucleophile
o	*ortho*
obs.	Observed
p	*para*
PD	Dispersity (for DLS analysis)
PEGA	Poly(ethylene glycol) methyl ether acrylate
PEGMA	Poly(ethylene glycol) monomethyl ether methacrylate
PMMA	Poly(methyl methacrylate)
p-NPBA	*para*-nitrophenyl boronic acid
ppm	Parts per million
PU	Polyurethane
q	Scattering vector
RAFT	Reversible Addition-Fragmentation Chain Transfer
RDRP	Reversible-Deactivation Radical Polymerisation
redox	Reduction Oxidation
R_f	Retardation factor
R_g	Radius of gyration
R_h	Hydrodynamic radius
RI	Refractive Index
rROP	Radical Ring-Opening Polymerisation
s	Dimension parameter
s	Singlet
SAXS	Small-Angle X-Ray Scattering
SEC	Size exclusion chromatography
t	Triplet
TDI	2,4-toluene diisocyanate
TEA	Triethylamine

TEGDMA	Tri(ethylene glycol) dimethacrylate
TEM	Transmission Electron Microscopy
theo.	Theoretical
TLC	Thin-layer chromatography
TMB	1,2,4-trimethoxy benzene
TMPDA	*N,N,N',N'*-tetramethyl-1,3-propanediamine
TMXDI	α, α, α', α'-tetramethyl-1,3-xylene diisocyanate
Tris	Tris(hydroxymethyl) aminomethane
UV	Ultraviolet
VT	Variable Temperature
XPS	X-Ray Photoelectron Spectroscopy
δ	Chemical shift
η	Weight-average intrinsic viscosity
λ	Wavelength
ρ	Shape factor

1. Introduction

1.1 Abstract

With the aim of the project to develop amine-functionalised polymeric stars as catalysts for the production of polyurethane foam, in this Chapter, two main concepts are introduced. The first focusses on introducing polymerisation methods, with emphasis placed on Reversible Addition-Fragmentation Chain Transfer (RAFT) polymerisation, and its application to the production of polymeric stars, with such synthetic methodologies applied within this Thesis. The second concept discussed is polyurethanes, including an introduction to formulation components, catalysts, and testing methods, and finishing with an in-depth review on blocked isocyanates, the chemistries of which are applied in Chapters 5 and 6.

1.2 Polymer Synthesis

A polymer is defined as a substance that is composed of molecules with long sequences of one or more species of atoms/groups linked to one another, usually by covalent bonds.[1] These atoms/groups are termed monomers, with the term "polymerisation" used to refer to the chemical reaction by which these monomers are joined. In general, there are two main classes of polymerisation: step-growth polymerisation and chain-growth polymerisation. In a step-growth polymerisation, polymer chains grow through step-wise reactions between two mutually-reactive monomers. Step-growth polymerisations involving the elimination of small molecules are termed polycondensations. Polycondensation reactions between two difunctional monomers allow for the synthesis of linear polymer chains, for example the production of linear polyesters from the reaction of a dicarboxylic acid and a diol (Scheme 1.11), or the production of nylon, prepared from the reaction of a diamine with a dicarboxylic acid. Conversely, step-growth polymerisations that do not involve the elimination of other molecules during polymerisation are termed polyadditions. Most applicable to this project, polyurethane is synthesised by a polyaddition reaction, with linear polyurethane synthesised by the reaction between a diisocyanate and a diol (Scheme 1.2). For a typical step-growth polymerization any two

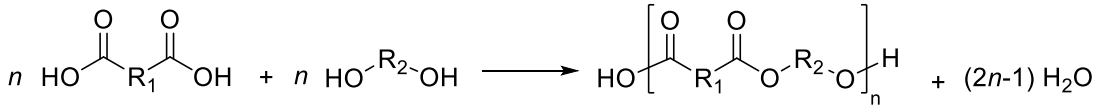

Scheme 1.1 Schematic representation of the polycondensation reaction for the synthesis of polyesters from a dicarboxylic acid and a diol.

monomers with differing functionalities can react, resulting in a random growth process.[2] Moreover, there is a rapid loss of monomer early in the reaction, with the average molecular weight increasing slowly at low conversions, and requiring high conversion to obtain high molecular weight polymers.[2] Step-growth polymerisations have the advantages of having no chain transfer or termination reactions as a result of utilising a single chemical reaction to grow the polymer chain, though they do suffer from side reactions as well as reacting with contaminants, which can have the same net effects as termination and chain transfer reactions.[3]

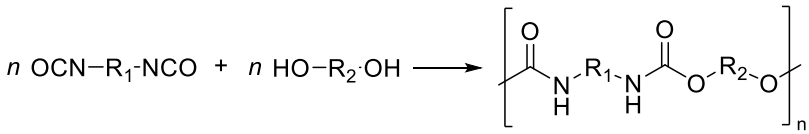

Scheme 1.2 Schematic representation of the polyaddition reaction for the synthesis of linear polyurethane from a diisocyanate and a diol.

The second class of polymerisation, chain-growth polymerisation, involves the growth of polymer chains through reaction of a monomer with a reactive end-group on the growing polymer chain. Unlike step-growth polymerisation which involves the reaction between two or more mutually-reactive functionalities to grow the polymer chain, chain-growth polymerisations typically involve initiation, propagation and termination reactions, all of which have different rates and mechanisms. Moreover, the molecular weight of the polymers increases rapidly in the early stage of polymerisation, with some monomer remaining even at long reaction times.

1.3 Radical Polymerisation

1.3.1 Conventional Free Radical Polymerisation

Conventional free radical polymerisation (FRP), a type of chain-growth polymerisation, is the most commonly applied method of radical polymerisation.[1] The mechanism of FRP can be divided into three basic stages: initiation, propagation and termination (Scheme 1.3).[4-6] Initiation involves the production of free radicals, formed from the homolytic scission of an initiator through, for example, the application of heat or radiation. These radicals react with the monomers to produce short polymeric chains (**RM·**, rate constant = k_i). The second stage, propagation, involves the rapid sequential addition of monomers to the growing polymer chains (**RM·$_{n+1}$**, k_p). Termination, the final stage, involves destruction of the radical species through an irreversible reaction. This may occur through recombination, in which two active radicals (for example growing polymer chains) couple together (**RM$_{p+n}$R**, k_{tc}). It may also occur through disproportionation, involving the abstraction of a hydrogen (**RM$_p$H** and **RM$_n$=**, k_{td}), with both termination mechanisms resulting in the production of dead polymer chains.

Due to the highly reactive nature of radical species, the fastest step in the process is termination, therefore resulting in termination of polymeric chains before complete monomer conversion, and reflected in the short-lifetime of propagating radicals ($k_{tc}/k_{td} > k_p$). Additionally,

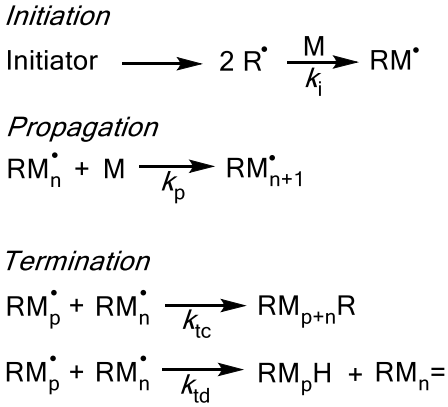

Scheme 1.3 Schematic representation for the key mechanistic steps in a free radical polymerisation.

the propagation rate is significantly faster than initiation ($k_i < k_p$) and therefore some polymer chains will have grown significantly whilst others are still initiating. Moreover, the kinetics are complicated further by chain transfer reactions, whereby radical species can react with the

solvent, the monomer and other polymer chains, which result in the formation of irregular "dead" polymer chains. As a consequence of these kinetics, polymers produced *via* FRP have broad, unpredictable molecular weight distributions.

1.3.2 "Living" Polymerisation

Conventional polymerisation methods, such as the aforementioned step-growth method used for polyurethane production and conventional FRP, are traditionally uncontrolled processes, with the resultant polymers having broad molecular weight distributions and large dispersities. The development of "living" polymerisation methods, for example anionic and cationic polymerisations, developed by Szwarc *et al.* and concurrently by Higashimura, Sawamoto, Faust and Kennedy respectively,[7-11] resulted in the synthesis of materials with low dispersities and with well-defined molecular weights. The main difference between these "living" polymerisation techniques and the aforementioned conventional processes is observed in the molecular weight evolution *vs* monomer conversion, with "living" polymerisation methods exhibiting a linear evolution of molecular weight *vs* conversion, compared to the rapid initial monomer consumption in chain-growth polymerisation, or the slow initial monomer consumption in step-growth polymerisation (Figure 1.1).[12]

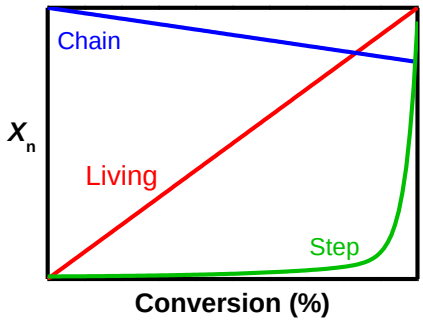

Figure 1.1 The difference in the evolution of molecular weight *vs* monomer conversion for chain-growth, step-growth and "living" polymerisations.

For a polymerisation to be classified as "living", certain criteria must be met:[13-15]

I. Polymerisation continues to 100% monomer conversion. Moreover, subsequent addition of monomer results in the continuation of polymerisation.

II. A single initiating species produces one active growing polymer chain. This ensures a constant number of active polymer chains.

III. The number-average molecular weight (M_n) is directly proportional to the monomer conversion.

IV. M_n is controlled by reaction stoichiometry.

V. The product polymer has a narrow dispersity ($Đ_M$)

VI. Block copolymers can be synthesised through the sequential addition of a second monomer.

VII. Chain-end functionalised polymers are able to be produced.

Though "living" polymerisation techniques realised great advances in the controlled synthesis of polymers, initial techniques required stringent reaction conditions and high monomer purity, and thus maintained the need to develop other polymerisation methods able to afford a similar level of control without such strict synthetic protocols.

1.3.3 Reversible Addition-Fragmentation Chain Transfer (RAFT) Polymerisation

Such developments resulted in the generation of reversible-deactivation radical polymerisation (RDRP) methods, which exhibit a large number of characteristics of a "living" polymerisation, yet cannot be termed as such owing to the presence of chain transfer and chain termination reactions. These methods are based on an equilibrium between the active propagating species and a deactivated dormant species. Once such RDRP method, Reversible Addition-Fragmentation Chain Transfer (RAFT) polymerisation involves the degenerative transfer between propagating and dormant species. Developed in the late 1990s at the Commonwealth

Scientific and Industrial Research Organisation,[14] simultaneous to the development by Rhodia Chimie of a similar technique, Macromolecular Design by Interchange of Xanthates (MADIX),[16] RAFT polymerisation has many advantages over other RDRP methods. For example, depending on selection of RAFT chain transfer agent (CTA), RAFT polymerisation can omit the use of metals, unlike Atom-Transfer Radical polymerisation,[17-19] nor requires high temperatures, such as those used in Nitroxide-Mediated polymerisation,[20] and has much greater tolerance to functional groups in comparison to anionic/cationic polymerisations.

Control over the polymerisation is introduced into a RAFT polymerisation through the addition of a CTA, with polymerisation proceeding *via* an addition-fragmentation mechanism. The overall mechanism is similar to conventional FRP (involving initiation, propagation and termination), with the addition of two significant steps: a pre-equilibrium and a chain equilibrium (Scheme 1.4, as *reversible chain transfer* and *chain equilibrium* respectively). Upon initiation, which, similar to FRP frequently results from the thermally induced decomposition of a radical initiator, the initiating radical reacts with the monomer to generate an initial polymer chain ($\mathbf{P_n\cdot}$, rate constant = k_i). This growing chain undergoes a rapid addition reaction (k_{add}) with the carbon-sulfur double bond in the RAFT CTA (compound **1**), generating a radical intermediate (product **2**). This intermediate subsequently fragments producing either the initial growing polymer chain, or to produce a reinitiating group (**R·**) and a polymeric thiocarbonyl compound (a macro-CTA, product **3**, $k_ß$). If fragmentation results in the evolution of a reinitiating group (**R·**), it is further able to re-initiate polymerisation with additional monomer ($k_{re\text{-}in}$), generating a new polymer chain ($\mathbf{P_m\cdot}$), and the process continues. Chain equilibrium is attained once all initial CTA has been consumed, leaving only the macro-CTA (product **5**) present. During chain equilibrium there is a rapid exchange between the active and dormant polymer chains ($\mathbf{P_n}$ and $\mathbf{P_m}$), ensuring an equal probability for chain growth for any of the polymer chains, therefore resulting in polymers with narrow dispersities.

Initiation

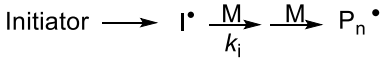

Reversible Chain Transfer

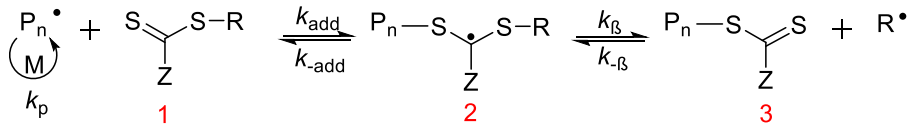

Reinitiation

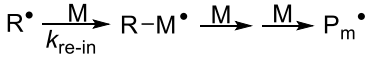

Chain Equilibrium

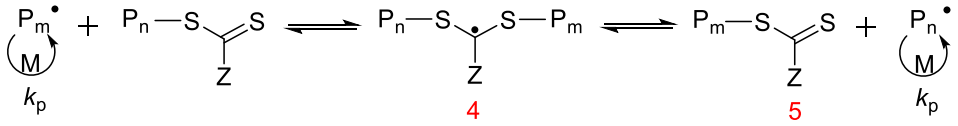

Termination

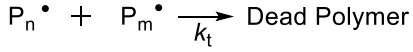

Scheme 1.4 Schematic representation for the main steps in the RAFT polymerisation mechanism.

For a RAFT polymerisation to be successful, the following criteria must be met:[13-15]

I. **R·** must efficiently instigate reinitiation.

II. To ensure fragmentation towards the reinitiating group is favoured, the rate of fragmentation ($k_ß$) must be high.

III. The CTA must have a reactive carbon-sulfur double bond to ensure rapid addition.

IV. Fragmentation of the radical intermediates (**2** and **4**) should occur rapidly and favour the formation of the product, as well as not participate in any side reactions.

V. To ensure a low steady-state concentration of **R·**, the equilibrium constant for reversible chain transfer must be significantly less than one.

VI. The polymers and R-initiators generated must be non-reactive.

Should all of these criteria be met, there are minimal destructive termination steps (k_t), which result in high dispersities and a loss of control over the molecular weight. It is this that is the defining component of a controlled radical polymerisation (CRP), and results in an equal probability of chain growth and therefore a narrow molecular weight distribution.

To ensure that these criteria are met, correct selection of the RAFT CTA is paramount. There are four main types of CTA: dithioester, trithiocarbonates, dithiocarbamates and xanthates (Figure 1.2). Within the pre-equilibrium, shown in Scheme 1.4 as the equilibrium between **1**, **2** and **3,** the stability of the thiocarbonyl-thio radical intermediate (**2**) depends on the attached Z group and its ability to stabilise the radical species produced (Scheme 1.5)[21]. Indeed, the Z group ensures sufficient activation of the carbon-sulfur double bond thus determining the rate of addition of the propagating radical, in addition to the rate of fragmentation of the RAFT agent.[22] The addition of electron-withdrawing groups, for example -CR_2 and -SR, increases the reactivity of the thiocarbonyl towards radicals, resulting in favouring the formation of the radical intermediate. Conversely, the addition of electron-donating groups does not stabilise the radical intermediate, and therefore does not result in the addition of radicals to the thiocarbonyl group.

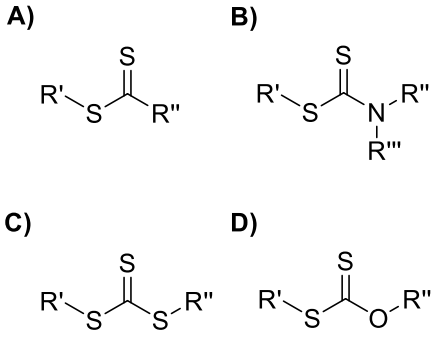

Figure 1.2 Schematic representation of the four main types of RAFT chain transfer agents used for RAFT polymerisations: (A) dithioester, (B) dithiocarbamate, (C) trithiocarbonate, and (D) xanthate.

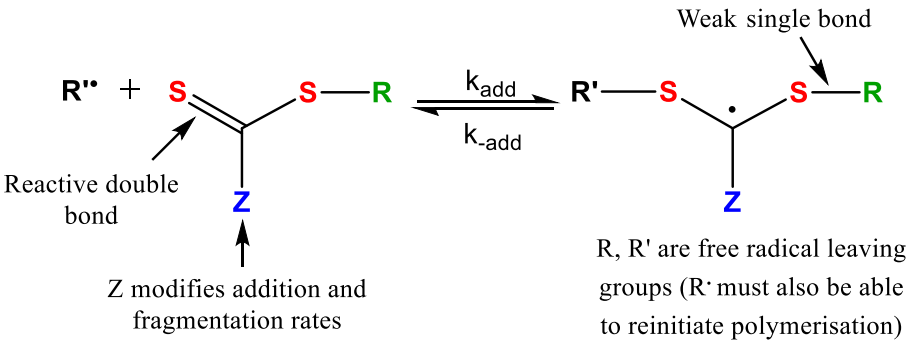

Scheme 1.5 Schematic representation for the generic structure of a RAFT chain transfer agent. Reproduced with permission from Moad *et al.*[21]

With regards to the R group, selection of the group must ensure stabilisation of the radical intermediate such that the equilibrium is shifted in favour of the production of the re-initiating **R·** species. Furthermore, the R group must be sufficiently unstable to be a good initiating species, yet also be stable enough to be a good homolytic leaving group to allow for cleavage of the radical intermediate. The structure of the CTA is chosen depending of the monomer selected for the polymerisation, with specific combinations of the Z and R groups being chosen to ensure controlled polymerisations (Figure 1.3).[14]

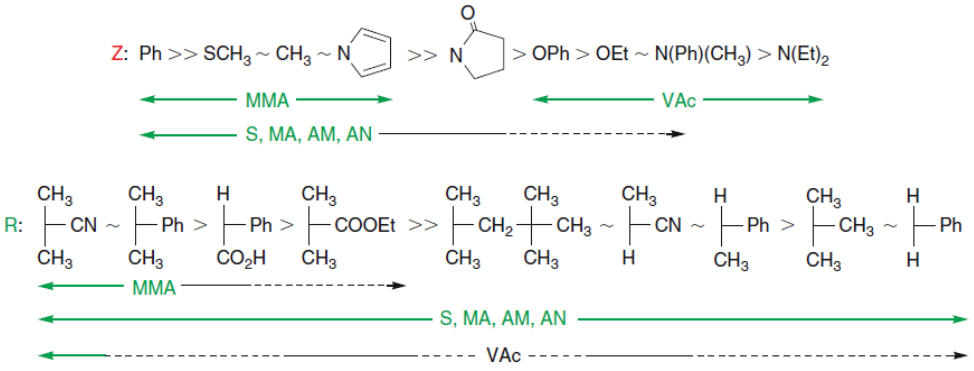

Figure 1.3 Guidelines for the selection of RAFT agent and monomer compatibility, where MMA = methyl methacrylate, S = styrene, MA = methyl acrylate, AM = acrylamide, AN = acrylonitrile, and VAc = vinyl acetate. For the Z-groups, addition rate decreases whilst fragmentation rate increases from left to right, and for the R-groups, fragmentation rate decreases from left to right. Reproduced with permission from Moad *et al.*[14]

1.3.4 Synthesis of complex architectures

Recent developments in CRP techniques have enabled the synthesis of polymers with complex, well-defined molecular architectures, including combs/brushes[23-26] and dendrimers.[27-29] One such architecture, readily synthesised using RAFT polymerisation,[30] is block copolymers. There are three different methods is which RAFT polymerisation can be used to form block copolymers: first, through sequential chain extension, in which a block of one monomer is chain extended with a block of a second monomer, secondly through two RAFT CTAs joined together *via* either the Z group or the R group, and thirdly through utilising a RAFT CTA with two leaving groups (Figure 1.4, pathways 1, 2 and 3, respectively).[31] Furthermore, the ability of the resultant block copolymers to self-assemble when placed in a specific environment allows for the production of even more complex morphologies, including spherical micelles,[32] cylindrical micelles[33, 34] and vesicles,[35] with different block compositions, *e.g.* block ratios and monomers, having an impact on the final morphology .[36, 37] Such morphologies have various applications, ranging from drug delivery[38, 39] to nanolithography[40, 41] and enhanced oil recovery.[42, 43]

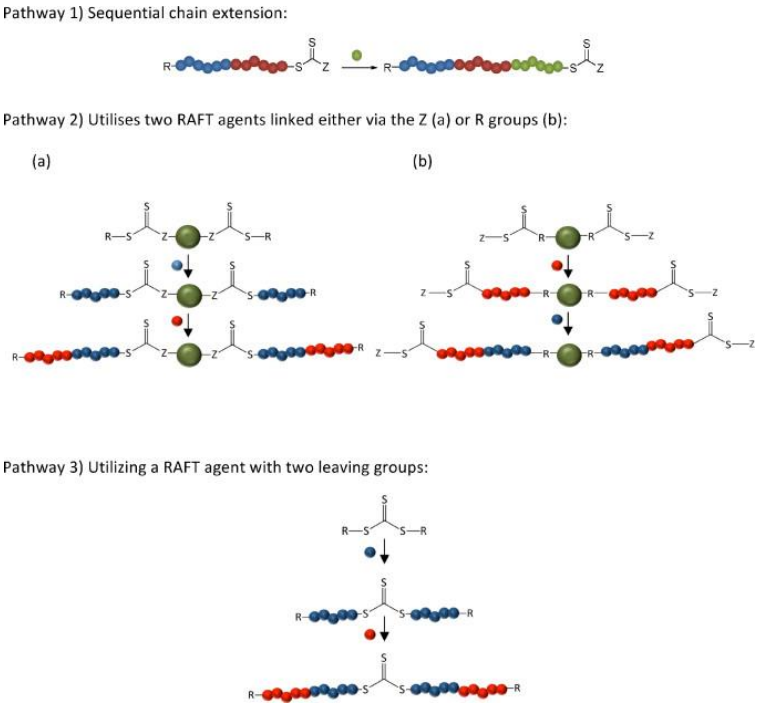

Figure 1.4 Schematic representation of the synthesis of block copolymers using RAFT polymerisation. Reproduced with permission from Gregory *et al.*[31]

Star polymers, an example of another complex molecular architecture, have a range of substructures, ranging from homopolymer stars through to Miktoarm stars and end-functionalised stars (Figure 1.5).[44, 45] Polymeric stars are synthesised *via* three different methods: a "core-first approach", an "arm-first" approach, and a "coupling-onto" approach (Scheme 1.6).[46] The "core-first" approach focusses on the growth of star arms from a multifunctional initiator. Whilst the core-first approach enables synthesis of stars with well-defined structures, with the precise number of arms predetermined by the number of initiating sites on the multifunctional initiator, the approach is not suitable for the synthesis of Miktoarm stars (though recently Tunca *et al.* have developed multifunctional initiators utilising orthogonal initiating functionalities for this purpose),[47] nor does it readily enable determination of the molecular weight of the arms. Additionally, the synthesis of stars with greater than 30 arms is difficult owing to the need to synthesise such highly functionalised initiators.[46] Moreover, the size of the core-domain is predetermined by the size of the macroinitiator, resulting in relatively small core domains, limiting applications involving encapsulation or functionalisation of the core.

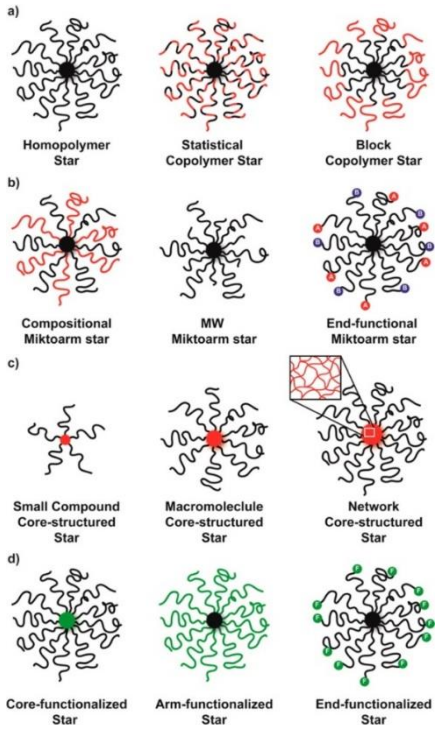

Figure 1.5 Different types of star polymers classified by (A) composition and sequence distribution of arms, (B) arm type, (C) core structure and (D) placement of functionality. Reproduced with permission from Ren *et al.*[44]

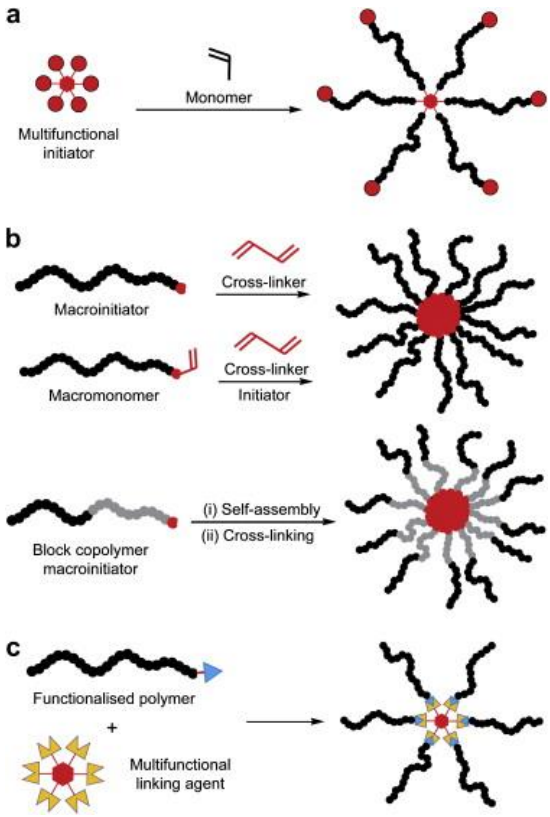

Scheme 1.6 Methods for the synthesis of polymeric stars: (A) "core-first", (B) "arm-first" and (C) "grafting-to". Reproduced with permission from Blencowe *et al*.[46]

The arm-first approach involves pre-synthesised linear polymers which are chain extended with a divinyl crosslinker to produce the polymeric stars, similar to the chain extension of a homopolymer with another monomer to produce a block copolymer. This technique overcomes many shortcomings of the core-first methodology, including the ability to fully characterise the star arms, owing to their prior synthesis. Additionally, the method allows for the production of Miktoarm stars, as well as the resultant stars produced having a large core domain which is able to be used for storage and encapsulation.[48] Moreover, it is significantly easier to produce stars with a large number of arms per star (>100). However, stars produced using this approach tend to have a relatively broad arm number distribution in comparison to the defined number of arms per star in the core-first method, owing to the random nature of arm incorporation.[49] Further disadvantages of the technique include low yields and the need for rigorous purification methods to obtain pure stars,[50] with disproportionation and bimolecular

termination during a radical based synthesis resulting in the formation of "dead" chains and low conversion to stars.[51-53]

The final method for polymeric star synthesis, the grafting-to approach, involves the coupling of pre-synthesised polymeric arms to a multifunctional linking agent. Whilst the grafting-to approach provides the best control over architecture of all the techniques, owing to the complete control over the synthesis of the arms and the core, it suffers from the same problems related to steric congestion of the core, as well as the need for the synthesis of multifunctional cores, as experienced in the core-first approach. Moreover, the method suffers from incomplete conversion, with reactions requiring an excess of arms in addition to long reaction times in order to produce defined polymeric stars.

Whilst RAFT polymerisation has been readily applied to the production of polymeric stars,[44, 50, 54-56] the efficacy of RAFT polymerisation for the synthesis of polymeric stars is easily influenced. For example, high chain end fidelity is important to ensure that arms are either successfully grown (core-first approach) or able to be chain extended with the divinyl crosslinking monomer (arm-first approach). Moreover, the steric congestion within the core, attributed to the bulky thiocarbonylthio group can result in problems during polymerisation.[44] To minimise these problems, additional care needs to be taken when selecting the R-and Z-group on the CTA, or through selecting either an R-group or Z-group approach for the core-first method of star synthesis (Figure 1.6).[55] One other disadvantage for the arm-first approach is the molecular weight of the arms. Whilst an arm-first approach allows for the incorporation of a large number of arms per star, it has been reported that short arms favour the formation of a star with a high number of arms and a large core domain, yet longer arms result in small core with fewer arms.[57] Therefore, to produce polymeric stars using RAFT polymerisation, a large number of factors must be considered, yet taking these into account can result in the successful synthesis of polymeric stars with defined structures which are able to be fully characterised.

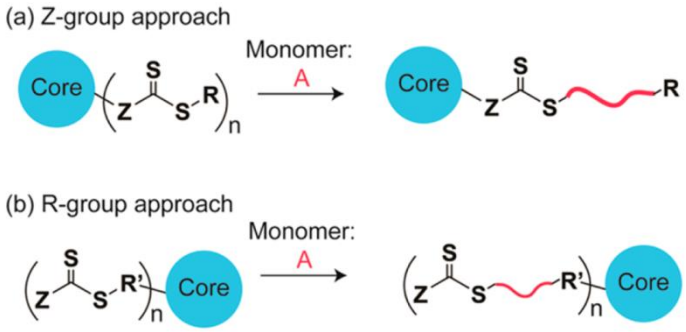

Figure 1.6 The Z-group approach and the R-group approach for the synthesis of polymeric stars using the core-first RAFT polymerisation method. Reproduced with permission from Ren *et al.*[44]

1.4 Polyurethane

1.4.1 Polyurethane Production

Since the discovery of polyurethane and its related chemistries by Otto Bayer in the late 1930s, significant developments have been made in the production of polyurethane based materials.[58, 59] The range of potential properties available results in a wide number of applications, including packaging,[60-63] adhesives,[64, 65] insulation,[66-68] coatings,[69, 70] and fire retardants.[71, 72] As introduced in section 1.2.1, polyurethane is produced *via* a step-growth polyaddition polymerisation mechanism, involving the reaction between two monomers, each with multiple isocyanate and hydroxyl functionalities,[1, 3, 73] and proceeds rapidly at room temperature, even without the addition of a catalyst. The basic synthesis of polyurethanes involves the reaction of an isocyanate with a hydroxyl-containing compound, such as an alcohol or water. The breadth in combinations of alcohols and hydroxyl compounds, alongside a vast catalogue of isocyanate compounds, produces an extensive collection of structurally different materials (Figure 1.7).[74]

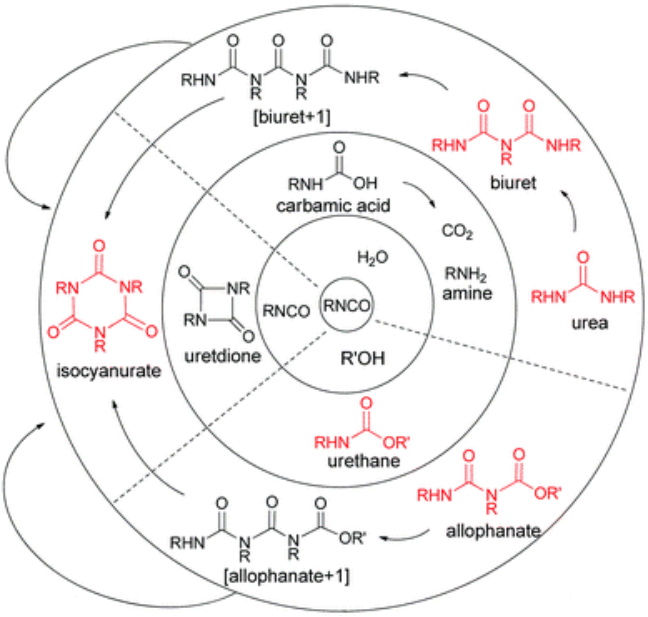

Figure 1.7 Examples of competing reactions in the synthesis of polyurethane foams. Reproduced with permission from Gibb *et al.*[74]

For the production of polyurethane foams, there are three main dominating reactions: the gelling reaction, the blowing reaction and the crosslinking reaction (Scheme 1.7). The gelling reaction involves the reaction between an isocyanate and an alcohol, resulting in the formation of a urethane linkage. The blowing reaction, involving the reaction of an isocyanate with water, results in the production of urea linkages and carbon dioxide. These two reactions must be carefully balanced in order to produce a structurally sound foam: the rate of formation of the polyurethane polymer and the production of carbon dioxide must be balanced to ensure the gas produced in the blowing reaction is trapped within cell walls that have sufficient strength to maintain the structure of the product. If the rate of gelling proves much faster, the foam will not rise, but if the rate of blowing is much faster than the gelling rate, the walls of the cells are insufficiently strong resulting in the foam collapsing.

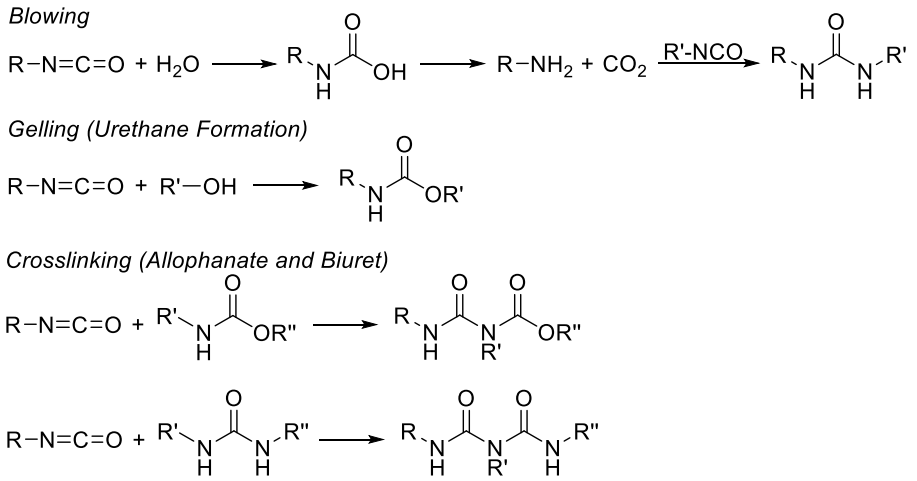

Scheme 1.7 Schematic representation for the main reactions involved in the production of polyurethane foam.

The production of rigid polyurethane foams is, in general, carried out in two stages. In the initial stage the polyol, a compound with multiple hydroxyl functional groups, is mixed with a series of additives selected to produce a polyurethane foam with specific desired properties. In the second stage, this mixture of polyol and additives, known as the premixture, is mixed with the isocyanate and results in the production of the polyurethane foam. Surfactants are added to ensure emulsification of the formulation and increase the compatibility of the formulation components, with reported surfactants ranging from ionic and non-ionic organics to silicon based compounds.[75-77] Moreover, surfactants assist in controlling the cell size and stabilisation of the cell membranes, preventing foam collapse.[75, 78, 79] Chain extenders are added to the formulation as they influence the polymer morphology through, for example, impacting phase separation.[80] Another formulation additive, paramount for polyurethane foam production, is the blowing agent. Blowing agents are added to the formulation to exert control over the blowing process and assert control over the foam density.[3] Originally introduced in the 1950s, halocarbons were traditionally the most prevalent type of blowing agents, but in recent years attempts have been made to phase out their use owing to environmental concerns.[81] Recently, owing to the depletion of the ozonosphere, the use of water as the only blowing agent to liberate

carbon dioxide in the formulation has been explored,[82-84] yet caution must be exercised as excessive water content has been reported to result in cell deformation.[85]

1.4.2 Catalysis

The final additive in the formulation is the catalyst, with correct selection important in achieving desired properties of the product polyurethane. The catalyst determines the precise rate of the gelling, blowing and crosslinking reactions and ultimately determines the final properties of the polyurethane product, with a combination of catalysts frequently applied in order to achieve the correct balance of reactions and desired polyurethane properties. [86] Industrially there are three major classes of catalyst: non-protic salts, organometallics and tertiary amines, the latter two of which will be introduced.

Frequently reported in the literature, organometallic catalysts are predominantly tin-based, with dibutyltin dilaurate (DBTL) and stannous octoate readily applied.[87, 88] In general, organo-tin catalysts strongly favour gelling reactions, catalysing the reaction between an isocyanate and an alcohol, and are mainly applied to aliphatic isocyanate polyurethane formulations.[89] Organo-tin compounds catalyse the formation of polyurethane through the N-coordination of the isocyanate with the tin alkoxide catalyst produced from the alcoholysis of the original tin compound. Subsequent transfer of the alkoxide anion to the isocyanate produces the product urethane and regenerates the tin alkoxide species (Scheme 1.8),[87, 90] with the steric hindrance of the isocyanate dominating the catalysis rate.

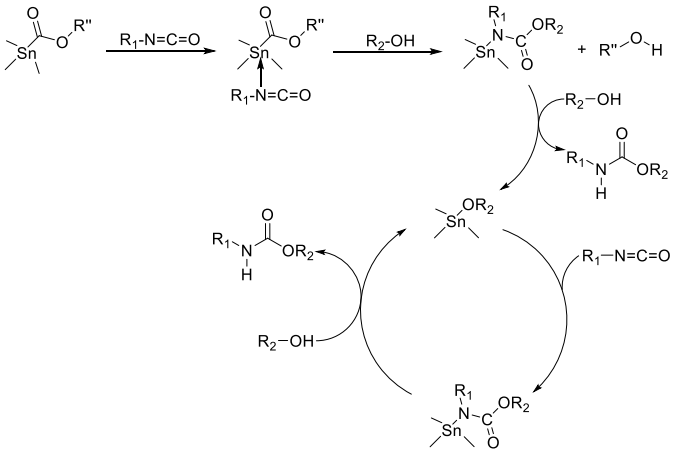

Scheme 1.8 Schematic representation for the mechanism of tin-catalysed polyurethane formation. Reproduced with permission from Sardon *et al.*[90]

Whilst tin catalysts are widely applied industrially, they are highly toxic, especially to aquatic organisms, which has resulted in attempts to ban the use of such compounds.[91] Another major disadvantage of organo-tin compounds is their inherent sensitivity towards moisture, as well as high temperatures, which both result in a sharp decrease in their catalytic activity. Additionally, certain organo-tin catalysts are unable to be applied in systems containing ester functionalities owing to their promotion of ester hydrolysis and transesterification.[92] It is because of these reactivity problems, coupled with being strong gelation catalysts, that organo-tin compounds have limited application in the synthesis of polyurethane foams. Indeed, the addition of water as a blowing agent results in a decrease in catalytic activity, and very strong gelators will prevent successful rise of the polyurethane foam. As a consequence, additional catalysts are used simultaneously in the formulation to allow for successful polyurethane production.

Contrastingly, the addition of water as a blowing agent, in addition to high temperatures, has little effect on tertiary amine catalysts. Tertiary amines, in addition to primary and secondary amines, comprise the largest class of industrially applied catalysts for polyurethane production.[86] Different tertiary amines have been reported as strong catalysts for either the gelling or the blowing reactions, with some tertiary amines described as being "balanced" catalysts, that is to say compounds which are able to catalyse both the gelling and blowing reactions to some extent (Figure 1.8). Blowing catalysts generally have an ether linkage two carbons away from the

tertiary amine, with Malwitz *et al.* reporting that the two carbon bridge restricts the movement of the two active sites, the ether oxygen atom and the amine nitrogen atom, increasing catalysis.[93] Gelling catalysts tend to contain alkyl-substituted nitrogen atoms (strong gelators) and ring-substituted nitrogen atoms (weak gelators), and balanced catalysts are likely to contain sterically unhindered amines to allow equal probability of amine access to both the hydroxyl functionalities and the isocyanates. It is widely accepted that an increase in the amine basicity results in an increase in catalytic activity, with steric hindrance reported to further impact catalytic activities. Indeed, Van Maris *et al.* reported that an increase in steric hindrance is shown to result in a decrease in catalytic activity with a trialkanolamine displaying a lower catalytic activity compared to the less sterically congested 2-dimethylaminoethanol (DMAE).[94] Furthermore, in spite of its relatively weak basicity which should render that catalyst less active, 1,4-diazabicyclo[2.2.2]octane (DABCO) is the most commonly employed tertiary amine catalyst, owing to being both a very strong gelling and blowing catalyst, with the high catalytic activity attributed to the lack of steric hindrance. Moreover, catalytic activity is further affected by the polarisability of the amine catalyst, and the presence of hydrogen bonding, as selectivity is greatly affected by spatial separation between active sites.[87]

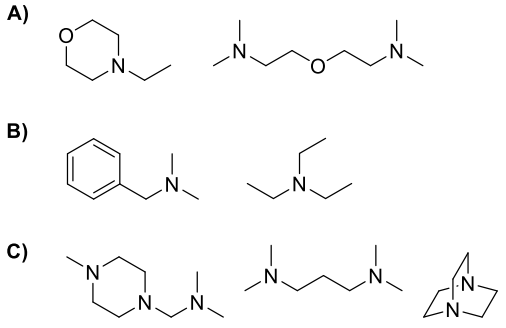

Figure 1.8 Schematic representation for examples of tertiary amine polyurethane catalysts: (A) blowing catalysts, (B) gelling catalysts and (C) balanced catalysts, including DABCO (*bottom right*).

Within the literature there are two proposed mechanisms by which tertiary amines catalyse the formation of polyurethane.[87] The first mechanism involves attack of the amine on the isocyanate, increasing the electrophilicity of the isocyanato carbon and rendering it more

susceptible to nucleophilic attack (Scheme 1.9A).[93] Experimental evidence for this mechanism is primarily based on the effects of sterics on catalytic activity, with Eley *et al.* reporting the activity of the tertiary amines being highly dependent on the steric hindrance of the nitrogen atom.[95] The second proposed mechanism comprises of a hydrogen-bonded complex of the amine catalyst and the nucleophilic alcohol or water in the formulation. This complex results in increasing the nucleophilicity of the attacking group, with subsequent attack of this complex on the isocyanate functionality (Scheme 1.9B).[90, 96] This mechanism is strongly supported by work carried out by Frisch *et al.*, which indicated a twelve times faster reaction rate in the production of polyurethane with the addition of 4-pyrdinyl methanol, with the catalytic increase attributed to the ability of the 4-pyridinyl methanol able to intramolecularly hydrogen bond and therefore further increasing the nucleophilicity of the hydroxyl functionality.[97]

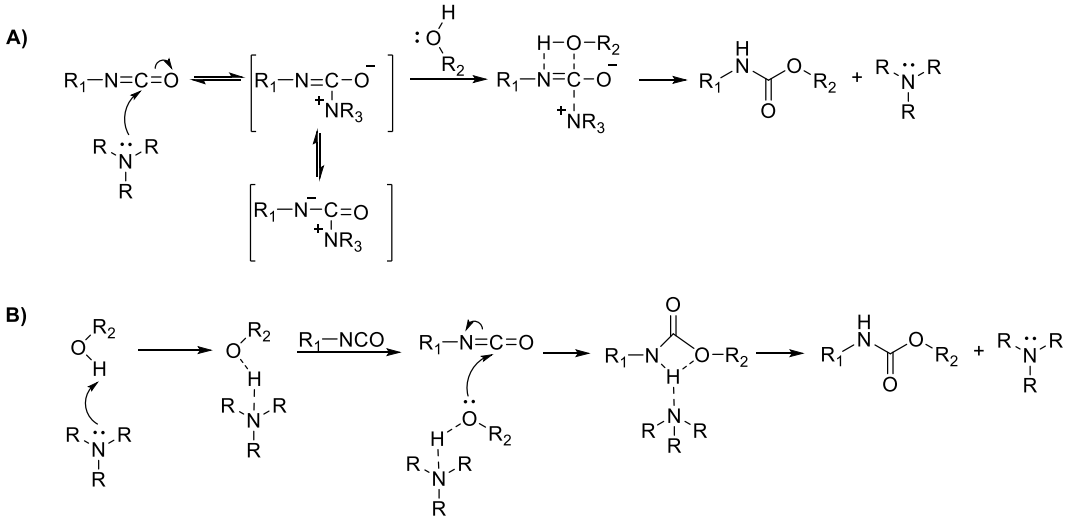

Scheme 1.9 Schematic representation for the synthesis of polyurethane catalysed by tertiary amines through (A) amine attack on the isocyanate, and (B) through amine coordination to the alcohol functionality.

In addition to their insensitivity to both moisture and high temperatures, tertiary amine catalysts have further advantages, including their lower toxicity compared to tin compounds, as well as their ability to activate aromatic isocyanates.[93] However, they are not without disadvantages. A large number of tertiary amine catalysts are highly hazardous materials, with the a currently applied commercial catalyst, *N,N,N',N'*-tetramethyl-1,3-propanediamine

(TMPDA) being both a flammable liquid and vapour, as well as being readily absorbed through the skin and causing skin, eye and respiratory tract burns, all of which contribute to problems with the handling of the catalyst.[98] Residual traces of catalyst in the product material may limit its applications, both due to the hazardous nature of the catalysts and also the potential of residual odour generated by the amine compounds.[86]

1.4.3 Evaluation of polyurethane formation

In order to probe the effect of the catalysts on the production of polyurethane foams, the formation of polyurethane has to be investigated. One commonly applied method for *in situ* analysis for the formation of polyurethane is the use of time-resolved Small-Angle X-Ray Scattering (SAXS) analysis. SAXS analysis involves the illumination of a sample with X-rays and measurement of the scattered radiation by a detector. The scattering patterns are then fitted to provide information on material morphology. Time-resolved SAXS, within the context of monitoring the production of polyurethane foam, has been demonstrated by Elwell *et al.* to allow for quantification over the different stages of the foaming process. Indeed, it was possible to determine at what time point the material changes from a homogenous liquid (little to no scattering intensity, Figure 1.9), to microphase separation (the first maxima), and finally the onset of vitrification *i.e.* when the glass transition temperature of the polymer is equal to the curing temperature (when the growth of the maxima slows and the maxima becomes constant).[99]

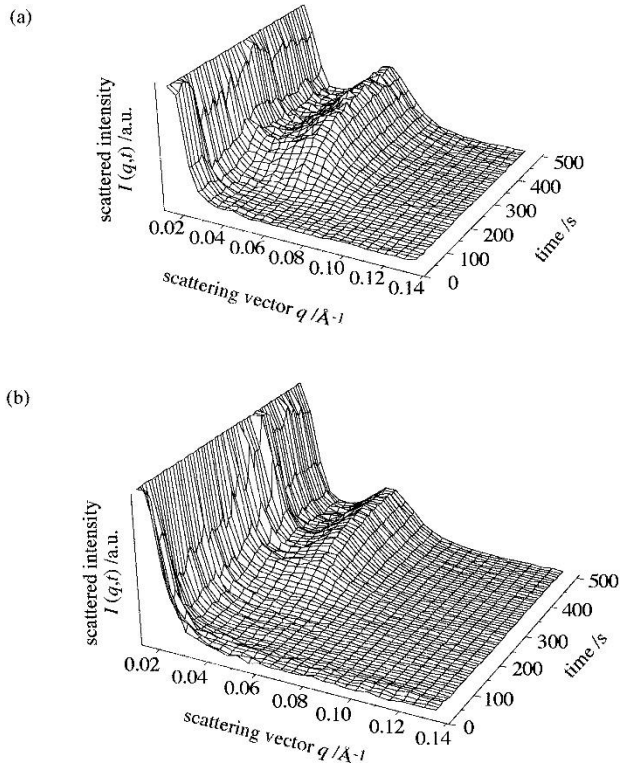

Figure 1.9 Time-resolved SAXS analysis on two different polyurethane formulations (a and b), showing the evolution of the formulation from a homogenous mixture (little to no scattering), through to microphase separation (first maxima) and vitrification (constant scattering intensity at maxima). Reproduced with permission from Elwell and Ryan.[99]

In addition to SAXS, Elwell *et al.* also investigated the foaming process using both Fourier-Transform Infra-red (FT-IR) spectroscopy and rheology. FT-IR spectroscopic analysis allows for direct monitoring of the characteristic peaks in the IR spectrum, including the disappearance of the isocyanate linkage (υ = 2270-2300 cm^{-1}), and the appearance of the urethane linkage (υ = 2270-2300 cm^{-1}) (Figure 1.10), with the former peak allowing for determination of the rate of isocyanate consumption. Rheology allows for further *in situ* investigations into the foaming process. Similar to the SAXS analysis producing information of different stages of the foaming process, Elwell *et al.* utilised rheology to further characterise the different foaming process stages, confirming four distinct regions during the foaming process: bubble nucleation, liquid foam and microphase separation, physical gelation, and foamed elastomer phase. Using a combination of these three techniques, a great deal of compositional information about the foaming process can be garnered, with a combination of two or three of

these analytical techniques frequently applied to the characterisation of polyurethane materials during formation.[80, 100-102]

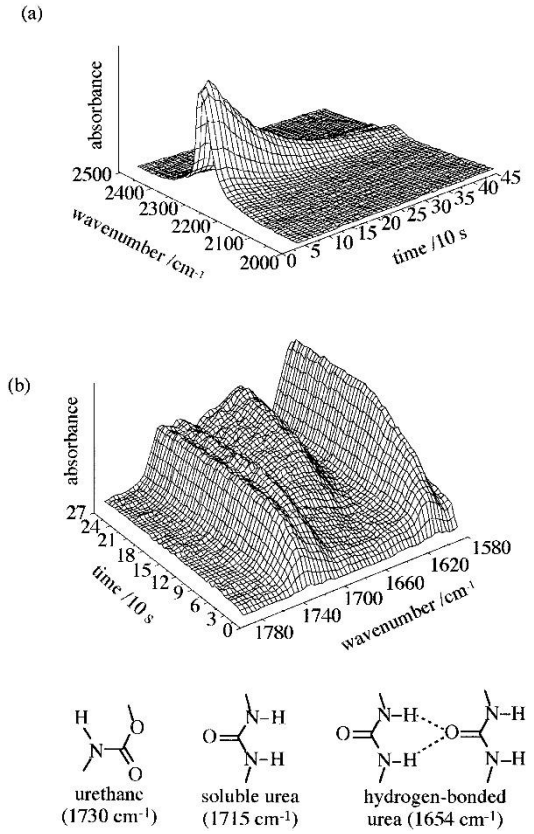

Figure 1.10 Time-resolved FT-IR analysis indicating (a) a decrease in the isocyanate concentration and (b) an increase in the urethane, urea and hydrogen-bonded urea peaks found in the product polyurethane material. Reproduced with permission from Elwell *et al*.[99]

Depsite providing a great deal of information on the foaming process, SAXS, FT-IR spectroscopy and rheology do not allow for determination of either the rise height, or the rise profile. Furthermore, such analytical methods are carried out on a small scale, which may not provide an accurate model for how well the bulk material will behave during processing. Industrially, the monitoring of the foaming process can be carried out using a Foamat® (Figure 1.11).[103] Here, the mixed formulation is added to a cup and placed underneath an ultrasonic detector. Once placed underneath the detector, the difference in distance between the detector

and the foam bun is measured using ultrasound, and the rise height is determined.

Figure 1.11 ATC container for the Foamat® set-up, featuring the thermostatically controlled foaming vessel and the ultrasonic sensor. Reproduced from Messtechnik GmbH.[103]

Whilst not providing as much in-depth information about the different stages in the foaming process when compared to SAXS analysis for example, it is able to provide further information other than rise height/profile through the introduction of a thermocouple into the foaming vessel, allowing for determination of the gel time, the internal temperature and pressure, and the viscosity (Figure 1.12).[103] Moreover, the addition of an advanced test container (ATC), a thermostatically controlled vessel, allows for probing the curing of materials at higher temperatures, and increases reproducibility of the foaming process by keeping a constant temperature around the vessel. Additionally, such temperature controlled foaming is more representative of the curing methods used industrially, for example in-mould curing, and therefore is a better production simulation.

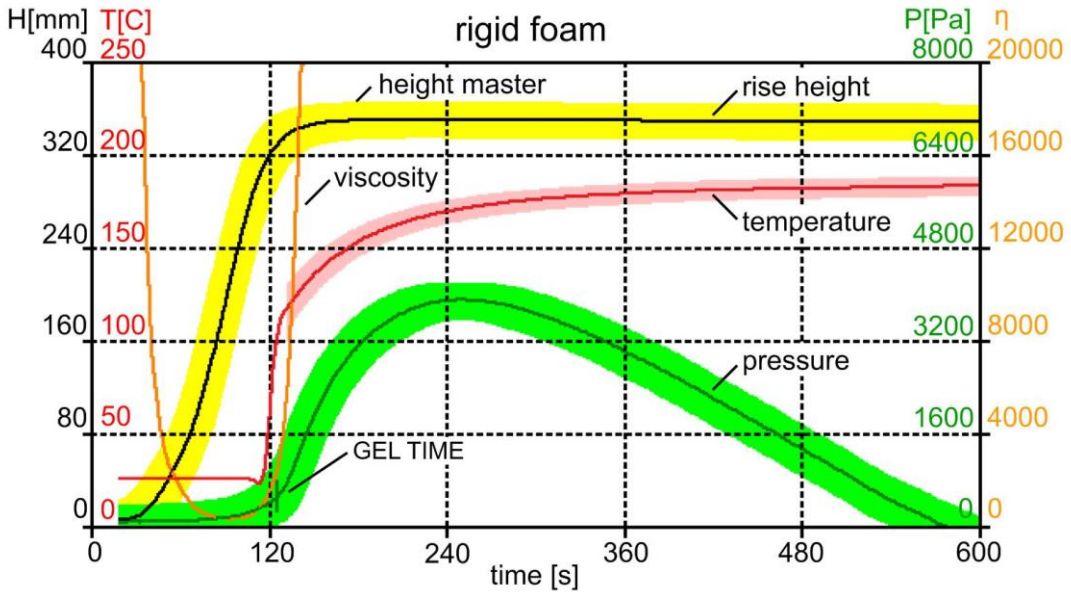

Figure 1.12 Output data from a Foamat® set-up, indicating rise height (black), viscosity (orange), internal temperature (red), and pressure (green). Reproduced from Messtechnik GmbH.[103]

1.5 Blocked Isocyanates

Despite significant developments in both additives and catalysts for the synthesis of polyurethane, a major industrial problem remains: formulation moisture sensitivity. With the inherent reactivity between hydroxyl functionalities and an isocyanate resulting in the formation of polyurethane without the addition of a catalyst, methods have been developed in order to overcome this problem. One such method is the use of blocked isocyanates, where the reversible reaction of an isocyanate and an active hydrogen-containing compound renders the isocyanate inert at room temperature (Scheme 1.10). Furthermore, the blocked isocyanates are found to be unreactive towards themselves and other nucleophiles, such as water, as well as being reported to have lower toxicities than the free isocyanate equivalents.[104, 105] Upon heating, the free isocyanate is liberated allowing for reactions to proceed.[106] It should be noted that, in addition to blocked isocyanates, one possibility to overcome moisture sensitivity is the use of "masked isocyanates". Frequently used incorrectly in the literature as synonymous to blocked isocyanates, masked isocyanates produce a reactive isocyanate *in situ* yet are not formed from

the reversible reaction of an isocyanate with an active-hydrogen containing compound. For example, Blencowe *et al.* reported the use of a heterocyclic bisulfide able to produce an isocyanate through the use of triphenyl phosphine mediated decomposition,[107] and Klinger *et al.* reported the *in situ* production of an isocyanate using the Curtius rearrangement of a benzoyl azide.[108]

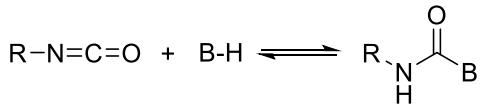

Scheme 1.10 Schematic representation for the synthesis of blocked isocyanates, where B-H is a blocking group with an active hydrogen.

A wide range of compounds have been reported for their use as blocking agents for isocyanates, with specific examples of blocking agents and the corresponding deblocking temperatures presented in Table 1.1. The list includes both external agents (*i.e.* where an additional compound is used to block the isocyanate) and internal blocking agents (where the isocyanate is used to block itself). It should be highlighted that the deblocking temperatures quoted must be taken as a range for which these functionalities deblock. The temperatures quoted result from a wide range of analytical techniques, and it is widely reported in the literature that different analytical techniques yield different deblocking temperatures, even for the same blocking agent.[109] Indeed, blocking agents are only able to be directly compared if analysed using the same technique and under identical conditions, as evidenced in the comprehensive study by Regulski *et al.* in which the crosslinking temperatures of various blocked isocyanatoethyl methacrylates were investigated.[110] Despite this, it is evident that there is a vast array of blocking agents available for use, encompassing a wide range of deblocking temperatures, with further temperatures able to be targeted through altering substituents on the blocking group, as well as changing the experimental conditions and the isocyanate to be blocked. It should also be noted that the term “deblocking temperature”, when referred to in the literature, frequently corresponds to the temperature at which a feature of deblocking is

observed. It is not, therefore, the exact temperature at which deblocking occurs, which would require determination of rates and extrapolation through the Arrhenius equation, plotting the natural logarithm of rate *vs* 1/temperature, the gradient of which is equal to the negative activation energy divided by the universal gas constant.

It is worth mentioning that the use of external blocking agents, whilst providing access to a greater temperature range of deblocking, is not without disadvantage. One particular problem is that once deblocked, unless the temperature range is similar to the boiling point of the blocking agent, the free blocking agent remains in the product material. However, the evaporation of, for example, an alcohol based blocking agent can provide a facile method of blocking agent removal from the product material. Meier-Westhues reported that, especially in a one-component system, the blocked isocyanate was responsible for increased thermal yellowing, though this could be mitigated through the use of correct stabilisers.[111] Moreover, it was noted that residual blocking agents within the paint film affected film quality, resulting in a lower etch resistance. In spite of the potential negative impact of residual blocking agent on the product material, the presence of blocking agent is not necessarily detrimental to the final product: Carter and co-workers found that ethyl acetoacetate oxime, upon deblocking, underwent intramolecular cyclisation to produce an unreactive oxazolone product, which then acted as a plasticiser.[112] Even if the blocking agent does evaporate, again this can be problematic and can result in the formation of bubbles in the product material, especially harmful for coating applications, and potentially disrupting the balance of gelling and blowing in the production of polyurethane foams.

Table 1.1 Common blocking agents and their corresponding deblocking temperature ranges.

Blocking Functional Group	Specific Examples	Additional Information	Deblocking Temp. (°C[a,b])
Alcohol	Butanol[113, 114] Ethanol[113] Isopropanol[115-117]	Generally found to have high deblocking temperatures. The presence of halogens found to significantly decrease the deblocking temperature.[118]	95-200
Phenol	Phenol[119-121] *o*-Cresol[122] *p*-Chlorophenol[123-125]	Easy to demonstrate the effect of substituent type and position on the deblocking temperature.[122]	60-180
Pyridinol	2-Pyridinol[118] 2-Chloro-3-pyridinol[118]	Deblocking at a lower temperature than phenol due the hydrogen bond formation between the amine and the urethane bond.[118]	110
Oxime	MEKO[126-129] Benzophenone Oxime[121, 130, 131]	MEKO found to be most common blocking agent in the literature, with the blocking reaction requiring no catalyst. Strong substituent effect on deblocking temperature.[130]	85-260
Thiophenol	Thiophenol[132] Pentafluorothiophenol[133]	Thiophenol found to have faster deblocking rates than phenol.[124]	130-170
Mercaptan	1-Dodecanethiol[134]	Restricted applicability due to odours produced in production and deblocking.[118]	75-115
Amide	Acetanilide[126] Methylacetamide[126]	Found to have lower deblocking temperatures than MEKO blocked isocyanates.[126]	100-130
Cyclic Amide	Pyrrolidinone[135] ε-Caprolactam[136-138]	ε-Caprolactam does not volatilise after deblocking and is able to act as a plasticiser.[139]	70-170
Imide	Succinimide[126] Hydroxyphthalimide[140]	Along with amines, the deblocking temperature is heavily influenced by the polarisation of the NH bond.[126]	110-145

Imidazole/ Imidazoline	Imidazole[141, 142] 2-Methylimidazole[141, 143, 144] 2-Phenylimidazole[145]	Basicity of imidazole able to accelerate the blocking reaction without additional catalyst.[105] Large substituent effect on deblocking temperature.[143]	120-290
Pyrazole	Dimethylpyrazole[146-148] 2-Methyl-4-ethyl-5-methylpyrazole[146]	When deblocked in the presence of amines, deblock *via* a cyclic transition state releasing the isocyanate, in contrast to phenol blocked isocyanates in which the amine attacks the urethane bond.[146] Deblocking temperature is lowered when the basicity of the pyrazole is increased.[118]	85-200
Triazole	Benzotriazole[109, 149] Triazole[150-152]	Along with pyrazoles, triazoles produce less yellowing than oximes.[118]	120-250
Amidine	Bicyclic amidine[153, 154]	Radical intermediates formed during cleavage.[154]	70-175
Hydroxamic Acid Ester	Benzylmethacrylo-hydroxamate[155]	Deblocking proceeds *via* a six membered transition state.[155]	50
Intra-molecular	Uretdione[156-158] 2-oxo-1,3-diazepane-1-carboxylate[159]	Uretdione is a self-condensation product, and can be further transformed into a trimeric species (isocyanurates).[160]	150-200
Other	Sodium bisulfite[161-163] *N*-Methylaniline[142, 164, 165]	Sodium bisulfite is frequently used in waterborne coatings as the blocked product is water soluble,[118] as well as being relatively cheap with no pollution.[163] *N*-methylaniline deblocks *via* a four membered transition state.[165]	50-160 -

[a] The deblocking temperatures are those quoted in the literature and as such are determined by varying methods. Different methods can yield different deblocking temperatures for the same blocking group and so these temperatures should only be taken as an approximate guide of the deblocking temperature range. Moreover, these can readily be influenced by the presence of catalysts and other additives.

[b] Blocking agents without deblocking temperatures have been found in literature in which the deblocking occurs during either curing or, kinetic studies at a constant temperature known to be greater than the deblocking temperature, or they are synthesised as a pre-polymer and so the deblocking temperature is not quoted.

Whilst variance in the blocking agent allows for different deblocking temperatures to be achieved, isocyanate structure is also integral in the deblocking temperature of isocyanates, with it being widely accepted that an aromatic blocked isocyanate undergoes deblocking at lower temperatures when compared to an aliphatic blocked isocyanate, as a consequence of both steric and electronic effects. The aromatic ring, in contrast to the alkyl functionality in aliphatic isocyanates, lowers the deblocking temperature through the conjugation of the π-electrons of the ring and the lone pair of electron on the nitrogen atom in the urethane bond.[166] Generally speaking, for a blocked isocyanate there is a partial positive charge on the carbonyl in the resonance forms. For an blocked aromatic isocyanate, conjugation between the π-electrons of the aromatic ring and the lone pair of electrons on the nitrogen atom has the net effect of increasing this partial positive charge and decreasing the deblocking temperature.[167] Moreover, substitution of the ring with electron-withdrawing groups amplifies this effect and further lowers the deblocking temperature. Nesterov reported that substitution on the aromatic ring resulted in increasing the blocking reaction rate with active hydrogen containing compounds, evidenced in the changing Hammett constants.[168] The Hammett constants, relating to the rate of a reaction when investigating a series of substituents, were found to be positive, indicating an acceleration of the reaction rate between the alcohol and isocyanate with the presence of electron-withdrawing groups. Conversely, the addition of electron-donating groups decreases the blocking rates. Indeed, in their study involving the reaction of different substituted phenyl isocyanates with alcohols, Bailey and co-workers noted that both nitrile and chlorine substituted phenyl isocyanate had much greater rates of reaction than that of the methyl groups which exhibited an inhibiting effect on the reaction.[169] Lee *et al.* further elaborated on substituent effects whilst reporting the deblocking of hydrogenated methylenediphenyl diisocyanate (H_{12}-MDI), (2,4-toluene diisocyanate) (TDI) and methylenediphenyl diisocyanate (MDI) (Figure 1.13): H_{12}-MDI was found to have the highest deblocking temperature owing to having no aromatic ring, followed by MDI and then TDI.[109] The conjugation between the π-electrons of the

ring and the lone pair of the nitrogen results in a slightly positive character on the nitrogen and thus weakening the bond between the hydrogen and the nitrogen.[109] This has the net result of making the hydrogen more labile and therefore decreasing the deblocking temperature.

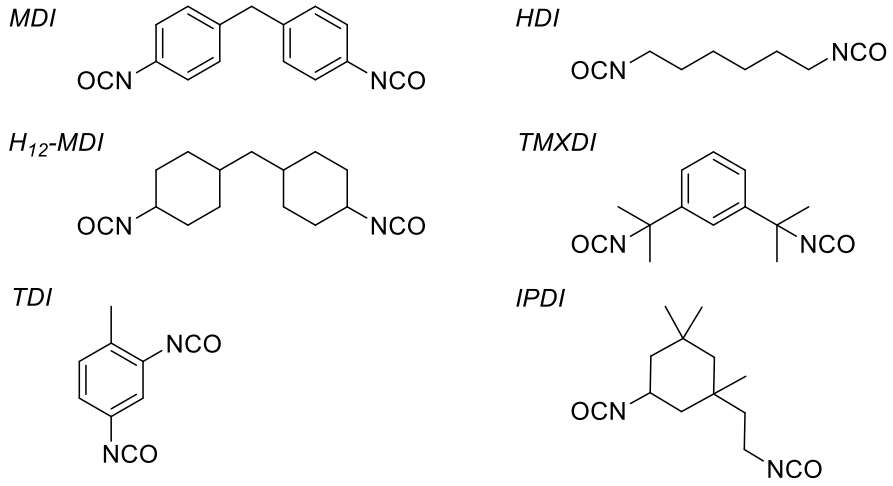

Figure 1.13 Schematic representation of the structure of various diisocyanates.

The combination of electronic and steric effects was further discussed by Muramatsu *et al.*, who demonstrated the methylethyl ketone oxime (MEKO) blocked isophorone diisocyanate (IPDI) deblocked at lower temperatures than hexamethylene diisocyanate (HDI) (Figure 1.13).[126] The lower deblocking temperature was attributed to the bulky nature of the cyclohexyl ring on the IPDI resulting in a more crowded isocyanate, further highlighted with the more sterically crowded α, α, α', α'-tetramethyl-1,3-xylene diisocyanate (TMXDI) having an even lower deblocking temperature. Interestingly, it was observed by Tassel *et al.* that the isocyanates on IPDI did not block at the same time, with the cyclic isocyanate blocking before the aliphatic isocyanate.[150] Indeed, this effect of isocyanate inequivalence was observed by Bailey and co-workers when working on isocyanate blocking in the mid-1950s: whilst phenylene diisocyanate was found to undergo a fast blocking reaction when reacted with alcohols, an additional isocyanate in a *meta* or *para* position relative to the first further increased reactivity (with *meta*- slightly more active than *para*-),[169] with this increase in reactivity attributed to the activating behaviour of the other isocyanate group positioned either *meta* or *para* to the first. This

substituent effect is further noted in the synthesis of uretdiones; Otto observed a significantly faster rate of synthesis for 4-nitrophenyl isocyanate based uretdiones than non-ring substituted uretdiones.[170]

Primarily, as indicated in Table 1.1, the blocking/ deblocking temperature is determined by the blocking agent. It is evident that different blocking agents have different deblocking temperatures, and as a result it is possible, to a certain degree, to tailor the deblocking temperature simply by selecting the correct blocking group. However, owing to the problems associated with high variance in deblocking temperature with detection method selected, it is important to have an alternative method to tailor the deblocking temperature. This is achieved through altering functional groups bound to the blocking agent. As previously mentioned, the deblocking temperature for aromatic systems, for example phenolic blocked isocyanates, can easily be tailored through varying the ring substituents from electron-withdrawing substituents to electron-donating substituents. Caution must be taken however in choosing the correct base agent: addition of the same functional groups to different aromatic systems has been demonstrated to have different effects. Mühlebach demonstrated that varying the substituents present on the pyrazole ring on the blocking agent from electron-withdrawing groups (decreased the curing rate), to electron-donating groups (increased the curing rate) was the opposite to the addition of these groups to phenolic blocking agents.[146, 171] For a pyrazole blocked isocyanate, the initial step of deblocking occurs *via* abstraction of the hydrogen from the urethane bond (Scheme 1.11A). The addition of electron withdrawing groups decreases the nucleophilicity of the ring nitrogen, rendering it less able to abstract the hydrogen and therefore increasing the deblocking temperature. Conversely, the phenol blocked isocyanates proceeded *via* attack of the tertiary amine on the partially positively charged blocked isocyanate carbonyl (Scheme 1.11B), with electron withdrawing groups on the aromatic ring increasing the rate of reaction through increasing the positive charge on the carbonyl.

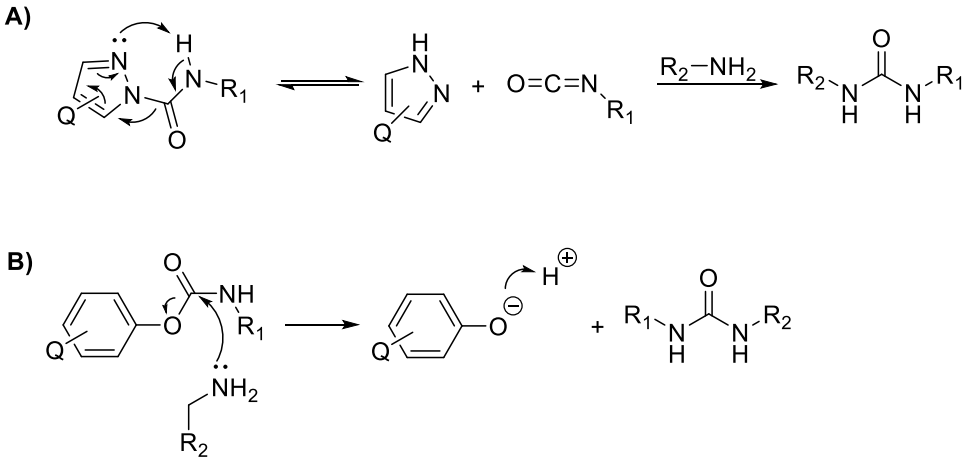

Scheme 1.11 Schematic representation for the proposed mechanisms for the deblocking of (A) pyrazole blocked isocyanates and (B) phenol blocked isocyanates. Reproduced with permission from Mühlebach.[146]

Work by Kothandaraman and Nasar further elaborated the effect that substituents had to play on deblocking temperature: the urethane carbonyl formed during the blocking reaction has a partial positive charge on the carbon and the addition of electron-donating substituents enhance the negative charge density on the blocking group and this intensification of charge difference between the urethane carbonyl and the blocking agent increases the bond strength and therefore increases the deblocking temperature.[122] It is not, however, just electronic effects of substituents that have an impact on deblocking temperature. In the same study as the investigation into electronic effects, Kothandaraman and Nasar concluded that sterics also had a significant impact, in line with the previously discussed steric influence, though the electronic effects predominated.

As well as the isocyanate structure, the reaction medium is also found to heavily influence deblocking studies. The majority of literature available stresses that the effects of reaction medium are mainly owing to the ability of the medium to hydrogen bond with the reactants.[164, 165, 172] Strong hydrogen bond-acceptor solvents have been shown to significantly

reduce the rate of recombination of a blocking agent and isocyanate (Scheme 1.12, k_{-1}), and therefore the rate of deblocking would increase in hydrogen bond-accepting solvents in comparison to aprotic solvents. Indeed, this effect was noted by Nasar and co-workers who reported a shorter reaction time when using hexamethyl phosphoric acid triamide and mesitylene when studying the impact of different solvents on the polymerisation rate of blocked isocyanate prepolymers.[164] It was suggested that the tertiary amine nitrogen in the solvent abstracts the proton from the blocked isocyanate nitrogen and facilitates transfer back to the blocking agent, increasing the rate of evolution of the free isocyanate. Gnanarajan *et al.* also investigated the effects of both dipolar aprotic solvents and non-polar solvents on the reaction between a *N*-methylaniline blocked polyurethane prepolymer, an isocyanate rich polymer produced from reacting an excess of diisocyanate with a polyol, and an anhydride, again concluding that the basicity and polarity of the solvents impacted the rate of deblocking. [165] Moreover, as reported by Baker and Gaunt for the blocking of phenyl isocyanate with alcohols/amines, the reaction proceeds faster in nonpolar solvents as these reduce the rate of deblocking (Scheme 1.12, k_1).[172]

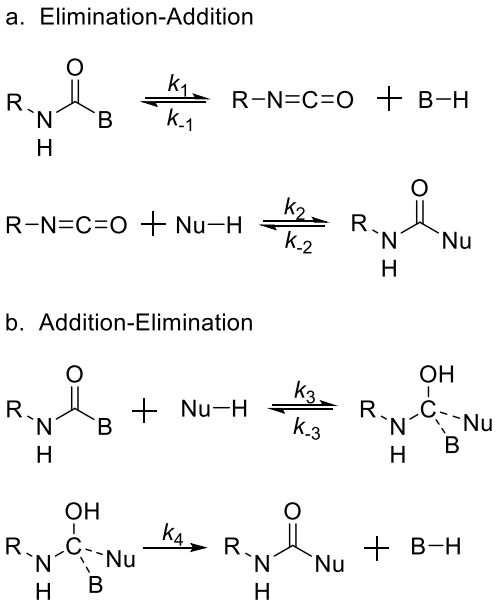

Scheme 1.12 Schematic representation for the proposed mechanism for isocyanate deblocking in the presence of a nucleophilic species: (A) Elimination-Addition mechanism, (B) Addition-Elimination mechanism, where B- blocking agent, Nu = nucleophilic species and R= additional functionality. Reproduced with permission from Wicks *et al.*[118]

The impact of reaction medium is not, however, singularly an effect of the H-bonding ability. Of potentially similar importance is the ability of the solvent to fully dissolve the blocked isocyanate. Noted by both Griffin and Willwerth, and by Mohanty and Krishnamurti, the higher the solubility of the adduct, the lower the observed deblocking temperature, with it being widely acknowledged that blocked isocyanates in the liquid state deblock at lower temperatures than those in the solid state.[134, 173]

Combining the topics introduced within this Chapter, the ultimate goal of the work is to produce an amine functionalised polymeric star that would be able to act as a polyurethane catalyst. Moreover, through the incorporation of a thermally responsive crosslinker, the polymeric star catalysts could remain dormant until thermally triggered. This would also allow for the deblocking of the formulation isocyanate and subsequently produce polyurethane foam.

1.6 Conclusion

Within this Chapter, several concepts and topics central to the work in this Thesis have been reviewed. With the focus of this work targeted towards a one-pot polyurethane formulation, whereby amine functionalised polymeric particles act as simultaneous isocyanate unblocking and polyurethane catalysts, basic principles in polyurethane chemistry have been introduced. Moreover, the two main categories of polyurethane catalysts have been discussed, in addition to an in-depth review on blocked isocyanates and factors affecting their deblocking temperature, a concept further explored in Chapter 6. With a view to the amine functionalised polymeric particles, the RAFT polymerisation methodology has been introduced, covering the basic concepts behind the technique, in addition to the synthetic methods used for the production of polymeric stars, with an arm-first methodology utilising RAFT polymerisation applied to polymeric star synthesis in Chapters 2-5.

1.7 Bibliography

1. Young, R. J., Lovell, P. A., *Introduction to Polymers, Third Edition*, Taylor & Francis, **2011**.
2. Stille, J., *J. Chem. Educ*, **1981**, 58, 862.
3. Szycher, M., *Szycher's Handbook of Polyurethanes, Second Edition*, Taylor & Francis, **2012**.
4. Odian, G., *Principles of Polymerization*, 4th ed.; John Wiley & Sons, **2007**.
5. Colombani, D., *Prog. Polym. Sci.*, **1997**, 22, 1649.
6. Zoller, A., Gigmes, D., Guillaneuf, Y., *Polym. Chem.*, **2015**, 6, 5719.
7. Szwarc, M., *Living Polymers and Mechanisms of Anionic Polymerization*, Springer, **1983**.
8. Ohtori, T., Hirokawa, Y., Higashimura, T., *Polym. J.*, **1979**, 11, 471.
9. Miyamoto, M., Sawamoto, M., Higashimura, T., *Macromolecules*, **1984**, 17, 265.
10. Faust, R., Fehérvári, A., Kennedy, J. P., *J. Macromol. Sci., Part A: Pure Appl. Chem.*, **1982**, 18, 1209.
11. Faust, R., Kennedy, J. P., *Polym. Bull.*, **1986**, 15, 317.
12. Darling, T. R., Davis, T. P., Fryd, M., Gridnev, A. A., Haddleton, D. M., Ittel, S. D., Matheson, R. R., Moad, G., Rizzardo, E., *J. Polym. Sci., Part A: Polym. Chem.*, **2000**, 38, 1706.
13. Quirk, R. P., Lee, B., *Polym. Int.*, **1992**, 27, 359.
14. Moad, G., Rizzardo, E., Thang, S. H., *Aust. J. Chem.*, **2005**, 58, 379.
15. Moad, G., Chong, Y. K., Postma, A., Rizzardo, E., Thang, S. H., *Polymer*, **2005**, 46, 8458.
16. Perrier, S., Takolpuckdee, P., *J. Polym. Sci., Part A: Polym. Chem.*, **2005**, 43, 5347.
17. Wang, J.-S., Matyjaszewski, K., *J. Am. Chem. Soc.*, **1995**, 117, 5614.
18. Kato, M., Kamigaito, M., Sawamoto, M., Higashimura, T., *Macromolecules*, **1995**, 28, 1721.
19. Matyjaszewski, K., Xia, J., *Chem. Rev.*, **2001**, 101, 2921.
20. Cacioli, P., Rizzardo, E., Solomon, D. H. US 4581429, 4581429, **1986**.
21. Moad, G., Rizzardo, E., Thang, S. H., *Polymer*, **2008**, 49, 1079.
22. Barner-Kowollik, C., *Handbook of RAFT Polymerization*, Wiley-VCH Verlag GmbH & Co. KGaA, **2008**.
23. Xie, M., Dang, J., Han, H., Wang, W., Liu, J., He, X., Zhang, Y., *Macromolecules*, **2008**, 41, 9004.
24. Stenzel, M. H., Zhang, L., Huck, W. T., *Macromol. Rapid Commun.*, **2006**, 27, 1121.
25. Runge, M. B., Dutta, S., Bowden, N. B., *Macromolecules*, **2006**, 39, 498.
26. Kizhakkedathu, J. N., Norris-Jones, R., Brooks, D. E., *Macromolecules*, **2004**, 37, 734.
27. Newland, B., Tai, H., Zheng, Y., Velasco, D., Di Luca, A., Howdle, S. M., Alexander, C., Wang, W., Pandit, A., *Chem. Commun.*, **2010**, 46, 4698.
28. Hao, X., Nilsson, C., Jesberger, M., Stenzel, M. H., Malmström, E., Davis, T. P., Östmark, E., Barner-Kowollik, C., *J. Polym. Sci., Part A: Polym. Chem.*, **2004**, 42, 5877.
29. Zheng, Q., Pan, C.-Y., *Macromolecules*, **2005**, 38, 6841.
30. Chong, Y., Le, T. P., Moad, G., Rizzardo, E., Thang, S. H., *Macromolecules*, **1999**, 32, 2071.
31. Gregory, A., Stenzel, M. H., *Prog. Polym. Sci.*, **2012**, 37, 38.
32. Riess, G., *Prog. Polym. Sci.*, **2003**, 28, 1107.
33. Huang, K., Rzayev, J., *J. Am. Chem. Soc.*, **2009**, 131, 6880.
34. Blanazs, A., Armes, S. P., Ryan, A. J., *Macromol. Rapid Commun.*, **2009**, 30, 267.
35. Qin, S., Geng, Y., Discher, D. E., Yang, S., *Adv. Mater.*, **2006**, 18, 2905.

36. Mai, Y., Eisenberg, A., *Chem. Soc. Rev.*, **2012**, 41, 5969.
37. Kim, J. K., Yang, S. Y., Lee, Y., Kim, Y., *Prog. Polym. Sci.*, **2010**, 35, 1325.
38. York, A. W., Kirkland, S. E., McCormick, C. L., *Adv. Drug Delivery Rev.*, **2008**, 60, 1018.
39. Bajpai, A., Shukla, S. K., Bhanu, S., Kankane, S., *Prog. Polym. Sci.*, **2008**, 33, 1088.
40. Park, M., Harrison, C., Chaikin, P. M., Register, R. A., Adamson, D. H., *Science*, **1997**, 276, 1401.
41. Kennemur, J. G., Yao, L., Bates, F. S., Hillmyer, M. A., *Macromolecules*, **2014**, 47, 1411.
42. Morgan, S. E., McCormick, C. L., *Prog. Polym. Sci.*, **1990**, 15, 103.
43. Taylor, K. C., Nasr-El-Din, H. A., *J. Petrol. Sci. Eng.*, **1998**, 19, 265.
44. Ren, J. M., McKenzie, T. G., Fu, Q., Wong, E. H., Xu, J., An, Z., Shanmugam, S., Davis, T. P., Boyer, C., Qiao, G. G., *Chem. Rev*, **2016**, 116, 6743.
45. Pal, S., Hill, M. R., Sumerlin, B. S., *Polym. Chem.*, **2015**, 6, 7871.
46. Blencowe, A., Tan, J. F., Goh, T. K., Qiao, G. G., *Polymer*, **2009**, 50, 5.
47. Tunca, U., Ozyurek, Z., Erdogan, T., Hizal, G., *J. Polym. Sci., Part A: Polym. Chem.*, **2004**, 42, 4228.
48. Adeli, M., Haag, R., *J. Polym. Sci., Part A: Polym. Chem.*, **2006**, 44, 5740.
49. Gao, H., Matyjaszewski, K., *Prog. Polym. Sci.*, **2009**, 34, 317.
50. Ferreira, J., Syrett, J., Whittaker, M., Haddleton, D., Davis, T. P., Boyer, C., *Polym. Chem.*, **2011**, 2, 1671.
51. Ren, J. M., Fu, Q., Blencowe, A., Qiao, G. G., *ACS Macro Lett.*, **2012**, 1, 681.
52. Goh, T. K., Yamashita, S., Satoh, K., Blencowe, A., Kamigaito, M., Qiao, G. G., *Macromol. Rapid Commun.*, **2011**, 32, 456.
53. Burdynska, J., Cho, H. Y., Mueller, L., Matyjaszewski, K., *Macromolecules*, **2010**, 43, 9227.
54. Stenzel, M. H., Davis, T. P., Barner-Kowollik, C., *Chem. Commun.*, **2004**, 1546.
55. Stenzel-Rosenbaum, M., Davis, T. P., Chen, V., Fane, A. G., *J. Polym. Sci., Part A: Polym. Chem.*, **2001**, 39, 2777.
56. Liu, J., Duong, H., Whittaker, M. R., Davis, T. P., Boyer, C., *Macromol. Rapid Commun.*, **2012**, 33, 760.
57. Dong, Z.-M., Liu, X.-H., Liu, H.-W., Li, Y.-S., *Macromolecules*, **2010**, 43, 7985.
58. Bayer, O., Siefhen, W., Rinke, H., Orther, L., Schild, H. DE 728981C, I.G.Farbenindustrie, **1937**.
59. Bayer, O., *Angew. Chem.*, **1947**, 59, 257.
60. Coppola, P. J. US 4087389 A, Olin Corporation, **1978**.
61. Raynor, R. J. US 4374934 A, Olin Corporation, **1983**.
62. Hnatow, M. F., Bonaddio, V. A., Chan, C. Y., Tursi, D. V., Rucker, J. R. US 6508362 B2, Foamex L.P., **2003**.
63. Mispreuve, H. L. S. A., Waddington, S., Tribelhorn, U. US 5484820 A, The Dow Chemical Company, **1996**.
64. Somani, K. P., Kansara, S. S., Patel, N. K., Rakshit, A. K., *Int. J. Adhes. Adhes.*, **2003**, 23, 269.
65. Du, H., Zhao, Y., Li, Q., Wang, J., Kang, M., Wang, X., Xiang, H., *J. Appl. Polym. Sci.*, **2008**, 110, 1396.
66. Schiller, C., Naumann, M., Landers, R., Eilbracht, C. US 8946311 B2, Evonik Degussa GmbH, **2015**.
67. Tilton, R. W. US 4477399 A, Gsw Inc., **1984**.
68. Demharter, A., *Cryogenics*, **1998**, 38, 113.
69. Chattopadhyay, D. K., Raju, K. V. S. N., *Prog. Polym. Sci.*, **2007**, 32, 352.
70. Melchiors, M., Sonntag, M., Kobusch, C., Jürgens, E., *Prog. Org. Coat.*, **2000**, 40, 99.
71. Statton, G. L., Gaul, J. M. US 4621105 A, Atlantic Richfield Company, **1986**.

72. Wu, G., Li, J., Luo, Y., *Polym. Degrad. Stab.*, **2016**, 123, 36.
73. Ashida, K., *Polyurethane and Related Foams: Chemistry and Technology*, CRC Press, **2006**.
74. Gibb, J. N., Goodman, J. M., *Org. Biomol. Chem.*, **2013**, 11, 90.
75. Zhang, X., Macosko, C., Davis, H., Nikolov, A., Wasan, D., *J. Colloid Interface Sci.*, **1999**, 215, 270.
76. McDermott, M. K., Schroeder, L. W., Balsis, S. L., Paradiso, N. A., Byrne, M. L., Briber, R. M., *J. Appl. Polym. Sci.*, **2004**, 91, 1086.
77. Zheng, J., Luo, J., Zhou, D., Shen, T., Li, H., Liang, L., Lu, M., *Colloids Surf., A*, **2010**, 363, 16.
78. Hill, R. M., *Curr. Opin. Colloid Interface Sci.*, **2002**, 7, 255.
79. Mondal, P., Khakhar, D., *Regulation of cell structure in water blown rigid polyurethane foam*, Wiley Online Library, **2004**.
80. Li, W., Ryan, A. J., Meier, I. K., *Macromolecules*, **2002**, 35, 6306.
81. Singh, S. N., *Rapra Review Reports, v. 12, No. 10, Report 142 : Blowing Agents for Polyurethane Foams*, iSmithers Rapra Publishing, **2002**.
82. Seo, W., Jung, H., Hyun, J., Kim, W. N., Lee, Y. B., Choe, K., Kim, S. B., *J. Appl. Polym. Sci.*, **2003**, 90, 12.
83. Li, X., Cao, H., Zhang, Y., *Sci. China, Ser. B: Chem.*, **2006**, 49, 363.
84. Thirumal, M., Khastgir, D., Singha, N. K., Manjunath, B., Naik, Y., *J. Appl. Polym. Sci.*, **2008**, 108, 1810.
85. Hee Kim, S., Lim, H., Chul Song, J., Kyu Kim, B., *J. Macromol. Sci., Part A: Pure Appl. Chem.*, **2008**, 45, 323.
86. Oertel, G., Abele, L., *Polyurethane Handbook: Chemistry, Raw Materials, Processing Applications and Properties*, Hanser-Gardner Publications, **1994**.
87. Silva, A. L., Bordado, J. C., *Catal. Rev. - Sci. Eng.*, **2004**, 46, 31.
88. Richter, F., Pires, R., Reiter, S., Krause, J., Jurkschat, K., Iovkova, L., Schürmann, M., Bradtmöller, G. US8946372 B2, Bayer Intellectual Property GmbH, **2015**.
89. Ni, H., Nash, H. A., Worden, J. G., Soucek, M. D., *J. Polym. Sci., Part A: Polym. Chem.*, **2002**, 40, 1677.
90. Sardon, H., Pascual, A., Mecerreyes, D., Taton, D., Cramail, H., Hedrick, J. L., *Macromolecules*, **2015**, 48, 3153.
91. Florio, J. J., Miller, D. J., *Handbook Of Coating Additives*, Taylor & Francis, **2004**.
92. Blank, W. J., He, Z. A., Hessell, E. T., *Prog. Org. Coat.*, **1999**, 35, 19.
93. Malwitz, N., Wong, S.-W., Frisch, K. C., Manis, P. A., *J. Cell. Plast.*, **1987**, 23, 461.
94. Van Maris, R., Tamano, Y., Yoshimura, H., Gay, K. M., *J. Cell. Plast.*, **2005**, 41, 305.
95. Eley, D. D., Frankenberg, W. G., Selwood, P. W., Weisz, P. B., *Advances in Catalysis*, Elsevier Science, **1962**.
96. Frisch, K. C., Rumao, L. P., *J. Macromol. Sci., Part C: Polym. Rev.*, **1970**, 5, 103.
97. Frisch, K. C., Klempner, D., *Advances in Urethane: Science & Technology*, Taylor & Francis, **1998**.
98. Albrecht, W. N., Stephenson, R. L., *Scand. J. Work Environ. Health*, **1988**, 14, 209.
99. Elwell, M. J., Ryan, A. J., Grünbauer, H. J. M., Van Lieshout, H. C., *Macromolecules*, **1996**, 29, 2960.
100. Bernal, M. M., Martin-Gallego, M., Romasanta, L. J., Mortamet, A.-C., López-Manchado, M. A., Ryan, A. J., Verdejo, R., *Polymer*, **2012**, 53, 4025.
101. Elwell, M. J., Ryan, A. J., Grünbauer, H. J. M., Van Lieshout, H. C., Lidy, W., Structure development via FT-IR spectroscopy, synchrotron SAXS and rheology during the reactive processing of flexible polyurethane foam. *IOM Polyurethanes Conference*, Institute of Materials: Blackpool, U.K., 1995; Vol. 23, pp 265.
102. Widya, T., Macosko, C. W., *J. Macromol. Sci., Part B: Phys.*, **2005**, 44, 897.

103. Foam Qualification System FOAMAT®, Messtechnik GmbH, http://www.format-messtechnik.eu/foamat.htm, October 2016.
104. Barceló, D., *Emerging Organic Pollutants in Waste Waters and Sludge*, Springer Berlin Heidelberg, **2004**.
105. Subramani, S., Sultan Nasar, A., Philip Gnanarajan, T., Padmanabha Iyer, N., Radhakrishnan, G., *Polym. Int.*, **2000**, 49, 546.
106. Eaves, D., *Handbook of Polymer Foams*, Rapra Technology, **2004**.
107. Blencowe, A., Clarke, A., Drew, M. G. B., Hayes, W., Slark, A., Woodward, P., *Reactive and Functional Polymers*, **2006**, 66, 1284.
108. Klinger, D., Chang, J. Y., Theato, P., *Macromol. Rapid Commun.*, **2007**, 28, 718.
109. Lee, J. M., Subramani, S., Lee, Y. S., Kim, J. H., *Macromol. Res.*, **2005**, 13, 427.
110. Regulski, T. W., Thomas, M. R. *Isocyanatoethyl Methacrylate III: Polymerization, Formulation and Evaluation of Blocked IEM Derivatives*, Organic Coatings and Applied Polymer Science Proceedings, 1983; Seattle, WA.
111. Meier-Westhues, U., *Polyurethanes: Coatings, Adhesives and Sealants*, Vincentz Network, **2007**.
112. Carter, J. W., Pappas, S. P., *J. Coat. Technol. Res.*, **1992**, 64, 29.
113. Wicks Jr, Z. W., *Prog. Org. Coat.*, **1975**, 3, 73.
114. Chang, W.-H., Scriven, R. L., Peffer, J. R., Porter, S., *Ind. Eng. Chem. Prod. Res. Dev.*, **1973**, 12, 278.
115. Gedan-Smolka, M., Haussler, L., Fischer, D., *Thermochim. Acta*, **2000**, 351, 95.
116. Wen, X., Mi, R., Huang, Y., Cheng, J., Pi, P., Yang, Z., *J. Coat. Technol. Res.*, **2010**, 7, 373.
117. Subrayan, R. P., Zhang, S., Jones, F. N., Swarup, V., Yezrielev, A. I., *J. Appl. Polym. Sci.*, **2000**, 77, 2212.
118. Wicks, D. A., Wicks, Z. W., *Prog. Org. Coat.*, **1999**, 36, 148.
119. Kothandaraman, H., Nasar, A. S., Lakshmi, R. K., *J. Appl. Polym. Sci.*, **1994**, 53, 31.
120. Gironès, J., Pimenta, M. T. B., Vilaseca, F., Carvalho, A. J. F., Mutjé, P., Curvelo, A. A. S., *Carbohydr. Polym.*, **2008**, 74, 106.
121. Sadoun, T., Clouet, G., Brossas, J., *Makromol. Chem.*, **1987**, 188, 1367.
122. Kothandaraman, H., Nasar, A. S., *Polymer*, **1993**, 34, 610.
123. Ho, K. S., Chen, L. W., *J. Polym. Sci., Part A: Polym. Chem.*, **1997**, 35, 1703.
124. Kamath, P., Srinivasan, M., *Polym. Int.*, **1993**, 32, 33.
125. Lei, G. Y., Angeli, S. R., Kristol, D. S., Snyder, W. H., *J. Polym. Sci., Part A: Polym. Chem.*, **1987**, 25, 607.
126. Muramatsu, I., Tanimoto, Y., Kase, M., Okoshi, N., *Prog. Org. Coat.*, **1993**, 22, 279.
127. Engonga, P. E., Marchetti, V., Gérardin, P., Tekely, P., Loubinoux, B., *J. Fluorine Chem.*, **2000**, 101, 19.
128. Subramani, S., Lee, J. M., Kim, J. H., Cheong, I. W., *Macromol. Res.*, **2005**, 13, 418.
129. Subramani, S., Park, Y.-J., Cheong, I.-W., Kim, J.-H., *Polym. Int.*, **2004**, 53, 1145.
130. Kothandaraman, H., Thangavel, R., *J. Polym. Sci., Part A: Polym. Chem.*, **1993**, 31, 2653.
131. Levine, A. W., Fech, J., *J. Org. Chem.*, **1972**, 37, 1500.
132. Phillips, D. C., Smith, J. D. B., Meier, J. F., Kaczmarek, T. D., *Microchem. J.*, **1978**, 23, 165.
133. Lonikar, S. V., Rungsimuntakul, N., Gilbert, R. D., Fornes, R. E., *J. Polym. Sci., Part A: Polym. Chem.*, **1990**, 28, 759.
134. Griffin, G. R., Willwerth, L. J., *Ind. Eng. Chem. Res.*, **1962**, 1, 265.
135. Fravel, H. G., Reguiski, T. W., Thomas, M. R., *Ind. Eng. Chem. Res.*, **1984**, 23, 586.
136. Subramani, S., Park, Y.-J., Lee, Y.-S., Kim, J.-H., *Prog. Org. Coat.*, **2003**, 48, 71.
137. Camberlin, Y., Michaud, P., Pesando, C., Pascault, J. P., *Makromol. Chem., Macromol. Symp.*, **1989**, 25, 91.

138. Premkumar, S., Karikal Chozhan, C., Alagar, M., *Polym. Eng. Sci.*, **2009**, 49, 747.
139. Dillard, D. A., Pocius, A. V., *Adhesion Science and Engineering: Surfaces, Chemistry and Applications*, Elsevier Science, **2002**.
140. Wei, W.-J., Guo, Z.-R., Zhang, Y.-F., Pan, E.-L., *J. Appl. Polym. Sci.*, **2002**, 84, 1346.
141. Nasar, A. S., Subramani, S., Radhakrishnan, G., *Polym. Int.*, **1999**, 48, 614.
142. Sankar, G., Yan, N., *J. Macromol. Sci., Part A: Pure Appl. Chem.*, **2015**, 52, 47.
143. Nasar, A. S., Jaisankar, S. N., Subramani, S., Radhakrishnan, G., *J. Macromol. Sci., Part A: Pure Appl. Chem.*, **1997**, 34, 1237.
144. Li, A., Fan, G., Chen, H., Zhao, Q., *Res. Chem. Intermed.*, **2012**, 39, 3565.
145. Wolf, H. E., Obendorf, D. J., Gras, H. R. US 4255551, Chemische Werke Huls Ag, **1981**.
146. Mühlebach, A., *J. Polym. Sci., Part A: Polym. Chem.*, **1994**, 32, 753.
147. Wang, T., Qi, S., Ren, B., Tong, Z., *Prog. Org. Coat.*, **2007**, 60, 132.
148. Gertzmann, R., Gürtler, C., *Tetrahedron Lett.*, **2005**, 46, 6659.
149. Wong, S. W., Damusis, A., Frisch, K. C., Jacobs, R. L., Long, J. W., *J. Elastom. Plast.*, **1979**, 11, 15.
150. Tassel, X., Barbry, D., Tighzert, L., *Eur. Polym. J.*, **2000**, 36, 1745.
151. Hoff, E. A., Abel, B. A., Tretbar, C. A., McCormick, C. L., Patton, D. L., *Macromolecules*, **2016**, 49, 554.
152. Decker, C., Masson, F., Schwalm, R., *Macromol. Mater. Eng.*, **2003**, 288, 17.
153. Rolf-Volker Meyer, K., Hans J. Kreuder, K., Eckhard de Cleur, D. US 4424353, Bayer AG, **1984**.
154. Polenz, I., Laue, A., Uhrin, T., Ruffer, T., Lang, H., Schmidt, F. G., Spange, S., *Polym. Chem.*, **2014**, 5, 6678.
155. Querat, E., Tighzert, L., Pascault, J.-P., *Angew. Makromol. Chem.*, **1994**, 219, 185.
156. Buckles, R. E., McGrew, L. A., *J. Am. Chem. Soc.*, **1966**, 88, 3582.
157. Spyrou, E., Metternich, H. J., Franke, R., *Prog. Org. Coat.*, **2003**, 48, 201.
158. Edelmann, M., Gedan-Smolka, M., Lehmann, D., *Prog. Org. Coat.*, **2006**, 57, 251.
159. Ubaghs, L., Keul, H., Höcker, H., *Polymer*, **2005**, 46, 1459.
160. Heift, D., Benko, Z., Grutzmacher, H., Jupp, A. R., Goicoechea, J. M., *Chem. Sci.*, **2015**, 6, 4017.
161. Viganò, M., Suriano, R., Levi, M., Turri, S., Chiari, M., Damin, F., *Surf. Sci.*, **2007**, 601, 1365.
162. Vorlop, K.-D., Muscat, A., Beyersdorf, J., *Biotechnol. Tech.*, 6, 483.
163. Zhang, Y., Gu, J., Jiang, X., Zhu, L., Tan, H., *Pigm. Resin Technol.*, **2011**, 40, 379.
164. Nasar, A. S., Raghavan, A., Kumar, V. S., *J. Macromol. Sci., Part A: Pure Appl. Chem.*, **2005**, 42, 309.
165. Gnanarajan, T. P., Nasar, A. S., Iyer, N. P., Radhakrishnan, G., *J. Polym. Sci., Part A: Polym. Chem.*, **2000**, 38, 4032.
166. Wicks, Z. W., Jones, F. N., Pappas, S. P., Wicks, D. A., *Organic Coatings: Science and Technology*, Wiley-VCH Verlag GmbH & Co. KGaA, **2006**.
167. Delebecq, E., Pascault, J.-P., Boutevin, B., Ganachaud, F., *Chem. Rev.*, **2013**, 113, 80.
168. Entelis, S. G., Nesterov, O. V., *Russ. Chem. Rev.*, **1966**, 35, 917.
169. Bailey, M. E., Kirss, V., Spaunburgh, R. G., *Ind. Eng. Chem.*, **1956**, 48, 794.
170. Otto, S. US 2671082 A, Du Pont, **1954**.
171. Rand, L., Lateef, A. B., Reeder, J. A., *J. Org. Chem.*, **1971**, 36, 2295.
172. Baker, J. W., Gaunt, J., *J. Chem. Soc.*, **1949**, 27.
173. Mohanty, S., Krishnamurti, N., *Eur. Polym. J.*, **1998**, 34, 77.

2. The Arm-First Synthesis of Amine-Functionalised Polymeric Stars as Catalysts for Rigid Polyurethane Foam

2.1 Abstract

In this Chapter, amine-functionalised polymeric stars have been synthesised using reversible addition-fragmentation chain transfer (RAFT) polymerisation and an arm-first methodology, with the resultant confinement of the amine within the core evaluated in a polyurethane foam formulation. Optimisation of the polymerisation conditions resulted in the synthesis of well-defined homopolymers of 2-hydroxyethyl methacrylate (HEMA), able to act as star arms, on both a small and a large scale whilst still maintaining control over the process (dispersity, $Đ_M$ <1.2). Chain extension of these homopolymers with different monomer feeds of the difunctionalised monomer tri(ethylene glycol) dimethacrylate (TEGDMA) and the amine-functionalised monomer *N,N'*-(dimethylamino)ethyl methacrylate (DMAEMA) allowed for the production of a series of polymeric stars. Furthermore, tuning of the degree of polymerisation for the homopolymer arms, the amine monomer and the crosslinking monomer allowed for a series of polymeric stars to be produced with varying crosslinking densities and arm lengths. The polymeric stars have been extensively characterised using a variety of spectroscopic techniques, confirming the successful incorporation of the amine and the crosslinked nature of the star polymer core. Evaluation of these polymers in a polyurethane foam formulation, allowing for determination of the amine shielding, revealed that there was little effect of both crosslinking density and arm length of the star polymers, with all polymers shown to afford approximately the same protection to the amine tethered in to the core, reflected in the polymers matching the foam rise profile of the blank formulation. Following these results, the star polymer synthesis has been successfully scaled, with star synthesis generated on a 30 g scale whilst still maintaining low dispersities ($Đ_M$ ~ 1.5).

2.2 Introduction

Reversible addition-fragmentation chain transfer (RAFT) polymerisation, in addition to other controlled radical polymerisation (CRP) techniques, has enabled for the synthesis of a vast range of well-defined materials of varying architectures, for example combs and brushes.[1-3] One such architecture, the polymeric star, consists of polymeric arms extending from a central branching point, or core, the synthesis of which has been described in section 1.3.4.[4-6] Owing to the defined nature of their structure, and associated properties (*e.g.* core density and arm length), there is a large number of applications for polymeric stars,[7-10] including their use as catalyst supports. In general, the binding of a catalyst to the polymer scaffold affords greater protection to the catalyst from, for example, deactivation, and improved recyclability,[11] additionally enabling reactions to be carried out in environments previously unsuitable or incompatible with reagents.[12] Most notable, Fréchet and co-workers have demonstrated a one-pot cascade catalysis utilising two separate star polymers, synthesised using nitroxide-mediated polymerisation, that have different internal environments (Figure 2.1).[13]

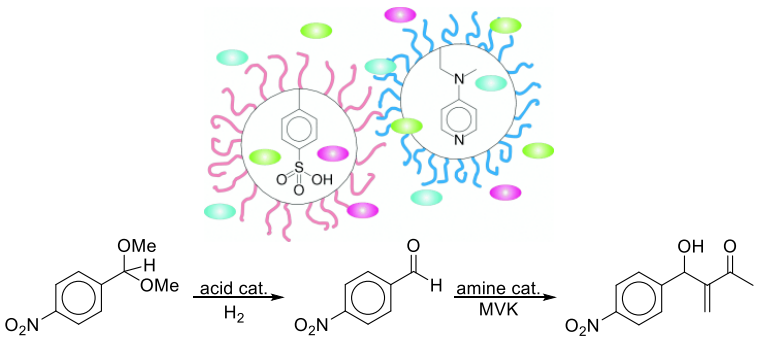

Figure 2.1 One-pot cascade catalysis of acid-catalysed acetal hydrolysis (pink armed star) of *para*-nitrobenzene and subsequent based-catalysed Baylis-Hillman reaction (blue armed star) with methyl vinyl ketone. Reproduced with permission from Fréchet and co-workers.[13]

The first core environment was acid-functionalised *via* the incorporation of *para*-toluene sulfonic acid groups, and enabled acid-catalysed acetal hydrolysis of nitrobenzene. The second star core environment was base-functionalised through the incorporation of 4-

(dialkylamino)pyridine, and allowed for the Baylis-Hillman reaction between the 4-nitrobenzaldehyde (the reaction product from the first star polymer) and methylvinyl ketone. Having both these stars in solution enabled a one-pot cascade catalysis despite the individual reactions requiring different conditions. Work by Sawamoto and co-workers further demonstrated the use of star polymers as supports for catalysis. Star polymers encapsulating a catalytic ruthenium complex, produced *in situ* by ruthenium-catalysed living radical polymerisation, were demonstrated to catalyse the oxidation of 1-phenylethanol to acetophenone (Figure 2.2).[14, 15] Further work by Sawamoto and co-workers has exploited ruthenium-functionalised polymeric stars for the polymerisation of methyl methacrylate.[15, 16]

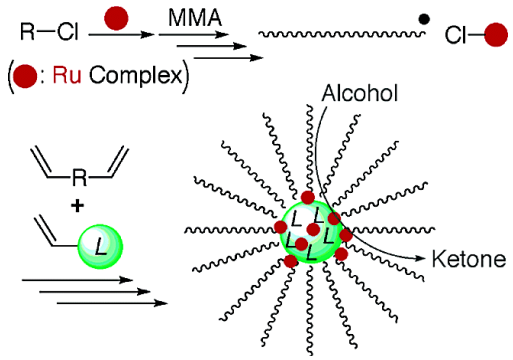

Figure 2.2 Star polymers containing a ruthenium complex in the core, prepared by ruthenium-catalysed living radical polymerisation, and used as catalysts for the oxidation of 1-phenylethanol to acetophenone. Reproduced with permission from Sawamoto *et al.*[14]

Introduced in Section 1.4.2, the production of polyurethane foams is, industrially, traditionally catalysed by either a metal-containing catalyst or a tertiary amine-functionalised organocatalyst, with the latter accounting for over 80% of polyurethane catalyst consumption.[17] In contrast to organo-metallic catalysts, for example, dibutyltin dilaurate (DBTL), tertiary amine catalysts have fewer associated environmental concerns, nor do they suffer from problems associated with deactivation of the catalyst as a consequence of hydrolysis. Moreover, unlike tin-based compounds such as DBTL which are strong gelators, a number of tertiary amine catalysts are described as "balanced" catalysts, enabling them to catalyse both the gelling and blowing reactions for the production of polyurethane foam

(Scheme 1.5). Additionally, it has been reported that tertiary amines have an increased catalytic effect for aromatic isocyanates compared to aliphatic isocyanates.[18] Previous work in our group assessing the catalytic ability of various mono-, bi- and multidentate amine-functionalised monomers revealed that *N,N'*-(dimethylamino)ethyl methacrylate (DMAEMA) produced one of the fastest foam rises compared to other small molecule amines when evaluated in a formulation for rigid polyurethane foam. It was hypothesised that, in comparison to the bi- and tri-dentate amine monomers and their corresponding polymers, the polymers produced using the mono-dentate amine monomer DMAEMA were a good mimic for the diamine commercial catalyst owing to the backbone providing the optimum distance between catalytic amine moieties, previously reported to be of importance in the formation of polyurethane foam.[19]

With the aim of the project to produce amine functionalised catalysts for a one-pot polyurethane foam formulation, it was hypothesised that amine-functionalised polymeric stars would be a suitable candidate as a latent catalyst. Indeed, tethering catalytically active amine functionality to the core of the polymeric star would ensure that the amine catalyst would be fully shielded from the formulation (itself inert owing to the isocyanate component existing as a blocked isocyanate inhibiting the reaction between the isocyanate and the polyol). Incorporation of a thermoresponsive crosslinker would allow for the latent catalyst to be thermally triggered. without the addition of heat, the amine functionality would remain confined within the core of the star, yet addition of heat would result in both the polymeric star either swelling or disintegrating depending on the thermoresponsive nature of the crosslinker incorporated, and the formulation blocked isocyanate deblocking. The swelling/disintegration of the polymeric star, in conjunction with the deblocking of the formulation isocyanate would enable the three main formulation components (the isocyanate, polyol and catalytic amine) to come into contact therefore resulting in the catalysed production of rigid polyurethane foam (Figure 2.3). Furthermore, the presence of polyol

soluble functionalities on the arm of the stars, for example hydroxyl or ester groups, should allow for improved dissolution and dispersion of the catalytic polymeric stars in the formulation polyol. Additionally the presence of tertiary amines should lower the deblocking temperature (discussed in detail in Chapter 6) therefore requiring less heat to trigger the foam synthesis.

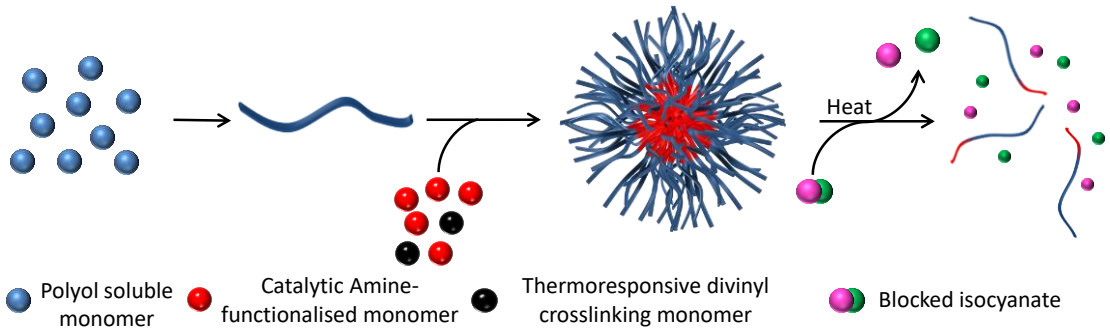

Figure 2.3 Pictorial representation of the aim of the project: the arm first synthesis of OH-functionalised responsive star polymers with catalytic amines tethered within the core, able to fall apart upon the addition of heat and result in catalysis of the polyurethane foam reaction.

2.3 Results and Discussion

2.3.1 Synthesis of homopolymer arms for star polymers

Polymeric stars were synthesised using the RAFT polymerisation method, with the chain transfer agent (CTA) 2-cyano-2-propyl benzodithioate (CPBD), synthesised according to a procedure previously developed by the group:[20] to a stirring solution of *S,S'*-bis(dithiobenzoate) in ethyl acetate, the radical initiator 2,2'-azobis(2-methylpropionitrile) (AIBN) was added, the flask degassed, and the solution refluxed for 24 hours. The solvent was evaporated under vacuum, and the resulting solution purified by column chromatography affording a viscous pink oil (in a yield of 62%).

An arm-first synthesis of the catalytic polymeric stars was employed to enable the production of polymeric stars with large numbers of arms without the need for the complex synthesis of a multifunctional initiator, and produce stars with a large core domain. To

ensure solubility within the formulation polyol, a compound with multiple hydroxyl functionalities, it was decided that the star arms should be hydroxy-functionalised, and as such the monomer 2-hydroxyethyl methacrylate (HEMA) was selected. In an initial experiment, the homopolymerisation was carried out using CPBD and the radical initiator AIBN in *N*,*N*'-dimethylformamide (DMF) at 70 °C, with a feed ratio of $[CTA]_0$:$[Initiator]_0$:$[Monomer]_0$ of 1:0.3:100 (Scheme 2.1). Following reaction for 3 hours, ^{1}H Nuclear Magnetic Resonance (NMR) spectroscopic analysis of the crude reaction sample revealed a monomer conversion of 63%, calculated through comparison of the integrals associated with the monomer vinyl peaks at δ = 5.66 ppm with the OCH_2CH$_2$ protons of the polymer (δ = 4.07 ppm) (Figure 2.4).

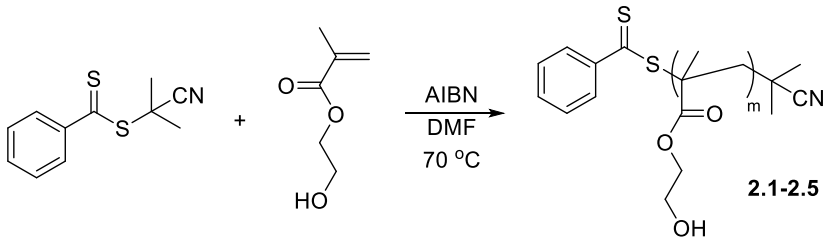

Scheme 2.1 Schematic representation for the synthesis of PHEMA homopolymers using RAFT polymerisation.

Purification of the reaction mixture by precipitation into diethyl ether afforded the pink homopolymer **2.1**. The theoretical number-average molecular weight ($M_{n,\ theo.}$) was found to be 8.2 kg/mol, determined by multiplying the equivalents of monomer added by the conversion determined from the ^{1}H NMR spectrum. This value was found to be lower than the observed number-average molecular weight ($M_{n,\ obs.}$), determined by end-group analysis using the ^{1}H NMR spectrum of the purified product through comparison of the integrals associated with the benzyl ring of the RAFT CTA (δ = 7.32 ppm) to the alkyl protons of the OCH_2CH$_2$ group (δ = 4.05 ppm), which generated a degree of polymerisation (DP) of 113 and $M_{n,\ obs.}$ of 14.9 kg/mol (Figure 2.5).

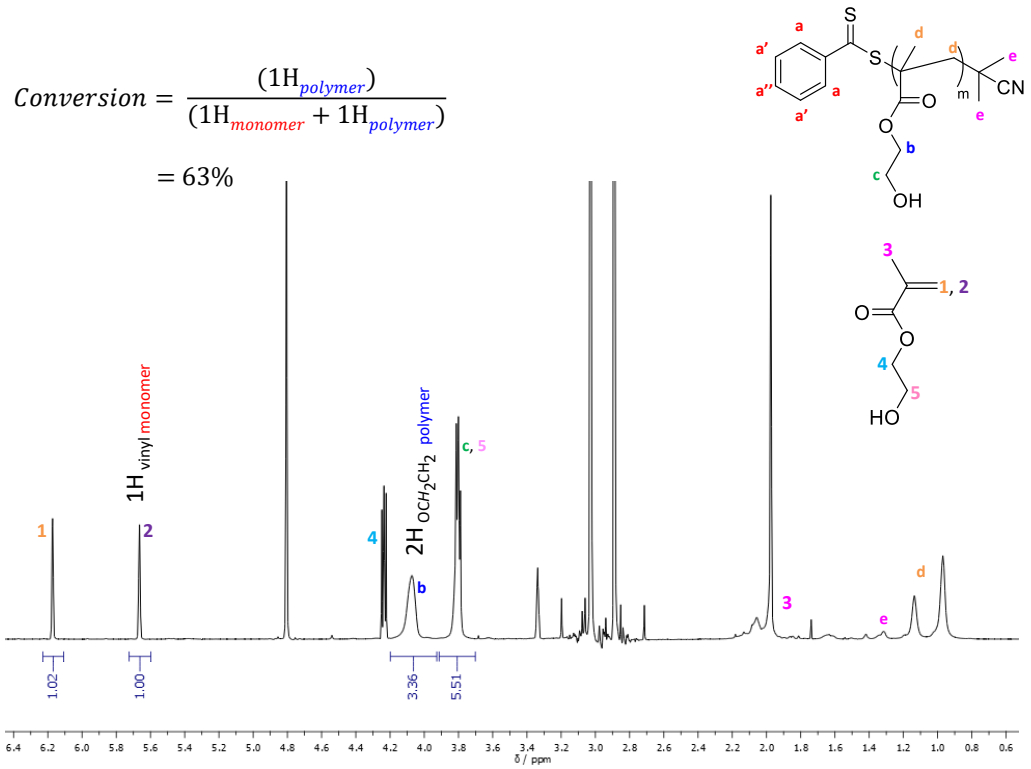

Figure 2.4 ^{1}H NMR spectrum used to calculate conversion for the synthesis of PHEMA homopolymer 2.1 (400 MHz, CD_3OD).

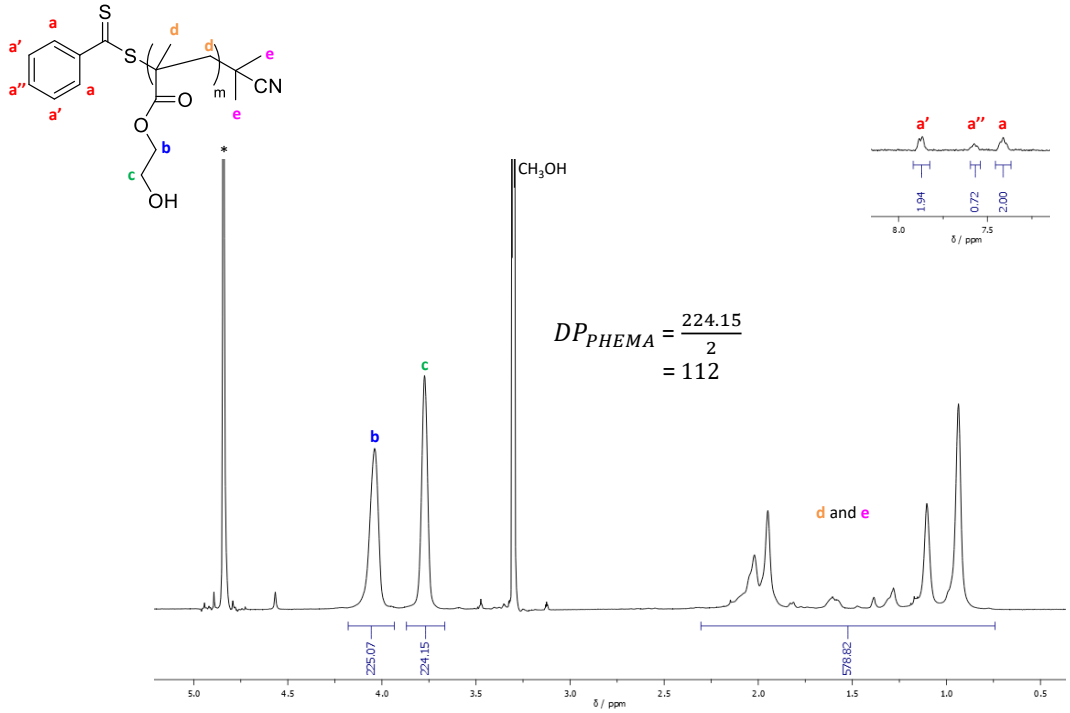

Figure 2.5 ^{1}H NMR spectrum showing calculation of the DP of the PHEMA homopolymer 2.1, by comparison of the aromatic integrals associated with the CTA end-group (proton 1, δ = 7.32 ppm, equal to 1H) and the alkyl OCH_2CH_2 protons (proton 3, δ = 3.80 ppm, equal to 2H in each monomer unit) where the DP = 224.15/2 = 112. *denotes H_2O (400 MHz, CD_3OD).

The number-average molecular weight by Size Exclusion Chromatography (SEC, $M_{n,\ SEC}$), carried out in DMF with PMMA standards, was found to be 16.3 kg/mol, with a polymer dispersity ($Đ_M$) of 1.14 (Figure 2.6B). In addition to the low dispersity value and narrow Gaussian distribution (Figure 2.6A), the kinetic analysis of the reaction demonstrated a linear increase in molecular weight *vs* conversion, with good correlation between the theoretical number-average molecular weight and the number-average molecular weight determined by SEC analysis, further confirming the controlled nature of the polymerisation (Figure 2.6 C and D).

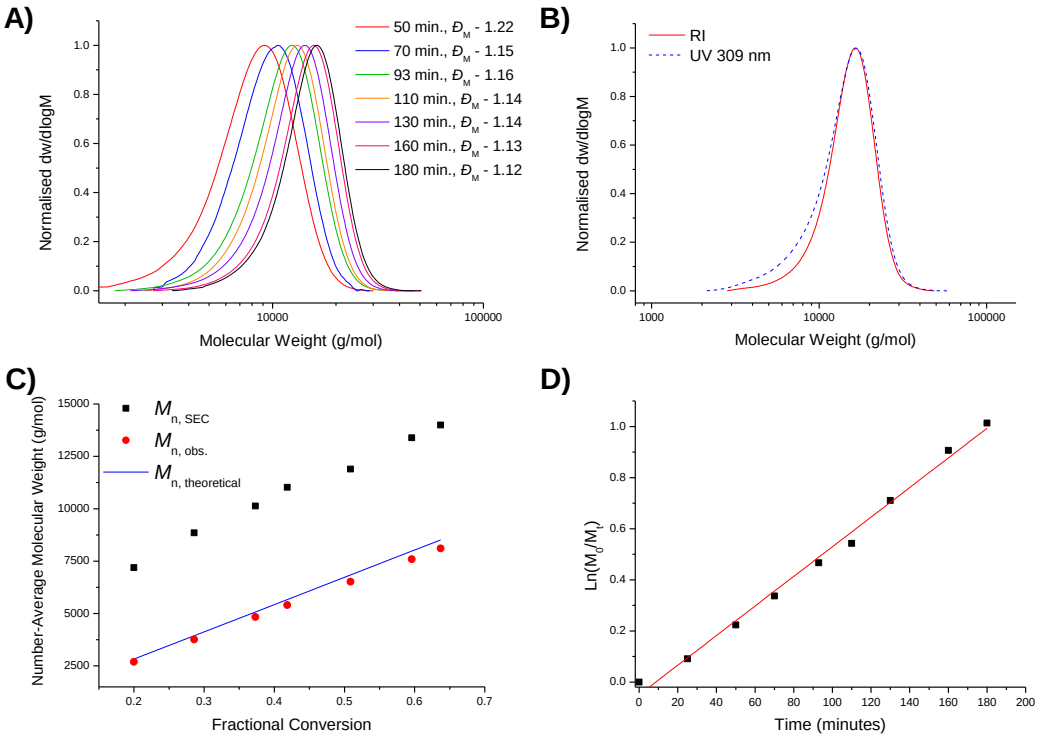

Figure 2.6 SEC analysis for the synthesis of PHEMA homopolymer 2.1. (A) normalised molecular weight distributions for PHEMA obtained at different reaction times, (B) overlay of the size exclusion chromatograms for polymer 2.1; red line generated using RI detection and the blue line generated using UV detection at λ = 309 nm, (C) linear increase in the number-average molecular weight with conversion (observed values calculated using ^{1}H NMR spectroscopy end-group analysis, theoretical values based on conversion determined by ^{1}H NMR spectroscopy), and (D) kinetic analysis of the polymerisation where the blue line is the trend line. (NMR analysis: 400 MHz, CD_3OD, SEC: DMF, PMMA standards).

Whilst a relatively good overlap between the SEC refractive index (RI) trace and ultraviolet (UV) trace at λ = 309 nm was observed (Figure 2.6B), confirming retention of the dithiobenzoate end-group, the significant difference (2.7 kg/mol) between the theoretical and

observed number-average molecular weight of the product polymer suggests that some control over the process has been lost, with some chains lacking the dithioester end-group. In order for successful chain extension into polymeric stars, the majority of PHEMA arms must contain the active end-group. In an attempt to improve the number of chains with the active end-group present, a series of experiments was carried out in which the feed ratio of AIBN and reaction time were varied (Table 2.1).

Polymer	Equivalents AIBN	Reaction Time (min.)	Conversion[a] (%)	$M_{n,\,SEC}$[b] (kg/mol)	$Đ_M$[b]	$M_{n,\,theo.}$[c] (kg/mol)	$M_{n,\,obs.}$[d] (kg/mol)
2.1	0.3	180	64	14.0	1.14	8.2	10.9
2.2	0.11	180	41	12.7	1.13	5.4	9.1
2.3	0.12	1440	97	14.5	1.14	9.8	10.2

Table 2.1 Characterisation data for PHEMA homopolymers investigating the effect of altering AIBN equivalents on the end-group fidelity of the reaction. [a] determined by ^{1}H NMR spectroscopy (400 MHz, CD_3OD), [b] measured by SEC (DMF, PMMA standards), [c] theoretical molar mass calculated based on monomer conversion (^{1}H NMR spectroscopy, CD_3OD), and [d] observed molar mass calculated based on the DP of the polymer, determined by ^{1}H NMR spectroscopy.

Decreasing the equivalents of AIBN from 0.3 to 0.11 was found to have little effect on the resultant polymerisation, with the product polymer (**2.2**) having a dispersity, $Đ_M$, of 1.13, compared to $Đ_M$ = 1.14 for the reaction involving greater equivalents of AIBN. It was also noted that fewer equivalents of AIBN produced a polymer with a theoretical number-average molecular weight significantly less that the observed number-average molecular weight, with polymer **2.2** found to have a difference of 4.5 kg/mol between the two values. The large difference was hypothesised to result from the lower conversion reached for the reaction with lower equivalents of AIBN over the three hour reaction period. As such, the reaction was repeated for 24 hours, achieving 97% conversion. SEC analysis on the product

polymer (**2.3**) confirmed that the reaction remained controlled, with a low dispersity value of $Đ_M$ = 1.14. Crucially, $M_{n,\,obs.}$, determined by end-group analysis using ^{1}H NMR spectroscopy, was found to be in good agreement with $M_{n,\,theo.}$., with molecular weights of 9.8 kg/mol and 10.2 kg/mol respectively, with the high end-group fidelity reflected in the overlap of the RI and UV at λ = 309 nm SEC traces.

In order to confirm the optimum conditions of the PHEMA homopolymerisation, a series of reactions were carried out for 24 hours using 0.1 equivalents of AIBN, varying the temperature (Table 2.2). Compensating for the lower temperatures by increasing the reaction time, it was found that the lower temperatures resulted in polymers with monomodal molecular weight distributions, as determined by SEC analysis, with similar narrow dispersities of 1.10 and 1.19 for the reaction at 65 and 60 °C, respectively (Figure 2.7). However, the observed number-average molecular weight, determined by ^{1}H NMR spectroscopy, was found to be much larger than that expected from monomer conversion ($M_{n,\,theo.}$). From these results it was concluded that the optimum conditions for the synthesis of PHEMA homopolymers was 0.1 eq. AIBN at 70 °C for 24 hours.

Polymer	Reaction Temperature (°C)	Conversion (%)	$M_{n,\,SEC}$[b] (kg/mol)	$Đ_M$[b]	$M_{n,\,theo.}$[c] (kg/mol)	$M_{n,\,obs.}$[d] (kg/mol)
2.3	70	97	14.5	1.14	9.8	10.2
2.4	65	87	15.7	1.11	8.6	14.8
2.5	60	73	15.0	1.13	7.6	10.5

Table 2.2 Characterisation data for PHEMA homopolymers investigating the effect of altering reaction temperature on the end-group fidelity of the reaction. [a] determined by ^{1}H NMR spectroscopy (400 MHz, CD_3OD), [b] measured by SEC (DMF, PMMA standards), [c] theoretical molar mass calculated based on monomer conversion (^{1}H NMR spectroscopy, CD_3OD), and [d] observed molar mass calculated based on the DP of the polymer, determined by ^{1}H NMR spectroscopy.

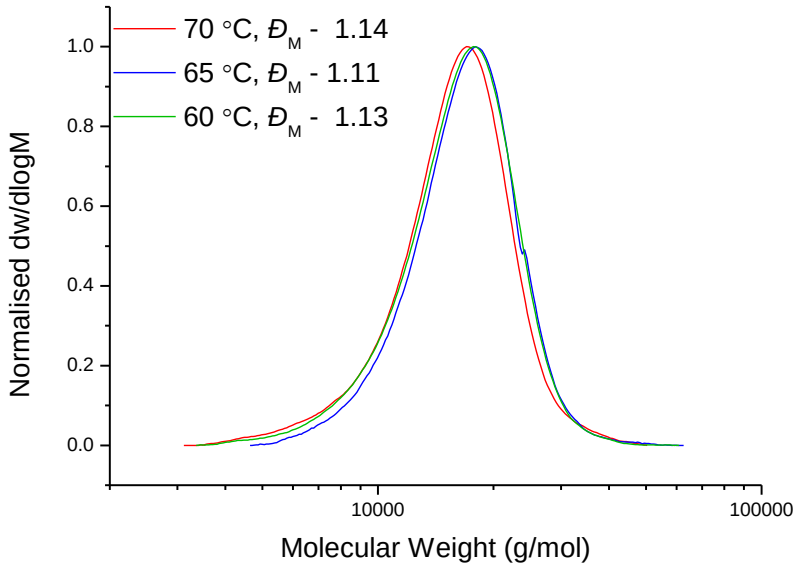

Figure 2.7 Overlay of normalised SEC chromatograms of product polymers 2.3 (red), 2.4 (blue) and 2.5 (green) obtained at different temperatures using RAFT polymerisation with 0.1 eq. AIBN for 24 hours.

Having optimised the conditions for HEMA homopolymerisation, the linear character of the HEMA arms was analysed using triple-detection SEC analysis. It is important for the arms to be linear in nature because it was hypothesised that arms with a brush-like character, or crosslinked owing to back-biting, may have an adverse effect on the diffusion of the polyol or isocyanate to the catalytically active amine in the core of the star polymer. Triple-detection SEC analysis, in which the SEC instrument is fitted with a viscometer, allows for determination of the Mark-Houwink characteristic constant *a*, derived from the linear fit of the Mark-Houwink curve generated by plotting log[η] *vs* log[MW], where MW is the viscosity-average molecular weight calculated by universal calibration and η is the weight-average intrinsic viscosity as measured by the viscometer.[21-24] For polymers, $a = 0.5$ for a polymer chain in a theta solvent, *i.e.* a solvent in which monomer-monomer interactions are equal to monomer-solvent interactions and therefore the polymer chains are referred to as ideal chains exhibiting random coil behaviour. In a good solvent, $a = 0.8$, and therefore for a flexible polymer (for example a linear polymer) $0.5 \leq a \leq 0.8$.[22] For a crosslinked or branched structure, $a < 0.5$. Mark-Houwink analysis of the PHEMA homopolymer produced an *a* value of 0.68, confirming the linear nature of the arms and in

good agreement of the literature value (a = 0.72) (Figure 2.8).[25] Additionally, no branching side reactions were detected in the ^{13}C NMR analysis of the resultant polymer, further confirming the linear nature of the PHEMA.

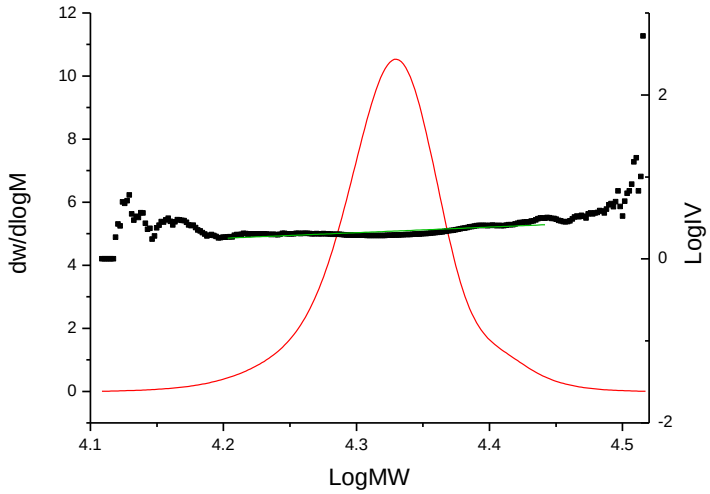

Figure 2.8 Triple-detection SEC analysis of PHEMA (2.3). Red line is the molecular weight distribution, black points are the Mark-Houwink plot, and the green line is the linear fit of the Mark-Houwink plot, of which the gradient is the *a* parameter. (DMF, PMMA standards)

2.3.2 Chain extension of PHEMA to produce polymeric stars

Polymeric stars were synthesised *via* an arm-first approach, by which PHEMA arms act as a macro-CTA for chain extension with the amine-functionalised monomer DMAEMA, and the divinyl crosslinking monomer tri(ethylene glycol) dimethacrylate (TEGDMA) (Scheme 2.2).

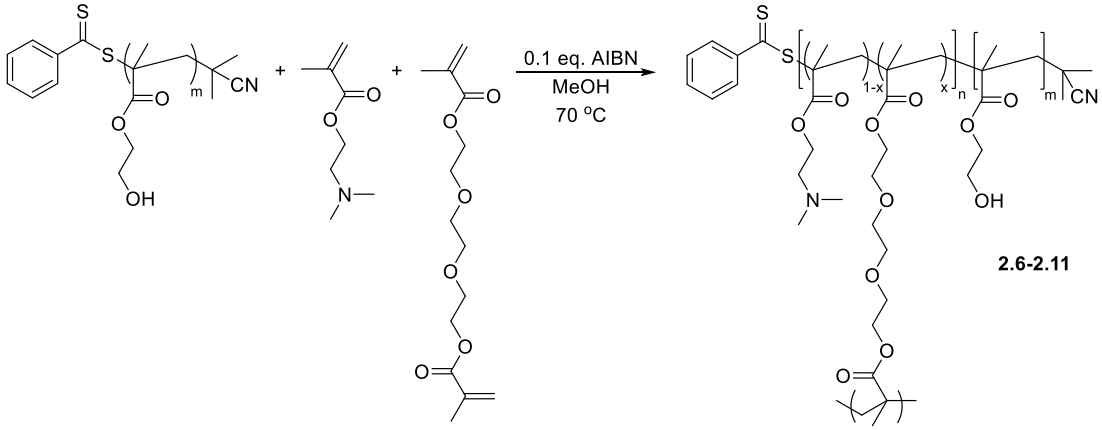

Scheme 2.2 Schematic representation of the synthesis of amine-functionalised polymeric stars *via* an arm-first approach using RAFT polymerisation chain extension of PHEMA arms with DMAEMA and TEGDMA.

Initially, chain extension was attempted using similar conditions to the PHEMA homopolymerisation, with 0.1 equivalents of AIBN at 70 °C, with methanol as solvent. To compensate the foreseen increase in viscosity as the crosslinked star polymers are formed, the concentration of the solution was decreased from the homopolymerisation conditions (5 M with respect to HEMA) to 1.5 M with respect to DMAEMA), and a relatively low initial crosslinking density of 10% was targeted. Following a reaction time of 300 minutes, the solution was found to gel. In addition to this, it was observed that monitoring of conversion by ^{1}H NMR spectroscopy was unsuitable, owing to the lack of non-overlapping peaks attributable to the vinyl protons and both monomers (Figure 2.9).

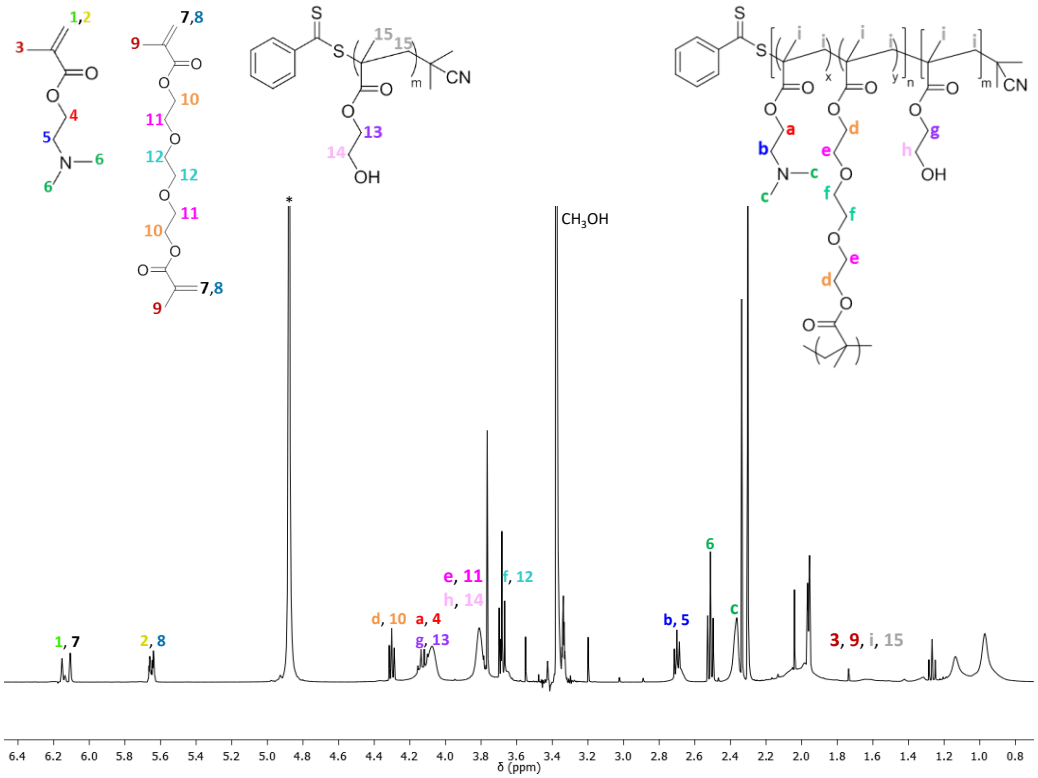

Figure 2.9 ^{1}H NMR spectrum of the crude reaction mixture for the PHEMA-*b*-(DMAEMA-*co*-TEGDMA) (2.6) showing the overlapping resonances *denotes H_2O (400 MHz, CD_3OD).

Consequently, a further method for determination of conversion had to be employed, and as such Gas Chromatography (GC) analysis was selected. Accordingly, the following experimental parameters were altered: to prevent gelation during polymerisation, the solution concentration was halved; to allow for conversion determination, chain extensions were

carried out with the addition of the GC internal standard 1,2,4-trimethoxy benzene (TMB); to use the GC, the reaction solvent was changed from methanol to DMF owing to the incompatibility of methanol with the non-bonded chiral column, with methanol resulting in GC column degradation during analysis.

Initially, 150 mg PHEMA macro-CTA (DP = 100) was chain extended with DMAEMA (100 eq.) and TEGMDA (10 eq.), with 0.1 eq. AIBN in DMF at 70 °C. The resulting polymer (**2.6**), following a reaction time of 240 minutes and a conversion of 52%, was isolated by precipitation into diethyl ether. The controlled nature of the polymerisation was confirmed by kinetic analysis which indicated a linear increase in molecular weight *vs* conversion, with a good correlation observed between the theoretical number-average molecular weight (based on conversion from GC analysis) and the number-average molecular weight by SEC analysis (Figure 2.10, A and B), with only a slight deviation at >50 % conversion. However, determination of the degree of polymerisation from end-group analysis of the extended ^{1}H NMR spectrum of the product polymer did not enable calculation of theoretical number-average molecular weight, likely as a result of the crosslinked core shielding both the amino methyl protons ($CH_2N(CH_3)_2$ and $N(CH_3)_2$) as well as the CTA chain end, resulting in the generation of nonsensical integrals. Despite this, the appearance of peaks associated with both the amine in addition to those associated with TEGDMA in the ^{1}H NMR spectrum (Figure 2.11, protons 1, 2, 3, and protons 4, 5, 6 for DMAEMA and TEGDMA respectively), as well as a noticeable shift in the molecular weight in the SEC trace from the PHEMA macro-CTA to the product polymer (Figure 2.10C) confirmed successful chain extension. SEC analysis also indicated a multimodal trace, frequently observed in the synthesis of polymeric stars, and likely as a result star-stars coupling as the growing crosslinking chains begin to agglomerate.[26] It is important to note, however, that star-star coupling is not likely to hinder the protection of the amine within the core, and therefore conditions were not further optimised.

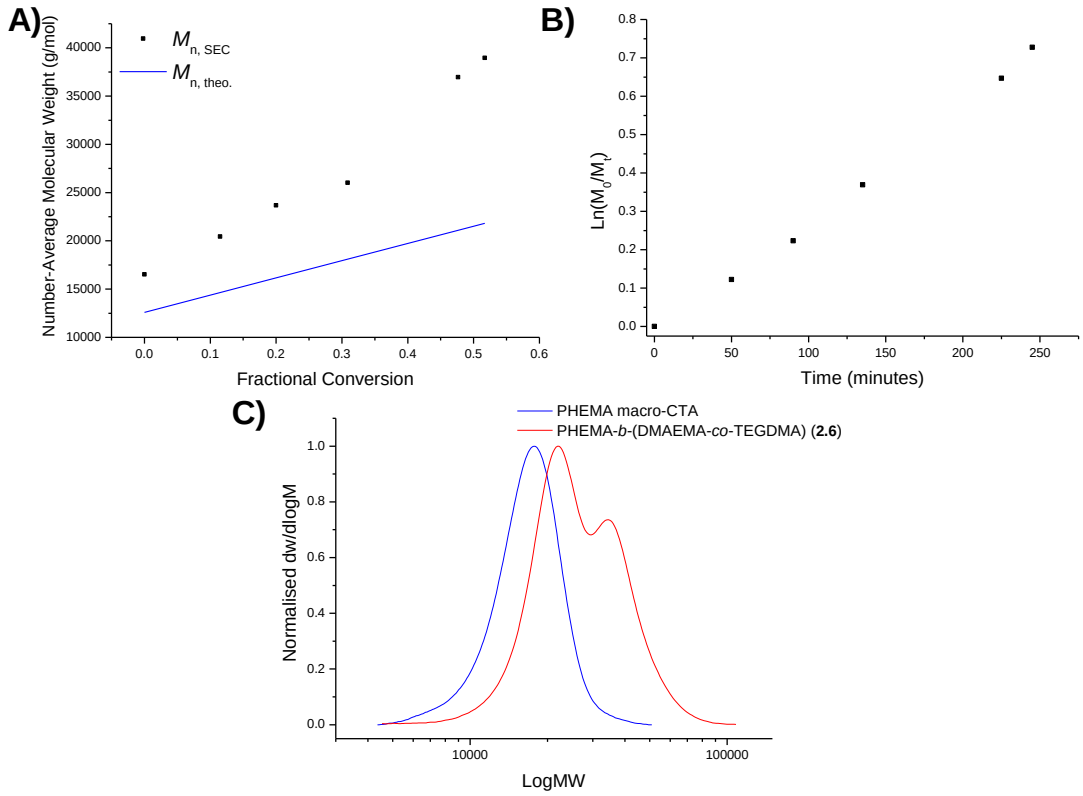

Figure 2.10 SEC analysis for the synthesis of PHEMA-*b*-(DMAEMA-*co*-TEGDMA) (2.6). (A) linear increase in the number-average molecular weight by SEC analysis ($M_{n, SEC}$) and the theoretical values based on conversion determined by GC analysis, (B) kinetic analysis of the polymerisation, and (C) normalised molecular weight distributions for PHEMA-*b*-(DMAEMA-*co*-TEGDMA and the PHEMA macro-CTA. (DMF, PMMA standards)

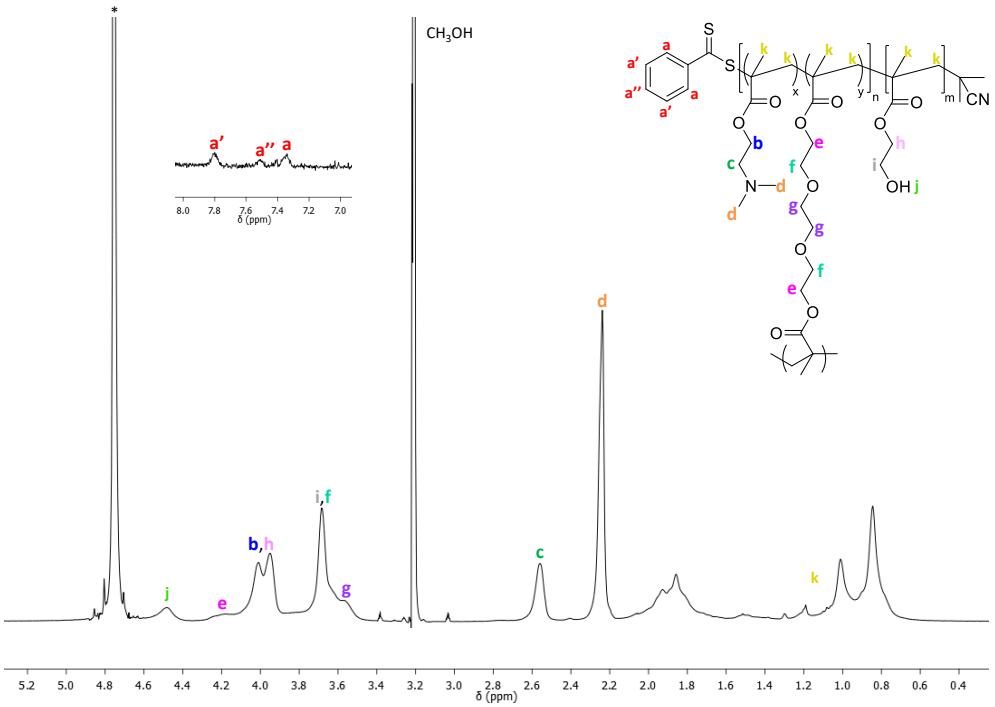

Figure 2.11 ^{1}H NMR spectrum of the PHEMA-*b*-(DMAEMA-*co*-TEGDMA) (2.6) *denotes H_2O (400 MHz, CD_3OD).

Owing to being unable to calculate the DP of DMAEMA from the ^{1}H NMR spectrum, and in order to enable testing of the polymeric catalysts, the polymer was submitted for elemental analysis to determine the nitrogen content. Control over the process was further confirmed in the relative agreement between the nitrogen content determined by elemental analysis with the theoretical content determined based on conversion.

Using these conditions, a series of polymeric stars of different theoretical crosslinking densities (20, 15 and 10%, determined by altering the monomer feed) were synthesised in order to investigate the effect of this structural parameter on the protection of amine within the core of the star polymer. At a larger scale of 1.5 g of macro-CTA, to allow for production of sufficient polymeric catalyst for evaluation in the small scale polyurethane foam formulation involving approximately 0.5 g catalyst per foam, and increasing the reaction time to 16 hours to account for the larger scale than the initial experiments, $PHEMA_{100}$ was chain extended with DMAEMA and TEGDMA, varying the monomer feed to produce differing theoretical crosslinking densities (Table 2.3).

Polymer	Monomer Feed $[PHEMA]_0$:$[DMAEMA]_0$:$[TEGDMA]_0$	Conversion[a] (%)	$M_{n,\,theo.}$[b] (kg/mol)	Theoretical Nitrogen Content [c] (%)	Actual Nitrogen Content[d] (%)
2.7-20	1:75:15	33%	16.7	2.16	2.01
2.7-15	1:75:11	37%	15.8	2.25	2.46
2.7-10	1:75:8	38%	17.5	2.41	2.85

Table 2.3 Characterisation data for PHEMA-*b*-(DMAEMA-*co*-TEGDMA) star polymers. [a] determined by GC, [b,c] calculated based on monomer conversion (GC), and [d] determined by elemental analysis.

Analysis of the resultant polymers by ^{1}H NMR spectroscopy indicated successful incorporation of the amine, with the appearance of characteristic peaks at δ = 2.55 ppm and δ = 2.25 ppm attributed to the CH_2N and N(CH_3)$_2$ protons of DMAEMA respectively. For all three polymers (**2.7-20**, **2.7-15** and **2.7-10** with a 20, 15 and 10% theoretical crosslinking density respectively), SEC analysis revealed a shift in the RI trace to a higher molecular weight than the macro-CTA (Figure 2.12A). SEC analysis further indicated the controlled nature of the process in the relatively low dispersity values obtained. Triple-detection SEC analysis, allowing for calculation of the Mark-Houwink *a* parameter, confirmed the crosslinked nature of the stars, producing *a* values ranging from 0.33-0.38 (Table 2.4). Moreover, the *a* values are significantly smaller than that of the linear PHEMA, further confirming the crosslinked nature of the polymeric stars. Additionally, all polymeric stars were found to exhibit an intrinsic viscosity lower than the linear polymer, consistent with the smaller size of the polymeric stars when compared to the macro-CTA (Figure 2.12B). To ensure that the TEGDMA was the source of crosslinking, a linear analogue PHEMA-*b*-DMAEMA was synthesised. Triple-detection SEC analysis on the linear polymer yielded an *a* value of 0.48, greater than the crosslinked polymer and in good agreement with the expected value for a linear polymer in a theta solvent (*a* = 0.50), further confirming the crosslinked character of the polymers.

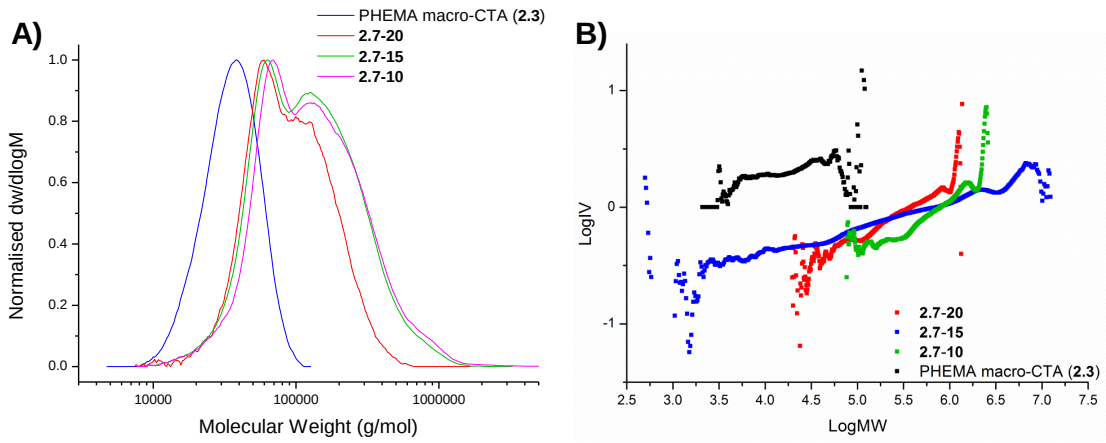

Figure 2.12 SEC analysis of polymers 2.7-20, 2.7-15 and 2.7-10. (A) molecular weight distributions of star polymers - in relation to the parent macro-CTA, and (B) triple-detection SEC Mark-Houwink curves for the polymeric stars and linear macro-CTA. (DMF, PMMA standards).

Polymer	$M_{n,\,SEC}$ (kg/mol)	$Đ_M$	*a*
2.7-20	71.4	1.49	0.40
2.7-15	84.0	1.76	0.25
2.7-10	88.4	2.04	0.38

Table 2.4 SEC Characterisation data for PHEMA-*b*-(DMAEMA-*co*-TEGDMA) star polymers of varying crosslinking density. (DMF, PMMA standards)

Star polymer size was analysed using Dynamic Light Scattering (DLS) analysis by direct dissolution of the polymers in methanol (2 mg/mL) at 25 °C. All polymers were found to be similar in size, with hydrodynamic diameters (D_h) ranging from 8 nm to 10 nm (Figure 2.13). Analysis by intensity also indicated the presence of larger entities of approximately 40 nm. In order to identify these species, the polymers were examined by Transmission Electron Microscopy (TEM) analysis using graphene oxide (GO) supported TEM grids, found to produce higher contrast images without staining.[27] TEM analysis revealed a star size in relatively good agreement, though slightly smaller, with that produced by DLS analysis (Figure 2.14). This size difference was attributed to the dehydration of the HEMA shell resulting in poor contrast between the shell and the GO grid. Moreover, TEM analysis identified the presence of larger species, likely produced through agglomeration of crosslinked polymer chains during star formation, and which were observed by DLS analysis in the volume and intensity traces.

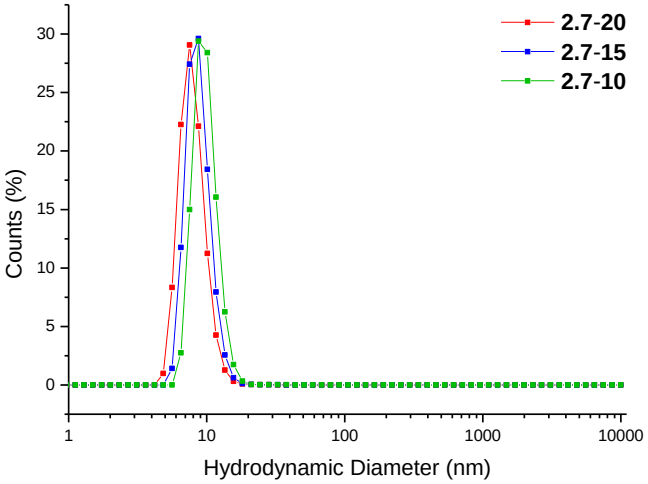

Figure 2.13 Size distributions and corresponding hydrodynamic diameters, by number, of PHEMA-*b*-(DMAEMA-*co*-TEGDMA) star polymers of varying crosslinking densities, obtained by DLS (detection angle = 173 °) at 2 mg/mL carried out in methanol at 25 °C (Dispersity, PD, given in brackets).

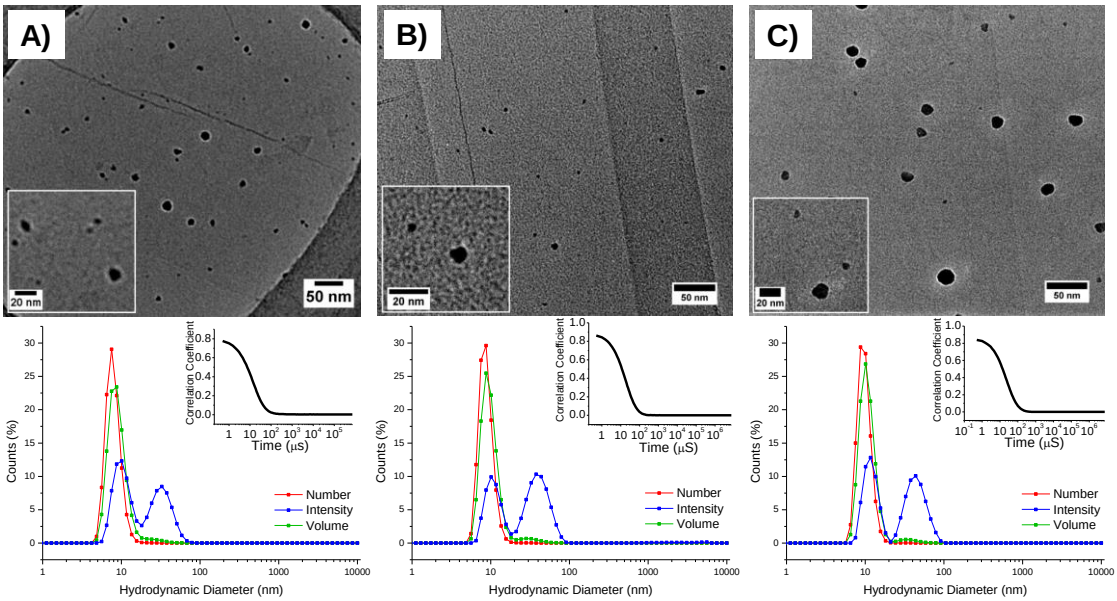

Figure 2.14 Representative TEM images and size distributions (inset - correlation function) determined by DLS (2 mg/mL in methanol) of polymers 2.7-20 (A), 2.7-15 (B), and 2.7-10 (C).

The star polymers were further characterised using Small-Angle X-ray Scattering (SAXS) analysis. Polymers were analysed in methanol, at 25 °C, with attempts made to analyse the samples in the formulation polyol found to be unsuccessful, likely as a result of the high viscosity of the polyol preventing accurate fitting of the results. Analysis of the Guinier-Porod plots *via* fitting of the graphs using the NIST models enables determination of the radius of gyration (R_g), determined from the gradient of the Guinier-Porod plot, where the gradient is equal to $-R_g^3/3$. Furthermore, analysis of the Guinier-Porod plot allows for determination of the dimension parameter, *s*, from the gradient of the slope (Table 2.5, Figure 2.15 *left*), with a sphere having a dimension parameter of $s = 0$. As can be seen in Table 2.5, the polymers were found to have dimension parameter close to those of spheres, with values ranging from 0.04 to 0.13. The Guinier-Porod plots did not fit the model for spherical micelles, nor did the fractal model in which aggregates are built based on spherical building blocks.[28] The best fit was found to be the Debye model, a model based on centro-symmetric particles with translation and rotational symmetry; in broad terms this model represents a polymer coil. The fit of a polymer coil was rationalised to be as a consequence of the high degree of solvation for HEMA arms.[29]

Polymer	Guinier-Porod Fit		R_h (nm)	Shape Factor, ρ R_g/R_h
	R_g (nm)	s		
2.70-20	5.5 ± 0.10	0.13	4.0	1.38
2.70-15	7.1 ± 0.10	0.04	4.5	1.58
2.70-10	6.9 ± 0.03	0.11	5.0	1.39

Table 2.5 Combined SAXS (Guinier-Porod Fit data) and DLS analysis (R_h for polymers 2.7-20, 2.7-15 and 2.7-10, both in methanol at 25 °C.

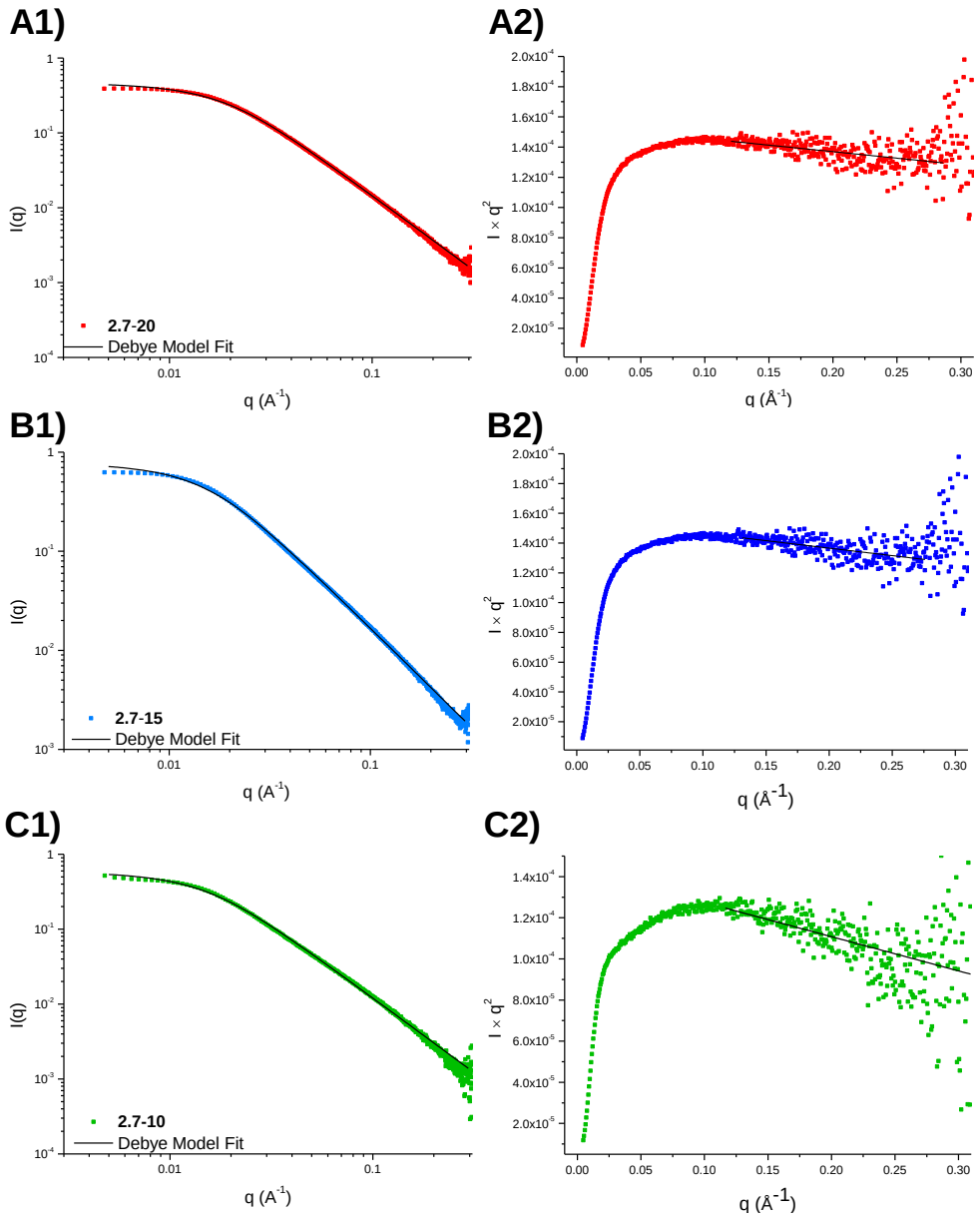

Figure 2.15 SAXS analysis for PHEMA-*b*-(DMAEMA-*co*-TEGDMA) star polymers carried out at 25 °C in methanol. (Left) Guinier-Porod plots for polymers with different crosslinking densities 2.7-20 (A1), 2.7-15 (B1) and 2.7-10 (C1). (Right) Kratky plots for polymers with different crosslinking densities 2.7-20 (A2), 2.7-15 (B2) and 2.7-10 (C2), with the linear fit of the asymptote.

Further analysis was carried out using the Kratky plot, which emphasises the morphological difference between, for example, a crosslinked polymer and a linear polymer chain.[30] Analysis of the Kratky plots clearly shows two major features (Figure 2.15, *right*). Firstly, the graph tends towards a horizontal asymptote, indicative of a spherical structure.[28] Secondly, the horizontal asymptote is approached from above, characteristic of a branched

polymer or network. Combining the Guinier-Porod plots and Kratky analyses, a polymer structure of spherical, crosslinked particles is obtained, with the polymer coil attributable to the highly solvated HEMA arms. Combination of the R_g value from SAXS analysis with the hydrodynamic radius (R_h) generated from the DLS analysis allows for determination of the shape factor, ρ. For hard spheres, ρ = 0.775 and for a random coil ρ = 1.505.[31, 32] As noted in Table 2.5, all polymers have shape factors that are close to random coils. This mixture of character generated by the Kratky analysis and the Guinier-Porod plots, and reflected in the shape factor, can be explained by the synthesis method for the star polymers. With an arm-first approach, arms are chain extended with a crosslinker, resulting in a morphological change from linear polymer (random coil morphology) towards a crosslinked star polymer (with a structure similar to a hard sphere when a high enough crosslinking density is achieved). [33, 34] Therefore, the SAXS analysis is likely to exhibit characteristics of both structures.

2.3.3 Evaluation of amine-functionalised polymeric stars in the polyurethane foam formulation

In order to evaluate the protection afforded to the amine when tethered into the core of a non-thermoresponsive star polymer, the polymers were sent to AWE for evaluation in the rigid polyurethane foam formulation, using the Foamat® set-up introduced in Chapter 1.4.3. In order to evaluate the protection, the polymeric catalysts were compared to a blank formulation allowing for observation of any additional catalytic behaviour for the polymeric catalysts. The polymers tested, and corresponding characterisation data, are listed in Table 2.6, allowing for comparison of the effect of crosslinking density and arm length. Shorter armed polymeric stars were re-synthesised with a greater number of equivalents of DMAEMA in the monomer feed (200 eq.) in order to allow for sufficient amine content in

the longer armed star polymers, without the need to make large quantities of the longer armed stars.

Polymer	Arm DP[a]	Monomer Feed $[PHEMA]_0$:$[DMAEMA]_0$:$[TEGDMA]_0$	$M_{n,\ theo.}$[b] (kg/mol)	$M_{n,\ SEC.}$[c] (kg/mol)	$Đ_M$[c]	Nitrogen Content[d] (%)
2.7-20	100	1:75:15	16.7	71.4	1.49	2.00
2.7-15	100	1:75:11	15.8	84.0	1.76	2.45
2.7-10	100	1:75:8	17.5	88.5	2.04	2.85
2.8-20	95	1:200:40	27.6	58.0	2.13	3.45
2.8-15	95	1:200:30	27.4	72.5	2.26	3.65
2.8-10	95	1:200:20	25.6	48.6	1.54	3.44
2.9-20	238	1:200:40	57.4	135.0	1.79	2.25
2.9-15	238	1:200:30	53.4	134.7	2.17	2.06
2.9-10	238	1:200:20	52.4	115.7	1.70	2.45

Table 2.6 Characterisation data for polymers evaluated in the rigid polyurethane foam formulation. [a] determined by end-group analysis (^{1}H NMR spectroscopy, 400 MHz, CD_3OD), [b] determined by GC, [c]determined using SEC (DMF, PMMA standards), and [d] determined by elemental analysis.

2.3.3.1 Evaluating the effect of arm length

It was hypothesised that an increase in arm length of the polymeric star would result in greater protection afforded to the amine tethered to the core, owing to prevention of diffusion of the reactants to the polymer core. Evaluation of the catalysts in the rigid polyurethane foam formulation revealed that there was little effect of arm length on the rate of rise, with both arm lengths producing similar foam rise profiles (Figure 2.16), in contrast to this hypothesis. It should be noted that, owing to a problem with the Foamat® set-up, repeat data was not successfully collected for the 10% crosslinked polymers.

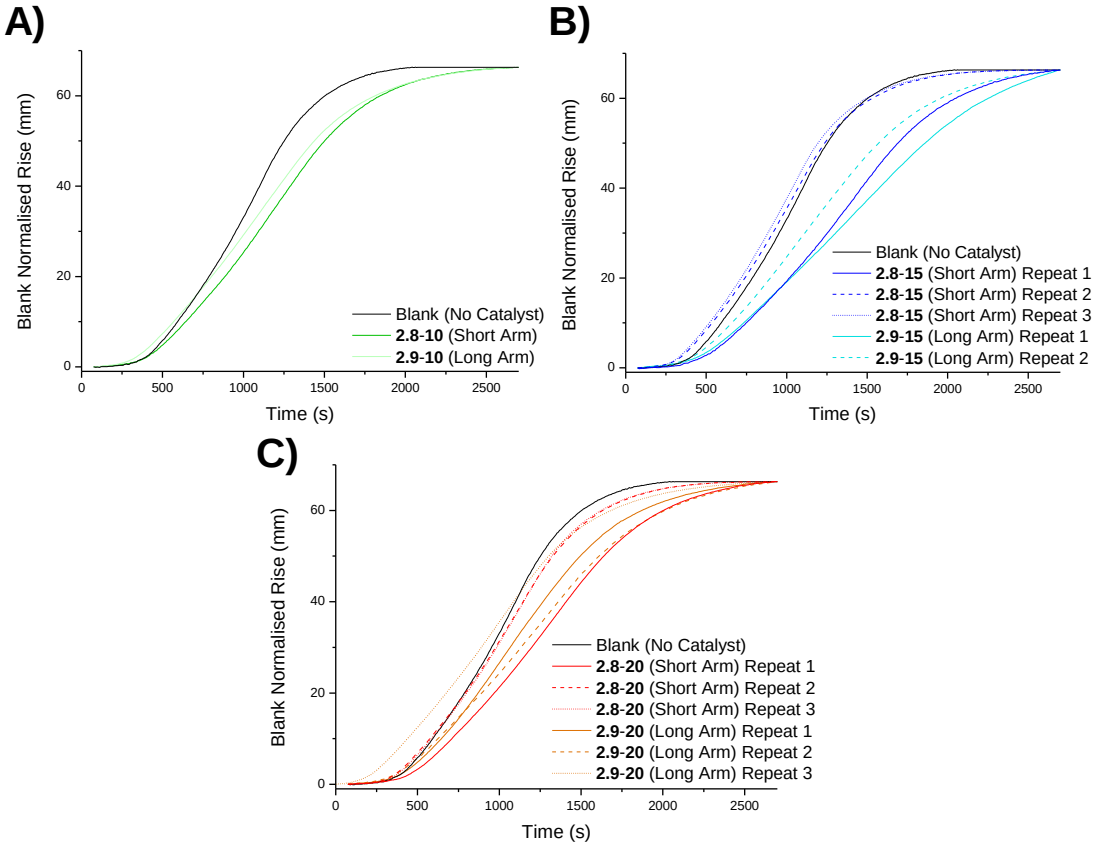

Figure 2.16 Foam rise profiles, normalised to the rise height of the blank (catalyst-free) formulation, showing the effect of arm length on the foam rise of formulations containing polymeric catalysts with (A) 10% crosslinking density, (B) 15% crosslinking density and (C) 20% crosslinking density.

Analysis of the rates of rise during constant foam growth (800-1200 seconds) further indicated little effect of arm length, with similar rates of rise to the blank profile for both the long and short armed polymeric stars (Table 2.7). The similarity in foam rise profiles and

rates of rise when compared to the blank formulation indicates that the amine was successfully shielded within the core of the polymeric star, regardless of arm length, and therefore unable to catalyse the various polyurethane reactions. The lack of an effect of catalyst arm length on catalyst protection may be attributable to the small number of lengths investigated; whilst the short arm afforded the same protection as the long arm, it may be that the short arm does not have a small enough DP for an effect to be noticeable.

Polymer	Repeat	Rate of rise (mm/sec × 10^{-2})
Blank	-	6.7
2.8-10	1	4.8
2.8-15	1	3.9
2.8-15	2	6.3
2.8-15	3	6.5
2.8-20	1	4.2
2.8-20	2	5.8
2.8-20	3	5.8
2.9-10	1	4.8
2.9-15	1	3.5
2.9-15	2	4.6
2.9-20	1	5.1
2.9-20	2	4.1
2.9-20	3	5.0

Table 2.7 Rates of foam rise for long and short-armed polymeric stars of varying crosslinking densities.

2.3.3.2 Evaluating the effect of crosslinking density

Similar to the effect of varying the polymeric star arm length, evaluation of the polymeric catalysts of differing crosslinking densities indicated little effect of crosslinking density on the protection afforded to the amine. All crosslinking densities were found to have similar rise profiles to the blank formulation (Figure 2.17), with analysis of rates during the period of constant foam growth (800-1200 seconds) confirming this result. What can be observed is

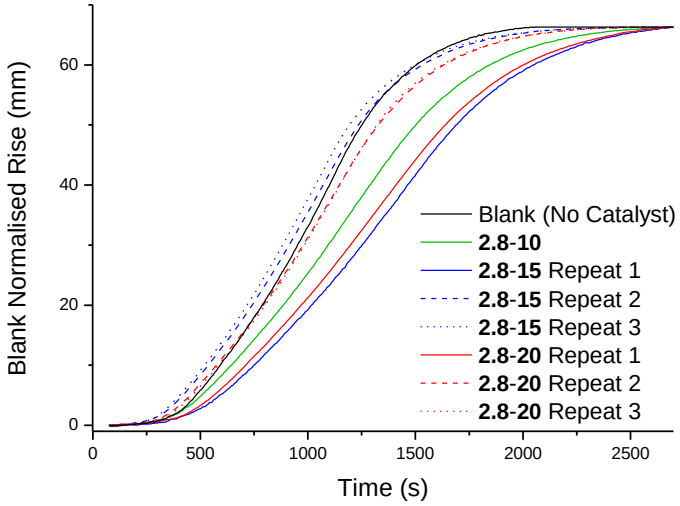

Figure 2.17 Foam rise profiles, normalised to the rise height of the blank (catalyst-free) formulation, showing the effect of crosslinking density on the foam rise of formulations containing short-armed polymeric catalysts of varying crosslinking densities.

that whilst all the rates are similar to the blank (ranging from 3.9-6.5 mm/sec × 10^{-2} compared to the blank rate of 6.7 mm/sec × 10^{-2}), there is a difference in rate of rise of between 20-40% for repeats of the same catalyst. This problem of reproducibility will be discussed later in the Chapter (section 2.3.3.4).

2.3.3.3 Evaluating the effect of amine content and core mobility

It was hypothesised that the polymeric catalysts synthesised using 75 equivalents of amine would have a less dense, and therefore more mobile, core in comparison to those synthesised using 200 equivalents of amine. This would be as a consequence of the equivalents of crosslinker added to ensure identical crosslinking densities; for the 20% crosslinked polymers, 15 equivalents of TEGDMA are added when using 75 equivalents of amine (**2.7-20**), in comparison to 40 added for the 200 equivalents of amine (**2.8-20**). As such, whilst the ratio of crosslinker:DMAEMA remains the same for both polymers, there would be more crosslinker in the 200 eq. polymers and therefore a less mobile core. This effect was studied as it is hypothesised that there may be an optimum distance between the catalytic nitrogens, and adding fewer equivalents would result in a decrease in the density of the core, potentially rendering it more mobile. Evaluation of the polymers in the formulation indicated that there

was no effect on the protection of the amine when using lower equivalents of amine and crosslinker, with rise profiles having similar shapes to the blank formulation, and with similar rates during the period of constant growth (Figure 2.18, Table 2.8).

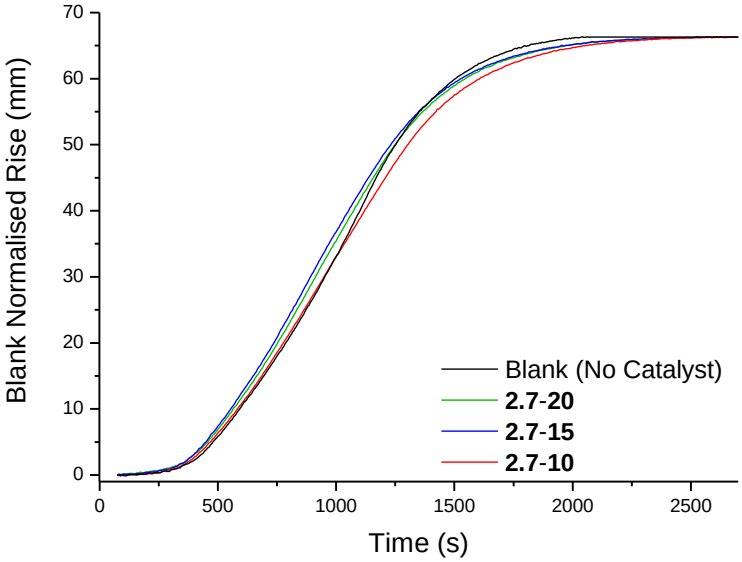

Figure 2.18 Foam rise profiles, normalised to the rise height of the blank (catalyst free) formulation, showing the effect of amine loading on the foam rise of formulations containing short-armed polymeric catalysts with varying core mobility.

Polymer	Repeat	Equivalents of DMAEMA:TEGDMA	Rate of rise (mm/sec × 10^{-2})
Blank	1	-	6.7
2.7-10	1	75:8	6.2
2.7-15	1	75:11	6.1
2.7-20	1	75:15	5.8
2.8-10	1	200:20	4.8
2.8-15	1	200:30	3.9
2.8-15	2	200:30	6.3
2.8-15	3	200:30	6.5
2.8-20	1	200:40	4.2
2.8-20	2	200:40	5.8

Table 2.8 Rates of foam rise for short-armed polymeric stars of varying crosslinking densities with different amine loadings.

2.3.3.4 Reproducibility and Repeatability

At this point, following earlier acknowledgment, it is important to mention that significant problems arose relating to the repeatability/reproducibility of the process. Indeed, the irreproducibility of the process was highlighted during a study into the reproducibility/repeatability of the foam testing process, involving a batch of new catalysts being tested at multiple times during a single foaming (reproducibility), and additional repeat tests run on the same batch of catalysts at a later time (repeatability). In order to carry out reproducibility/repeatability tests, a new batch of polymers was synthesised, producing polymeric stars with an arm DP of 165 and with a theoretical crosslinking density of 20, 15 and 10% (**2.10-20**, **2.10-15** and **2.10-10**). From the reproducibility/repeatability foam tests on these polymers, it became evident that the process was relatively irreproducible, with different rates of rise found for the same catalysts when tested at the same time. For example the 20% crosslinked polymer displayed rates which differed by just over 20% (Figure 2.19, solid red line *vs* dashed red line).

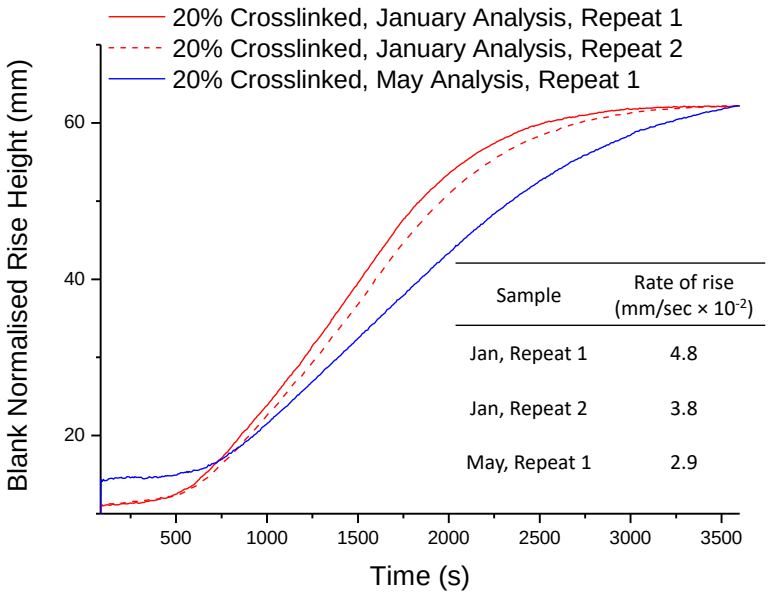

Figure 2.19 Foam rise profiles for a new batch of 20% crosslinked polymers (2.10-20), normalised to the rise height of the blank (catalyst free) formulation, highlighting the problems of reproducibility (red lines) and repeatability (red *vs* blue lines).

Whilst the rise profiles were similar in shapes, suggesting a similar water content for both runs, the difference in rates is likely to result from an alternative experimental parameter. Particle size of the catalyst (once ground up for evaluation in the formulation) was initially considered as a likely source of the discrepancy. Particle size analysis, carried out by AWE using a particle size analyser, was determined for three different samples of the ground 20% crosslinked polymers and revealed significantly different particle sizes, with a span ranging from 1.88–2.44, and a large difference between surface and volume weighted mean size (Figure 2.20). An additional source of irreproducibility was thought to relate to the method and length of mixing of the formulation prior to addition to the Foamat®, with changes made by AWE to improve on the reproducibility in this area.

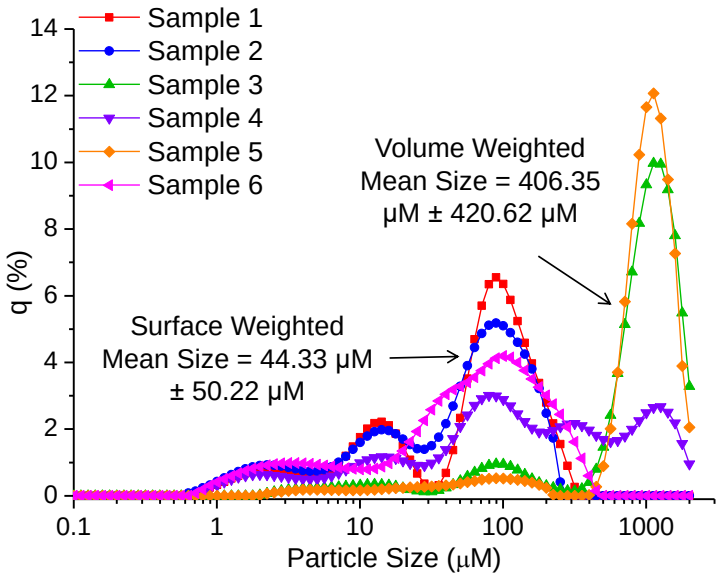

Figure 2.20 Particle size distributions for 3 samples of the same ground catalyst (2.10-20) (calculated using a particle size analyser).

The study also highlighted the irrepeatability of the process which was evident from the significant differences between tests run 4 months after the initial testing (Figure 2.19, red lines *vs* blue line). Indeed, whilst some difference in rate can be attributed to the aforementioned irreproducibility likely attributable to the catalyst particle size, such significant differences in rate of rise cannot be explained by these parameters. In a bid to investigate the irreproducibility, a series of blank tests were run to determine the error of the

blank foaming process, as this is what the formulations foamed with a catalyst are compared to. Whilst irreproducibility had been previously observed in the blank formulation (Figure 2.21), statistical analysis revealed an error of 19% for the rate of rise in the blank when foaming was carried out at 25 °C, calculated from the standard deviation of the rates of rise for all the blank samples. Moreover, a statistical analysis of the foaming process at 30 °C produced an error in the rate of raise for blank samples of 23%. Owing to the data being normalised to the blank formulation, it is likely that the irreproducibility between tests is actually a consequence of comparison to vastly different blank profiles, and therefore it is hypothesised that comparison to a more reproducible rise profile, for example that of a current commercial catalyst such as *N,N,N',N'*-tetramethyl-1,3-propanediamine (TMPDA), would likely improve the reproducibility of results.

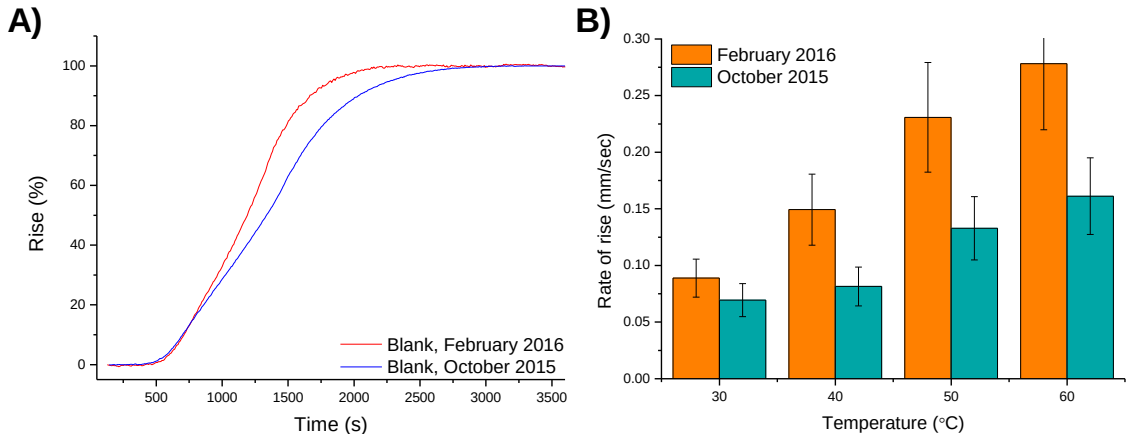

Figure 2.21 Foam rise data for blank formulations run at different temperatures in February 2016 and October 2015: (A) foam rise profiles for a blank formulation foamed at 30 °C, and (B) comparison of rates of rise for foams produced using blank formulations at different temperatures.

2.3.4 Scaling-up of star polymer synthesis

One way to improve on reproducibility/repeatability is to increase the quantity of catalyst tested allowing for the use of the advanced test container (ATC) with the Foamat®. All results reported in this Chapter (up to Figure 2.19) have been analysed in a non-temperature controlled vessel, allowing for evaluation of the polymers on a smaller scale. To allow for

evaluation in the ATC, the synthesis of both the arms and the star polymers was increased in scale to produce significantly greater quantities of polymeric catalyst.

2.3.4.1 Scaled-up synthesis of PHEMA arms

In order to scale up the synthesis of the polymeric stars, the scale of the arm synthesis was scaled 10 fold, aiming to go from producing approximately 3 g of PHEMA to 30 g. As a consequence of the foam rise results, the target DP of the PHEMA arms was kept relatively short at DP = 100. To that end, the quantity of CTA was increased from 75 mg to 300 mg, and the reaction time increased from 16 hours to 20 hours. In order to compensate for the increase in reaction time, the equivalents of AIBN were increased slightly from 0.1 to 0.12 equivalents. Owing to the large volume of DMF in the reaction mixture, precipitation was found to be unsuitable, likely as a result of re-solvation of the precipitated polymer as more reaction solution, and therefore DMF, was added. This could be overcome by precipitating into an increased volume of solvent, however, 1 litre of solvent was already being used for 8 g of polymer, and therefore an alternative purification method was used: dialysis to remove the DMF followed by precipitation. The water solubility of PHEMA homopolymers is subject to debate in the literature, with some arguing solubility below certain molecular weights (2.5 kg/mol),[35] whilst others describe it as water-swellable.[36] It was found that none of the PHEMAs synthesised were water-soluble, and so dialysis was carried out in a 50% v/v methanol and water solution. Following removal of the DMF, the polymer was dialysed against pure methanol allowing for subsequent concentration of the polymer solution under vacuum, and finally precipitation of this significantly smaller volume of polymer solution into diethyl ether.

In an initial experiment, homopolymerisation of HEMA was carried out using 300 mg of CPBD and 0.12 eq. of AIBN at 70 °C for 19 hours, reaching 94% conversion and producing 23 g of PHEMA. SEC analysis of the resultant polymer (**2.11**) revealed a narrow

monomodal peak with a low dispersity ($Đ_M$ = 1.12), confirming the absence of any back-biting reactions (Table 2.9). Whilst a narrow Gaussian distribution confirmed control over the process, it was noted that the theoretical number-average molecular weight, determined by conversion calculated by ^{1}H NMR spectroscopy, was significantly lower than the observed number-average molecular weight, based on the DP of the final polymer calculated using ^{1}H NMR spectroscopy; this discrepancy indicated some loss of control over the polymerisation process.

Polymer	Conversion[a] (%)	$M_{n,\,SEC}$[b] (kg/mol)	$Đ_M$[b]	$M_{n,\,theo.}$[c] (kg/mol)	$M_{n,\,obs.}$[d] (kg/mol)
2.11	94	24.7	1.12	16.4	23.4
2.12	85	22.2	1.17	15.4	11.9
2.13	80	17.8	1.12	13.7	10.9

Table 2.9 Characterisation data for the large scale synthesis of PHEMA homopolymers [a] determined by ^{1}H NMR spectroscopy (400 MHz, CD_3OD), [b] measured by SEC (DMF, PMMA standards), [c] theoretical molar mass calculated based on monomer conversion (^{1}H NMR spectroscopy, CD_3OD), and [d] observed molar mass calculated based on the DP of the polymer, determined by ^{1}H NMR spectroscopy.

It was hypothesised that the loss of control may be related to the high conversion of the reaction; hence the experiment was repeated with a shorter reaction time (16 hours) in order to reach a lower conversion (85%). Analysis of the resultant polymer (**2.12**) confirmed that control was maintained, with the theoretical number-average molecular weight in relatively good agreement with the observed number-average molecular weight (15.2 kg/mol *vs* 11.9 kg/mol respectively), in addition to a narrow monomodal distribution by SEC analysis ($Đ_M$ = 1.17) (Table 2.9). Moreover, retention of the end-group was confirmed by good overlap of the UV SEC trace at λ = 309 nm, with the RI trace (Figure 2.22A). Linearity

of the polymer was further confirmed using triple-detection SEC, producing a Mark-Houwink *a* parameter of 0.73 (Figure 2.22B).

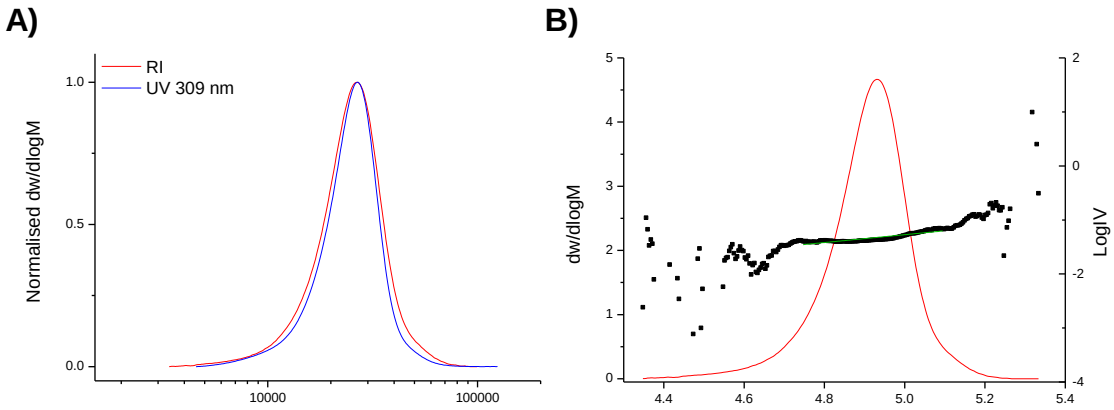

Figure 2.22 SEC analysis of PHEMA homopolymer 2.12: (A) overlay of the size exclusion chromatograms for polymer 2.10, red line generated using RI detection and the blue line generated using UV detection at λ = 309 nm, and (B) triple-detection SEC analysis of PHEMA (2.10); red line is the molecular weight distribution, black points are the Mark-Houwink plot, and the green line is the linear fit of the Mark-Houwink plot, of which the gradient is the *a* parameter (DMF, PMMA standards).

Scaling of the reaction was further increased, in order to achieve 30 g of polymer, increasing the mass of CTA to 650 mg and the reaction time to 24 hours. Using the aforementioned reaction conditions, 30.1 g of PHEMA (**2.13**) was produced maintaining reaction control, evidenced in the monomodal SEC trace and agreement in number-average molecular weights, and with good end-group retention, enabling chain extension to produce polymeric stars (Table 2.9).

2.3.4.2 Scaled-up synthesis of polymeric stars

Following successful production of PHEMA on a larger scale, the scale of chain extension to produce polymeric stars was also increased. Based on an approximation that, for a star polymer with a nitrogen content of 2.5%, the mass required for evaluation in the larger temperature controlled foam set-up is 8.6 g (2 × 4.3 g to allow for tests with and without a thermocouple), it was decided that 10 g batches of each polymer were to be targeted. Taking into consideration that the data produced from the evaluation of the polymeric catalysts in a

rigid polyurethane formulation indicated that neither arm length nor crosslinking density had an impact on amine protection, the synthesis was only scaled for polymers with a 10% crosslinking density and a short arm length (DP = 100).

To that end, 4.3 g of PHEMA macro-CTA was chain extended with DMAEMA and TEGDMA, with an increased reaction time of 24 hours and with slightly increased equivalents of AIBN (0.17 *vs* 0.1 equivalents). Following purification by precipitation into diethyl ether, analysis of the resultant polymer (**2.14**) indicated successful extension, with a clear shift in the molecular weight from the macro-CTA to the polymeric star (Figure 2.23A), and with an *a* parameter of 0.27 confirming the crosslinked nature of the polymer (Figure 2.23B). As observed in the small scale reactions, there is a slight high molecular weight shoulder indicative of star-star coupling, yet the distribution remains relatively narrow, with a dispersity of $Đ_M$ = 1.27 (Table 2.10). Similar to the smaller scale polymeric stars, analysis of the polymers by DLS revealed a hydrodynamic diameter of 9 nm. The nitrogen content of the product polymer, determined using elemental analysis, was found to be 2.89%, ensuring that the 7.4 g polymer produced was sufficient for the larger scale evaluation.

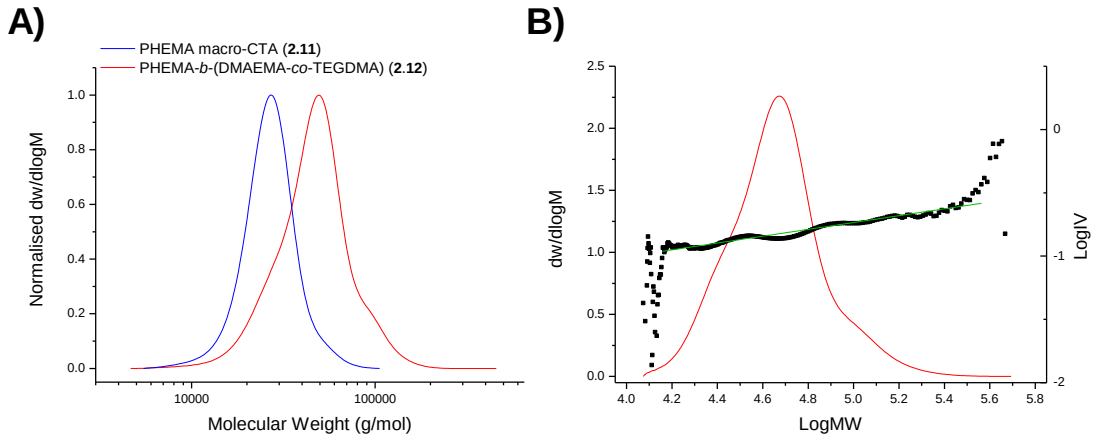

Figure 2.23 SEC analysis of PHEMA-*b*-(DMAEMA-*co*-TEGDMA) (2.14): (A) Normalised molecular weight distributions for PHEMA-*b*-(DMAEMA-*co*-TEGDMA (2.12) and the PHEMA macro-CTA (2.11), and (B) Triple-detection SEC analysis (DMF, PMMA standards). Red line is the molecular weight distribution, black points are the Mark-Houwink plot, and the green line is the linear fit of the Mark-Houwink plot, of which the gradient is the *a* parameter (DMF, PMMA standards).

Polymer	$M_{n,\,SEC}$[a] (kg/mol)	$Đ_M$[a]	a[b]	$M_{n,\,theo.}$[c] (kg/mol)	Nitrogen Content[d] (%)	D_h[e] (nm)
2.14	41.0	1.27	0.27	35.5	2.89	9
2.15	37.7	1.52	0.40	44.2	3.95	8

Table 2.10 Characterisation data for the large scale synthesis of PHEMA-*b*-(DMAEMA-*co*-TEGDMA): [a] measured by SEC (DMF, PMMA standards), [b] measured by triple detection SEC (DMF, PMMA standards),[c] theoretical molar mass calculated based on monomer conversion (GC), [d] determined by elemental analysis, CHN in duplicate, and [e] determined by DLS (3 mg/mL in methanol at 25 °C).

Despite the successful scaling, the reaction only produced enough material for a single test with and without the thermocouple. In order to enable more repeat measurements, particle synthesis was further scaled, aimed at producing 30 g of polymeric stars. Using the conditions which produced 7.4 g of product, the chain extension was repeated with an increased quantity of macro-CTA (19.5 g). Following the reaction for 24 hours and precipitation into diethyl ether, the product polymer (**2.15**) was successfully isolated as a pink solid, with a mass of 30.1 g. With a nitrogen content of 3.95 %, determined by elemental analysis, this quantity of material allows for 10 foaming experiments, therefore 5 repeats. Triple-detection SEC analysis confirmed the crosslinked nature of the star polymers, with an *a* value of 0.40 (Table 2.10), and a shift in the molecular weight of the RI trace to higher molecular weights indicated successful extension. Akin to the previous scaling experiment, the hydrodynamic radius of the polymer, as determined by DLS, was found to be 8 nm. Evaluation of these polymers as catalysts in the polyurethane formulation, in addition to their thermoresponsive behaviour, is discussed in Section 4.3.1.

2.4 Conclusion

An arm-first methodology has been successfully applied to the synthesis of polymeric stars using the RAFT polymerisation technique, producing a series of stars in which a catalytically active amine functionality is tethered into the core of the polymer. Polymeric stars have been

synthesised with varying structural parameters, such as arm length and crosslinking density, and have been fully characterised using various techniques, including triple-detection SEC, DLS and SAXS. Despite problems related to reproducibility and repeatability arising when the polymeric catalysts were evaluated in a rigid polyurethane foam formulation, analysis of the foam rise data indicated that neither crosslinking density, arm length, nor the density of the core had an impact on the shielding of the amine. Indeed, all parameters investigated produced foam rise profiles with rates of rise comparable to that of the blank formulation, indicating that the amine does not come into contact with the polyurethane formulation. Following evaluation of the polymers in the formulation, synthesis of both the PHEMA arms and the polymeric stars has been scaled up to produce sufficient quantity of material to allow for testing in the Foamat® fitted with an ATC. These scaling conditions enabled the controlled synthesis of both arms and stars, reflected in both the ^{1}H NMR spectroscopic analysis and SEC analysis and produced sufficient polymeric material for five tests with and without the thermocouple. The successful scaling allowing for the use of the ATC is highly important for enabling the introduction of a thermoresponsive crosslinker into the particles, as without it evaluation of such polymers at raised temperatures (Chapter 4) would not be possible.

2.5 Experimental

2.5.1 Materials

The following reagents were used as received: 2-hydroxyethyl methacrylate (HEMA, Sigma-Aldrich, 97%), 1,2,4-trimethoxy benzene (TMB, Sigma-Aldrich, 97%), *N,N'*-(dimethylamino) ethyl methacrylate (DMAEMA, Sigma-Aldrich, 98%), and tri(ethylene glycol) dimethacrylate (TEGDMA, Sigma-Aldrich, 99%). Inhibitor was removed by passing through a plug of basic alumina. *S,S'*-Bisdithiobenzoate was made by Dr Daniel Wright.[20] The following solvents were used as received: dimethyl

formamide (DMF, Fisher Scientific, Laboratory grade), methanol (CH_3OH, Fisher Scientific, LT grade), petroleum ether 40-60 °C (pet. ether, Fisher Scientific, LT grade), ethyl acetate (EtOAc, Fisher Scientific, LT grade) and diethyl ether (Et_2O, Sigma-Aldrich, AR grade). 2,2'-Azobis(isobutyronitrile) (AIBN) was received from Molekula, recrystallized from methanol and stored at 4 °C. Deuterated solvents and silica gel (40-63 μM) were received from Apollo Scientific.

2.5.2 Instrumentation

Nuclear Magnetic Resonance (NMR) spectra were recorded on a Bruker DRX-400 spectrometer. Chemical shifts are reported as δ in parts per million and quoted downfield from the internal standard tetramethylsilane (δ = 0 ppm). Spectral analysis was carried out using MestReNova software v.6.0.2. Gas Chromatography (GC) conversion analysis was run on a Varian 450-GC fitted with a Varian Factor Four column, with a column flow of 1.5 mL/min, nitrogen as the carrier gas, and using TMB as an internal standard. Size Exclusion Chromatography (SEC) measurements were carried out using an Agilent 390-MDS multi detector suite fitted with a viscometer, a refractive index (RI) and a light scattering (LS) detector, and equipped with a guard column (Varian PLGel) and two PLGel 5 μm mixed-D columns. The mobile phase was DMF with 5 mM NH_4BF_4 with a flow rate of 1 mL/min. All data was analysed using Cirrus v3.3 and Agilent GPC/SEC software v1 with calibration curves produced using Varian Polymer Laboratories linear PMMA standards. Dynamic Light Scattering was conducted using a Malvern Zetasizer NanoS instrument equipped with a 4 mW He-Ne 633 nm laser module at 25 °C, with data analysis using Malvern DTS 6.20 software. Measurements were carried out at a detection angle of 173° (backscattering). All determinations were made in triplicate unless otherwise stated (with 10 measurements recorded for each run). Mass spectra were recorded on an Agilent 6130B single Quad using electrospray ionisation. Infrared spectra were recorded on a Perkin Elmer Spectrum 100 FT-

IR spectrometer, neat. Transmission Electron Microscopy (TEM) solutions were made up at 2 mg/mL in methanol. TEM samples were prepared on graphene oxide (GO)-coated carbon grids (Quantifoil R2/2). Generally, a drop of sample was pipetted onto a grid and left to dry overnight. Samples were analysed with a JEOL-2100 microscope, operating at 200 keV. All TEM images were collected by Miss Maria Inam (O'Reilly Group, University of Warwick). Small-angle X-ray scattering (SAXS) analyses were carried out on the SAXS-WAXS beamline at the Australian Synchrotron facility at a photon energy of 15 keV. Samples were prepared in methanol and were run using 1.5 mm diameter quartz capillaries. The measurements were collected at 25 °C with a detector-to-sample distance of 7.160 m to give a q range of 0.0015 to 0.08 $Å^{-1}$, where q is the scattering vector and is related to the scattering angle (2θ) and the photon wavelength (λ) by the following equation:

$$q = \frac{4\pi \sin(\theta)}{\lambda}$$

All patterns were normalised to fixed transmitted flux using a quantitative beam stop detector. The scattering from a blank (methanol) was measured in the same location as the sample collection and was subtracted for each measurement. The two-dimensional SAXS images were converted into one-dimensional SAXS profiles (I(q) *vs* q) by circular averaging, where I(q) is the scattering intensity. ScatterBrain and NCNR Data Analysis IGOR PRO software were used to plot and analyse SAXS data.[37] The scattering length density of the solvents and monomers were calculated using the "Scattering Length Density Calculator" provided by NIST Centre for Neutron Research. All SAXS data was collected and analysed by Dr Anaïs Pitto-Barry (O'Reilly Group, University of Warwick). Elemental analysis was performed in duplicate by Warwick Analytical Services. Catalyst particle size analysis and foam rise analysis was performed by Dr Anna Markowska at AWE (Aldermaston, UK).

2.5.3 Synthetic Methods and Procedures

Synthesis of 2-cyano-2-propyl benzodithioate (CPBD)

The synthesis of CPBD was based on a procedure previously developed by the group.[20] To a stirring solution of *S,S'*-bis(dithiobenzoate) (13.1 mmol, 1.0 eq.) in EtOAc (300 mL), AIBN (19.5 mmol, 1.5 eq.) was added and the flask degassed by purging with nitrogen. The solution was refluxed for 24 hours, the solvent evaporated under vacuum, and the resulting solution purified by column chromatography (silica gel, 98:2 pet. ether/EtOAc) affording a viscous pink oil (3.6 g, 62%). R_f (98:2 pet. ether/EtOAc): 0.19. ^{1}H NMR (400 MHz, CD_3OD): δ (ppm) 7.83 (appt. d, 2H, *ortho*-Ar*H*, appt. $^3J_{H\text{-}H}$ = 7.7 Hz), 7.51 (appt. t, 1H, *para*-Ar*H*, appt. $^3J_{H\text{-}H}$ = 7.5 Hz), 7.34 (appt. t, 2H, *meta*-Ar*H*, appt. $^3J_{H\text{-}H}$ = 7.5 Hz), 1.85 (s, 6H, (C*H*$_3$)$_2$). ^{13}C NMR (100 MHz, CD_3OD): δ (ppm) 146.6, 136.2, 130.3, 127.7 (Ar*C*), 121.1 (*C*N), 43.2 (*C*(CN)), 26.6 ((*C*H$_3$)$_2$). IR (neat) max/cm^{-1}: 3060 ($\upsilon_{Ar\text{-}H}$), 2980 ($\upsilon_{C\text{-}H}$), 2230 ($\upsilon_{C\equiv N}$), 1050 ($\upsilon_{C=S}$). *m/z* [ESI MS]: 243.7 (M+Na)

Typical procedure for the synthesis of PHEMA (**2.3**)

CPBD (1.5 g, 1 eq.) and HEMA (100 eq.) were dissolved in DMF (2.5 mL) with radical initiator AIBN (0.1 eq.). Following four freeze-pump-thaw cycles, the ampoule was refilled with nitrogen and the solution heated to 70 °C for 24 hours (97% conversion). The reaction was quenched in liquid nitrogen and purified by precipitation in Et_2O until vinyl signals were no longer observed in the ^{1}H NMR spectrum, affording a light pink solid (0.37 g, 48%). ^{1}H NMR (400 MHz,CD_3OD): δ (ppm) 7.91 (br s, 2H, *ortho*-Ar*H)*, 7.52 (br s,1H, *para*-Ar*H*), 7.37 (br s, 2H, *meta*-Ar*H*), 4.05 (br s, OC*H*$_2$CH$_2$), 3.79 (br s, OCH$_2$C*H*$_2$), 2.20-0.87 (m, C*H*$_2$C*H*$_3$ backbone). ^{13}C NMR (100 MHz, CD_3OD): δ (ppm) 178.3 (*C*=O), 66.4 (O*C*CO), 59.4 (OC*C*O), 46.8 (C(CH$_3$)*C*H$_2$), 18.4 (C(*C*H$_3$)). IR (neat) max/cm^{-1}: 3435 (υ_{OH}), 2961 ($\upsilon_{C\text{-}H}$), 1725 ($\upsilon_{C=O}$), 1157 ($\upsilon_{C\text{-}O}$). $M_{w,\,SEC}$ = 16.5 kg/mol, $M_{n,\,SEC}$ = 14.5 kg/mol $Đ_M$ = 1.14.

Typical procedure for the chain extension of PHEMA with DMAEMA and TEGDMA to produce PHEMA-*b*-(DMAEMA-*co*-TEGDMA) (**2.7-20**, **2.7-15**, **2.7-10, 2.8-20**, **2.8-15**, **2.8-10, 2.9-20**, **2.9-15**, and **2.9-10**)

PHEMA macro-CTA (1 eq., 1.5 g), DMAEMA (200 eq.), and TEGDMA (40 eq.) were dissolved in DMF (5 mL) together with the radical initiator AIBN (0.1 eq.) and the GC standard TMB. The solution was degassed by purging with nitrogen and the mixture heated for 16 hours at 70 °C (64% conversion). The reaction was quenched by immersion in liquid nitrogen and purified by precipitation into Et_2O three times, affording a pink-orange solid (1.70 g, 85%). ^{1}H NMR (400 MHz, CD_3OD): δ (ppm) 7.90 (br s, 2H, *ortho*-Ar*H)*, 7.57 (br s, 1H, *para*-Ar*H*), 7.35 (br s, 2H, *meta*-Ar*H*), 4.44 (br s, CH_2OH), 4.21-3.93 (m, $C(O)OCH_2CH_2$, CH_2CH_2N, CH_2CH_2OH), 3.77-3.50 (m, $C(O)OCH_2CH_2$, $OCH_2CH_2OCH_2CH_2O$, CH_2CH_2OH), 2.55 (br s, CH_2CH_2N), 2.25 (br s, $N(CH_3)_2$), 2.17-0.69 (m, CH_2CH_3 backbone).^{13}C NMR (100 MHz, CD_3OD): δ (ppm) 178.3 (*C*=O), 66.3 (O*C*CO), 62.5 (O*C*CN), 59.7 (OC*C*O), 56.7 (OC*C*N), 45.0 ($C(CH_3)CH_2$), 44.6 ($N(CH_3)_2$), 18.4 ($C(CH_3)$). IR (neat) max/cm^{-1}: 3454 (υ_{OH}), 2962 (υ_{C-H}), 2786 (υ_{N-CH_3}), 1725 ($\upsilon_{C=O}$), 1153 (υ_{C-O}). $M_{w,\ SEC}$ = 106.2 kg/mol, $M_{n,\ SEC}$ = 71.4 kg/mol, $Đ_M$ = 1.49. Anal. Calcd. For PHEMA-*b*-(DMAEMA-*co*-TEGDMA): C 55.27; H 8.06; N 2.01%. Found: C 55.9; H 8.05; N 2.0%.

Synthesis of PHEMA-*b*-(DMEAMA)

PHEMA macro-CTA (200 mg, 1 eq.) and DMAEMA (200 eq.) were dissolved in DMF (2 mL) with radical initiator AIBN (0.2 eq.). Following four freeze-pump-thaw cycles the ampoule was refilled with nitrogen and the solution heated to 60 °C for 6 hours. Following quenching of the reaction with liquid nitrogen (55% conversion), the polymer was purified

by precipitation in Et_2O until no vinyl signals were observed in the ^1H NMR spectrum, affording a pale pink solid. ^1H NMR (400 MHz, CD_3OD): δ (ppm) 7.92 (br s, *ortho*-Ar*H)*, 7.62 (br s, *para*-Ar*H*), 7.46 (br s, *meta*-Ar*H*), 4.13-4.07 (m, CH_2CH_2N, CH_2CH_2OH), 3.80 (br s, CH_2CH_2OH), 2.67 (br s, CH_2CH_2N), 2.37 (br s, N(CH_3)$_2$), 2.05-0.96 (m, CH_2CH_3 backbone). $M_{w,\,SEC}$ = 41.3 kg/mol, $M_{n,\,SEC}$ = 35.3 kg/mol, $Đ_M$ = 1.17.

Typical procedure for the large scale PHEMA macro-CTA synthesis (**2.11**):

CPBD (1 eq., 650 mg) and HEMA (100 eq.) were dissolved in DMF (90 mL) with radical initiator AIBN (0.12 eq.). Following degassing by purging with nitrogen, the solution was heated to 70 °C for 24 hours (80% conversion). The reaction was quenched in liquid nitrogen and purified by dialysis in 1:1 CH_3OH:H_2O, followed by dialysis in H_2O and subsequent concentration of polymer solution under vacuum. Precipitation into Et_2O afforded a pink-orange solid. ^1H NMR (400 MHz, CD_3OD): δ (ppm) 7.91 (br s, 2H, *ortho*-Ar*H)*, 7.61 (br s, 1H, *para*-Ar*H*), 7.45 (br s, 2H, *meta*-Ar*H*), 4.07 (br s, OCH_2CH_2), 3.81 (br s, OCH_2CH_2), 2.06-0.77 (m, CH_2CH_3 backbone). ^{13}C NMR (100 MHz, CD_3OD): δ (ppm) 178.3 (*C*=O), 66.4 (O*C*CO), 59.4 (OC*C*O), 44.7 (C(CH$_3$)*C*H$_2$), 16.2 (C(*C*H$_3$)). IR (neat) max/cm^{-1}: 3426 (υ_{OH}), 2957 (υ_{C-H}), 1723 ($\upsilon_{C=O}$), 1158 (υ_{C-O}). $M_{w,\,SEC}$ = 19.9 kg/mol $M_{n,\,SEC}$ = 17.8 kg/mol, $Đ_M$ = 1.12.

Typical procedure for the large scale chain extension of PHEMA with DMAEMA and TEGDMA (**2.12**)

PHEMA macro-CTA (1 eq., 19.5 g), DMAEMA (200 eq.), and TEGDMA (40 eq.) were dissolved in DMF (120 mL) together with the radical initiator AIBN (0.17 eq.) and the GC standard TMB. The solution was degassed by purging with nitrogen and the mixture heated

for 16 hours at 70 °C (66% conversion). The reaction was quenched by immersion in liquid nitrogen and purified by precipitation into Et_2O three times, affording an orange-pink solid. ^{1}H NMR (400 MHz, CD_3OD): δ (ppm) 7.91 (br s, 2H, *ortho*-Ar*H)*, 7.54 (br s, 1H, *para*-Ar*H*), 7.47 (br s, 2H, *meta*-Ar*H*), 4.31-4.07 (m, C(O)OCH_2CH_2, CH_2CH_2N, CH_2CH_2OH), 3.80-3.67 (m, C(O)OCH$_2$CH_2, OCH$_2$CH$_2$OCH_2CH_2O, CH$_2$CH_2OH), 2.66 (br s, CH$_2$CH_2N), 2.40 (br s, N(CH_3)$_2$), 2.18-0.96 (m, CH_2CH_3 backbone).). ^{13}C NMR (100 MHz, CD_3OD): δ (ppm) 178.3 (*C*=O), 66.4 (O*C*CO), 62.6 (O*C*CN), 59.4 (OC*C*O), 56.7 (OC*C*N), 46.8 (C(CH$_3$)*C*H$_2$), 44.7 (N(*C*H$_3$)$_2$), 18.4 (C(*C*H$_3$)). IR (neat) max/cm^{-1}: 3455 (υ_{OH}), 2949 ($\upsilon_{C\text{-}H}$), 2774 ($\upsilon_{N\text{-}CH_3}$), 1725 ($\upsilon_{C=O}$), 1148 ($\upsilon_{C\text{-}O}$). $M_{w,\ SEC}$ = 57.3 kg/mol, $M_{n,\ SEC}$ = 37.7 kg/mol, $Đ_M$ = 1.52. Anal. Calcd. For PHEMA-*b*-(DMAEMA-*co*-TEGDMA): C 55.68; H 8.43; N 4.46%. Found: C 55.78; H 8.59; N 4.38%.

2.6 Bibliography

1. Boyer, C., Stenzel, M. H., Davis, T. P., *J. Polym. Sci., Part A: Polym. Chem.*, **2011**, 49, 551.
2. Matyjaszewski, K., Tsarevsky, N. V., *Nature Chem.*, **2009**, 1, 276.
3. Matyjaszewski, K., Davis, T. P., *Handbook of Radical Polymerization*, Wiley-VCH Verlag GmbH & Co. KGaA, **2002**.
4. Gao, H., Matyjaszewski, K., *Prog. Polym. Sci.*, **2009**, 34, 317.
5. Wu, W., Wang, W., Li, J., *Prog. Polym. Sci.*, **2015**, 46, 55.
6. Lapienis, G., *Prog. Polym. Sci.*, **2009**, 34, 852.
7. Jeong, B., Choi, Y. K., Bae, Y. H., Zentner, G., Kim, S. W., *J. Control. Release*, **1999**, 62, 109.
8. Qiu, L., Bae, Y., *Pharm. Res.*, **2006**, 23, 1.
9. Whittell, G. R., Hager, M. D., Schubert, U. S., Manners, I., *Nature Mater.*, **2011**, 10, 176.
10. Forman, D. C., Wieberger, F., Gröschel, A., Müller, A. H. E., Schmidt, H.-W., Ober, C. K. *Advances in Resist Materials and Processing Technology XXVII*, 2010.
11. Lu, A., O'Reilly, R. K., *Curr. Opin. Biotechnol.*, **2013**, 24, 639.
12. Lu, J., Toy, P. H., *Chem. Rev.*, **2009**, 109, 815.
13. Helms, B., Guillaudeu, S. J., Xie, Y., McMurdo, M., Hawker, C. J., Frechet, J. M. J., *Angew. Chem. Int. Ed.*, **2005**, 44, 6384.
14. Terashima, T., Kamigaito, M., Baek, K.-Y., Ando, T., Sawamoto, M., *J. Am. Chem. Soc.*, **2003**, 125, 5288.
15. Terashima, T., Nomura, A., Ito, M., Ouchi, M., Sawamoto, M., *Angew. Chem., Int. Ed.*, **2011**, 50, 7892.

16. Terashima, T., Nomura, A., Ouchi, M., Sawamoto, M., *Macromol. Rapid Commun.*, **2012**, 33, 833.
17. Harper, C. A., Petrie, E. M., *Plastics Materials and Processes: A Concise Encyclopedia*, Wiley-VCH Verlag GmbH & Co. KGaA, **2003**.
18. Florio, J. J., Miller, D. J., *Handbook Of Coating Additives*, Taylor & Francis, **2004**.
19. Cotanda Santapau, M. J., Amino-containing polymers for catalysis using RAFT polymerisation, PhD Thesis, University of Warwick, 2012.
20. Wright, D. B., The synthesis and characterisation of pH-responsive polymers, understanding their self-assembly and their development as ashless detergents, PhD Thesis, University of Warwick, 2015.
21. Zeng, W., Du, Y., Xue, Y., Frisch, H. L., Mark–Houwink–Staudinger–Sakurada Constants, *Physical Properties of Polymers Handbook*, Springer New York, **2007**.
22. Hiemenz, P. C., Lodge, T. P., *Polymer Chemistry, Second Edition*, Taylor & Francis, **2007**.
23. James, A. B., David, M. H., Becer, C. R., Synthesis and SEC Characterization of Poly(methyl methacrylate) Star Polymers, *Progress in Controlled Radical Polymerization: Materials and Applications*, American Chemical Society, **2012**.
24. Radke, W., Chromatography of Polymers, *Macromolecular Engineering*, Wiley-VCH Verlag GmbH & Co. KGaA, **2007**.
25. Brandrup, J., Immergut, E. H., Grulke, E. A., *Polymer Handbook*, 4th ed.; Wiley-VCH Verlag GmbH & Co. KGaA, **1999**.
26. Barner-Kowollik, C., *Handbook of RAFT Polymerization*, Wiley-VCH Verlag GmbH & Co. KGaA, **2008**.
27. Patterson, J. P., Sanchez, A. M., Petzetakis, N., Smart, T. P., Epps III, T. H., Portman, I., Wilson, N. R., O'Reilly, R. K., *Soft Matter,* **2012**, 8, 3322.
28. Teixeira, J., *J. Appl. Crystallogr.*, **1988**, 21, 781.
29. Lee, J. M., Subramani, S., Lee, Y. S., Kim, J. H., *Macromol. Res.*, **2005**, 13, 427.
30. Moatsou, D., Li, J., Ranji, A., Pitto-Barry, A., Ntai, I., Jewett, M. C., O'Reilly, R. K., *Bioconjugate Chem.*, **2015**, 26, 1890.
31. Patterson, J. P., Robin, M. P., Chassenieux, C., Colombani, O., O'Reilly, R. K., *Chem. Soc. Rev.*, **2014**, 43, 2412.
32. Schärtl, W., *Light Scattering from Polymer Solutions and Nanoparticle Dispersions*, Springer Berlin Heidelberg, **2007**.
33. Blencowe, A., Tan, J. F., Goh, T. K., Qiao, G. G., *Polymer*, **2009**, 50, 5.
34. Burchard, W., Solution Properties of Branched Macromolecules, *Branched Polymers II*, Springer Berlin Heidelberg, **1999**.
35. Paterson, S. M., Brown, D. H., Chirila, T. V., Keen, I., Whittaker, A. K., Baker, M. V., *J. Polym. Sci., Part A: Polym. Chem.*, **2010**, 48, 4084.
36. Weaver, J. V. M., Bannister, I., Robinson, K. L., Bories-Azeau, X., Armes, S. P., Smallridge, M., McKenna, P., *Macromolecules*, **2004**, 37, 2395.
37. Kline, S., *J. Appl. Crystallogr.*, **2006**, 39, 895.

3. The Hydrolytic Behaviour of *N,N'*-(dimethylamino)ethyl acrylate Functionalised Polymeric Stars Towards Modelling Amine Protection for the Analogous Methacrylate Polymeric Stars

3.1 Abstract

In this Chapter, the arm-first synthesis of polymeric stars, first introduced in Chapter 2, was extended to the synthesis of acrylate based polymeric stars with a view to modelling the effect of different structural parameters on the shielding of the amine. To that end, well-defined *N,N'*-(dimethylamino)ethyl acrylate (DMAEA) functionalised polymeric stars have been synthesised utilising Reversible Addition-Fragmentation Chain Transfer (RAFT) polymerisation. Linear homopolymers of poly(ethylene glycol) methyl ether acrylate (PEGA) and 2-hydroxyethyl acrylate (PHEA) were chain extended with DMAEA and a divinyl crosslinker, di(ethylene glycol) diacrylate (DEGDA), to produce a series of crosslinked polymeric stars, which have been characterised using a range of techniques. The hydrolytic susceptibility of DMAEA, whereby acrylic acid and the small molecule *N,N'*-dimethylaminoethanol (DMAE) are produced, was intended to act as a model enabling investigation of structural parameters on the protection afforded to the amine when tethered into the core of the star, without the necessity of evaluation in the irreproducible foam set-up reported in Chapter 2. The hydrolytic behaviour of the DMAEA was investigated by ^{1}H Nuclear Magnetic Resonance (NMR) spectroscopy and was found to be strongly dependent on temperature. At elevated temperature either a higher crosslinking density or a longer arm length was found to offer greater protection to the amine resulting in slower hydrolysis, with hydrolysis found to level off at a lower final percentage of hydrolysis with greater crosslinking density and increased arm length. In contrast, the composition and nature of the arm was found to have little impact on the hydrolysis, with the same trends relating to the effect of temperature and crosslinking density observed with a linear (PHEA) and a brush (PEGA) arm. Additionally, the diffusion based release of DMAE from the polymeric stars was successfully confirmed through the use of an enzymatic assay, producing a concentration of DMAE in good agreement with the theoretical concentration based on the ^{1}H NMR spectroscopic analysis.

3.2 Introduction

Numerous studies report the formation of well-defined polymeric stars through the use of controlled radical polymerisation (CRP) techniques, including Reversible Addition-Fragmentation Chain Transfer (RAFT) polymerisation.[1-6] A structurally well-defined star polymer has one defined branching point, or core, from which multiple arms extend, and thus exhibit a globular shape and, commonly, a core-shell microstructure.[7-9] As introduced in section 1.3.4, star polymers can be synthesised through both a core-first and an arm first method, with the former producing stars with a well-defined number of arms, and the latter allowing for a larger number of arms per star without the need to use complex syntheses to produce a multifunctional initiator. Due to the defined nature of their structure and associated properties (for example core density and arm length), there is a large number of applications for polymeric stars that range from drug delivery to nanoelectronics.[10-15] Through varying the size, crosslinking density and arm composition, the physical properties of the stars can be tailored for various applications.[16]

The hydrolysis of an ester bond is one of the most fundamental reactions in organic chemistry.[17] It is generally accepted that ester hydrolysis proceeds *via* one of 8 mechanisms proposed by Ingold,[18, 19] through either acid catalysed or base catalysed mechanisms, to produce the parent carboxylic acid and an alcohol (Scheme 3.1),[20] though proposed mechanisms for neutral ester hydrolysis have also been reported.[21-24]

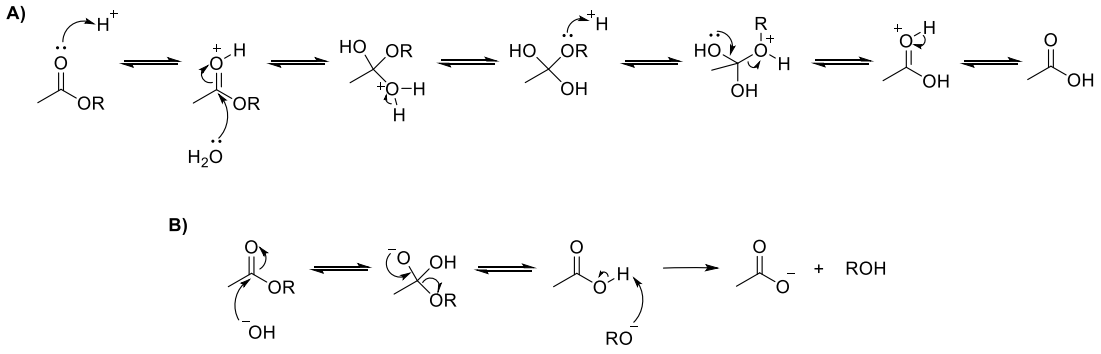

Scheme 3.1 Schematic representation for the mechanisms of ester hydrolysis: (A) acid catalysed and (B) base catalysed.

Owing to the reversibility of the acid catalysed ester hydrolysis (Scheme 3.1A), an excess of water is required to force the equilibrium to the carboxylic acid product, in contrast to the base catalysed reaction (Scheme 3.1B) where irreversible deprotonation of the carboxylic acid product renders the reaction irreversible. The hydrolysis of ester linkages has been widely exploited in the synthesis of degradable polymers, with the majority of the work focused on hydrolysing the polymer backbone (Scheme 3.2A).[25-28] Backbone hydrolysis enables degradation of the polymer into smaller molecular weight oligomers each maintaining functionalities that have been initially tethered to the backbone. One such method of incorporating the degradable ester linkages is the radical Ring-Opening polymerisation (rROP) of cyclic ketene acetal based monomers, which allows for the production of degradable polyesters.[29, 30] Indeed, work by Hedir *et al.* used the copolymerisation of 2-methylene-1,3-dioxepane with a functionalised hydrophilic vinyl monomer, vinyl bromobutanoate, to produce copolymers with tuneable incorporations of ester repeat units, therefore allowing for control over the polymer degradability.[31]

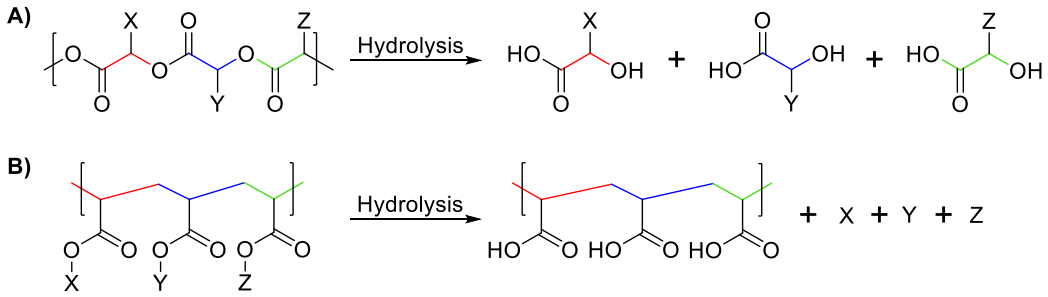

Scheme 3.2 Schematic representation of ester hydrolysis (A) in the polymer backbone and (B) of pendent functionalities.

In contrast, relatively little work has been reported on the hydrolytic behaviour of pendent ester functionalities, especially for either acrylate or methacrylate based materials (Scheme 3.2B). Here, following hydrolysis, the polymer backbone remains intact with the release of the pendent functionalities. Despite the relatively limited literature available, it is still widely accepted that methacrylate-based polymers are significantly more stable to

hydrolysis than their acrylate-based equivalents,[32-34] proposed to be as a result of the increased hydrophobicity of the methacrylate backbone preventing water from reaching the ester linkage.[35] Indeed, van de Wetering *et al.* demonstrated the increased reactivity of the acrylate *vs* the methacrylate in their study into the hydrolytic stability of *N,N'*-(dimethylamino)ethyl methacrylate (DMAEMA). Comparing both the monomeric acrylate, methacrylate and polymeric equivalents, it was shown that polymerisation increased the hydrolytic stability of both monomers (at pH = 1 and 37 °C), with the poly(methacrylates) found to be one hundred times more stable than their monomers, and the poly(acrylates) ten times more stable. Additionally, in comparing the acrylates to methacrylates, the hydrolysis rate of the poly(acrylate) was found to be three times faster than the poly(methacrylate). Recently, Monteiro *et al.* carried out an in-depth study into the self-catalysed hydrolysis of linear homopolymers of the amino-functionalised monomer *N,N'*-(dimethylamino)ethyl acrylate (DMAEA) (Scheme 3.3).[36] The self-catalysed nature of the hydrolysis, in which the rate of catalysis is further accelerated by the carboxylic acid by-product, forms poly(acrylic acid) and a small molecule of *N,N'*-dimethylaminoethanol (DMAE). The rate of hydrolysis was found to be independent of both the pH of the solution as well as the molecular weight of the polymer, confirming the self-catalysed nature of the process.

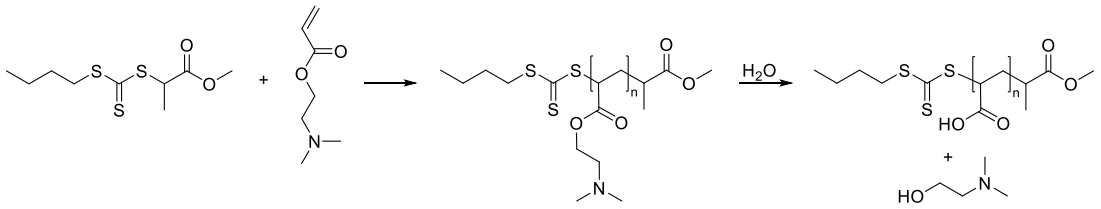

Scheme 3.3 Schematic representation of the homopolymerisation of DMAEA and subsequent hydrolysis of the polymer to produce poly(acrylic acid) and *N,N'*-dimethylaminoethanol, reproduced with permission from Truong *et al.*[34]

Further work by Monteiro and co-workers demonstrated that copolymerisation of this monomer with thermoresponsive and hydrophobic monomers was able to produce polymers which could self-assemble to produce small micellar structures which used the hydrolysis of the P(DMAEA) to trigger disassembly of the polymeric structures, owing to

the change in the hydrophilic nature of the core during hydrolysis. Additionally, through tuning of the copolymer composition and conditions, the possibility to control the start of degradation and disassembly of the micelles could be tuned.[37, 38] More recently, our group reported the hydrolysis of DMAEA within a DMAEA-methyl acrylate copolymer.[39] It was reported that the pK_a of the copolymers was found to increase with an increasing distance between the amine repeat units, varied through changing the incorporation of methyl acrylate, owing to the ability of the DMAE unit to form a cyclic transition state in which the free electron pair from the amine is delocalised through an interaction with the acrylate carbonyl rendering the amine less available for protonation (Figure 3.1). Despite this, and in agreement with the work by Monteiro, hydrolysis was found to be independent of the amount of amino groups present.

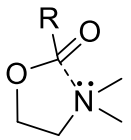

Figure 3.1 Proposed cyclic transition state for DMAEA, where R = C=CH$_2$. Reproduced, with permission from Van de Wetering *et al*.[35]

The lack of requirement for an internal or external stimulus in order to trigger hydrolytic degradation, coupled with the resultant change in environment from basic to acidic (attributed to the acrylic acid moieties), results in these materials having the potential to be used in a vast range of applications, for example in the release of siRNA complexes from cationic polymers, as well as DNA release.[37, 38, 40, 41]

Even though the hydrolysis of DMAEA is widely acknowledged in the literature, as well as the proposed multiple potential applications for these materials, the self-catalysed hydrolysis has not yet been extensively studied. Indeed the outcomes of such studies would potentially have a significant impact on, for example, the self-assembly of DMAEA-containing polymers amongst other applications.[42] Moreover, the influence of structural

parameters of the polymer architecture on the hydrolytic rate would provide an indication to the how well the amine is shielded from the external environment when tethered into the core of the star polymer. This would enable the system to act as a model to the analogous methacrylate star polymers introduced in Chapter 2, without the need to use the irreproducible foam testing methodology to evaluate the effect of structural parameters on the shielding of the amine from its surrounding environment. Hence, in this Chapter, the hydrolytic behaviour of DMAEA-containing polymeric stars is studied to determine the effect of temperature and structural parameters on the hydrolytic behaviour of the polymers.

3.3 Results and Discussion

RAFT polymerisation, with its compatibility towards amine-functionalised monomers, allows for the synthesis of DMAEA-containing polymeric stars with defined arm lengths and crosslinking densities. Star polymers were synthesised *via* an arm-first approach, with initial synthesis of the polymeric arms, and subsequent extension with DMAEA and the difunctionalised crosslinking monomer di(ethylene glycol) diacrylate (DEGDA).

3.3.1 Synthesis and characterisation of polymeric stars

3.3.1.1 PEGA armed stars

The synthesis of poly(ethylene glycol) monomethyl ether acrylate (PEGA, M_n = 480 g/mol) polymeric arms of varying arm length was carried out using RAFT polymerisation at 70 °C, with the radical initiator 2,2'-azobis(2-methylpropionitrile) (AIBN, 0.3 eq.) in 1,4-dioxane, and in the presence of the chain transfer agent (CTA) cyanomethyl dodecyl trithiocarbonate (Scheme 3.4).

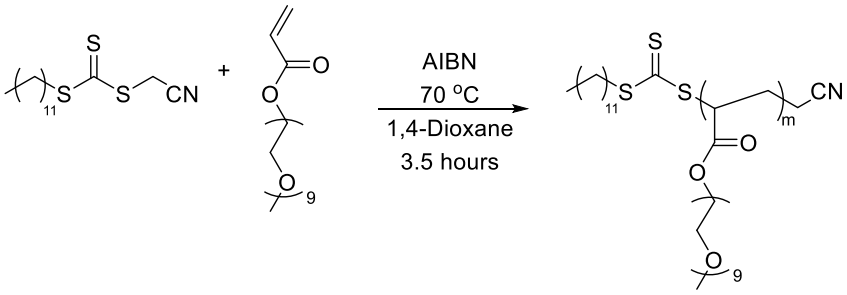

3.1, 3.2 and 3.3

Scheme 3.4 Synthesis of PEGA homopolymers of different lengths (polymers 3.1, 3.2 and 3.3) using RAFT polymerisation.

In an initial experiment, the polymerisation was performed at 70 °C for 3.5 hours with a ratio of $[CTA]_0$:$[Initiator]_0$:$[Monomer]_0$ of 1:0.2:110, targeting a short arm length with a degree of polymerisation (DP) of 100. ^{1}H NMR spectroscopic analysis of the crude reaction sample, through comparison of the vinyl signals at δ = 5.81 ppm to the monomer $OCH_2CH_2(OCH_2CH_2)_8$ signal at δ = 4.10 ppm, afforded a monomer conversion of 80% (Figure 3.2, protons 2 and a respectively).

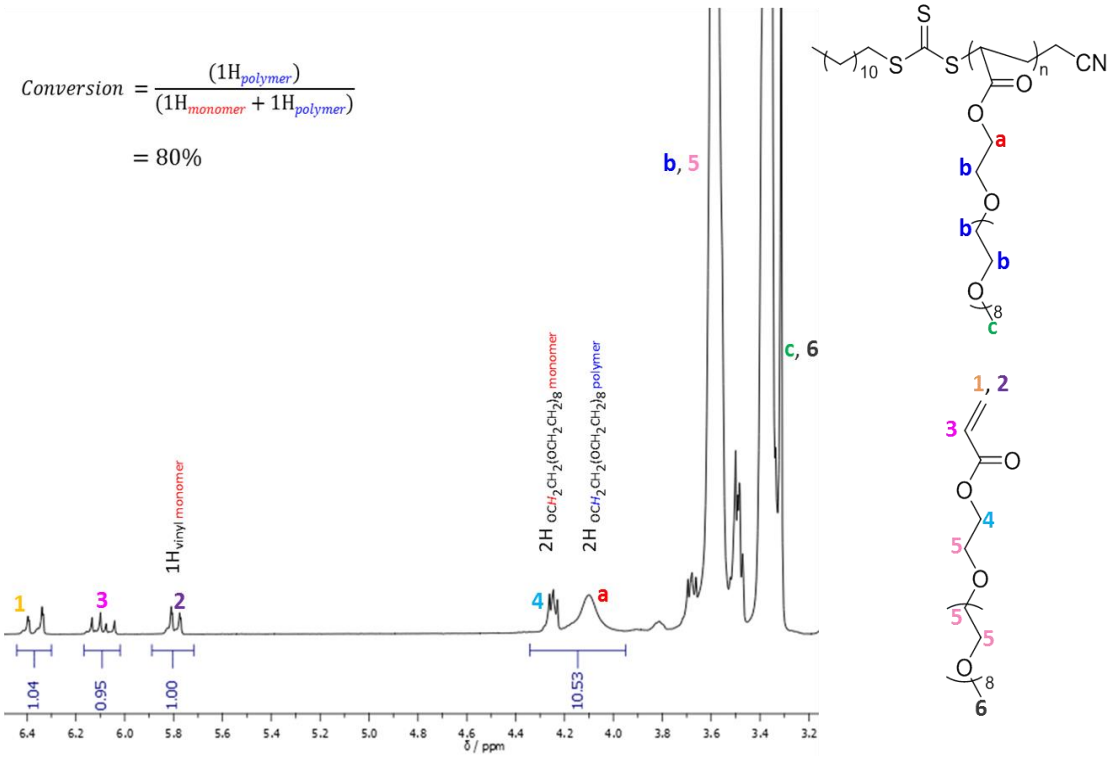

Figure 3.2 ^{1}H NMR spectrum used to calculate conversion for the synthesis of homopolymer PEGA arms 3.1 (400 MHz, $CDCl_3$).

Purification of the crude reaction mixture, through exhaustive dialysis against deionised water and subsequent lyophilisation, afforded a viscous yellow polymer, **3.1**, in a yield of 73%. The theoretical number-average molecular weight ($M_{n,\,theo.}$), determined by conversion from the ^{1}H NMR spectrum, was found to be in good agreement with the observed number-average molecular weight ($M_{n,\,obs.}$) (Table 3.1), as calculated by ^{1}H NMR spectroscopic analysis through comparison of the integrals attributed to the CTA methyl end group (δ = 0.80 ppm, proton a) to the methyl ester protons in the PEGA repeat unit (δ = 3.30 ppm, proton d) (Figure 3.3), indicating the controlled nature of the polymerisation.

Polymer	DP [a]	$M_{n,\,SEC}$ [b] (kg/mol)	$Đ_M$ [b]	$M_{n,\,theo}$ [c]. (kg/mol)	$M_{n,\,obs.}$ [d] (kg/mol)
3.1	98	44.7	1.51	53.1	47.4
3.2	148	46.2	1.64	89.4	71.4
3.6	288	47.0	1.52	114.4	138.6

Table 3.1 Characterisation data for PEGA homopolymers of different DPs. [a] DPs calculated by ^{1}H NMR spectroscopy ($CDCl_3$), [b] measured by SEC (DMF, PMMA standards), [c] theoretical molar mass calculated based on monomer conversion (^{1}H NMR spectroscopy, 400 MHz,$CDCl_3$), and [d] observed molar mass calculated based on the DP of the polymer.

Analysis of polymer **3.1** by Size Exclusion Chromatography (SEC, in DMF with PMMA standards) further demonstrated the controlled nature of the polymerisation, with a monomodal peak of relatively narrow dispersity ($Đ_M$ = 1.51) (Figure 3.4A). Additionally, a good overlap was observed between the refractive index (RI) trace and the UV trace at λ = 309 nm (Figure 3.4B), the wavelength attributed to the trithiocarbonate of the CTA, indicated the presence of the trithiocarbonate functionality in the polymer, rendering it suitable to act as a macro-CTA for further chain extension to produce polymeric stars.

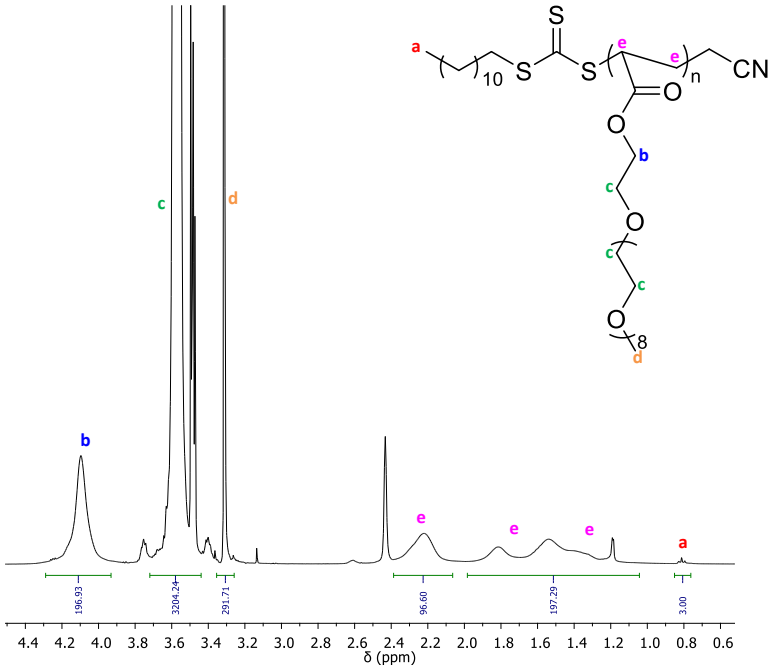

Figure 3.3 Calculation of the DP of the PEGA homopolymer 3.1 by comparison of the ^{1}H NMR spectrum integrals associated with the CTA end group (δ = 0.80 ppm, a) and the methyl ester (δ = 3.30 ppm, d) (400 MHz, $CDCl_3$).

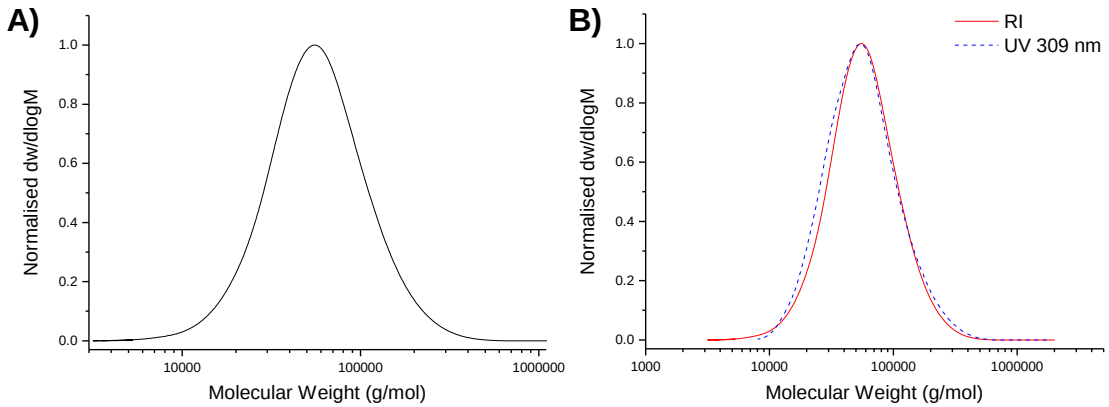

Figure 3.4 SEC analysis of polymer 3.1: (A) Molecular weight distribution and (B) overlay of the RI and UV trace at λ = 309 nm (DMF, PMMA standards).

To enable investigation into the effect of arm length on the hydrolytic behaviour, two further arm lengths were synthesised. To that end, the monomer feed was altered from $[CTA]_0$:$[Initiator]_0$:$[Monomer]_0$ of 1:0.2:100, to 1:0.2:200 for the medium DP homopolymer arm, and 1:0.2:300 for the longer DP homopolymer arm. Using the previous polymerisation conditions, SEC analysis of the resultant polymers indicated monomodal traces and

relatively low dispersity values of 1.64 and 1.52 for the medium DP homopolymer (DP = 148, **3.2**) and longer DP homopolymer (DP = 288, **3.3**), respectively (Table 3.1).

Following the successful synthesis of the three arm lengths, the polymers were chain extended and crosslinked with the amino-functionalised monomer DMAEA and the divinyl crosslinking monomer DEGDA (Scheme 3.5).

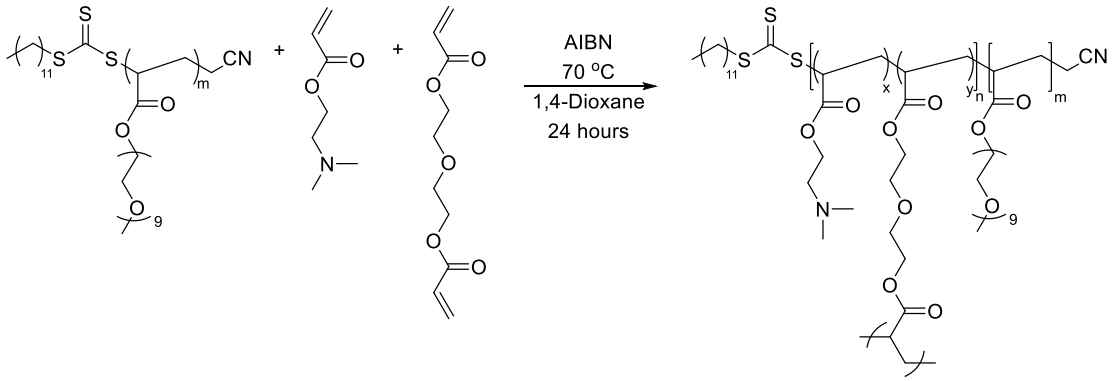

3.1-20, 3.1-15, 3.1-10, 3.2-20 and 3.3-20

Scheme 3.5 Schematic representation of the synthesis of PHEA armed, amine functionalised, polymeric stars (3.4-20, 3.4-15 and 3.4-10) *via* an arm-first approach using RAFT polymerisation chain extension of PHEA arms with DMAEA and the crosslinker DEGDA.

In an initial experiment, the shortest DP homopolymer (**3.1**) was chain extended, altering the monomer feed to produce polymeric stars with approximately 20, 15, and 10% crosslinking density (**3.1-20**, **3.1-15**, and **3.1-10**, respectively, Table 3.2). ^{1}H NMR spectroscopic analysis indicated the successful incorporation of the amine, with the characteristic resonances at δ = 2.27 and 2.54 ppm (N(CH_3)$_2$ and CH_2N respectively) (Figure 3.5, protons d and c, respectively). SEC analysis demonstrated a shift in molecular weight from the macro-CTA to the chain extended polymeric star, confirming successful chain extension (Figure 3.6).

olymer	Structure [a]	$M_{n,\,SEC}$ [b] (kg/mol)	$Đ_M$ [b]	a [c]	f [d]	$M_{n,\,theo.}$ [e] (kg/mol)	$M_{n,\,obs.}$ [f] (kg/mol)
3.1-20	PEGA$_{98}$-*b*-(DMAEA$_{86}$-*co*-DEGDA$_{16}$)	23.8	2.25	0.37	12	63.6	62.7
3.1-15	PEGA$_{98}$-*b*-(DMAEA$_{67}$-*co*-DEGDA$_{11}$)	39.9	2.88	0.40	13	65.1	59.3
3.1-10	PEGA$_{98}$-*b*-(DMAEA$_{72}$-*co*-DEGDA$_{8}$)	43.8	2.25	0.40	14	67.6	59.4
3.2-20	PEGA$_{148}$-*b*-(DMAEA$_{100}$-*co*-DEGDA$_{18}$)	66.3	1.73	0.40	16	96.9	91.4
3.3-20	PEGA$_{288}$-*b*-(DMAEA$_{71}$-*co*-DEGDA$_{7}$)	43.6	1.81	0.46	-	165.8	153.8

Table 3.2 Characterisation data for PEGA armed stars. [a] DPs calculated by ^{1}H NMR spectroscopy (400 MHz, $CDCl_3$), [b] measured by SEC (DMF, PMMA standards), [c] calculated using triple-detection SEC (DMF, PMMA standards), [d] star functionality calculated using Agilent GPC/SEC software version 1.2, with branching model set to "star branched-regular" and a branching frequency of 1, [e] theoretical molar mass calculated based on monomer conversion (^{1}H NMR spectroscopy, 400 MHz,$CDCl_3$), and [f] observed molar mass calculated based on the DP.

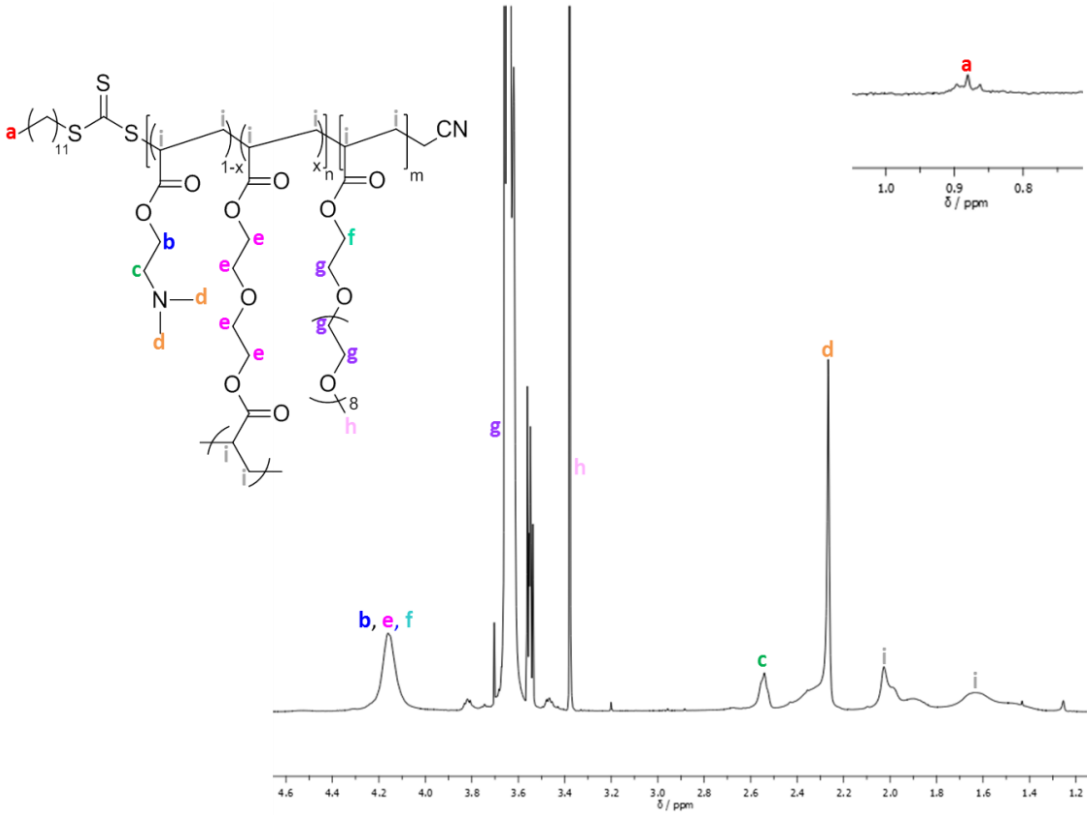

Figure 3.5 ^{1}H NMR spectrum of polymeric star 3.1-20 (400 MHz, $CDCl_3$).

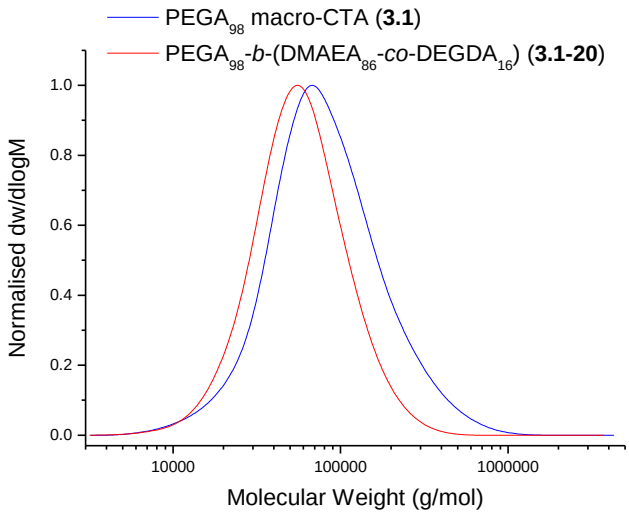

Figure 3.6 SEC analysis of polymer 3.1-20. RI traces of the linear $PEGA_{98}$ macro-CTA (3.1, blue) and $PEGA_{98}$-*b*-($DMAEA_{86}$-*co*-$DEGDA_{16}$) (3.1-20, red) (DMF with PMMA standards.

Analysis of the polymeric stars by SEC with viscometry detection enabled calculation of the Mark-Houwink characteristic constant *a*, derived from the linear fit of the Mark-Houwink curve generated by plotting log[η] *vs* log[MW], where η is the intrinsic viscosity and MW the molecular weight of the polymer.[43-46] As introduced in section 2.3.1, for polymers, $a = 0.5$ for a polymer chain in a theta solvent, $a = 0.8$ for a polymer in a good solvent, and therefore for a flexible polymer (for example a linear polymer) $0.5 \leq a \leq 0.8$; for crosslinked /branched polymers, $a < 0.5$.[44] Measuring the gradient of the linear fit for the Mark-Houwink plots for all the short-armed stars (**3.1-20**, **3.1-15**, and **3.1-10**, Figure 3.7A-C) generated *a* values ranging from 0.37-0.40, consistent with the crosslinked nature of the particles (Table 3.2). Moreover, *a* was found to be less than the linear PEGA macro-CTA, where $a = 0.52$, confirming a structural change from a linear polymer to a branched architecture.

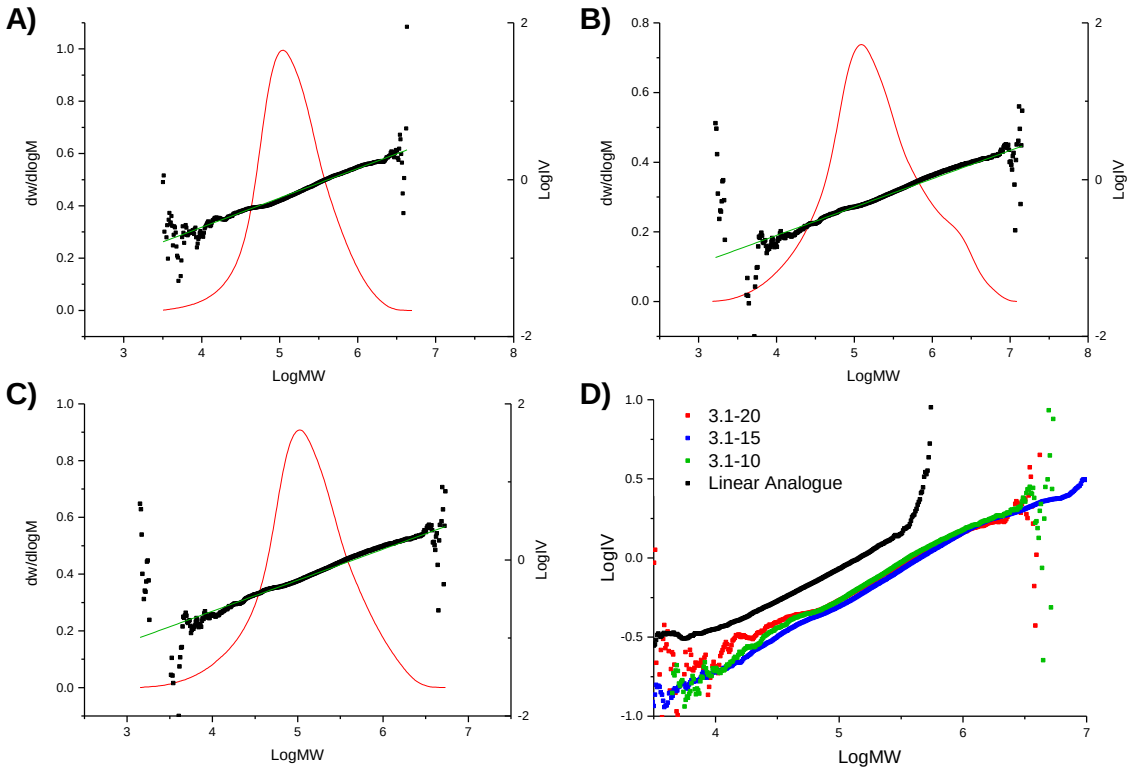

Figure 3.7 Triple detection SEC analysis of PEGA$_{98}$ (3.1) armed particles 3.1-20 (A), 3.1-15 (B), and 3.1-10 (C) with the Mark-Houwink curve overlaid on the molecular weight distribution (DMF with PMMA standards). Red line is the molecular weight distribution, black points are the Mark-Houwink plots, and the green line is the linear fit of the Mark-Houwink plot, of which the gradient is the *a* parameter.

To confirm that the introduction of the divinyl crosslinker DEGDA had resulted in the branched nature of the polymer, a linear analogue omitting DEGDA was synthesised. Using the conditions previously described for the synthesis of the polymeric stars, the same PEGA$_{98}$ macro-CTA was chain extended with DMAEA in 1,4-dioxane with radical initiator AIBN, and with methyl acrylate (MA) in the place of crosslinking DEDGA, to produce a polymer of approximately the same molecular weight, PEGA$_{98}$-*b*-(DMAEA$_{60}$-*co*-MA$_{13}$). Comparison of the star polymers **3.1-20**, **3.1-15** and **3.1-10** to the linear analogue indicated that all particles displayed lower intrinsic viscosities than the linear analogue, hence further confirming the structural change from a linear to a branched polymer (Figure 3.7D). Moreover, the similarity in the intrinsic viscosities of the particles is likely an indication of a similar number of arms per star. To probe the structure of the polymers and confirm this theory, the star functionality, *f*, was calculated (Table 3.2). Star functionality, in this instance

referring to the number of arms attached to the core of the star, was determined using the branching function in the Agilent software,[47] with the triple-detection SEC data for the linear PEGA arm used as the linear reference for branching calculations. All particles were found to have a similar number of arms, ranging from 12- 14 arms per star.

Particle size was analysed by Dynamic Light Scattering (DLS) in chloroform at 25 °C, at a concentration of 5 mg/mL. All the shortest DP particles were found to have similar hydrodynamic diameters (D_h), ranging in size from 9-11 nm (Figure 3.8A).

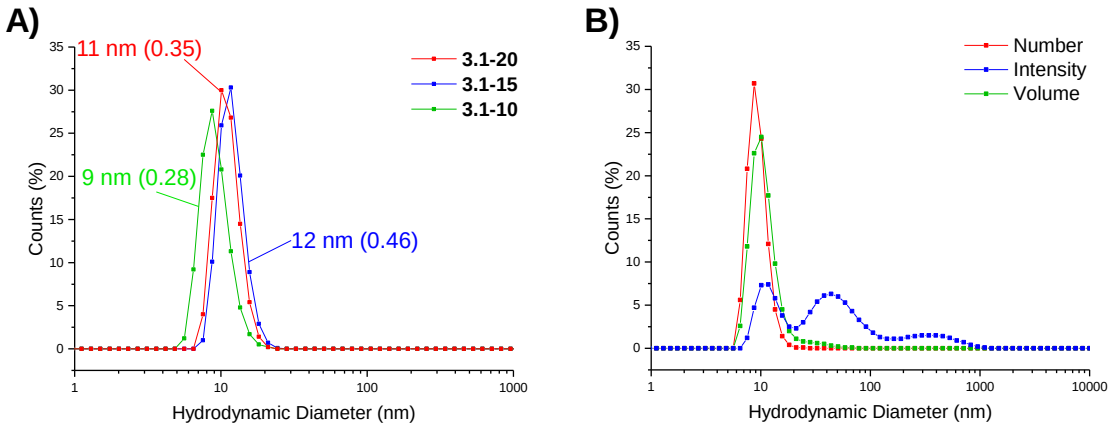

Figure 3.8 Size distributions of short armed PEGA particles obtained by DLS (detection angle = 173 °) at 5 mg/mL carried out in chloroform at 25 °C. (A) Size distribution, by number, for short armed PEGA particles 3.1-20, 3.1-15 and 3.1-10, and (B) size distribution, by number, intensity and volume for 3.1-15.

Light scattering analysis indicated the presence of larger entities alongside the small particles, potentially caused by aggregation (Figure 3.8B). Examination of the particles by Transmission Electron Microscopy (TEM) analysis using graphene oxide (GO) supported TEM grids, found to produce higher contrast images without staining,[48] confirmed that theses larger species were agglomerated particles as a consequence of star-stars coupling of the growing crosslinking chains during polymerisation (Figure 3.9). The particle diameter produced by TEM analysis was significantly smaller than that obtained by DLS analysis, with a particle size of approximately 3 nm. The smaller size produced by TEM analysis can be attributed to the dry-state of the TEM samples in which the PEGA shell is not hydrated,

resulting in poor contrast between the shell of the polymer and the GO grid, and therefore only the particle core is imaged, commonly observed for such dry-state analysis.[49]

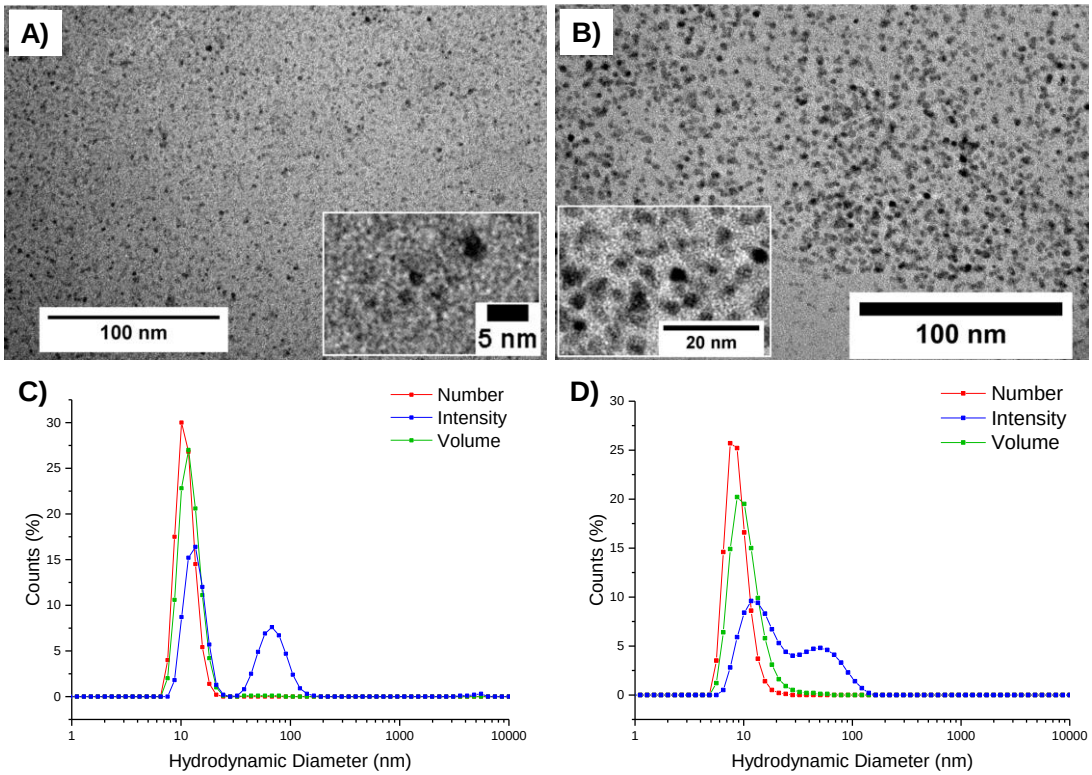

Figure 3.9 Representative TEM images and size distributions, as determined by DLS (5 mg/mL in chloroform), of polymers 3.1-20 (A and C) and 3.1-10 (B and D).

3.3.1.2 HEA armed stars

In order to investigate the effect of arm type, a non-brush type linear polymer of 2-hydroxyethyl acrylate (HEA) was synthesised. Using the same RAFT based methodology, an initial experiment was performed at 65 °C for 3 hours with a ratio of $[CTA]_0$:$[Initiator]_0$:$[Monomer]_0$ of 1:0.2:100, targeting a similar DP to the shortest PEGA arms (DP = 120) (Scheme 3.6).

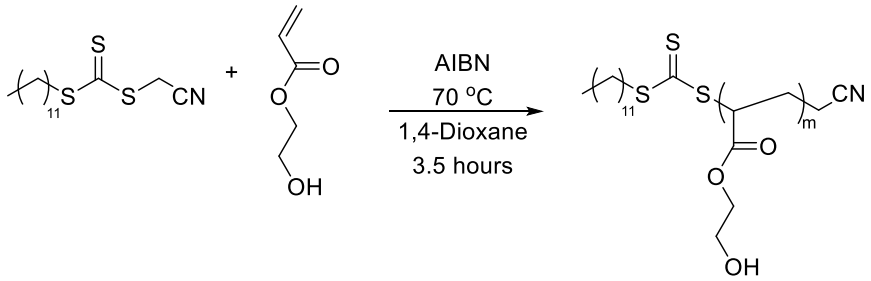

Scheme 3.6 Schematic representation of the synthesis of a PHEA homopolymer (3.4) using RAFT polymerisation.

After quenching of the reaction, ^{1}H NMR spectroscopic analysis of the crude reaction sample, through comparison of the vinyl signals at δ = 5.90 ppm to the monomer signals at δ = 4.77 ppm, attributed to the CH_2OH protons, revealed a reaction conversion of 60%. Following purification of the polymer (**3.4**), ^{1}H NMR spectroscopic analysis revealed a DP of 104, calculated through comparison of the integrals attributed to the CTA methyl end group (δ = 0.80 ppm) to the protons of the CH_2OH (δ = 4.01 ppm) (Figure 3.10 protons a and c, respectively), producing a $M_{n,obs.}$ of 12.5 kg/mol (Table 3.3).

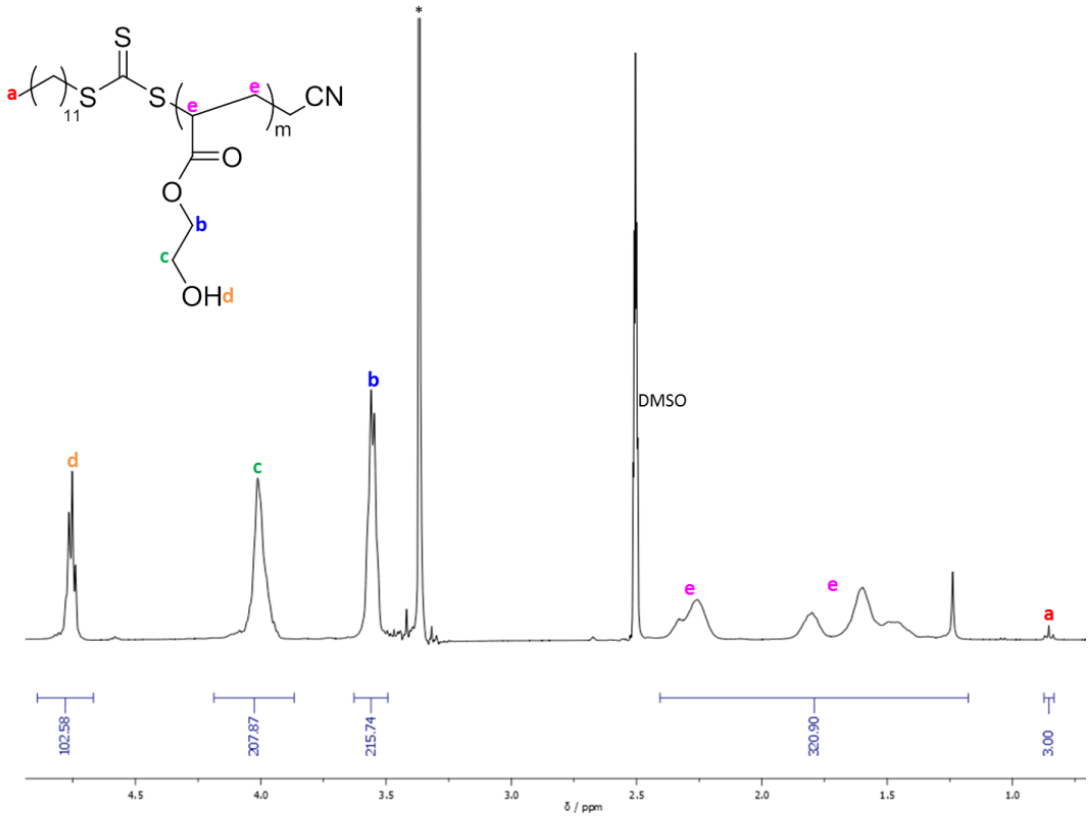

Figure 3.10 Calculation of the DP of the PHEA homopolymer 3.4 by comparison of the ^{1}H NMR spectrum integrals associated with the CTA end group (δ = 0.80 ppm, a) and the CH_2OH protons (δ = 4.01 ppm, d) * denotes water (400 MHz, DMSO-d_6).

Polymer	Structure [a]	$M_{n,\,SEC}$ [b] (kg/mol)	$Đ_M$ [b]	a [c]	f [d]	$M_{n,\,theo.}$ [e] (kg/mol)	$M_{n,\,obs.}$ [f] (kg/mol)
3.4	$pHEA_{104}$	20.2	1.10	0.50	-	7.8	12.4
3.4-20	$pHEA_{104}$-*b*-($DMAEA_{74}$-*co*-$DEGDA_{14}$)	29.1	1.56	0.34	12	32.0	23.4
3.4-15	$pHEA_{104}$-*b*-($DMAEA_{69}$-*co*-$DEGDA_{10}$)	27.8	1.25	0.32	11	31.8	24.8
3.4-10	$pHEA_{104}$-*b*-($DMAEA_{71}$-*co*-$DEGDA_{7}$)	24.9	1.31	0.40	14	35.7	24.4

Table 3.3 Characterisation data for PHEA armed stars. [a] DPs calculated by ^{1}H NMR spectroscopy (400 MHz, DMSO-d_6), [b] measured by SEC (DMF, PMMA standards), [c] calculated using triple-detection SEC (DMF, PMMA standards), [d] Star functionality calculated using Agilent GPC/SEC software version 1.2, with branching model set to "star branched-regular" and a branching frequency of 1, [e] theoretical molar mass calculated based on monomer conversion (^{1}H NMR spectroscopy, 400 MHz, DMSO-d_6), and [f] observed molar mass calculated based on the DP of the polymer.

Analysis of the resultant polymer by SEC analysis indicated that the value for $M_{n,\,theo.}$ was slightly smaller than the observed number-average molecular weight, indicating some loss of control over the process. Indeed, unlike the methacrylate equivalent discussed in Chapter 2, there is an appearance of a high molecular weight shoulder visible in the SEC RI trace (Figure 3.11).

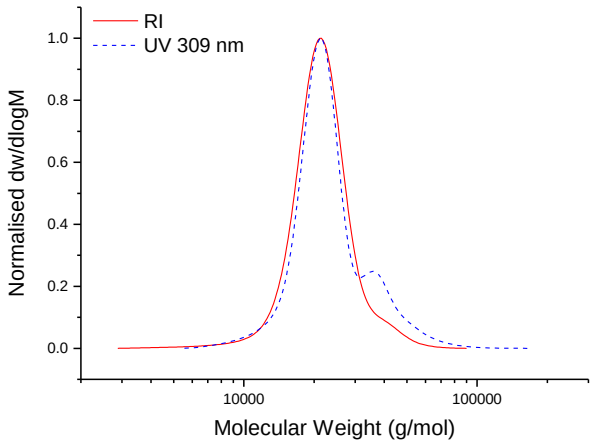

Figure 3.11 SEC analysis of polymer 3.4 (DMF PMMA standards) showing the RI trace and an overlaid UV λ = 309 nm trace.

The high molecular weight shoulder is likely to result from the formation of some branches as a result of chain transfer through hydrogen abstraction of the CH radical (known as back-

biting, Scheme 3.7),[50] a common side reaction for acrylate monomers, though this is likely only to be slight as the dispersity remains low ($Đ_M$ = 1.10), and the Mark-Houwink parameter *a* was only 0.50. Whilst some branching will detract from the linear nature of the arms, a significant difference in architecture between the brush-like PEGA arms and the largely linear HEA arms will remain, allowing for differencesin the effect of arm architecture on the hydrolytic behaviour to still be observed. Confirmation of the attachment of the trithiocarbonate end-group, evidenced through the UV SEC trace analysis at λ = 309 nm overlapping with the RI trace (Figure 3.11), confirmed that the PHEA was able to act as a macro-CTA for further chain extensions.

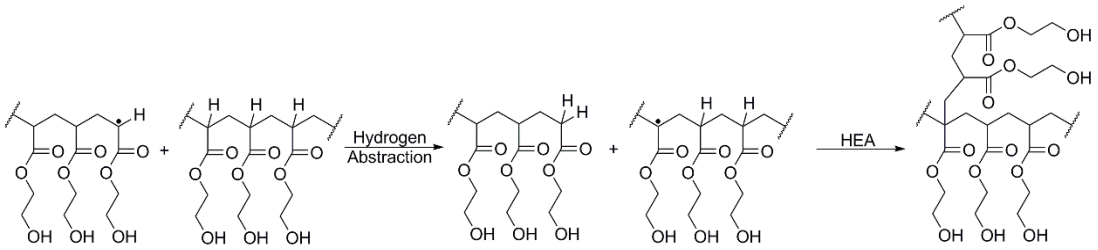

Scheme 3.7 Schematic representation for the back-biting reaction during the polymerisation of HEA, resulting in the production of branching points.

Subsequent chain extension of the PHEA arms with DMAEA and DEGDA, using the identical initiator and macro-CTA, produced a series of PHEA armed polymeric stars with varying crosslinking densities (Scheme 3.8, **3.4-20**, **3.4-15**, and **3.4-10**) and with similar arm lengths to the smallest PEGA.

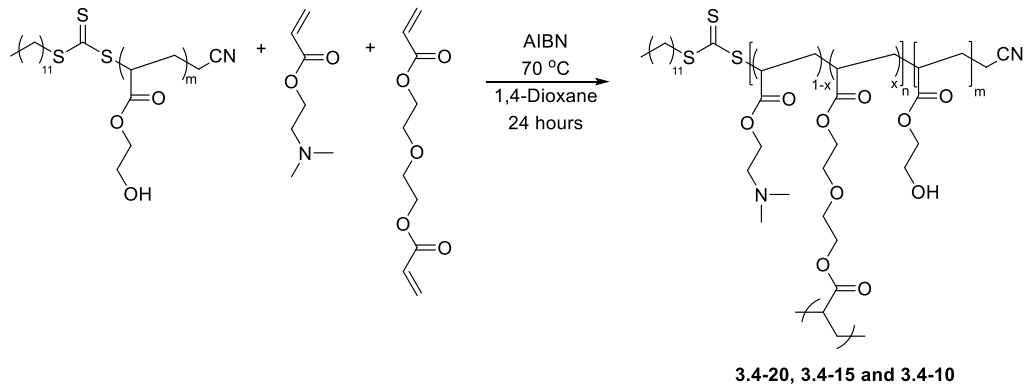

Scheme 3.8 Schematic representation of the synthesis of PHEA armed, amine functionalised, polymeric stars (3.4-20, 3.4-15 and 3.4-10) *via* an arm-first approach using RAFT polymerisation chain extension of PHEA arms with DMAEA and DEGDA.

In an initial experiment, performed at 65 °C for 24 hours, the monomer feed was set to $[PHEA]_0$:$[Initiator]_0$:$[DMAEA]_0$:$[DEGDA]_0$ = 1:0.25:200:40, targeting a 20% crosslinking density. ^{1}H NMR spectroscopic analysis of the crude reaction sample, through comparison of the vinyl signal at δ = 5.92 ppm to the DMAEA monomer signal at δ = 2.47 ppm and to the DEGDA signal at δ = 4.24 ppm, produced a DMAEA conversion of 53% and a DEGDA conversion of 56%. ^{1}H NMR spectroscopic analysis on the purified viscous yellow product (**3.4-20**) revealed a slight difference between the values of $M_{n,\ theo.}$ (32.0 kg/mol) and $M_{n,obs.}$ (23.4 kg/mol), indicating a loss in control over the polymerisation (Table 3.3).

Analysis of the polymers using triple-detection SEC revealed, similar to the $PEGA_{98}$ armed particles, that the PHEA armed stars were found to be crosslinked in nature (with Mark-Houwink *a* values ranging from 0.25-0.41, Figure 3.12), and displayed a similar number of arms, with a star functionality ranging from 11 to 14, determined using the Agilent software using the macro-CTA $PHEA_{104}$ as the linear analogue. Analysis of particle size by DLS yielded slightly larger particle sizes of 23-25 nm compared to the PEGA armed particles, and also indicated the presence of larger agglomerates for the polymers with a crosslinking density of 20% and 15% (Figure 3.13).

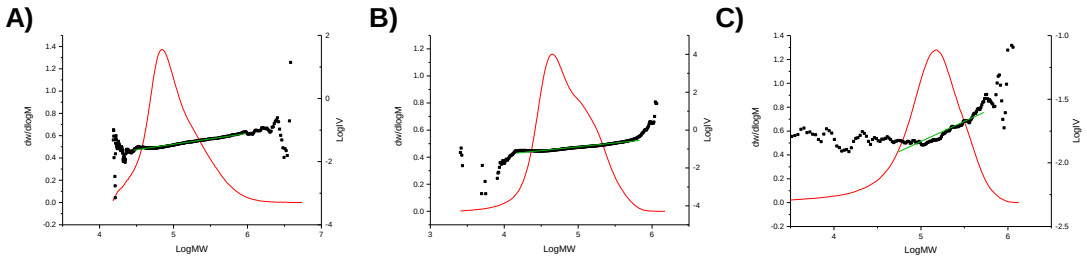

Figure 3.12 Triple-detection SEC analysis of $PHEA_{104}$ (3.4) armed particles 3.4-20 (A), 3.4-15 (B) and 3.4-10 (C) with the Mark-Houwink curve overlaid on the molecular weight distribution (DMF with 5 mM NH_4BF_4 and PMMA standards). Red line is the molecular weight distribution, black points are the Mark-Houwink plots, and the green line is the linear fit of the Mark-Houwink plot, of which the gradient is the *a* parameter.

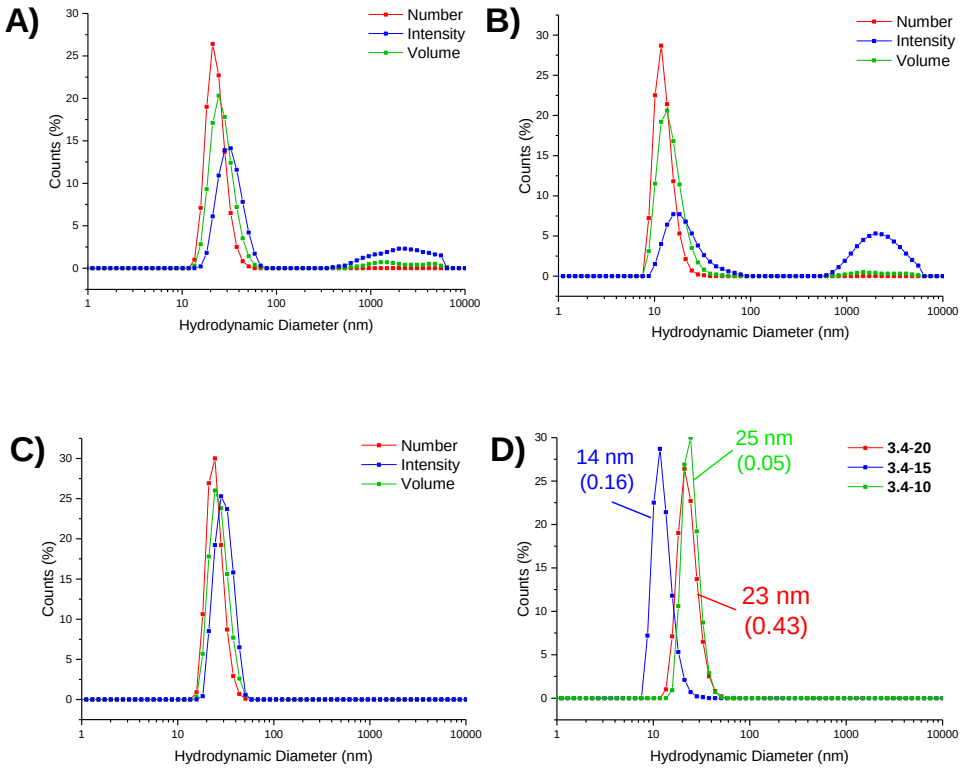

Figure 3.13 Size distributions of HEA_{104} armed particles obtained by DLS (detection angle = 173 °) at 5 mg/mL carried out in chloroform at 25 °C: (A-C) Size distribution, by number, intensity and volume, for particles 3.4-20, 3.4-15 and 3.4-10 respectively, and (D) size distribution, by number of all the PHEA armed particles.

3.3.2 Evaluation of hydrolytic behaviour

Evaluation of the hydrolytic stability of the DMAEA when tethered to the core of star polymers with different structural parameters (Figure 3.14) was investigated using ^{1}H NMR spectroscopic analysis of the particles in D_2O (50 mg/mL).

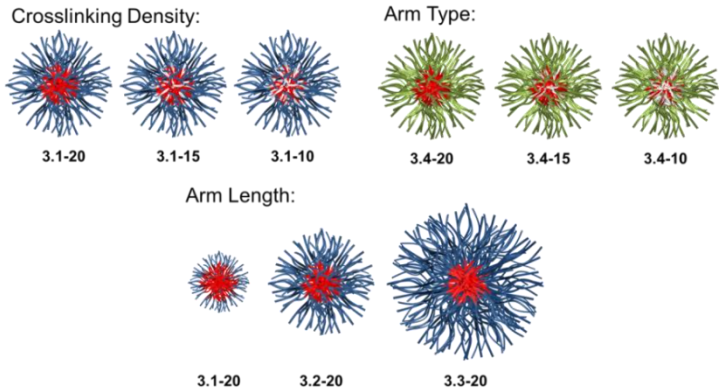

Figure 3.14 Schematic representation of the polymeric stars with varying structural parameters evaluated for hydrolytic stability, where blue arms = PEGA arms, green arms = PHEA arms, and the red core represents DMAEA.

The resulting spectrum of the particles hydrolysed at 25 °C (Figure 3.15, representative of the PEGA armed polymers (**3.1-20**, **3.1-15**, **3.1-10**, **3.2-20**, **3.3-20**)), clearly displays the protons associated with the incorporated amine monomer, observed at δ = 2.65 ppm for the methyl groups bound to the nitrogen and at δ = 3.08 ppm for the methylene protons bound to the amine (Figure 3.15, protons 3 and 2, respectively), with the intensity of two new signals at δ = 2.90 and 3.20 ppm, corresponding to the equivalent protons in the hydrolytically released small molecule 2-dimethylaminoethanol (DMAE, Figure 3.15, protons c and b respectively). From these signals, which confirm hydrolysis through the ester linkage within the amine-functionalised monomer in the polymer, the percentage of hydrolysis can be estimated based on the ratio between hydrolysed and non-hydrolysed amine integrals at δ = 3.20 ppm and δ = 3.08 ppm respectively. It should be noted that hydrolysis calculated using the ratio of polymer proton 3(at δ = 2.65 ppm) to the small molecule proton c (at δ = 2.90 ppm) was found to produce the same percentage hydrolysis.

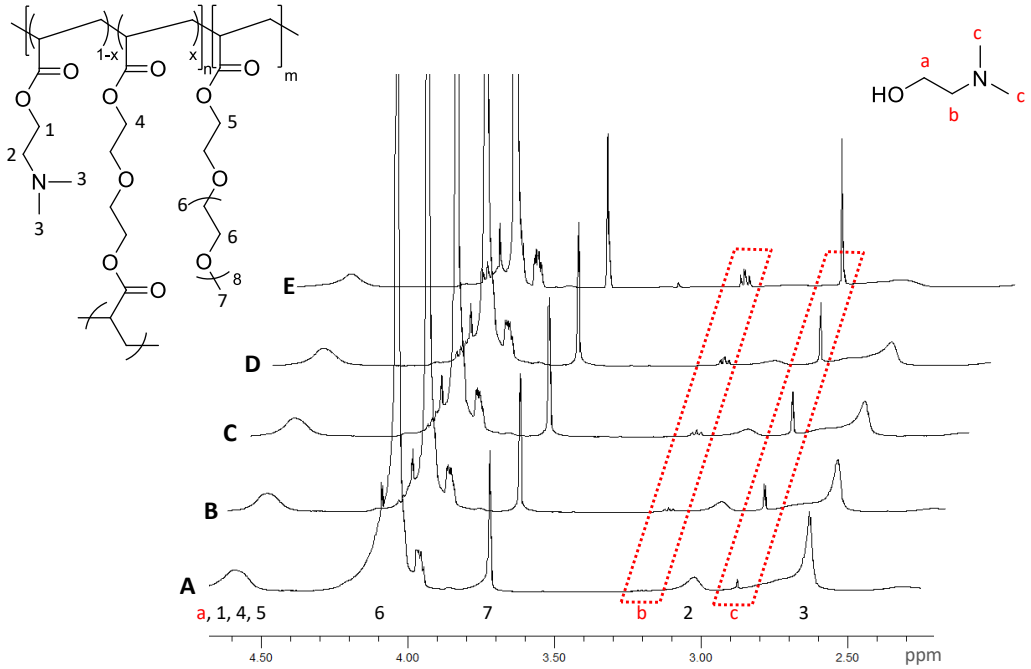

Figure 3.15 ^{1}H NMR spectra of PEGA$_{98}$-*b*-(DMAEA$_{86}$-*co*-DEGDA$_{16}$) (3.1-20) for (A) 1 h., (B) 2 h., (C) 4 h., (D) 6 h., and (E) 24 h at 25 °C. Spectra normalised to the resonance at δ = 3.72 ppm (protons 7) (D$_2$O, 400 MHz).

3.3.2.1 Influence of temperature on the rate of hydrolysis for different crosslinking densities

An initial set of hydrolysis experiments was carried out to investigate the influence of temperature on the rate of hydrolysis for different crosslinking densities (Figure 3.16). Reactions performed at 50 °C resulted in a significantly faster rate of hydrolysis, with 20% of the amino-functionalised repeat units in **3.1-10** hydrolysed after 21 minutes, but 230 minutes was required at 25 °C to achieve the same degree of hydrolysis (Figure 3.16A). Subsequent heating of the particles already hydrolysed at 25 °C to the increased temperature of 50 °C resulted in an increase in the rate of hydrolysis, with the overall hydrolysis tailing off at the same level as those initially hydrolysed at 50 °C (Figure 3.16B). Through comparison of the hydrolysis at both 25 °C and 50 °C it is evident that at the lower temperature crosslinking density has little effect on the observed hydrolysis, with all crosslinking densities exhibiting approximately the same degradation rate and with hydrolysis of all polymers falling within error regardless of the crosslinking density (Figure 3.16C). In contrast, at the raised temperature there is a clear influence of crosslinking density, with the most highly crosslinked particle (**3.1-20**) displaying the slowest rate of hydrolysis, followed by **3.1-15**, and with the lowest crosslinking density (**3.1-10**) demonstrating both the greatest hydrolysis over the period of 4 hours in addition to the fastest initial rate of hydroysis (Figure 3.16D).

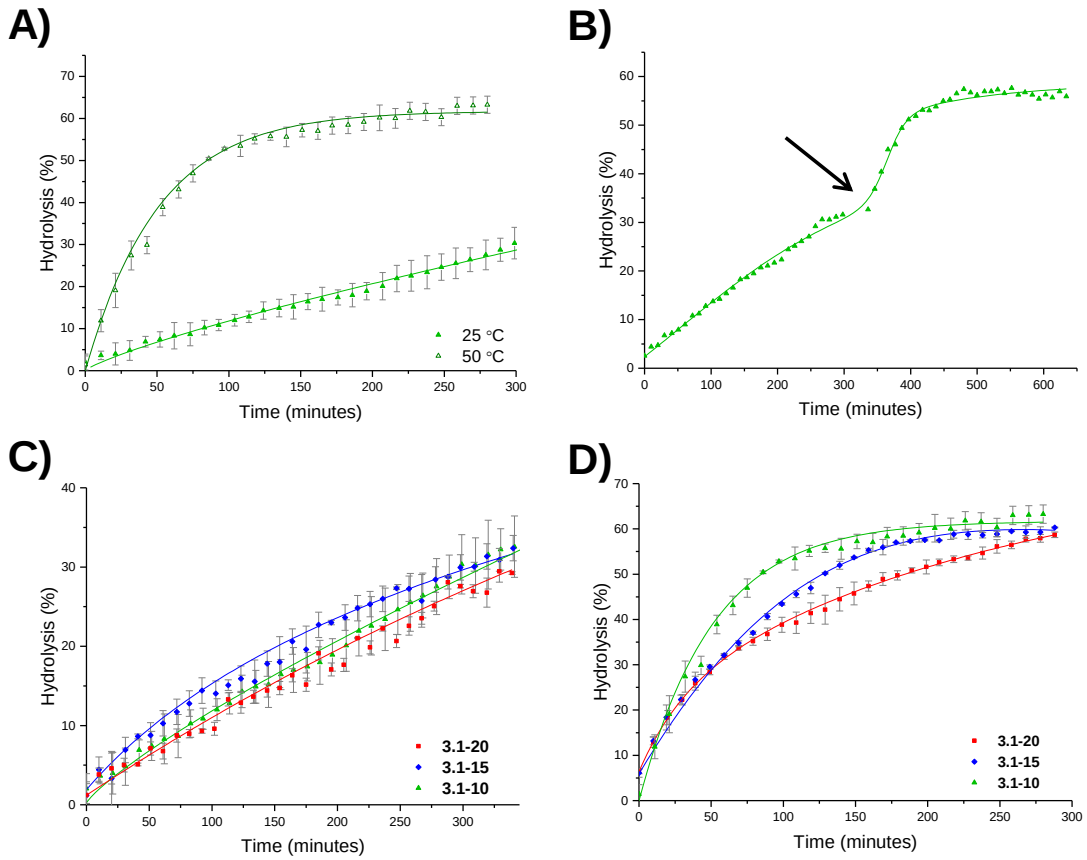

Figure 3.16 Hydrolysis kinetics of PEGA-*b*-(DMAEA-*co*-DEGDA) polymers in D_2O: (A) hydrolysis of 3.1-10 carried out at 25 °C and 50 °C; (B) 3.1-10 initially heated at 25 °C with an increase in temperature to 50 °C at 320 minutes; (C) hydrolysis at 25 °C with different crosslinking densities, and (D) hydrolysis at 50 °C with different crosslinking densities. Error bars produced from the standard deviation of three repeats.

It was hypothesised that the decrease in the rate of hydrolysis over time is likely a consequence of one of two theories. The first suggests that the decrease in the rate of hydrolysis over time is a result of the build-up of electrostatic repulsion throughout the reaction. At the beginning of the hydrolysis, the DMAEA units begin with no adjacent units hydrolysed. As the reaction proceeds, the adjacent units begin to hydrolyse and the DMAEA repeat unit progresses from having no adjacent units hydrolysed, to one adjacent unit hydrolysed and then both hydrolysed. The formation of polyacrylic acid groups within the core increases the electrostatic repulsion between the non-hydrolysed ester linkages, the acrylic acid moieties, and the hydrolysing water molecule, slowing the rate of hydrolysis. Moreover, as demonstrated by Higuchi and Senju for acrylamide hydrolysis,[51] this electrostatic repulsion between the hydrolysed groups and the water results in an increase in

the activation free energy required to hydrolyse the ester bond thus rendering further hydrolysis energetically unfavourable. An increase in crosslinking density results in a less mobile core and subsequently a less mobile amine functionality. Upon hydrolysis, the polyacrylic acid product is therefore in a more fixed position in the core giving rise to a build-up of localised negative charge, attributed to the carboxylic acid moieties. Therefore, in a more crosslinked particle, the build-up of a localised more negative environment is greater owing to lower core mobility, resulting in both a slower rate of hydrolysis as well as a lower overall percentage hydrolysis.

An alternative to the electrostatic argument is that at raised temperatures the particles swell resulting in a greater ingress of water thus producing a faster rate of hydrolysis. An increase in crosslinking density is thought to result in less swelling of the particle and as such lower hydrolysis. To exclude the possibility of particle swelling having an impact on the rate of hydrolysis, DLS analysis of the particles (**3.1**-**20**) was carried out both before and after hydrolysis at 25 °C, and additionally measured at 50 °C (Figure 3.17).

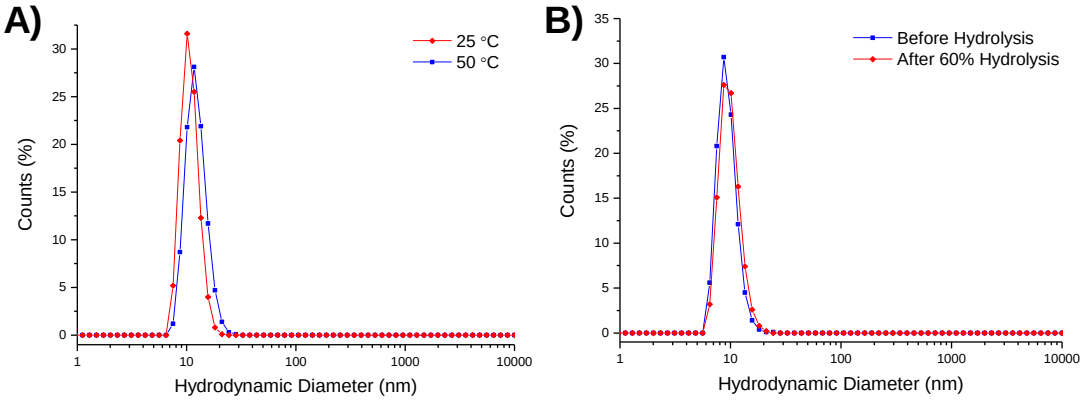

Figure 3.17 Size distribution, by number, of 3.1-20 at 5 mg /mL in chloroform. (A) at 25 °C and 50 °C before hydrolysis, and (B) before and after hydrolysis at 50 °C, obtained by DLS (detection angle = 173 °).

Particle size was found to remain approximately the same at both 25 °C and 50 °C regardless of the crosslinking density (Table 3.4, Figure 3.17). Moreover, hydrolysis had minimal effect on the particle size, with no size changes observed following 60% hydrolysis.

Additionally, the integrals in the ^{1}H NMR spectrum assigned to the crosslinker (Figure 3.15, protons 4) remained unchanged throughout the hydrolysis confirming that only the amine was hydrolysed.

Polymer	D_h, by number, at 25 °C	D_h, by number, at 25 °C
3.1-20	11 (0.35)	12 (0.38)
3.1-15	12 (0.46)	12 (0.33)
3.1-10	9 (0.28)	12 (0.38)

Table 3.4 Size distribution analysis, obtained by DLS (detection angle=173 °) in chloroform at 5 mg/mL. PD is given in brackets.

3.3.2.2 Influence of particle arm length

To further probe the effect of star composition on the protection afforded to the amine, hydrolysis kinetics at the raised temperature of 50 °C were measured for short, medium, and long armed PEGA particles all with approximately 20% crosslinking density (**3.1-20**, **3.2-20**, and **3.3-20,** respectively). As an increase in arm length would result in lower core mobility, it was expected that an increase in arm length would result in lower hydrolysis. Whilst an increase in arm length did result in a decrease in hydrolysis (Figure 3.18), the initial rates of hydrolysis for all arm lengths are similar suggesting that arm length does not have such as significant impact on hydrolysis compared to crosslinking density. This may be attributed to the properties of the star polymer: as the arm length increases, the density of the shell decreases which allows for greater influx of water into the core.[8] Therefore, there is little difference between the initial rates of hydrolysis. However, longer arms result in a less mobile core; therefore there is a greater build-up of electrostatic repulsion in the polymers with larger PEGA DPs, thus resulting in a lower final percentage hydrolysis.

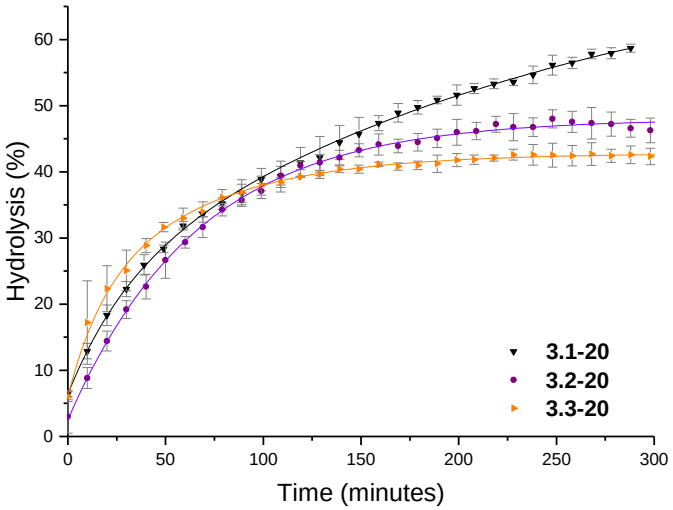

Figure 3.18 Hydrolysis kinetics of 3.1-20, 3.2-20 and 3.3-20 at 50 °C in D_2O. Error bars produced from the standard deviation of three repeats.

3.3.2.3 Effect of polymer architecture

The hydrolysis rate observed for the polymeric particles was found to be noticeably higher than that previously reported, with Truong *et al.* reporting only 13% hydrolysis in a linear PDMAEA (with a similar DP with respect to the amine) after 7 hours at 25 °C.[36] To ascertain whether tethering the amine functionality in a polymeric particle has afforded protection against hydrolysis, the hydrolytic behaviour of a linear analogue, in which the 20% crosslinking monomer was replaced with non-crosslinking methyl acrylate (MA), was evaluated. Hydrolysis at room temperature showed little difference in the rate of hydrolysis between the linear and star hydrolysis kinetics, with the star polymer reaching 26% hydrolysis over 300 minutes compared to 34% hydrolysis of the linear polymer (Figure 3.19A). At 50 °C, however, the rate of hydrolysis for the linear polymer begins to deviate from the star polymer, with a much faster hydrolysis rate observed for the linear copolymer (Figure 3.19B). The rigid core of the stars gives rise to a more confined build-up of acrylic acid moieties as hydrolysis proceeds, resulting in increased electrostatic repulsion thus generating both a lower overall hydrolysis and a slower rate of hydrolysis for the star polymer in comparison to the linear analogue. Nonetheless, whilst the star appears to afford

protection, the linear MA based analogue was still found to have higher hydrolysis than the DMAEA homopolymers previously reported. This can be attributed to the MA group acting as a spacer: in the copolymer there is less electrostatic repulsion between the hydrolysed and non-hydrolysed groups as the MA lies between them on the polymer backbone, disrupting the build-up of electrostatic repulsion along the backbone thus increasing hydrolysis. In contrast, the build-up of electrostatic repulsion along the backbone in the homopolymer does not have this spacer to disrupt the electrostatic charge, therefore resulting in a slower hydrolysis rate.

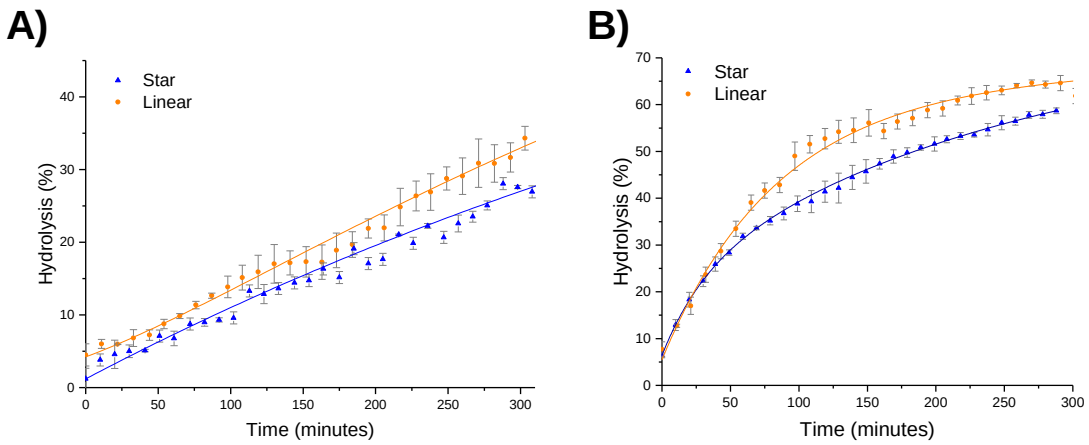

Figure 3.19 Hydrolysis kinetics of polymeric star 3.1-20 and the linear analogue PEGA$_{98}$-*b*-(DMAEA$_{60}$-*co*-MA$_{13}$) at (A) 25 °C and (B) at 50 °C, in D_2O. Error bars produced from the standard deviation of three repeats.

3.3.2.4 Influence of the polymer arm type at different crosslinking densities

The brush-like character of the PEGA arms may influence the hydrolysis rate, for example by affecting diffusion of water into the particle. To this end, the hydrolytic stability of a series of analogous particles using PHEA$_{104}$ as the star arms was evaluated. Similar to the analogous PEGA armed star polymers, stars were synthesised with varying crosslinking densities of approximately 20, 15 and 10% (**3.4-20**, **3.4-15** and **3.4-10**, Table 3.3). Whilst investigating the effect of temperature, at 25 °C it was observed that crosslinking density again has little effect on the hydrolysis rate (Figure 3.20A), similar to the PEGA armed counterparts. At raised temperatures (50 °C) the same trend as for the PEGA armed particles

was observed: increasing the crosslinking density lowered the hydrolysis rate (Figure 3.20B).

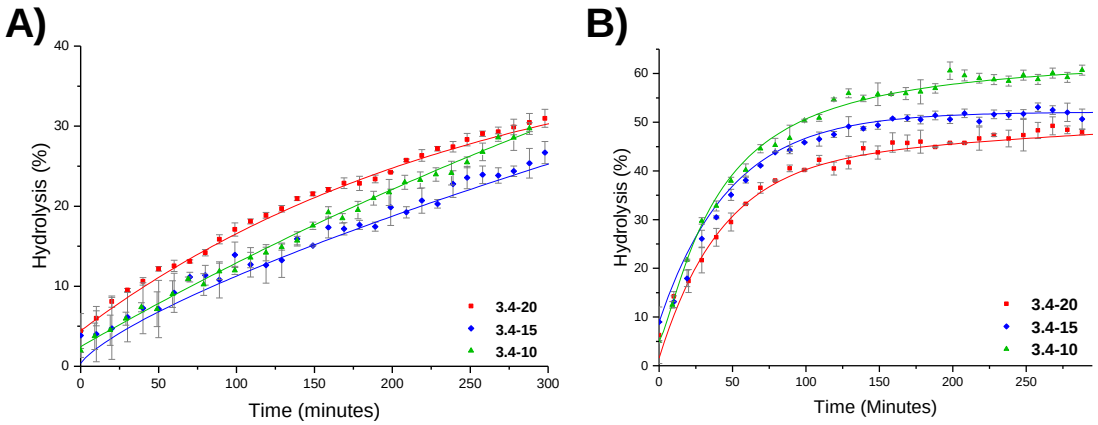

Figure 3.20 Hydrolysis kinetics of PHEA armed polymers of varying crosslinking densities, in D_2O at (A) 25 °C and (B) 50 °C. Error bars produced from the standard deviation of three repeats.

Direct comparison to the PEGA analogues at different crosslinking densities confirmed that arm identity had little effect (Figure 3.21). At 25 °C both PEGA and PHEA arms produced similar profiles for the hydrolysis kinetics. Further analysis suggests that at 50 °C, whilst both arms produced similar profiles, the PEGA armed particles achieved a slightly higher overall hydrolysis in 300 minutes. Whilst there is almost no difference for the 10% crosslinked particle (Figure 3.21C), there is a 3% difference at 15% crosslinking density (**3.1-15** and **3.4-15,** Figure 3.21B), rising to 6% at 20% crosslinking density (**3.1-20** and **3.4-20,** Figure 3.21A). Whilst the 3% difference for the 15% crosslinked particles could be within error, the error associated with the 10% crosslinked PEGA armed particles (**3.1-10)** at 50 °C is ± 1.3%, and for the 10 % crosslinked PHEA particles (**3.4-10**) it is ± 0.6%, suggesting that the 6% difference between the PHEA and PEGA particle hydrolysis is increasing as the crosslinking density increases. This could be attributed to the more dense PEGA shell slowing diffusion of the dimethylaminoethanol out of the core in comparison to the PHEA shell. Moreover, an increase in crosslinking density will create a more densely packed core which would further prevent the release of the small molecule DMAE, which would be able to buffer the hydrolysis in the core which would further slowdown hydrolysis.

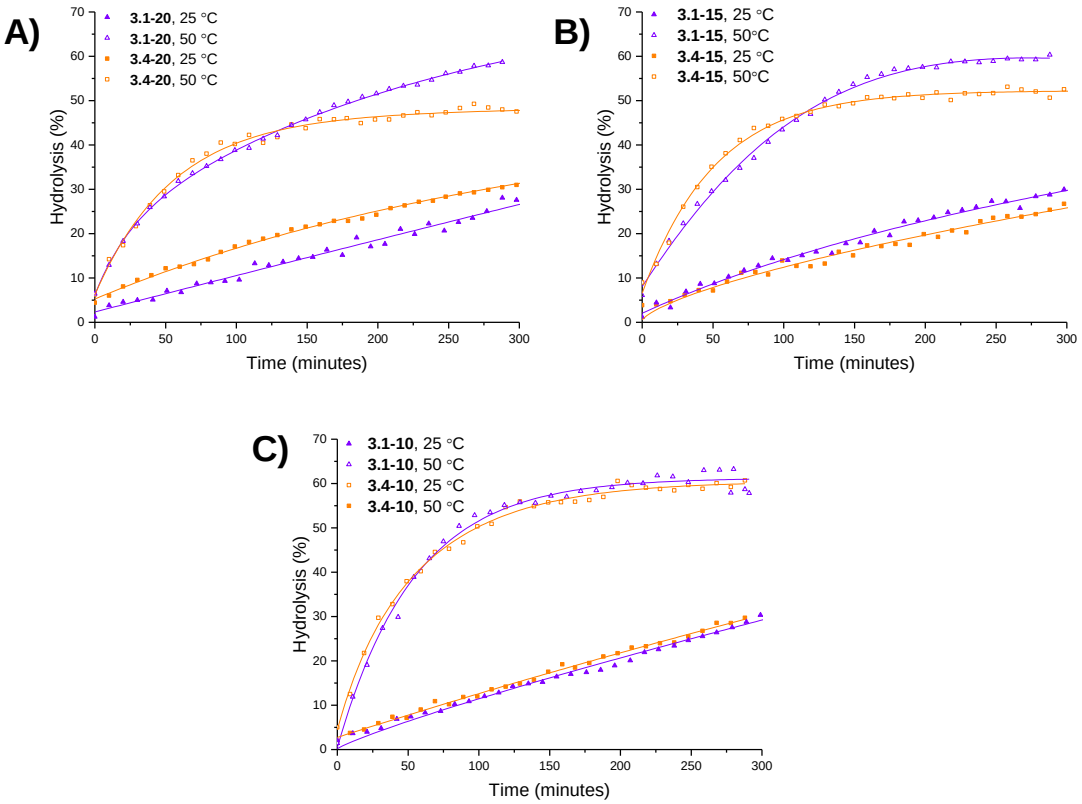

Figure 3.21 Hydrolysis kinetics of both PHEA (3.4) and PEGA (3.1) armed particles with (A) 20% crosslinking density (3.1-20 and 3.4-20), (B) 15% crosslinking density (3.1-15 and 3.4-15) and (C) 10% crosslinking density (3.1-10 and 3.4-10), in D_2O.

3.3.3 Enzymatic confirmation of small molecule release

Whilst ^{1}H NMR spectroscopy confirms the successful hydrolysis of PDMAEA, it does not, however, confirm release of the small molecule from within the polymeric star. Indeed, the changing integrals attributed to the PDMAEA (at δ = 3.08 ppm) observed by ^{1}H NMR spectroscopy may not accurately reflect the degree of hydrolysis, as the resonances may be distorted through shielding of the protons as a consequence of their location within the core of the polymeric star. To this end, a release study was undertaken to enable calculation of the concentration of DMAE, which could be compared to the theoretical concentration based on the conversion values obtained by ^{1}H NMR spectroscopy, with the aim to confirm the release of the small molecule and validate the ^{1}H NMR spectroscopy results.

The study chosen would have to be suitable for use in aqueous conditions, as well as only reacting with DMAE and not the acrylic acid moieties remaining after hydrolysis. Choline oxidase, an oxidoreductase enzyme, catalyses the oxidation of choline to produce betaine aldehyde and hydrogen peroxide (Scheme 3.9).

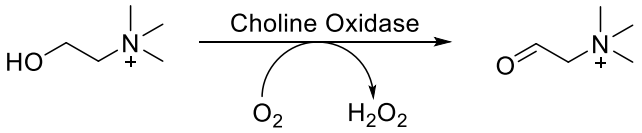

Scheme 3.9 Schematic representation for the production of betaine aldehyde from choline using the enzyme choline oxidase.

It has been shown that whilst DMAE is a competitive inhibitor of choline oxidase,[52] the enzyme does catalyse the oxidation of the small molecule, with the Michaelis-Menten constant (K_m) reported to be approximately 10 times greater for choline oxidase (K_m = 1.3 mM) than DMAE (K_m =14 mM).[53] The production of hydrogen peroxide from the process can then be monitored using a widely accepted colorimetric test,[54] in which *para*-nitrophenyl boronic acid (*p*-NPBA) is reacted with hydrogen peroxide resulting in the production of *para*-nitrophenol, which has an intense absorption at λ = 405 nm (Scheme 3.10).

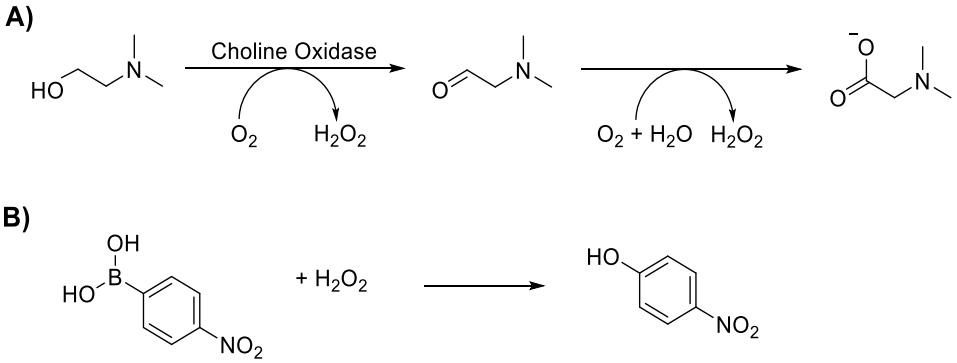

Scheme 3.10 Colorimetric determination of [DMAE] *via* (A) oxidation of DMAE by choline oxidase releasing hydrogen peroxide and (B) production of *p*-nitrophenol by the reaction of hydrogen peroxide with *p*-NPBA.

To enable calculation of the concentration of released DMAE, a calibration curve was first generated, relating the absorbance at λ = 405 nm to the concentration of DMAE. To

that end, a series of solutions of DMAE were analysed, ensuring the maximum concentration of DMAE was 150 μM, as the theoretical maximum concentration based on 100% polymer hydrolysis is 130 μM. Upon addition of *p*-NPBA (4 mM in DMSO) and choline oxidase (7.5 μM in Tris-HCl pH = 8 buffer), the absorbance at λ = 405 nm was monitored for 10 hours (Figure 3.22).

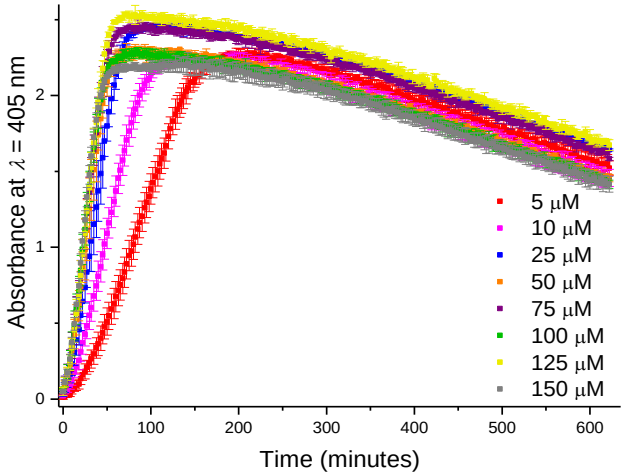

Figure 3.22 UV absorbance profiles at λ = 405 nm for solutions of DMAE of varying concentrations. Error bars produced from the standard deviation of 3 repeats.

Owing to all concentrations reaching approximately the same final absorbance after 10 hours, the initial rate of rise was calculated for all solutions. Plotting the initial rate of rise for the absorbance *vs* concentration of DMAE resulted in a calibration curve which was fitted using an exponential equation (Figure 3.23).

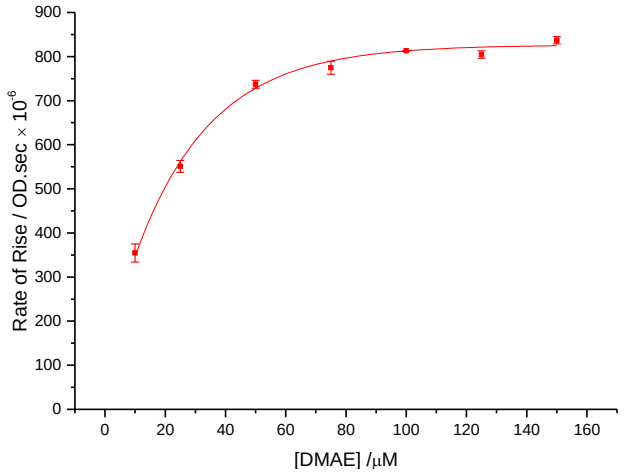

Figure 3.23 Calibration curve for the initial rate of rise of absorbance at λ = 405 nm *vs* the concentration of DMAE. Error bars produced from the standard deviation of 3 repeats.

Following development of the calibration, analysis was carried out on the 20% crosslinked PEGA armed star polymer (**3.1-20**). Polymer was dissolved in 18.2 MΩ.cm water (50 mg/mL) and stirred slowly at room temperature. Aliquots were removed at regular time intervals, the polymer removed from solution using a spin concentrator (5 kDa MWCO) and the resultant supernatant was stored in the freezer until analysis. Using the calibration curve, it can be seen that the concentration of DMAE released is in relatively good agreement with the theoretical concentration based on ^{1}H NMR spectroscopy (Figure 3.24), confirming the release of the small molecule from the core of the star. Moreover, the similarity between the theoretical and enzymatically determined values ratifies the hydrolysis results produced by ^{1}H NMR spectroscopic analysis. It should be noted that the levelling off of the calibration curve to a maximum value of approximately 900 OD/sec × 10^{-6} is attributed to the maximum activity of the enzyme, in which the active site is completely saturated and no increase in substrate concentration will result in a faster rate of rise.

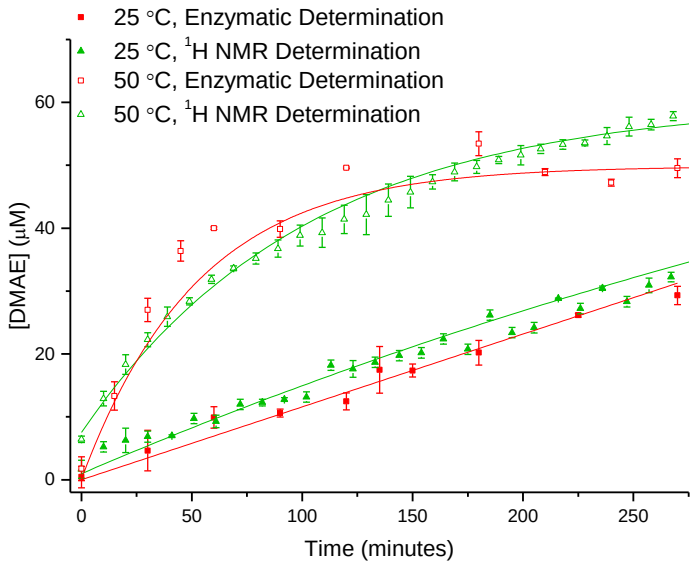

Figure 3.24 Comparison between the theoretical concentration of DMAE released based on ^{1}H NMR spectroscopic analysis (*green*) and enzymatically determined (*red*) at 25 and 50 °C. Error bars produced from the standard deviation of three repeats.

3.4 Conclusion

RAFT polymerisation has been successfully applied to the synthesis of amino-functionalised polymeric stars with differing arm lengths, arm types and varying crosslinking densities in the core of the particles. To understand the hydrolytic behaviour of the amine tethered within the core of the particle, the polymers were studied *in situ* by ^{1}H NMR spectroscopy through monitoring of the signals attributed to both the polymer and the released dimethylaminoethanol. Results indicated that at 25 °C there is little effect of crosslinking density but at the raised temperature of 50 °C an increase in crosslinking density results in lower overall hydrolysis. Moreover, increasing the length of arm was found to demonstrate the same effect, though not as significantly as increasing crosslinking density. It was also indicated that the type of arm had little effect on hydrolysis, suggesting therefore that amines tethered within other architectures, for example self-assembled polymeric micelles, would be expected to exhibit similar hydrolytic behaviour. Analysis of the polymers using an enzymatic assay confirmed that DMAE was released from the polymeric star following hydrolysis, with the assay allowing for determination of the concentration of DMAE which was found to be in good agreement with the theoretical value obtained from ^{1}H NMR spectroscopy.

3.5 Experimental

3.5.1 Materials

The following reagents were used as received: poly(ethylene glycol) methyl ether acrylate (PEGA, M_n – 480 g/mol, Sigma-Aldrich), *N,N'*-(dimethylamino) ethyl acrylate (DMAEA, Sigma-Aldrich, 98%), di(ethylene glycol) diacrylate (DEGDA, Sigma-Aldrich, 75%), methyl acrylate (MA, Sigma-Aldrich, 99%), tris(hydroxymethyl)amine methane hydrochloride

(Tris-HCl, Sigma-Aldrich, 98%) and *para*-nitrophenyl boronic acid (*p*-NPBA, Sigma-Aldrich, 95%). Inhibitor was removed by passing through a plug of basic alumina. The following solvents were used as received: methanol (CH_3OH, Fisher Scientific, LT grade), diethyl ether (Et_2O, Sigma-Aldrich, AR grade), dimethylsulfoxide (DMSO, Fisher Scientific, analytical grade), and hexane (C_6H_{14}, Sigma-Aldrich, laboratory grade). 2,2'-Azobis(isobutyronitrile) (AIBN) was received from Molekula, recrystallised from methanol and stored at 4 °C. Deuterated solvents were received from Apollo Scientific. Dialysed water was used for dialysis. Corning Spin-X UF concentrators (500 μL, 5 kDa MWCO) and the lyophilized powder Choline Oxidase from *Alcaligens sp.* were purchased from Sigma-Aldrich.

3.5.2 Instrumentation

In addition to the instrumentation introduced in section 2.5.2, and with the omission of gas chromatography, mass spectrometry, elemental analysis, foam testing and particle size analysis, and small-angle X-ray scattering, the following instrumentation was used in this Chapter: UV measurements were carried out in triplicate using a FLUO-star Optima plate reader, fitted with an excitation filter at λ = 405 nm, with data analysed using MARS data analysis software v3.01. All TEM images were collected by Dr Anaïs Pitto-Barry (O'Reilly Group, University of Warwick).

3.5.3 Synthetic Methods and Procedures

*Typical procedure for PEGA macro-CTA synthesis (**3.1**, **3.2**, **3.3**):*

*$PEGA_{98}$ (**3.1**)*

Cyanomethyl dodecyl trithiocarbonate (1.0 eq.) and poly(ethylene glycol) monomethyl ether acrylate (PEGA, M_n = 480, 100 eq.) were dissolved in 1,4-dioxane (10 mL) with radical

initiator AIBN (0.2 eq.). Following four freeze-pump-thaw cycles the ampule was refilled with nitrogen and the mixture heated to 70 °C for 3.5 hours (79% conversion). The reaction was quenched by immersion in liquid nitrogen and dialysed extensively against deionized water. The solution was lyophilized yielding a viscous yellow liquid (2.61 g, 70%). ^{1}H NMR (400 MHz, $CDCl_3$): δ (ppm) 4.14 (br s, OCH_2CH_2), 3.39-3.62 (m, $O(CH_2CH_2)_8$) and $SCH_2(CH_2)_9$), 3.32 (s, CH_2OCH_3), 1.20-2.33 (m, CH_2 backbone, $CH_2(CH_2)_{10}$ CTA), 0.80 (t, 3H, $(CH_2)_{10}CH_3$, $^{3}J_{H\text{-}H}$ = 6.1 Hz). $M_{w,\,SEC}$ = 67.5 kg/mol, $M_{n,\,SEC}$ = 44.7 kg/mol, $Đ_M$ = 1.51.

PEGA$_{148}$ (**3.2**)

^{1}H NMR (400 MHz, $CDCl_3$): δ (ppm) 4.16 (br s, OCH_2CH_2), 3.47-3.89 (m, $O(CH_2CH_2)_8$ and $SCH_2(CH_2)_9$), 3.38 (s, CH_2OCH_3), 1.25-2.29 (m, CH_2 backbone, $CH_2(CH_2)_{10}$ CTA), 0.88 (t, 3H, $(CH_2)_{10}CH_3$, $^{3}J_{H\text{-}H}$ = 6.0 Hz). $M_{w,\,SEC}$ = 75.8 kg/mol, $M_{n,\,SEC}$ = 46.2 kg/mol, $Đ_M$ = 1.64.

PEGA$_{288}$ (**3.3**)

^{1}H NMR (400 MHz, $CDCl_3$): δ (ppm) 4.17 (br s, OCH_2CH_2), 3.47-3.82 (m, $O(CH_2CH_2)_8$ and $SCH_2(CH_2)_9$), 3.38 (s, CH_2OCH_3), 1.26-2.67 (m, CH_2 backbone, $CH_2(CH_2)_{10}$ CTA), 0.88 (t, 3H, $(CH_2)_{10}CH_3$, $^{3}J_{H\text{-}H}$ = 6.1 Hz). $M_{w,\,SEC}$ = 71.4 kg/mol, $M_{n,\,SEC}$ = 47.0 kg/mol, $Đ_M$ = 1.52.

*Typical procedure for the chain extension of PEGA with DMAEA and DEGDA (**3.1-20**, **3.1-15**, **3.1-10**, **3.2-20**, **3.3-20**)*

PEGA macro-CTA (**1**, 1.0 eq.), DMAEA (200 eq.), and DEGDA (40 eq.) were dissolved in 1,4-dioxane (7 mL) together with radical initiator AIBN (0.2 eq.). Following four freeze-pump-thaw cycles the ampule was refilled with nitrogen and the mixture heated to 70 °C for 24 hours (58% conversion). The reaction was quenched by immersion in liquid nitrogen and purified by precipitation into 5:1 hexane/ diethyl ether, affording a viscous pale yellow liquid (0.24 g, 70%).

*20% Crosslinked Polymer (**3.1-20**)*

^{1}H NMR (400 MHz, $CDCl_3$): δ (ppm) 4.16 (br s, OCH_2CH$_2$, OCH_2CH$_2$O(CH$_2$CH$_2$O)$_7$ and CH_2CH$_2$N), 3.46-3.80 (m, O(CH_2CH_2O)$_8$ and OCH$_2$CH_2O), 3.38 (s, CH$_2$OCH_3 and SCH_2(CH$_2$)$_9$), 2.62 (br s, CH_2N), 2.23 (br s, N(CH_3)$_2$), 1.24-2.06 (m, CH_2 backbone, CH$_2$(CH_2)$_{10}$ CTA), 0.88 (t, 3H, (CH$_2$)$_{10}$CH_3, $^{3}J_{H\text{-}H}$ = 6.1 Hz. ^{13}C NMR (100 MHz, $CDCl_3$): δ (ppm) 178.2 (*C*=O), 66.9 (O*C*CO), 63.2 (O*C*CN), 62.2 (OC*C*O), 58.8 (O*C*H$_3$), 57.4 (OC*C*N), 45.6 (N(*C*H$_3$)$_2$), 41.1 (C(*C*H)CH$_2$). IR (neat) max/cm^{-1}: 2929, 2866 ($\upsilon_{C\text{-}H}$), 2768 ($\upsilon_{N\text{-}CH_3}$), 1732 ($\upsilon_{C=O}$), 1451 ($\upsilon_{C\text{-}O,\ ester}$), 1099 ($\upsilon_{C\text{-}O}$). $M_{w,\ SEC}$ = 53.6 kg/mol, $M_{n,\ SEC}$ = 23.8 kg/mol, $Đ_M$ = 2.25. D_h = 11 nm ± 1 nm (PD = 0.35).

*15% Crosslinked Polymer (**3.1-15**)*

^{1}H NMR (400 MHz, $CDCl_3$): δ (ppm) 4.17 (br s, OCH_2CH$_2$O, OCH_2CH$_2$O(CH$_2$CH$_2$O)$_7$, and CH_2CH$_2$N), 3.47-3.70 (m, O(CH_2CH_2)$_8$, SCH_2(CH$_2$)$_9$ and OCH$_2$CH_2O), 3.32 (s, CH$_2$OCH_3), 2.54 (br s, CH_2N), 2.27 (br s, N(CH_3)$_2$), 1.25-2.03 (m, CH_2 backbone, CH$_2$(CH_2)$_{10}$ CTA), 0.88 (t, 3H, (CH$_2$)$_{10}$CH_3, $^{3}J_{H\text{-}H}$ = 6.2 Hz). ^{13}C NMR (100 MHz, $CDCl_3$): δ (ppm) 178.3 (*C*=O), 68.7 (O*C*CO), 63.2 (O*C*CN), 62.2 (OC*C*O), 58.9 (O*C*H$_3$), 57.4 (OC*C*N), 45.6 (N(*C*H$_3$)$_2$), 40.9 (C(*C*H)CH$_2$). IR (neat) max/cm^{-1}: 2929, 2866($\upsilon_{C\text{-}H}$), 2777 ($\upsilon_{N\text{-}CH_3}$), 1732 ($\upsilon_{C=O}$), 1447 ($\upsilon_{C\text{-}O,\ ester}$), 1106 ($\upsilon_{C\text{-}O}$). $M_{w,\ SEC}$ = 114.9 kg/mol, $M_{n,\ SEC}$ = 39.9 kg/mol, $Đ_M$ = 2.88. D_h = 9 nm ± 1 nm (PD = 0.28).

*10% Crosslinked Polymer (**3.1-10**)*

^{1}H NMR (400 MHz, $CDCl_3$): δ (ppm) 4.18 (br s, OCH_2CH$_2$O, OCH_2CH$_2$O(CH$_2$CH$_2$O)$_7$ and CH_2CH$_2$N), 3.45-3.80 (m, O(CH_2CH_2)$_8$, SCH_2(CH$_2$)$_9$ and OCH$_2$CH_2O), 3.32 (s, CH$_2$OCH_3), 2.62 (br s, CH_2N), 2.23 (br s, N(CH_3)$_2$), 1.29-2.06 (m, CH_2 backbone, CH$_2$(CH_2)$_{10}$ CTA), 0.90 (t, 3H, (CH$_2$)$_{10}$CH_3, $^{3}J_{H\text{-}H}$ = 6.0 ^{13}C NMR (100 MHz, $CDCl_3$): δ (ppm) 178.2 (*C*=O), 66.9 (O*C*CO), 63.2 (O*C*CN), 62.1 (OC*C*O), 58.7 (O*C*H$_3$), 57.7 (OC*C*N), 45.6 (N(*C*H$_3$)$_2$),

41.1 (C(*C*H)CH_2). IR (neat) max/cm^{-1}: 2929, 2856 (υ_{C-H}), 2768 (υ_{N-CH_3}), 1732 ($\upsilon_{C=O}$), 1450 ($\upsilon_{C-O,\ ester}$), 1100 (υ_{C-O}). $M_{w,\ SEC}$ = 98.6 kg/mol, $M_{n,\ SEC}$ = 43.8 kg/mol, $Đ_M$ = 2.25. D_h = 10 nm ± 1 nm (PD = 0.46).

*20% Crosslinked Polymer (**3.2-20**)*

^{1}H NMR (400 MHz, $CDCl_3$): δ (ppm) 4.16 (br s, OC$H_2$$CH_2$, OC$H_2$$CH_2$O($CH_2CH_2$O)$_7$ and C$H_2$$CH_2$N), 3.47-3.82 (m, O(C$H_2CH_2$)$_8$, SC$H_2$($CH_2$)$_9$ and OCH_2CH_2O), 3.38 (s, CH_2OCH_3), 2.54 (br s, CH_2N), 2.27 (br s, N(CH_3)$_2$), 1.25-2.10 (m, CH_2 backbone, CH_2(CH_2)$_{10}$ CTA), 0.88 (t, 3H, (CH_2)$_{10}$CH_3, $^3J_{H-H}$ = 6.2 Hz). ^{13}C NMR (100 MHz, $CDCl_3$): δ (ppm) 178.2 (*C*=O), 66.9 (O*C*CO), 63.2 (O*C*CN), 62.3 (OC*C*O), 58.4 (O*C*H_3), 57.5 (OC*C*N), 45.9 (N(*C*H_3)$_2$), 41.0 (C(*C*H)CH_2). IR (neat) max/cm^{-1}: 2948, 2868 (υ_{C-H}), 2763 (υ_{N-CH_3}), 1732 ($\upsilon_{C=O}$), 1452 ($\upsilon_{C-O,\ ester}$), 1100 (υ_{C-O}). $M_{w,\ SEC}$ = 16.5 kg/mol, $M_{n,\ SEC}$ = 66.3 kg/mol, $Đ_M$ = 114.7. D_h = 11 nm ± 1 nm (PD = 0.54).

*20% Crosslinked Polymer (**3.3-20**)*

^{1}H NMR (400 MHz, $CDCl_3$): δ (ppm) 4.12 (br s, OC$H_2$$CH_2$, OC$H_2$$CH_2$O($CH_2CH_2$O)$_7$ and C$H_2$$CH_2$N), 3.41-3.73 (m, O(C$H_2CH_2$)$_8$, SC$H_2$($CH_2$)$_9$ and OCH_2CH_2O), 3.24 (s, CH_2OCH_3), 2.57 (br s, CH_2N), 2.15 (br s, N(CH_3)$_2$), 1.13-2.00 (m, CH_2 backbone, CH_2(CH_2)$_{10}$ CTA), 0.78 (t, 3H, (CH_2)$_{10}$CH_3, $^3J_{H-H}$ = 6.2 ^{13}C NMR (100 MHz, $CDCl_3$): δ (ppm) 178.2 (*C*=O), 66.9 (O*C*CO), 63.0 (O*C*CN), 62.3 (OC*C*O), 58.6 (O*C*H_3), 57.4 (OC*C*N), 45.7 (N(*C*H_3)$_2$), 41.1 (C(*C*H)CH_2). IR (neat) max/cm^{-1}: 2948, 2867 (υ_{C-H}), 2761 (υ_{N-CH_3}), 1732 ($\upsilon_{C=O}$), 1452 ($\upsilon_{C-O,\ ester}$), 1098 (υ_{C-O}). $M_{w,\ SEC}$ = 78.9 kg/mol, $M_{n,\ SEC}$ = 43.6 kg/mol, $Đ_M$ = 1.81. D_h = 11 nm ± 1 nm (PD = 0.33).

*Typical procedure for HEA macro-CTA synthesis (**3.4**):*

Cyanomethyl dodecyl trithiocarbonate (1.0 eq.), HEA (120 eq.) and radical initiator AIBN (0.25 eq.) were dissolved in methanol (10 mL). Following four freeze-pump-thaw cycles the ampule was refilled with nitrogen and the mixture heated to 60 °C for 3 hours (86% conversion). The mixture was quenched by immersion in liquid nitrogen and purified by precipitation into cold diethyl ether, yielding a viscous yellow liquid (2.89 g, 74%). ^{1}H NMR (400 MHz, DMSO-d_6): δ (ppm) 4.77 (br s, CH_2OH) 4.12 (br s, $CO_2CH_2CH_2$), 3.56 (br s, CH_2CH_2OH and $SCH_2(CH_2)_9$), 1.24-2.26 (m, CH_2 backbone, $CH_2(CH_2)_{10}$ CTA), 0.85 (t, 3H, $(CH_2)_{10}CH_3$, $^{3}J_{H\text{-}H}$ = 7.0 Hz). ^{13}C NMR (100 MHz, DMSO-d_6): δ (ppm) 174.6 (C=O), 66.1 (OCCO), 59.3 (OCCO), 41.3 ((C=O)CHCH$_2$). IR (neat) max/cm^{-1}: 3403 (υ_{OH}), 2951 ($\upsilon_{C\text{-}H}$), 1723 ($\upsilon_{C=O}$), 1158 ($\upsilon_{C\text{-}O}$). $M_{w,\,SEC}$ = 22.2 kg/mol, $M_{n,\,SEC}$ = 20.2 kg/mol, $Đ_M$ = 1.10.

*Typical procedure for the chain extension of HEA with DMAEA and DEGDA (**3.4-20**, **3.4-15**, **3.4-10**):*

PHEA macro-CTA (**3**, 1.0 eq.), DMAEA (200 eq.) and DEGDA (40 eq.) were dissolved in 1,4-dioxane (5 mL) together with radical initiator AIBN (0.25 eq.). Following four freeze-pump-thaw cycles the ampule was refilled with nitrogen and the mixture heated to 65 °C for 24 hours (53% conversion). The reaction was quenched by immersion in liquid nitrogen, and purified by precipitation into 5:1 hexane/diethyl ether, affording a viscous pale yellow liquid (0.14 g, 27%).

*20% Crosslinked Polymer (**3.4-20**)*

^{1}H NMR (400 MHz, DMSO-d_6): δ (ppm) 4.75 (br s, CH_2OH), 4.02 (br s, OCH_2CH_2OH and OCH_2CH_2O), 3.33 (br s, OCH_2CH_2OH, $SCH_2(CH_2)_9$ and OCH_2CH_2O), 2.50 (br s, CH_2N), 2.17 (br s, $N(CH_3)_2$), 1.60-1.80 (m, CH_2 backbone, $CH_2(CH_2)_{10}$ CTA), 0.88 (br s, 3H,

$(CH_2)_{10}CH_3$). $M_{w,\ SEC}$ = 45.4 kg/mol, $M_{n,\ SEC}$ = 29.1 kg/mol, $Đ_M$ = 1.56. D_h = 23 nm ± 1 nm (PD = 0.43).

*15% Crosslinked Polymer (**3.4-15**)*

^{1}H NMR (400 MHz, DMSO-d_6): δ (ppm) 4.73 (br s, CH_2OH), 4.01 (br s, OCH_2CH_2OH and OCH_2CH_2O), 3.31 (br s, OCH_2CH_2OH, $SCH_2(CH_2)_9$ and OCH_2CH_2O), 2.49 (br s, CH_2N), 2.15 (br s, $N(CH_3)_2$), 1.58-1.79 (m, CH_2 backbone, $CH_2(CH_2)_{10}$ CTA),), 0.87 (br s, 3H, $(CH_2)_{10}CH_3$). $M_{w,\ SEC}$ = 33.9 kg/mol, $M_{n,\ SEC}$ = 27.1 kg/mol, $Đ_M$ = 1.25. D_h = 14 nm ± 1 nm (PD = 0.16).

*10% Crosslinked Polymer (**3.4-10**)*

^{1}H NMR (400 MHz, DMSO-d_6): δ (ppm) 4.73 (br s, CH_2OH), 4.00 (br s, OCH_2CH_2OH and OCH_2CH_2O), 3.34 (br s, OCH_2CH_2OH, $SCH_2(CH_2)_9$ and OCH_2CH_2O), 2.44 (br s, CH_2N), 2.25 (br s, $N(CH_3)_2$), 1.39-1.90 (m, CH_2 backbone, $CH_2(CH_2)_{10}$ CTA),), 0.88 (br s, 3H, $(CH_2)_{10}CH_3$).). $M_{w,\ SEC}$ = 32.6 kg/mol, $M_{n,\ SEC}$ = 24.9 kg/mol, $Đ_M$ = 1.31. D_h = 25 nm ± 1 nm (PD = 0.05).

Typical procedure for the chain extension of PEGA with DMAEA and MA:

PEGA macro-CTA (1.0 eq.), DMAEA (200 eq.) and MA (40 eq.) were dissolved in 1,4-dioxane (1.5 mL) together with radical initiator AIBN (0.2 eq.). Following four freeze-pump-thaw cycles the ampule was refilled with nitrogen and the mixture heated to 70 °C for 24 hours (67 % conversion). The reaction was quenched by immersion in liquid nitrogen and purified by precipitation into 5:1 hexane/ diethyl ether, affording a viscous pale yellow liquid (0.18 g, 57 %). ^{1}H NMR (400 MHz, $CDCl_3$): δ (ppm) 4.15 (br s, OCH_2CH_2), 3.55-3.65 (m, OCH_3, $O(CH_2CH_2)_8$, and $SCH_2(CH_2)_9$), 3.38 (s, CH_2OCH_3), 2.54 (br s, CH_2N), 2.27 (br s, $N(CH_3)_2$), 1.25-1.89 (m, CH_2 backbone, $CH_2(CH_2)_{10}$ CTA), 0.87 (t, 3H, $(CH_2)_{10}CH_3$, $^3J_{H\text{-}H}$ =

6.1 Hz). IR (neat) max/cm^{-1}: 3415 (υ_{OH}), 2962 (υ_{C-H}), 1712 ($\upsilon_{C=O}$), 1445 ($\upsilon_{C-O,\ ester}$), 1158 (υ_{C-O}). $M_{w,\ SEC}$ = 57.0 kg/mol, $M_{n,\ SEC}$ = 33.5 kg/mol, $Đ_M$ = 1.70.

Hydrolysis Analysis:

Polymers (30 mg,) were dissolved in D_2O (0.6 mL) and stirred for 5 minutes. The solution was transferred into an NMR tube. Measurements were taken at various time intervals at both 25 °C and 50 °C. The percentage hydrolysis was calculated according to Equation 3.1, using the integrals for the CH_2N of the dimethylaminoethanol and the corresponding polymer resonance at δ = 3.20 ppm and δ = 3.08 ppm, respectively (PEGA armed particles), and δ =2.85 and δ = 2.64 ppm for HEA particles.

$$\%\ \text{hydrolysis} = \frac{I_{3.20\ ppm}}{I_{3.20\ ppm} + I_{3.08\ ppm}}$$

Equation 3.1: Hydrolysis Determination

Enzymatic determination of [DMAE]:

For the production of the calibration curve, solutions of DMAE of varying concentrations (0-150 μM in 18.2 MΩ.cm water) were produced. 50 μL samples of each concentration (3 repeats) were added to the 96 well plate, and *p*-NPBA(4 mM in DMSO) and choline oxidase (7.5 μM in Tris-HCl pH = 8 buffer) were added and the assay analysed for 10 hours, monitoring the initial rate of raise for the UV absorbance at λ = 405 nm, attributed to the *p*-nitrophenol produced. Fitting of the resultant data produced a calibration of:

$$\text{Rate of Rise} = 826.41 + (-712.02e^{(-0.04x)})$$

Equation 3.2: Exponential fit for calibration data allowing for determination of [DMAE]

For analysis of the polymer samples, preparation of the 96 well plate was a follows: at each time point a 250 μL aliquot of the polymer solution (50 mg/ mL in 18.2 MΩ.cm water) was purified twice through removal of the polymer (Corning Spin-X UF concentrators, 500μL 5kDa MWCO) and the resultant supernatant stored in the freezer. Upon completion of sampling, 50 μL samples of each time point (3 repeats) were added to the 96 well plate, and *p*-NPBA(4 mM in DMSO) was added. Following addition of all the samples and *p*-NPBA solution, choline oxidase (7.5 μM in Tris-HCl pH = 8 buffer) was added and the plate analysed for 10 hours.

3.6 Bibliography

1. Barner-Kowollik, C., Davis, T. P., Stenzel, M. H., *Aust. J. Chem.*, **2006**, 59, 719.
2. Mayadunne, R. T. A., Jeffery, J., Moad, G., Rizzardo, E., *Macromolecules*, **2003**, 36, 1505.
3. Stenzel-Rosenbaum, M., Davis, T. P., Chen, V., Fane, A. G., *J. Polym. Sci., Part A: Polym. Chem.*, **2001**, 39, 2777.
4. Quinn, J. F., Chaplin, R. P., Davis, T. P., *J. Polym. Sci., Part A: Polym. Chem.*, **2002**, 40, 2956.
5. Zheng, G., Pan, C., *Polymer*, **2005**, 46, 2802.
6. Chaffey-Millar, H., Stenzel, M. H., Davis, T. P., Coote, M. L., Barner-Kowollik, C., *Macromolecules*, **2006**, 39, 6406.
7. Gao, H., Matyjaszewski, K., *Prog. Polym. Sci.*, **2009**, 34, 317.
8. Wu, W., Wang, W., Li, J., *Prog. Polym. Sci.*, **2015**, 46, 55.
9. Lapienis, G., *Prog. Polym. Sci.*, **2009**, 34, 852.
10. Jeong, B., Choi, Y. K., Bae, Y. H., Zentner, G., Kim, S. W., *J. Control. Release*, **1999**, 62, 109.
11. Qiu, L., Bae, Y., *Pharm. Res.*, **2006**, 23, 1.
12. Whittell, G. R., Hager, M. D., Schubert, U. S., Manners, I., *Nature Mater.*, **2011**, 10, 176.
13. Helms, B., Guillaudeu, S. J., Xie, Y., McMurdo, M., Hawker, C. J., Fréchet, J. M. J., *Angew. Chem., Int. Ed.*, **2005**, 44, 6384.
14. Kobayashi, S., Akiyama, R., *Chem. Commun.*, **2003**, 449.
15. Liu, J., Duong, H., Whittaker, M. R., Davis, T. P., Boyer, C., *Macromol. Rapid Commun.*, **2012**, 33, 760.
16. Hadjichristidis, N., Hirao, A., Tezuka, Y., Du Prez, F., *Complex Macromolecular Architectures: Synthesis, Characterization, and Self-Assembly*, Wiley-VCH Verlag GmbH & Co. KGaA, **2011**.
17. Carey, F. A., Sundberg, R. J., *Advanced Organic Chemistry: Part A: Structure and Mechanisms*, Springer US, **2007**.
18. Datta, S., Day, J., Ingold, C., *J. Chem. Soc.*, **1939**, 838.
19. Day, J., Ingold, C., *Transactions of the Faraday Society*, **1941**, 37, 686.
20. Clayden, J., Greeves, N., Warren, S., *Organic Chemistry*, Oxford University Press, **2012**.

21. da Silva, P. L., Guimarães, L., Pliego, J. R., *J. Phys. Chem. B*, **2013**, 117, 6487.
22. Wolfenden, R., Yuan, Y., *J. Am. Chem. Soc.*, **2011**, 133, 13821.
23. Kanerva, L. T., Euranto, E. K., *J. Am. Chem. Soc.*, **1982**, 104, 5419.
24. Euranto, E. K., Cleve, N. J., *Acta Chem. Scand.*, **1963**, 17, 1584.
25. Jo, Y. S., Gantz, J., Hubbell, J. A., Lutolf, M. P., *Soft Matter*, **2009**, 5, 440.
26. Nair, L. S., Laurencin, C. T., *Prog. Polym. Sci.*, **2007**, 32, 762.
27. Chandra, R., Rustgi, R., *Prog. Polym. Sci.*, **1998**, 23, 1273.
28. Uhrich, K. E., Cannizzaro, S. M., Langer, R. S., Shakesheff, K. M., *Chem. Rev.*, **1999**, 99, 3181.
29. Agarwal, S., *Polym. Chem.*, **2010**, 1, 953.
30. Tsarevsky, N. V., Sumerlin, B. S., Matyjaszewski, K., Chiefari, J., *Controlled Radical Polymerization: Mechanisms*, American Chemical Society, 2015; Vol. 1187.
31. Hedir, G. G., Bell, C. A., O'Reilly, R. K., Dove, A. P., *Biomacromolecules*, **2015**, 16, 2049.
32. Bevington, J. C., Eaves, D. E., Vale, R. L., *J. Polym. Sci., Part A: Polym. Chem.*, **1958**, 32, 317.
33. Mallik, K. L., Das, M. N., *Naturwissenschaften*, **1964**, 51, 37.
34. Freidig, A. P., Verhaar, H. J. M., Hermens, J. L. M., *Environ. Toxicol. Chem.*, **1999**, 18, 1133.
35. van de Wetering, P., Zuidam, N. J., van Steenbergen, M. J., van der Houwen, O. A. G. J., Underberg, W. J. M., Hennink, W. E., *Macromolecules*, **1998**, 31, 8063.
36. Truong, N. P., Jia, Z., Burges, M., McMillan, N. A. J., Monteiro, M. J., *Biomacromolecules*, **2011**, 12, 1876.
37. Gillard, M., Jia, Z., Gray, P. P., Munro, T. P., Monteiro, M. J., *Polym. Chem.*, **2014**, 5, 3372.
38. Truong, N. P., Gu, W., Prasadam, I., Jia, Z., Crawford, R., Xiao, Y., Monteiro, M. J., *Nat. Commun.*, **2013**, 4, 1902.
39. Cotanda, P., Wright, D. B., Tyler, M., O'Reilly, R. K., *J. Polym. Sci., Part A: Polym. Chem.*, **2013**, 51, 3333.
40. Gu, W., Jia, Z., Truong, N. P., Prasadam, I., Xiao, Y., Monteiro, M. J., *Biomacromolecules*, **2013**, 14, 3386.
41. Hartono, S. B., Phuoc, N. T., Yu, M., Jia, Z., Monteiro, M. J., Qiao, S., Yu, C., *J. Mater. Chem. B*, **2014**, 2, 718.
42. Zhao, W., Fonsny, P., FitzGerald, P., Warr, G. G., Perrier, S., *Polym. Chem.*, **2013**, 4, 2140.
43. Zeng, W., Du, Y., Xue, Y., Frisch, H. L., Mark–Houwink–Staudinger–Sakurada Constants, *Physical Properties of Polymers Handbook*, Springer New York, **2007**.
44. Hiemenz, P. C., Lodge, T. P., *Polymer Chemistry, Second Edition*, Taylor & Francis, **2007**.
45. James, A. B., David, M. H., Becer, C. R., Synthesis and SEC Characterization of Poly(methyl methacrylate) Star Polymers, *Progress in Controlled Radical Polymerization: Materials and Applications*, American Chemical Society, **2012**.
46. Radke, W., Chromatography of Polymers, *Macromolecular Engineering*, Wiley-VCH Verlag GmbH & Co. KGaA, **2007**.
47. McEwan, K., Randev, R. K., Haddleton, D. M., *Analysis of Star Polymers Using the Agilent 1260 Infinity Multi-Detector GPC/SEC System*, Agilent Technologies, Inc., **2013**.
48. Patterson, J. P., Sanchez, A. M., Petzetakis, N., Smart, T. P., Epps III, T. H., Portman, I., Wilson, N. R., O'Reilly, R. K., *Soft Matter*, **2012**, 8, 3322.
49. Patterson, J. P., Robin, M. P., Chassenieux, C., Colombani, O., O'Reilly, R. K., *Chem. Soc. Rev.*, **2014**, 43, 2412.

50. Bian, K., Cunningham, M. F., *Macromolecules*, **2005**, 38, 695.
51. Higuchi, M., Senju, R., *Polym. J.*, **1972**, 3, 370.
52. Lohr, J., Acara, M., *J. Pharmacol. Exp. Ther.*, **1990**, 252, 154.
53. Yamada, H., Mori, N., Tani, Y., *Agric. Biol. Chem.*, **1979**, 43, 2173.
54. Lu, C.-P., Lin, C.-T., Chang, C.-M., Wu, S.-H., Lo, L.-C., *J. Agric. Food Chem.*, **2011**, 59, 11403.

4. The Synthesis and Catalytic Evaluation of Responsive Polymeric Stars through the Introduction of Responsive Crosslinkers

4.1 Abstract

The potential to exploit the responsive behaviour of polymers for catalysis was explored, through either probing the swelling of the polymeric stars introduced in Chapter 2, which contain a tri(ethylene glycol) dimethacrylate (TEGDMA) crosslinker, by the introduction of a thermoresponsive crosslinker utilising Diels-Alder chemistry, or through the introduction of a redox responsive disulfide crosslinker. Initial tests examining the swelling properties of the TEGDMA crosslinked particles suggested some thermoresponsive behaviour, with apparent catalytic activity in the polyurethane (PU) formulation attributed to both the catalyst swelling and the ability of the polymers to act as a nucleating agent and improve formulation mixing. Introduction of a furan-maleimide based crosslinker, through continuation of the arm-first methodology for star polymer synthesis applied in the previous Chapters, produced thermoresponsive polymeric stars utilising Diels-Alder chemistry. The thermoresponsive behaviour has been spectroscopically investigated, confirming the retro Diels-Alder reaction occurs within the desired temperature range (50-60 °C). Evaluation of these polymers in the rigid polyurethane formulation was found to be inconclusive, with little to no difference in the foam rise profiles. Moreover, catalytic evaluation of these polymers for the Knoevenagel reaction further indicated no difference on catalytic ability between the non-responsive TEGDMA crosslinked polymers and the responsive Diels-Alder crosslinked polymers, except when the experimental set-up was tailored to favour the Diels-Alder crosslinked polymer. Incorporation of the disulfide crosslinker bis(2-methacryloyl)oxyethyl disulfide and analysis in the rigid PU formulation confirmed the suitability of the catalyst towards the one pot formulation, with foam rise profiles matching the blank profile prior to addition of the reducing agent, yet demonstrating accelerated foam rise upon addition of the reducing agent.

4.2 Introduction

Reversible-covalent chemistry allows for the production of polymers with increased structural stability owing to the stronger covalent bonds compared to other weaker supramolecular interactions, yet still maintains the reversibility exhibited by supramolecular interactions.[1] Readily applied to the field of polymers, reversible-covalent chemistry allows for the production of multiple polymeric architectures. Indeed, the use of such chemistries has been reported for the production of hyperbranched,[2-4] cyclic,[5-7] and star polymers.[1, 8] Moreover, the dynamic nature of this chemistry has significantly advanced the field of self-healing and responsive materials, with the reversibility of dynamic disulfide bonds, in addition to Diels-Alder reactions, most prevalent in the literature.[9-14]

Commonly encountered in nature, where the formation of new disulfide bonds between cysteine residues results in protein folding and is therefore instrumental in protein function, the reversibility of disulfide bonds is readily exploited for polymeric materials through either redox cleavage/coupling or by using thiol/disulfide exchange (Scheme 4.1).[1, 15]

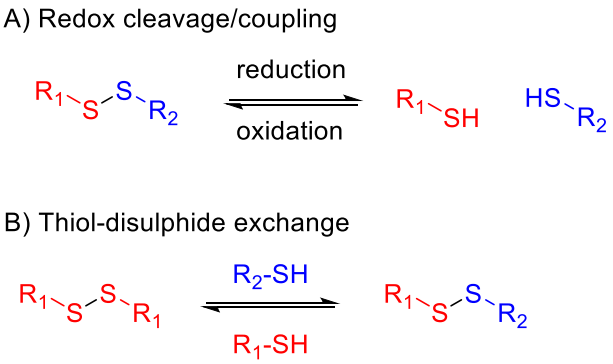

Scheme 4.1 Schematic representation of the reversible-covalent reactions which disulfides are able to undergo (A) redox cleavage/coupling, and (B) thiol-disulfide exchange. Reproduced with permission from Gao *et al.*[7]

Tsarevsky and Matyjaszweski reported the use of the redox cleavage of disulfides in the production of degradable poly(methyl methacrylate) gels, with reduction producing free thiols allowing the material to act as a "superinitiator" for the polymerisation of styrene (Scheme 4.2).[16]

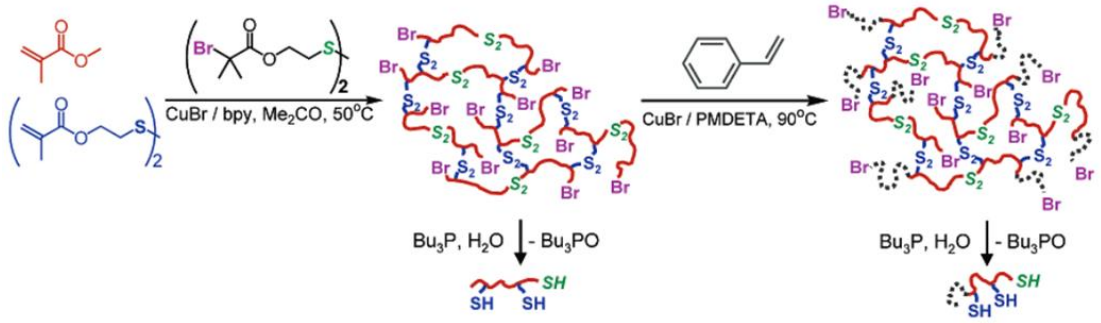

Scheme 4.2 Schematic representation of the preparation of degradable poly(methyl methacrylate) based gels using atom-transfer radical polymerisation, and their use as "supermacroinitiators". Reproduced with permission from Tsarevsky *et al.*[16]

Pal *et al.* further demonstrated the use of the disulfide redox chemistry, producing responsive hyperbranched polymers with the ability to reversibly produce core-crosslinked star polymers.[17] Upon reduction of the hyperbranched poly(*N*-isopropylacrylamide-*co*-*N,N'*-bis(acryloyl)cystamine)-*star*-(dimethyl acrylamide), the resultant polymer could be further oxidised to produce core-crosslinked star copolymers (Scheme 4.3). In addition to the production of responsive materials using the redox chemistry of disulfides, the thiol/disulfide exchange reaction has also been applied to self-healing materials.[18-20] In order to investigate the mechanism of disulfide exchange, Pepels and co-workers developed pH sensitive disulfide crosslinked self-healing thermoset materials.[21] It was noted that the thiol curing agent underwent good exchange with the commercial polysulfide during curing, resulting in a different network morphology, with the same mechanism responsible for the self-healing ability.

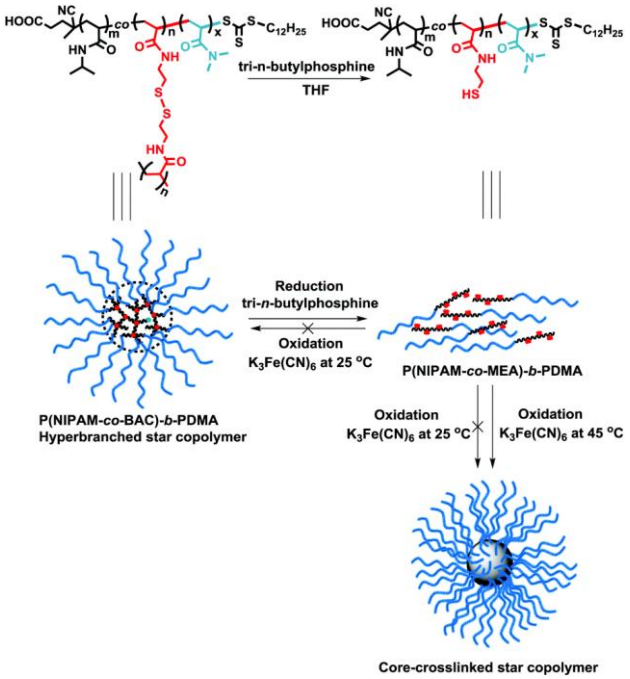

Scheme 4.3 Schematic representation of the degradation of a hyperbranched star polymer and formation of a core-crosslinked star copolymer *via* redox reactions. Reproduced with permission from Pal *et al.*[17]

A commonly applied alternative to disulfide chemistry, the application of Diels-Alder chemistry to the development of responsive polymers has been greatly reported over the last couple of decades,[22, 23] with numerous studies applying different Diels-Alder chemistries to produce thermoresponsive materials.[22, 24] Applications of such polymers range from biomedical applications such as drug delivery,[25, 26] through to self-healable materials.[27-30] One advantage of such chemistry is the requirement for only heat to be applied in order to trigger a reaction, whereas the addition of a reducing/oxidation agent, or a thiol, is required in order to instigate a change in the disulfide crosslinking which may have a detrimental impact for certain applications, for example affecting the final cure in PU foams.

A thermally reversible reaction, the Diels-Alder reaction was developed by Otto Diels and Kurt Alder in the late 1920s.[31] The reaction proceeds *via* a concerted [4+2] cycloaddition reaction involving the transfer of 4 π electrons from the electron rich diene and 2 π electrons from the electron poor dienophile, and driven by the formation of energetically more stable σ

bonds (Scheme 4.4). Commonly used dienes include anthracene, cyclopentadiene and furan, with maleimides and alkenes frequently employed as the dienophile.[22, 32]

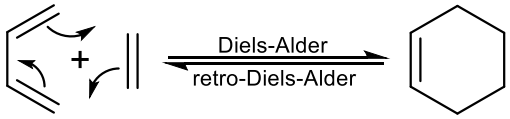

Scheme 4.4 Schematic representation for the general mechanism for the Diels-Alder/retro-Diels-Alder reaction between a diene and a dienophile.

One of the earliest reports of using Diels-Alder chemistry with a view towards polymers was reported by Stille and Plummer, using biscyclopentadienes and benzoquinone to produce high molecular weight polymers.[33] The copolymerisation of a biscyclopentadiene with either *p*-benzoquinone or bismaleimide allowed to the production of high molecular weight polymers by utilising the Diels-Alder reaction between the maleimide and cyclopentadiene as a propagating mechanism for the polymerisation.

Frequently used in conjunction with controlled polymerisation methods, the Diels-Alder conjugation reaction is also used to produce polymers with complex architectures. Indeed, Diels-Alder chemistry has been applied to the synthesis of telechelic polymers, block copolymers and, frequently, star polymer architectures.[22, 34, 35] Indeed, Bapat *et al*. demonstrated the ability to produce dynamic-covalent star polymers able to reversibly transition from unimers to stars through the use of pendent furans and bismaleimides (Scheme 4.5).[1]

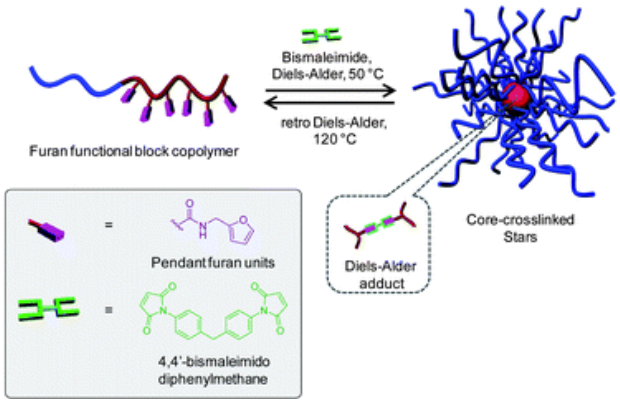

Scheme 4.5 Schematic representation of dynamic-covalent stars through the use of Diels-Alder chemistry. Reproduced with permission from Bapat *et al*.[1]

Additionally, studies by Altinbasak and co-workers combined both the disulfide and Diels-Alder covalent chemistry to encapsulate bovine serum albumin within a hydrogel which, upon addition of a reducing agent, released the protein (Scheme 4.6).[36] Similar to the application of the dynamic disulfide chemistry, the Diels-Alder reaction is highly prevalent in the field of self-healable materials, with polymers using the furan-maleimide Diels-Alder reaction readily reported.[37-40] In contrast to the disulfide based materials, the material only has to be heated in order for the retro-Diels-Alder reaction to occur and heal the material. Indeed, the process can be repeated multiple times, with both Kötteritzsch *et al.* and Peterson *et al.* both reporting healing efficiencies averaging over 70%.[41, 42]

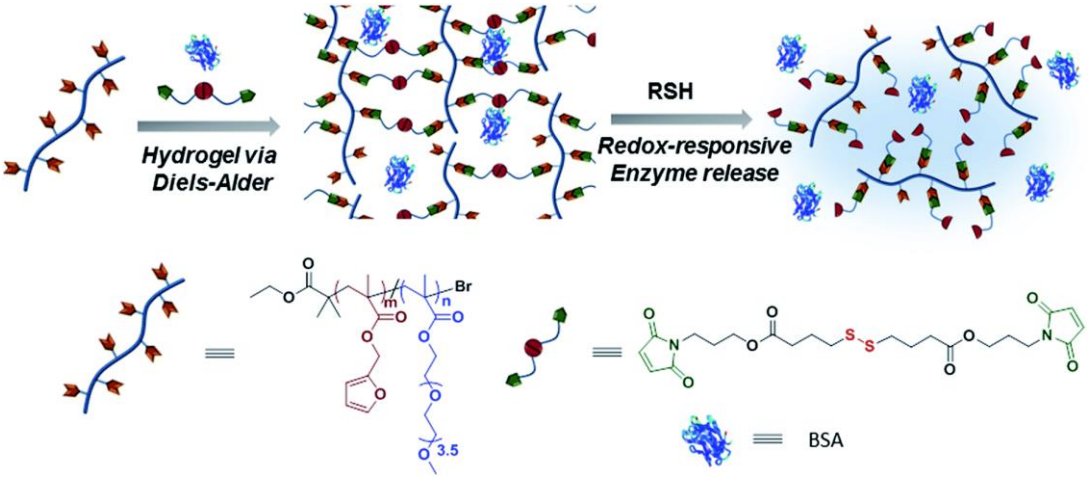

Scheme 4.6 Schematic representation of the use of both Diels-Alder and disulfide chemistry to produce responsive hydrogels. Reproduced with permission from Altinbasak *et al.*[36]

Given the responsive behaviour of these functionalities, it was hypothesised that the introduction of such chemistries into the polymeric star catalysts reported in Chapter 2 would allow for a one-pot polyurethane formulation, with the catalysts remaining dormant until the stimulus (heat or reducing agent) is applied, triggering release of the catalytic amine through disintegration of the polymeric stars. In this Chapter, work focusses on investigating the synthesis and catalytic ability of polymeric stars incorporating responsive crosslinkers.

4.3 Results and Discussion

4.3.1 Probing the requirement of a thermoresponsive crosslinker

Following on from the successful synthesis of amine-functionalised polymeric stars in Chapter 2, the focus was shifted to the incorporation of a responsive crosslinker into the catalysts, aiming at developing a thermoresponsive amine-functionalised polymeric star able to remain dormant within the formulation until stimulated. However, prior to investigating these responsive stars, further investigation into the "non-responsive" tri(ethylene glycol) dimethacrylate (TEGDMA) crosslinked stars was carried out, to confirm the requirement of a responsive crosslinker. Indeed, whilst TEGDMA has, until this point, been described as a "non-responsive" crosslinker, it was hypothesised that the TEGDMA crosslinker may swell upon increasing temperature, and such swelling of the particle may be sufficient to expose the amine to the polyurethane formulation and catalyse the production of rigid polyurethane foam.

Using the arm-first synthetic methodology introduced in Chapter 2, a PHEMA-*b*-(DMAEMA-*co*-TEGDMA) polymeric star, with a theoretical crosslinking density of 10%, was synthesised in sufficient quantity to allow for evaluation in the polyurethane formulation (> 10 g). Initially, a poly(hydroxyethyl methacrylate) (PHEMA) macro-CTA was synthesised by RAFT polymerisation using the RAFT agent 2-cyano-2-propyl benzodithioate (CPBD), used previously for the synthesis of polymeric stars in Chapter 2, and subsequently chain extended with the amine-functionalised monomer *N,N'*-(dimethylamino)ethyl methacrylate, DMAEMA, and the divinyl crosslinker TEGDMA. Size Exclusion Chromatography (SEC) analysis of the resultant polymer (**4.1**) confirmed successful extension, with a shift in the number-average molecular weight from SEC analysis ($M_{n,\,SEC.}$) from 25.9 kg/mol to 37.7 kg/mol, with control over the polymerisation process reflected in the dispersity ($Đ_M$ = 1.52) (Figure 4.1A). The crosslinked nature of the polymeric star was confirmed using triple-detection SEC analysis (introduced in Chapter 2.3.1.1) allowing for determination of the Mark-Houwink parameter *a*.

The *a* value was found to be 0.41, significantly lower that for the linear PHEMA (*a* = 0.68) and the linear PHEMA-*b*-(DMAEMA) (*a* = 0.48), confirming the crosslinked nature of the polymeric stars. Particle size, as determined by Dynamic Light Scattering (DLS) analysis, revealed a particle size of 8 nm ± 1 nm (Figure 4.1B), in good agreement with the particle size for similar polymers reported in Chapter 2.

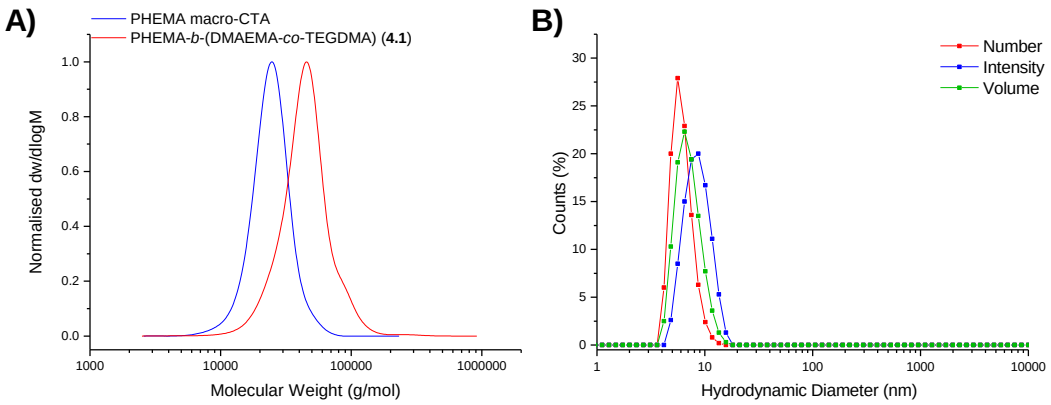

Figure 4.1 (A) Normalised molecular weight distributions for PHEMA-*b*-(DMAEMA-*co*-TEGDMA) and the PHEMA macro-CTA (DMF, PMMA standards), and (B) size distribution analysis by number, intensity and volume, obtained by DLS (detection angle = 173 °) at 3 mg/mL carried out in methanol at 25 °C.

In order to probe any swelling of the polymeric particles, initial studies focussed on the use of variable temperature Nuclear Magnetic Resonance (VT-NMR) spectroscopy were conducted. As reported in Chapter 2, the ^{1}H NMR spectrum of the star polymers did not allow for determination of the degree of polymerisation (DP) from end-group analysis, as a consequence of the crosslinked core shielding both the amino methyl protons ($CH_2N(CH_3)_2$, $N(CH_3)_2$) and the CTA chain end (as well as likely preventing complete solvation of the core of the polymeric star) and resulting in the generation of nonsensical integrals. However, should the polymeric star swell upon an increase in temperature, it is hypothesised that the shielding of these protons would decrease and therefore a change in the integrals would be observed.

Evaluation of the polymeric stars at different temperatures was carried out in deuterated dimethyl sulfoxide (DMSO-d_6) at 25 °C at 5 mg/mL, and at 10 °C intervals between 30 - 80 °C. Setting the integral of the HEMA hydroxy proton (δ = 4.80 - 4.50 ppm, Figure 4.2 proton a) to

equal 1, analysis of the integrals of proton resonances associated with the DMAEMA (N(CH_3)$_2$, δ = 2.25 ppm, Figure 4.2 proton b) revealed an increase in the DMAEMA integrals with an increase in temperature, suggesting a less shielded core environment, consistent with an increase in polymeric star size (Table 4.1). It should be noted that the resonance associated with the HEMA hydroxyl proton was found to shift upfield with increasing temperature, consistent with a decrease in hydrogen bonding between the hydroxyl protons and the DMSO at raised temperatures. Moreover, in addition to an increase in the integrals associated with the DMAEMA increasing temperature, the integrals were found to return to pre-heating values upon cooling and reanalysis of the sample, indicating that cooling results in the particles contracting back to their non-swollen size.

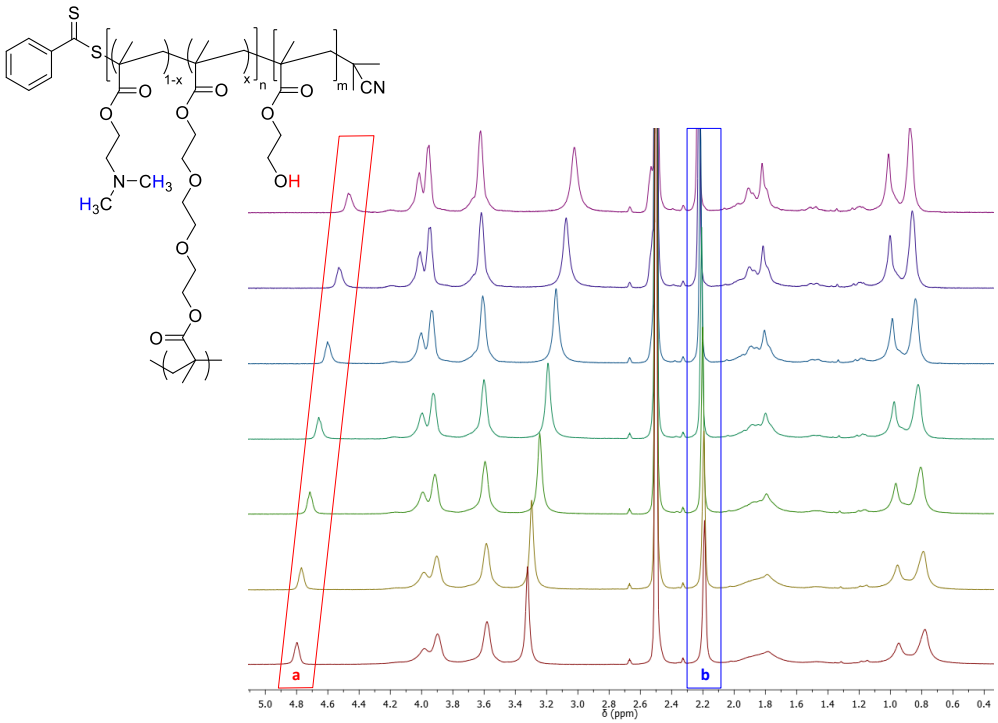

Figure 4.2 Overlaid ^{1}H VT-NMR spectra of 4.1 at 25 °C (*red*), 30 °C (*yellow*), 40 °C (*green*), 50 °C (*turquoise*), 60 °C (*blue*), 70 °C (*purple*), and 80 °C (*pink*), highlighting the HEMA O*H* proton (a) and the DMAEMA N(C*H*$_3$)$_2$ protons (b) (400 MHz, DMSO-d_6).

Temperature (°C)	CH_2OH (HEMA) (proton a)	OCH_2CH_2 (HEMA, TEGDMA, DMAEMA)	$(CH_3)_2$ (DMAEMA) (proton b)
25	1	3.38	3.73
30	1	3.46	3.80
40	1	3.64	3.99
50	1	3.82	4.17
60	1	3.96	4.16
70	1	4.12	4.27
80	1	4.21	4.25
25	1	3.37	3.74

Table 4.1 Changing integrals for the polymeric star PHEMA-*b*-(DMAEMA-*co*-TEGDMA), 4.1, at different temperatures and after cooling. (400 MHz, DMSO-d_6)

To confirm that the polymeric stars do change in size, variable temperature DLS analysis was carried out. Ethylene glycol was chosen as the solvent for the analysis as it best represents the foaming conditions in which the catalyst is dissolved in a polyol rich formulation. DLS analysis confirmed those results obtained by VT-NMR spectroscopic analysis, with a clear increase in the polymer size as the temperature increased (Figure 4.3).

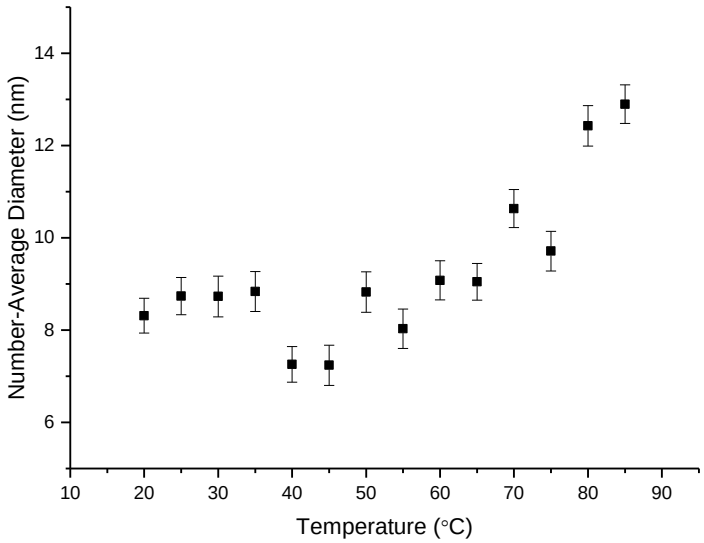

Figure 4.3 Number-average diameter of 4.1, as determined by variable temperature DLS in ethylene glycol (2 mg/mL).Error bars produced as the standard deviation of 5 runs.

As a consequence of the increase in star size at raised temperatures, the polymer was evaluated in the polyurethane foam formulation using the Foamat® set-up introduced in section 1.4.3. Tests were conducted by incubating the formulation premixture, containing both the polyol, the ground catalyst and additives, for 16 hours at a predetermined temperature prior to mixing with the isocyanate and evaluation in the Foamat® set-up. Analysis of the percentage foam rise indicated that there was some catalytic effect, with a notably faster rate of rise at 30 and 40 °C when compared to the catalyst free formulation (Figure 4.4, Table 4.2). However, it was noted that at temperatures above and including 50 °C the percentage rise for the formulation containing catalyst appears to indicate much less catalytic effect, with much smaller differences in the rate of rise at 60 °C compared to 40 °C, reflected in the rate of rise. One reason for this decrease in catalytic effect as the temperature increases may be attributed to the rate of the polyurethane forming reactions being sufficiently fast at 50 °C without a catalyst that any increase in rate brought about by the presence of catalyst will be less easily observed, hence the smaller difference in rates of rise for the catalyst free formulation and the formulation containing catalyst. It is for this reason that no higher temperature were investigated, as the reaction would be sufficiently fast at >70 °C to negate the addition of a catalyst.

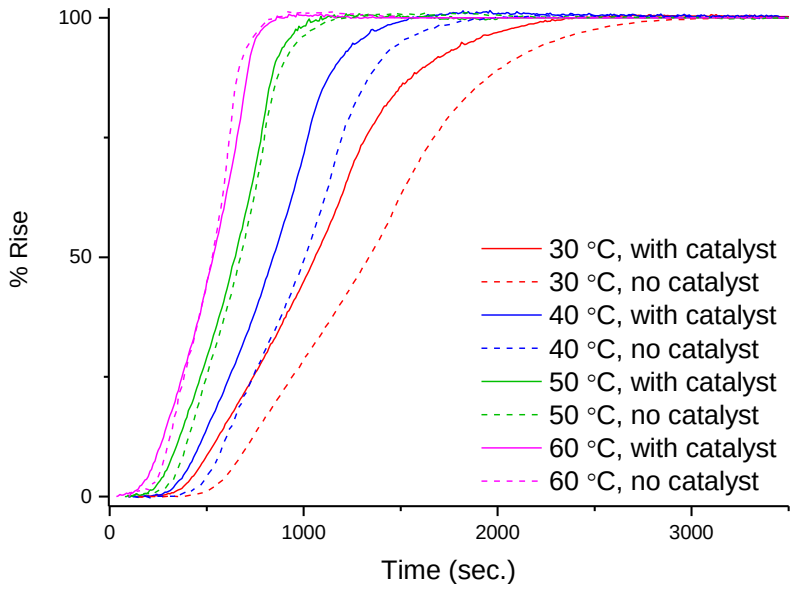

Figure 4.4 Foam rise profiles, plotted as % rise, for foams produced at different foaming temperatures with and without the addition of catalyst 4.1.

Table 4.2 Rates of foam rise for formulations heated to different temperatures with and without catalyst 4.1.

Temperature (°C)	Rate of rise (mm/sec. × 10^{-2})	
	With Catalyst	No Catalyst
30	11.3 ± 0.4	7.1 ± 0.2
40	15.5 ± 0.4	8.5 ± 0.4
50	16.1 ± 0.6	12.9 ± 0.6
60	17.4 ± 0.7	15.4 ± 1.1

During the foaming process it was noted that, at both higher temperatures and in catalyst-free formulations, there was greater separation of the isocyanate from the formulation. It was hypothesised that the lower degree of separation in the catalyst-containing formulation was as a consequence of the catalyst acting as a nucleating agent and allowing for conservation of the mixing of the formulation during the foaming process. As visually observed in Figure 4.5, there is noticeably much more isocyanate separated out of the foam, for both the raised temperatures (C and D) and the catalyst-free formulations (A and C), observable in the pooling of the isocyanate at the base of the foams. Additionally, there is noticeably less separation in the catalyst-containing foams (B and D) *vs* the catalyst-free foams (A and B).

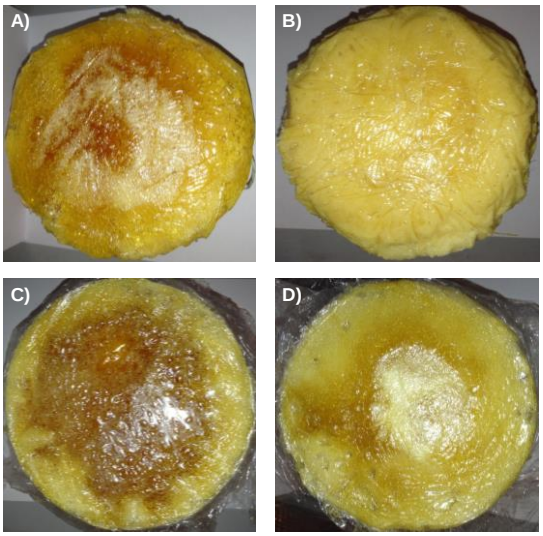

Figure 4.5 Photographs of the base of the rigid polyurethane foams, produced at (A) 30 °C with no catalyst, (B) 30 °C with catalyst 4.1, (C) 60 °C with no catalyst, and (D) 60 °C with catalyst 4.1.

In order to investigate the theory of catalysts acting as nucleating agents, the foaming process was repeated with ground-up polyurethane foam added to the formulation to mimic the nucleating capability of the catalyst within the formulation. It was visually observed that there was significantly less separation of the isocyanate from the formulation at the base of the foams when ground polyurethane was added (Figure 4.6A-B). Additionally, the crude rise height of the foam was much greater for the foam containing the ground-up polyurethane than the completely blank formulation, indicating greater mixing of the isocyanate allowing for more to be consumed during the foaming process (Figure 4.6C).

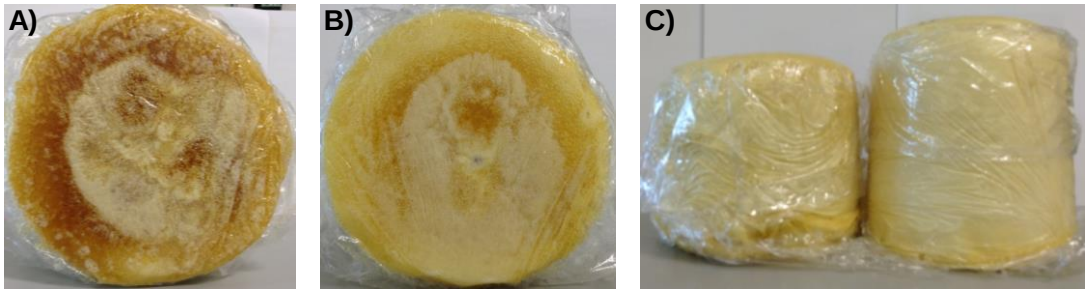

Figure 4.6 Photographs of the base of the foam produced at 30 °C: (A) using no ground-up polyurethane and (B) with added ground-up polyurethane in the formulation, and (C) The side profiles of the foams (*left*) without and (*right*) with added ground-up polyurethane.

Interestingly, in spite of the visually confirmed improvement of mixing, analysis of the rates of rise indicated little to no difference between the blank formulation and that containing ground-up polyurethane, with a blank rate of rise of 1.3 ± 0.3 mm/g/sec $\times 10^{-2}$ when compared to 1.0 ± 0.1 mm/g/sec $\times 10^{-2}$ for the ground-up polyurethane formulation at 30 °C. Moreover, when comparing the TEGDMA catalysed foams *vs* the catalyst-free formulations, the crude rise height and the rates of rise for all the foams produced from catalyst-containing formulations indicated an increase in rise height and rate of rise with increasing temperature, at all temperatures investigated (Figure 4.7).

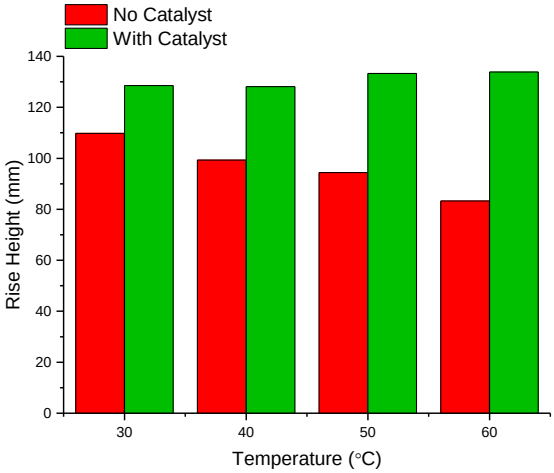

Figure 4.7 The crude rise height of rigid polyurethane foams produced with and without catalyst 4.1 at different foaming temperatures.

It would be expected that, even with improved mixing as a consequence of the polymer, the rise height of the foam is expected to be lower at higher temperatures as a consequence of greater separation of the isocyanate resulting in less isocyanate being available for the foaming process, as observed in the catalyst free foams. However, the rise height remains relatively constant, even as the foaming temperature, and therefore isocyanate separation, increases. Taking into account that, from the ground-up polyurethane experiments, the nucleating effect doesn't appear to have an impact on the rate of rise and only the crude rise height, the almost constant rise height suggests that there is some catalysis occurring, likely favouring the blowing reaction, resulting in greater rise heights of the foams at raised temperatures. Without such catalysis the rise height would decrease as the temperature increased. Consequently, it is probable that a combination of both the nucleating effect of the catalyst ensuring improved isocyanate incorporation in the formulation, in addition to swelling of the catalyst allowing for the amines to become exposed to the formulation, is resulting in the catalysed production of the PU foam.

4.3.2 Incorporation of a Diels-Alder crosslinker

Whilst analysis of the TEGDMA crosslinked polymers indicated that the particles did increase in size, the confusion surrounding the foam results with regards to the contribution from catalysis and the contribution from nucleating effect prompted investigations into responsive

crosslinkers. The incorporation of a responsive crosslinker would ensure that catalysis of the PU production should be the dominant driving force in the foaming process, with any beneficial nucleating effects an added benefit. As a consequence of the foam rise set-up containing a temperature controlled foaming vessel (ATC vessel, Figure 1.12), it was decided that a thermoresponsive crosslinker would be most suited in the development of a one-pot formulation.

4.3.2.1 Synthesis of the Diels-Alder crosslinker

A furan-maleimide based crosslinker was chosen as a consequence of this chemistry having a relatively low retro-Diels-Alder temperature,[23] with a reported retro-Diels-Alder temperature of 80 °C,[43] falling close to the desired temperature range required for the one-pot formulation. Commonly, furan-maleimide Diels-Alder crosslinkers involve a crosslinking dimaleimide which, upon heating, is released and results in the breakdown of the crosslinker (Scheme 4.5 and Scheme 4.6).[1, 36] However, the release of such dimaleimide into the polyurethane foam formulation may have detrimental effects on the foaming process through, for example, affecting the cure of the foam. Therefore, the crosslinker chosen, based on an acrylate equivalent in the literature,[37, 44] contains a single furan and a single maleimide functionality to allow for breakdown of the crosslinker without additional molecules being released into the formulation.

The Diels-Alder crosslinker was synthesised according to a modified previously reported crosslinker synthesis by Syrett *et al*. and Heo and Sodano,[37, 44] with a generalised reaction scheme shown in (Scheme 4.7).The initial starting material dioxatricyclodecene dione (**4.2**), formed as a result of the reaction between furan and maleic anhydride, was obtained as a crystalline white solid in relatively good yield (79%) compared to the literature yield (86%). Characterisation of **4.2** by ^{1}H and ^{13}C NMR spectroscopy confirmed the successful synthesis of the dione product (Figure 4.8), with the integrals associated with the product in the proton NMR in good agreement with the product structure, and the carbon NMR spectrum containing no

resonances attributable to the furan or maleic anhydride. Moreover, elemental analysis confirmed the successful synthesis and isolation of **4.2**.

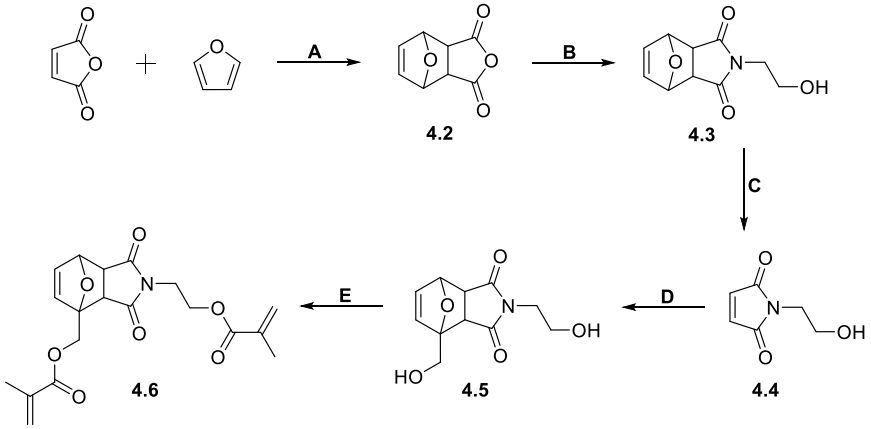

Scheme 4.7 Schematic representation for the synthesis of Diels-Alder crosslinker 4.6. *Reagents and conditions*: (A) toluene, 25 °C; (B) ethanolamine, triethylamine, methanol, 0- 70 °C; (C) toluene, reflux; (D) furfuryl alcohol, benzene, 85 °C; (E) methacryloyl chloride, dichloromethane, 0 – 25 °C.

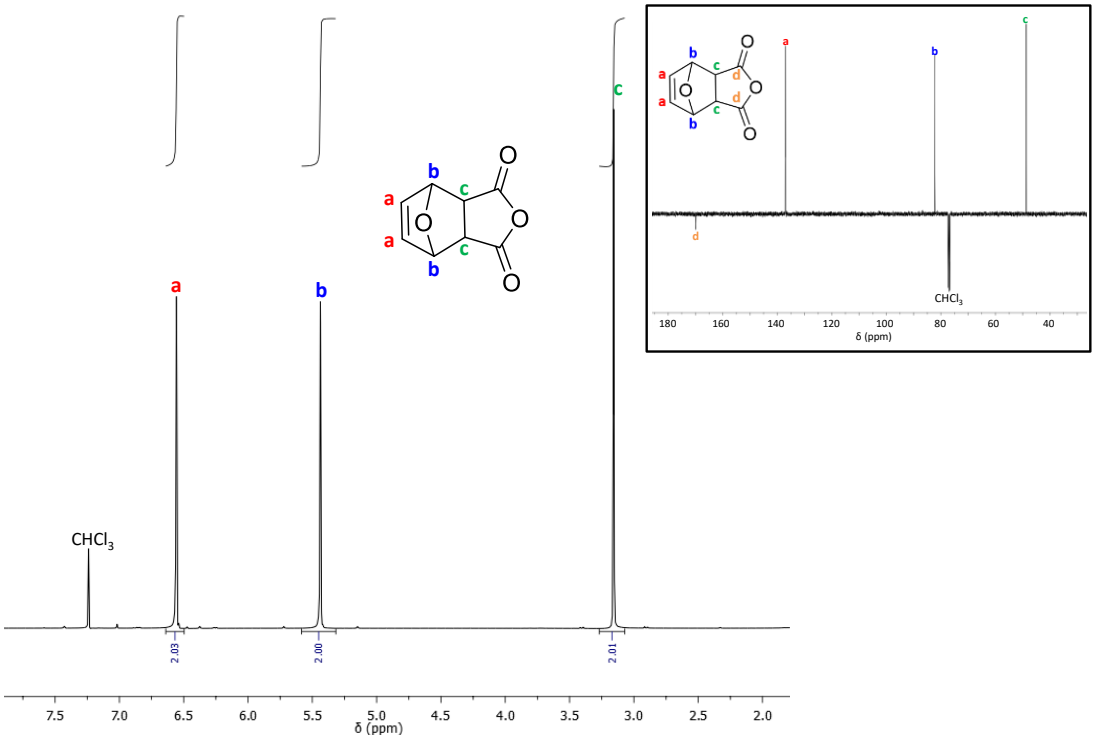

Figure 4.8 NMR spectra of dioxatricyclodecene dione (4.2): (*main*) ^{1}H NMR spectrum (400 MHz, $CDCl_3$) and (*inset*) ^{13}C NMR spectrum (100 MHz, $CDCl_3$).

Following the synthesis of the dioxatricyclodecene dione, hydroxyethyloxa-aza-tricyclodecene dione (**4.3**) was synthesised by the reaction of **4.2** with ethanolamine, under reflux for 16 hours, obtaining a white crystalline solid in a good yield (66%). Analysis of the resultant solid by ^{1}H and ^{13}C NMR spectroscopy confirmed the synthesis of **4.3** (Figure 4.9), with the infrared (IR) spectrum confirming the incorporation of the hydroxyl functionality.

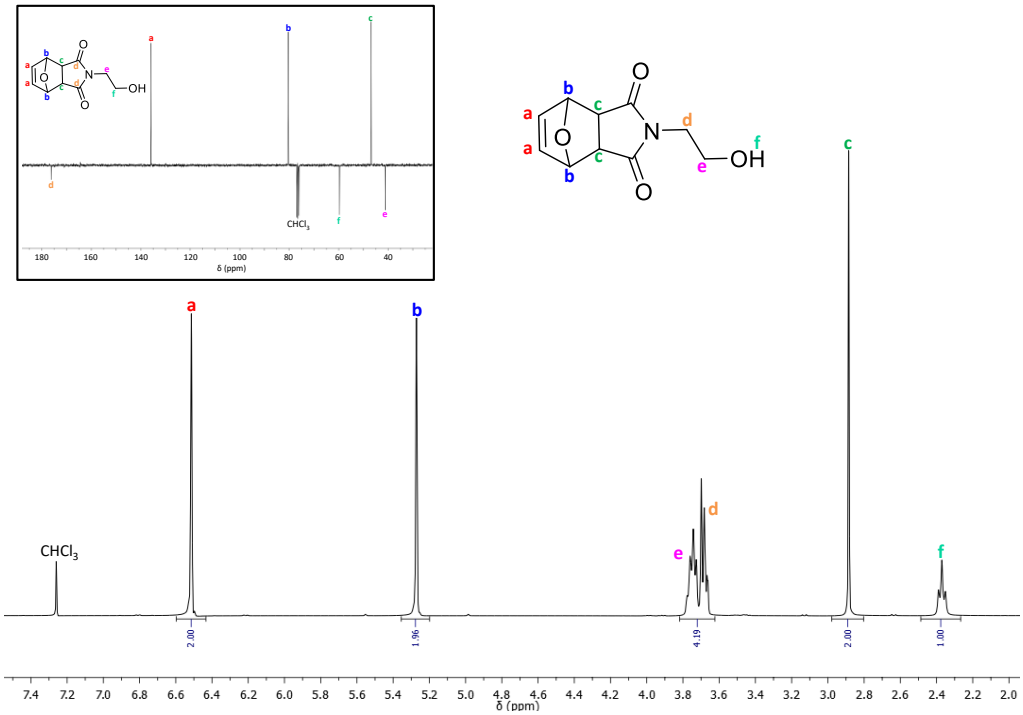

Figure 4.9 NMR spectra of hydroxyethyloxa-aza-tricyclodecene dione (4.3): (*main*) ^{1}H NMR spectrum (400 MHz, $CDCl_3$) and (*inset*) ^{13}C NMR spectrum (100 MHz, $CDCl_3$).

Hydroxyethyl pyrrole dione (**4.4**) was prepared by refluxing **4.3** in toluene for 16 hours, allowing for the retro-Diels-Alder reaction between the maleimide and the furan to occur. Analysis of the resultant white crystalline solid (yield = 95 %) by ^{1}H and ^{13}C NMR spectroscopy confirmed the successful synthesis of **4.4** (Figure 4.10). The Diels-Alder reaction between **4.4** and furfuryl alcohol afforded hydroxyethyloxatricyclodecene dione aminoethanol (**4.5**) in a good yield (66%), with the successful synthesis confirmed by ^{1}H NMR spectroscopy (Figure 4.11). The pair of doublet of doublets can be attributed to the inequivalce of the two methylene protons (labelled as protons *h*), each coupling to one another in addition to the hydroxyl proton (labelled as proton *i*).

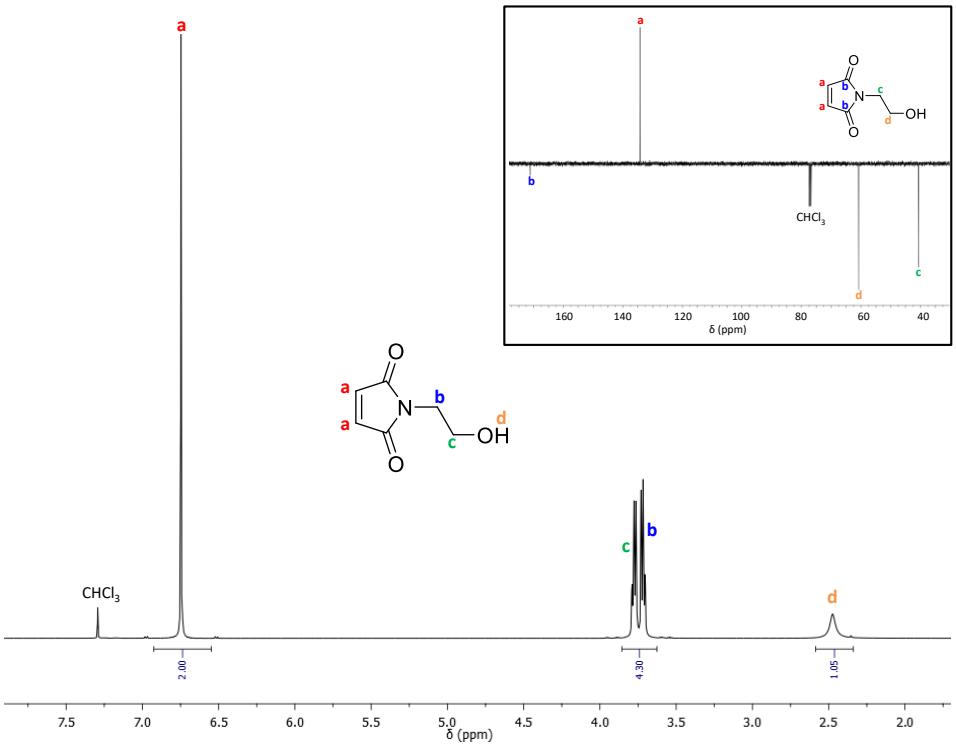

Figure 4.10 NMR spectra of hydroxyethyl pyrrole dione (4.4): (*main*) ^{1}H NMR spectrum (400 MHz, $CDCl_3$) and (*inset*) ^{13}C NMR spectrum (100 MHz, $CDCl_3$).

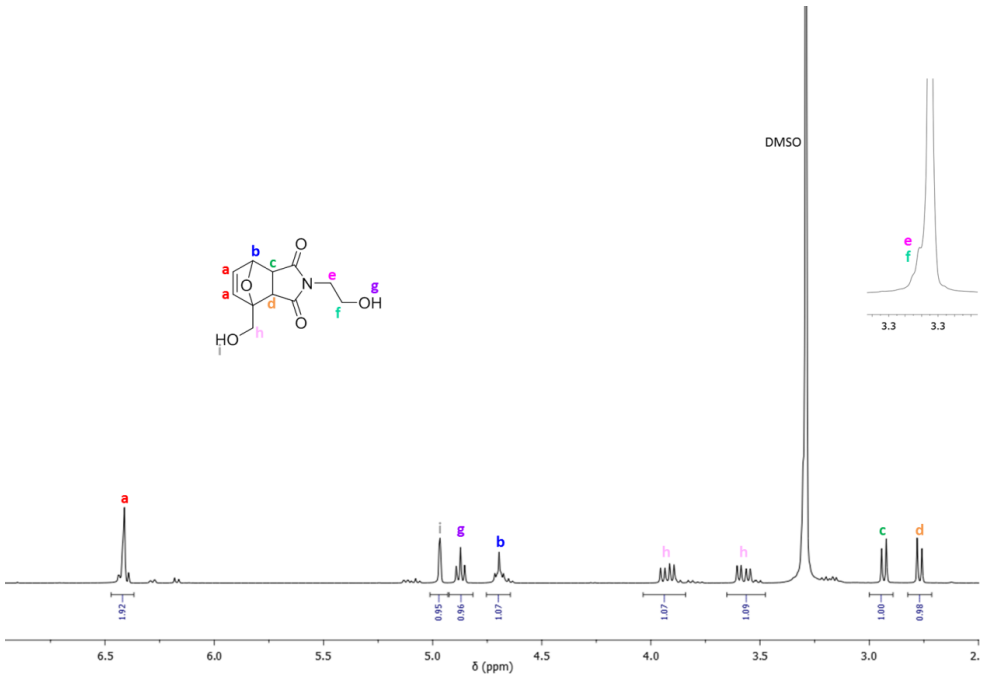

Figure 4.11 ^{1}H NMR spectrum of hydroxyethyloxatricyclodecene dione amino ethanol (4.5) Protons e and f are obscured by the solvent signal at δ = 3.33 ppm. The unlabelled peaks correspond to unreacted furfuryl alcohol (400 MHz, DMSO-d_6).

Initial attempts to produce the dimethacrylate crosslinker were carried out by reaction of **4.5** (200 mg) with methacryloyl chloride (2.15 eq.). Extraction of the crude reaction mixture with ammonium chloride and brine, and subsequent removal of the reaction solvent under vacuum, afforded an off-white solid. However, ^{1}H NMR spectroscopic analysis revealed the presence of a large number of impurities in addition to the product signals. In order to allow for further purification, the reaction was repeated on a larger scale, using 5 g of **4.5**. Using this larger scale, thin-layer chromatography (TLC) analysis indicated the presence of both the product and multiple impurities, hence the solvent was removed *in vacuo* to allow for purification of the crude solid using column chromatography; however, removal of the solvent afforded a non-soluble gel. It was hypothesised that residual methacrylic acid may have resulted in the polymerisation of the reaction mixture, producing a highly insoluble crosslinked polymer gel. In order to minimise the methacrylic by-product in the solution, subsequent work-up of reactions involved an increase in washes with basic water and with saturated ammonium chloride being performed, in addition to concentration of the sample in contrast to complete solvent removal. Following this procedure, the crude reaction mixture was purified by column chromatograph. However, column fractions were found to gel upon complete removal of the solvent. Analysis of the column fractions by ^{1}H NMR spectroscopy prior to complete solvent evaporation indicated the presence of product in addition to some furan impurities (Figure 4.12), with analysis of the gel product not-possible owing to its insolubility in deuterated NMR solvents. The ^{1}H NMR spectrum also indicated the presence of both the *exo* and *endo* isomers of the product crosslinker. These isomers arise from the alignment of the highest occupied molecular orbital (HOMO) of the diene and the lowest unoccupied molecular orbital (LUMO) of the dieneophile within the reaction transition state. The kinetic product, the more sterically unfavourable *endo* isomer, is formed as a consequence of the non-bonding interactions betwwen the diene HOMO and the dienophile LUMO which stabilises the endo isomer transistion state and therefore overcomes the steric disadvanatage of the *endo* isomer *vs* the *exo* isomer.[45]

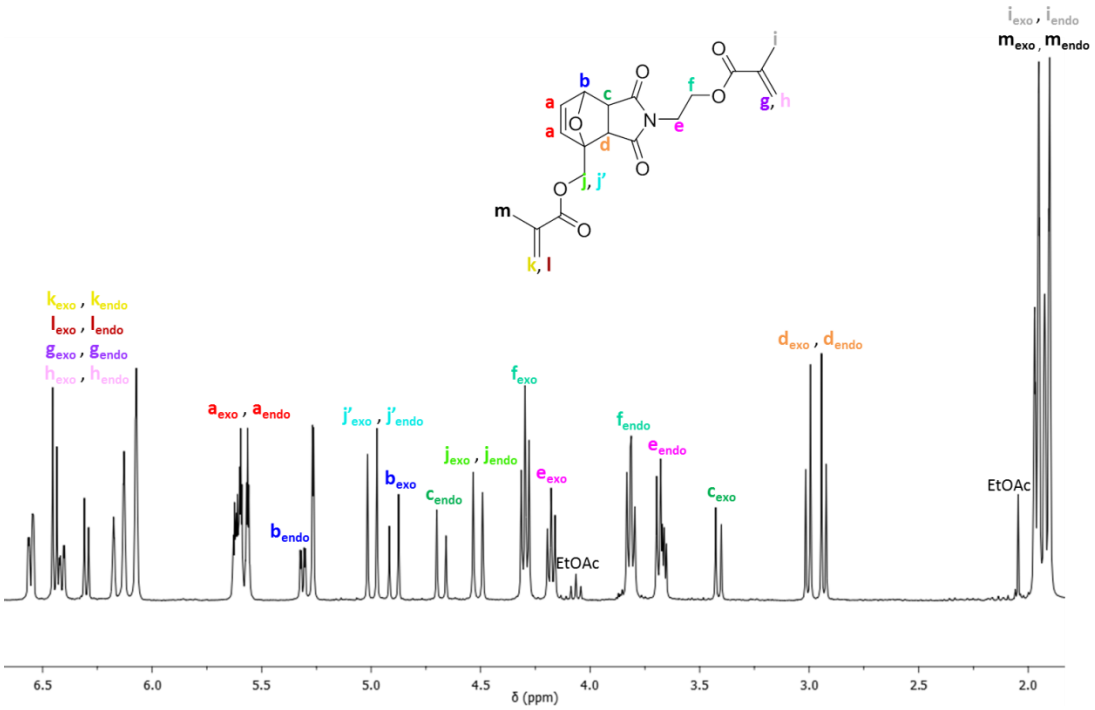

Figure 4.12 ^{1}H NMR spectroscopic analysis of column fractions after concentration, containing a mixture of isomers of Diels-Alder crosslinker 4.6 (400 MHz, $CDCl_3$).

It was assumed that, owing to the much increased scale of the reaction (> 10 g of **4.5**), the work-up procedure was no longer sufficient for removal of the methacrylic acid, resulting in the gelation of the column fractions. In order to overcome this, an alternative synthetic route was selected (Scheme 4.8), in which the hydroxyethyl pyrrole dione (**4.4**) was first reacted with methacryloyl chloride and purified, followed by reaction with furfuryl methacrylate.

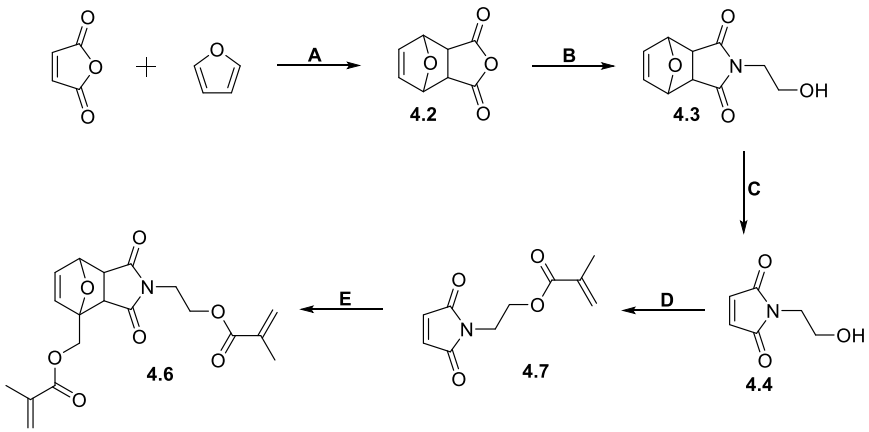

Scheme 4.8 Schematic representation for the synthesis of Diels-Alder crosslinker 4.6. *Reagents and conditions*: (A) toluene, 25 °C; (B) ethanolamine, triethylamine, methanol, 0- 70 °C; (C) toluene, reflux; (D) methacryloyl chloride, dichloromethane, 0 – 25 °C; (E) furfuryl methacrylate, toluene, 25 °C.

Purification of the resultant methacryloylethyl pyrrole dione (**4.7**), obtained as a white crystalline solid (14 g), was carried out by extraction and column chromatography which should allow for complete removal of gel-inducing impurities. The successful synthesis was confirmed by ^{1}H and ^{13}C NMR spectroscopy (Figure 4.13), with the purity confirmed by elemental analysis.

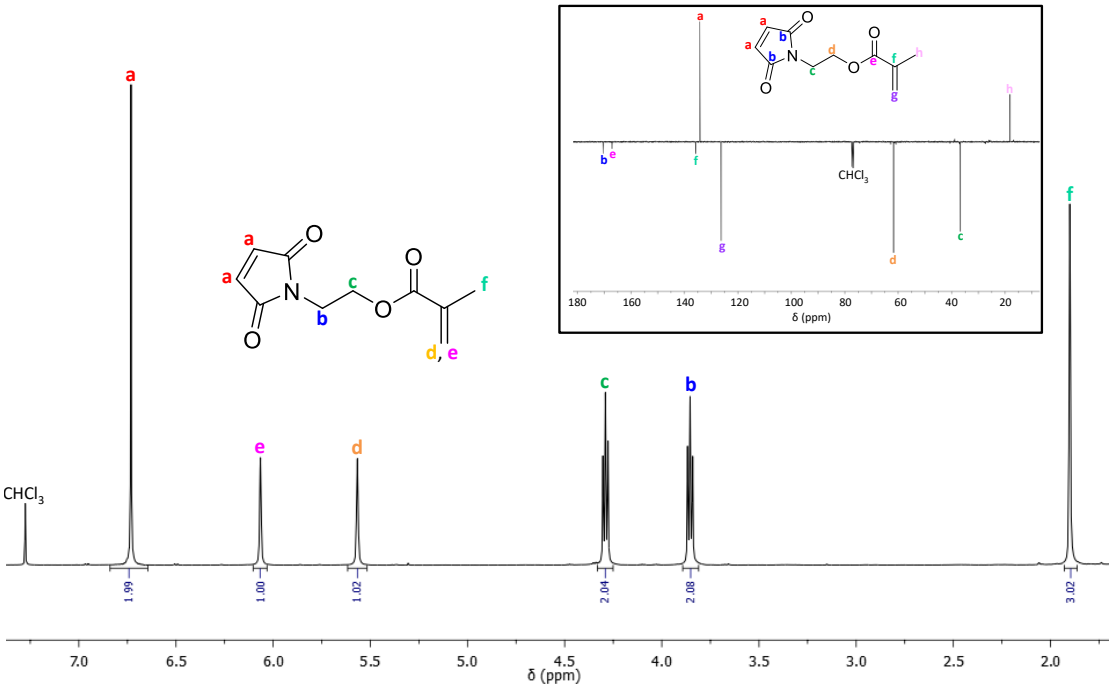

Figure 4.13 ^{1}H NMR spectra of methacryloylethyl pyrrole dione (4.7): (*main*) ^{1}H NMR spectrum (400 MHz, $CDCl_3$) and (*inset*) ^{13}C NMR spectrum (100 MHz, $CDCl_3$).

Synthesis of the crosslinker **4.6** was carried out utilising the Diels-Alder reaction between furfuryl methacrylate and methacryloylethyl pyrrole dione (**4.7**), and purification by column chromatography. ^{1}H NMR spectroscopic analysis of the produced fractions revealed the synthesis of both the *exo* and *endo* isomers, with almost complete isomeric separation (Figure 4.14). The isomers were produced in a 3:1 ratio of the thermodynamically more stable *exo* isomer compared to the *endo* isomer.

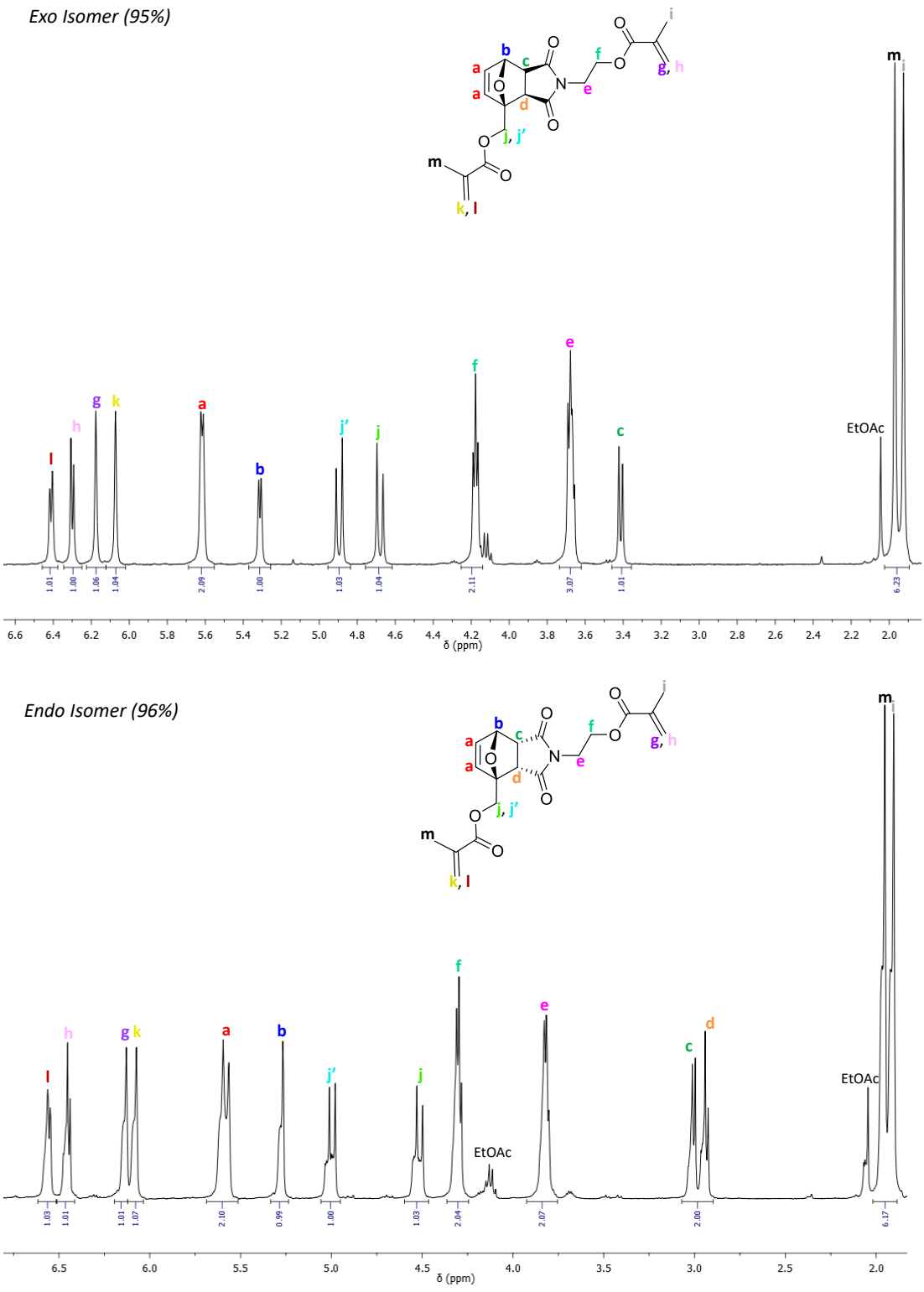

Figure 4.14 ^{1}H NMR spectra of Diels-Alder crosslinker 4.6, with the *exo* isomer (*top*) and *endo* isomer (*bottom*). The percentage of each isomer is given in brackets, and determined by the ratio of integrals associated with each isomer. (400 MHz, $CDCl_3$).

4.3.2.2 Polymerisation of the Diels-Alder crosslinker to produce polymeric stars

Following the successful synthesis of the Diels-Alder crosslinker, the synthesis of thermoresponsive star polymers was carried out using the same arm-first methodology applied earlier in section 4.3.1. To that end, PHEMA was chain extended with DMAEMA and the crosslinker **4.6**, with the monomer feed modified to target a 10% crosslinking density.

In an initial experiment, 300 mg PHEMA macro-CTA (DP = 170, $M_{n,obs.}$ = 22.3 kg/mol, $Đ_M$ = 1.13) was chain extended with DMAEMA (200 eq.) and crosslinker **4.6** (20 eq.), with 0.17 eq. AIBN in DMF at 50 °C (Scheme 4.9). The reaction temperature chosen was lower than previous chain extensions to ensure that the crosslinker did not undergo the retro-Diels-Alder reaction during polymerisation, and was based on the temperature used in the literature.[37]

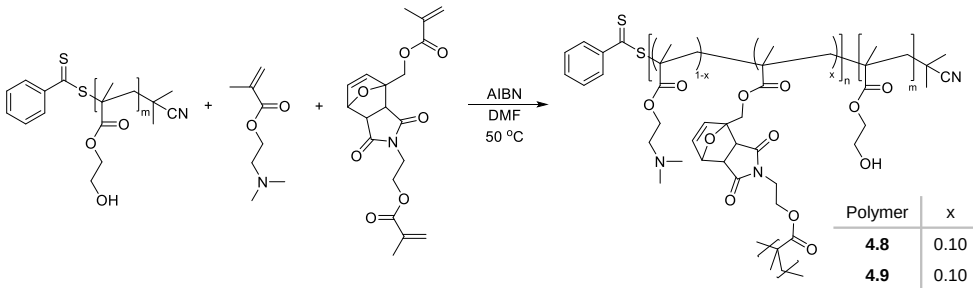

Polymer	x	n	m
4.8	0.10	70	170
4.9	0.10	80	180
4.12	0.10	80	80
4.14	0.20	90	80
4.16	0.35	90	80

Scheme 4.9 Schematic representation of the synthesis of amine-functionalised polymeric stars *via* an arm-first approach using RAFT polymerisation chain extension of PHEMA arms with DMAEMA and the Diels-Alder crosslinker 4.6.

Following reaction for 200 minutes, producing conversions of 61% and 38% for DMAEMA and **4.6**, respectively, the resultant polymer (**4.8**) was isolated by precipitation into diethyl ether. Successful extension of the PHEMA macro-CTA was observed by SEC analysis, with a shift in the molecular weight in the SEC refractive index (RI) trace from the PHEMA macro-CTA to a higher molecular weight (Figure 4.15A). Moreover, the polymodal trace of the SEC data, common during the arm-first synthesis of polymeric stars, is likely attributable to the agglomeration of growing stars during polymerisation.

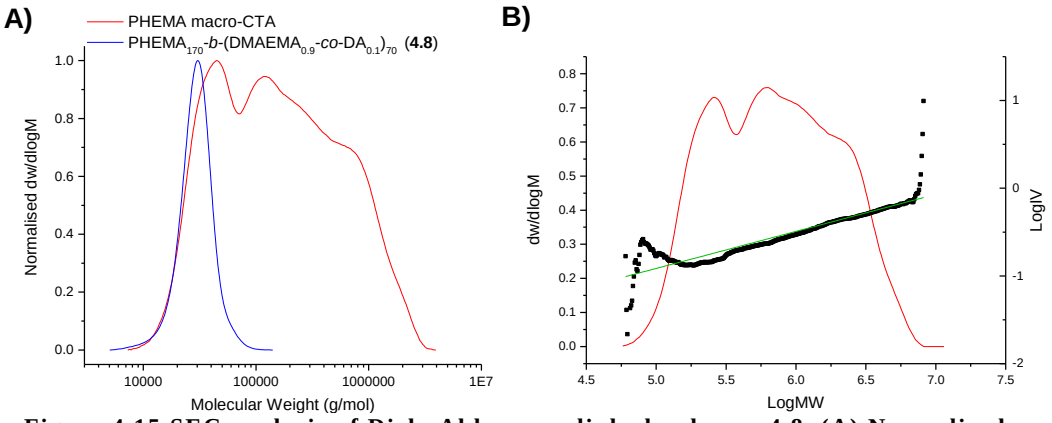

Figure 4.15 SEC analysis of Diels-Alder crosslinked polymer 4.8. (A) Normalised molecular weight distributions for PHEMA$_{170}$-*b*-(DMAEMA$_{0.9}$-*co*-DA$_{0.1}$)$_{70}$ and the PHEMA macro-CTA, where DA = Diels-Alder crosslinker, and (B) Mark-Houwink analysis of 4.8 (DMF, PMMA standards).

Analysis of the resultant polymer using ^{1}H NMR spectroscopy further confirmed the extension, with the appearance of signals at δ = 2.59 ppm and δ = 2.28 ppm attributable to the CH_2N and N(CH_3)$_2$ of the DMAEMA, respectively, in addition to those attributable to the Diels-Alder crosslinker at δ = 5.28-6.70 ppm (Figure 4.16). Mark-Houwink analysis (Figure 4.15B), as discussed in section 2.3.1.1, confirmed the crosslinking of the polymer, with an *a* value of 0.42, significantly lower than the *a* values of 0.68 for the linear PHEMA.

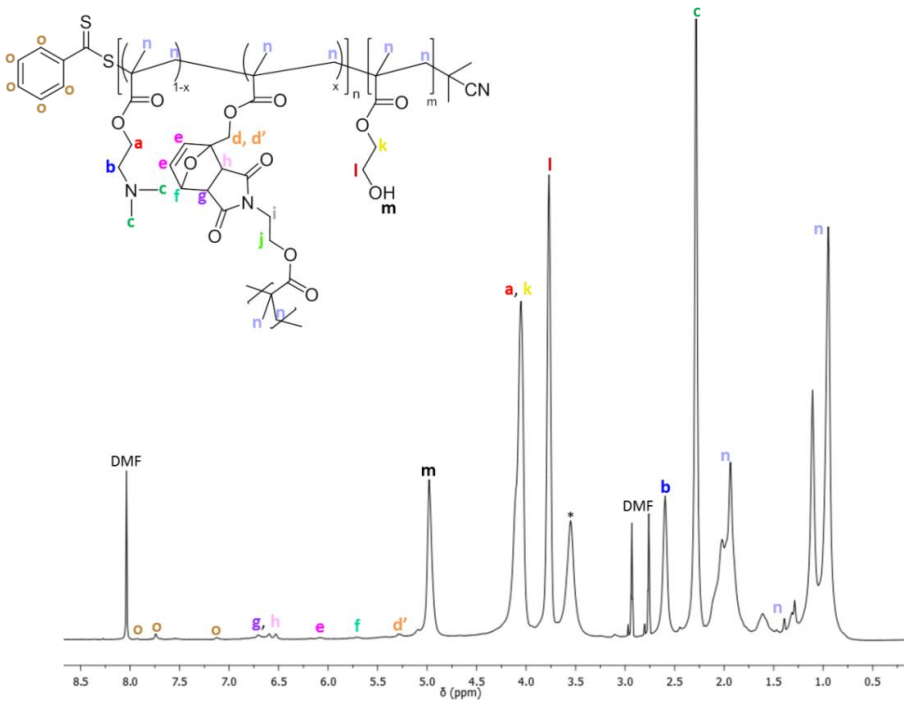

Figure 4.16 ^{1}H NMR spectrum of the PHEMA$_{170}$-*b*-(DMAEMA$_{0.9}$-*co*-DA$_{0.1}$)$_{70}$ (4.8) *denotes H_2O (400 MHz, DMF-d_7).

Having demonstrated the suitability of the Diels-Alder crosslinker in the production of polymeric stars, the scale of the reaction was increased to allow for the production of a suitable quantity to enable evaluation in the rigid polyurethane formulation. To this end, 10 g PHEMA macro-CTA (DP = 180, $M_{n,obs.}$ = 23.4 kg/mol, $Đ_M$ = 1.12) was chain extended with DMAEMA and crosslinker **4.6**, at half the concentration of the initial experiment in order to reduce the coupling reactions and account for an increase in viscosity at the larger scale. Analysis of the resultant polymer (PHEMA$_{180}$-*b*-(DMAEMA$_{0.9}$-*co*-DA$_{0.1}$)$_{80}$, **4.9**) by ^{1}H NMR spectroscopy confirmed successful chain extension, through the appearance of resonances associated with DMAEMA and the crosslinker. Moreover, a clear shift to higher molecular weights in the SEC analysis was observed (Figure 4.17), as well as an *a* value of 0.32 generated from the Mark-Houwink SEC analysis confirming the successful chain extension to form crosslinked polymeric stars. Further analysis confirmed the controlled nature of the polymerisation, with a relatively narrow dispersity ($Đ_M$ = 1.41), in addition to the theoretical number-average molecular weight ($M_{n,\,theo.}$), based on monomer conversion, being in good agreement with the observed number-average molecular weight ($M_{n,obs.}$), as determined by ^{1}H NMR spectroscopic analysis (37.3 kg/mol and 37.6 kg/mol, respectively). Furthermore, these values were similar in value to the number-average molecular weight determined by triple-detection SEC analysis ($M_{n,\,SEC.}$), which was found to be 37.9 kg/mol.

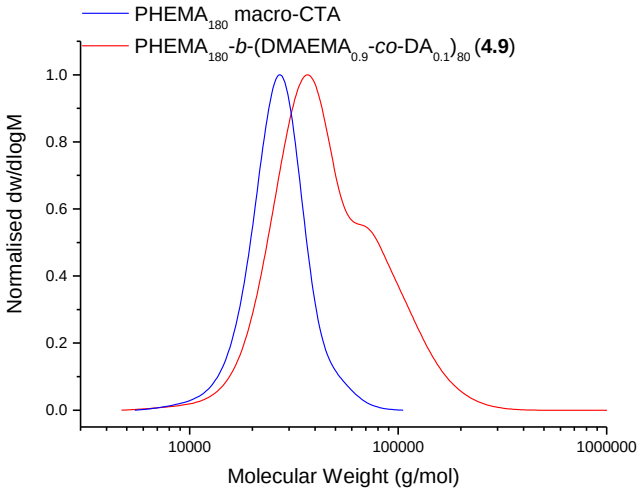

Figure 4.17 Normalised molecular weight distributions for PHEMA$_{180}$-*b*-(DMAEMA$_{0.9}$-co-DA$_{0.1}$)$_{80}$ (4.9), and the PHEMA$_{180}$ macro-CTA (DMF, PMMA standards).

Further analysis of the star polymers was carried out using DLS analysis to determine the polymeric star size. DLS analysis, by direct dissolution of the polymer in methanol (2 mg/mL) at 25 °C, afforded a star polymer size of 7 nm ± 1 nm (PD = 0.24, Figure 4.18), slightly larger than the TEGDMA crosslinked polymers. This difference in size is hypothesised to result from the bulkier nature of the Diels-Alder crosslinker resulting in the crosslinker requiring more space within the core, and therefore creating a larger hyperbranched core within the star polymer. It was hypothesised that the appearance of a second peak in the intensity signal is as a consequence of both a small number of aggregates and agglomeration of growing star chains, which were observed in the TEGDMA crosslinked polymers in section 2.3.2

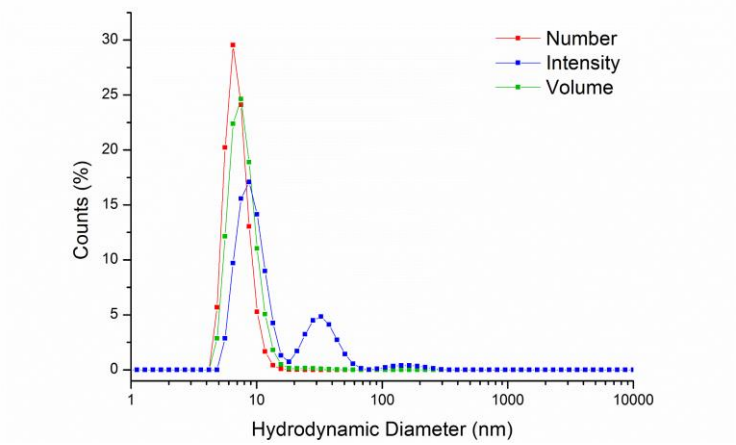

Figure 4.18 Size distribution of 4.9, determined by DLS analysis (2 mg/mL in methanol).

4.3.2.3 Confirmation of the retro-Diels-Alder reaction

The thermoresponsive behaviour of the polymer was evaluated to confirm that the crosslinker undergoes the retro-Diels-Alder reaction within the desired temperature range. Initially, Differential Scanning Calorimetry (DSC) analysis was carried out on the non-polymerised crosslinker, revealing a retro-Diels-Alder reaction temeprature of 70 °C for the *endo* isomer, and a slightly higher temperature of 112 °C for the *exo* isomer (Figure 4.19), in good agreement with the literature.[43]

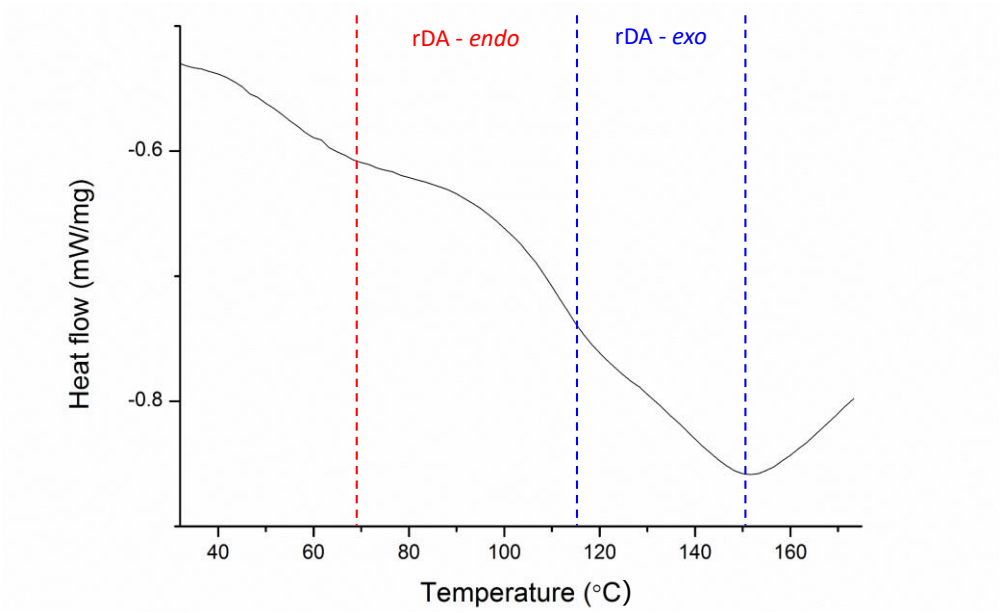

Figure 4.19 DSC thermogram of the Diels-Alder crosslinker (4.6). Heating rate = 10 °C/min.

Analysis of the crosslinker once incorporated within the polymer was found to be more problematic. Indeed, attempts to use variable temperature ^{1}H NMR spectroscopy in deuterated DMF were complicated by the resonance for the released furan being masked by the solvent, in addition to the resonances associated with both the DMAEMA and the HEMA. Moreover, the relatively low intensity of the resonances associated with the crosslinker render it difficult to observe any resonances associated with the product of the retro-Diels-Alder reaction. Nevertheless, it is possible to see the formation of the free maleimide resonances in the ^{1}H VT-NMR spectroscopic analysis at δ = 6.97 ppm, producing a retro-Diels-Alder temperature of 70 °C, though integration to determine the extent of the retro-Diels-Alder reaction was unsuccessful owing to the weakness of the resonances (Figure 4.20).

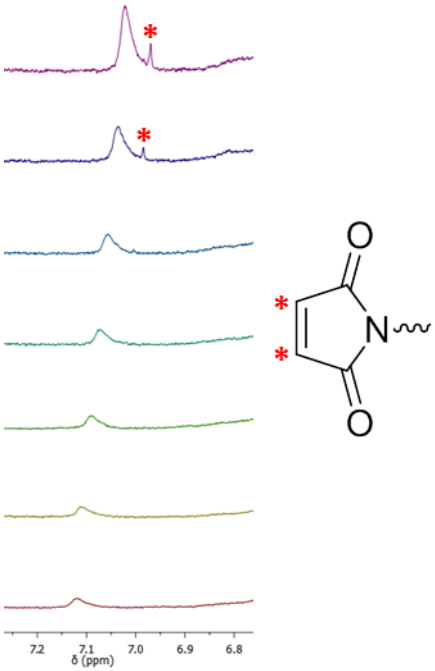

Figure 4.20 Expanded region of the overlaid ^{1}H VT-NMR spectra of 4.9 at 25 °C (*red*), 30 °C (*yellow*), 40 °C (*green*), 50 °C (*turquoise*), 60 °C (*purple*) and 70 °C (*pink*), showing the evolution of the furan resonances (* at δ = 6.97 ppm) generated by the retro-Diels-Alder reaction (400 MHz, DMF-d_7).

Both DSC and VT-NMR spectroscopic analysis revealed a retro-Diels-Alder temperature that was slightly higher than the desired temperature range for the one-pot formulation (50 - 60 °C). In order for the catalysts to be suitable for the formulation, only a small portion of the crosslinker would have to undergo the retro-Diels-Alder reaction, as the exotherm produced from the catalysed reaction of the polyol and isocyanate to produce polyurethane would generate increased heat within the reaction vessel and therefore result in further retro-Diels-Alder reactions. As such, it was decided that the polymeric catalysts should be heated at 50 °C to determine whether even a small number of crosslinking monomers would undergo the retro-Diels-Alder reaction. In order to probe this, a thiol-functionalised coumarin was selected, allowing for monitoring of the reaction through the use of fluorescence spectroscopy. It was hypothesised that, should the polymeric catalyst undergo the retro-Diels-Alder reaction, the released maleimide would react with the thiol, resulting in a quenching of the fluorescence intensity in comparison to the non-reacted coumarin (Scheme 4.10).

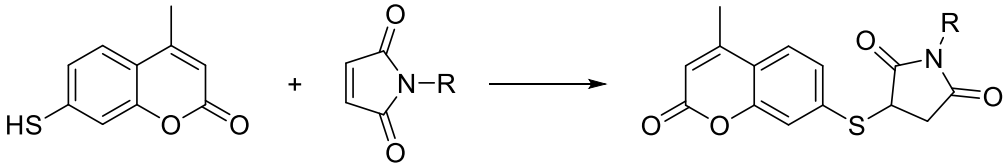

Scheme 4.10 Schematic representation for the reaction of 7-mercapto-4-methyl coumarin and the released maleimide.

To this end, a 20 mM solution of 7-mercapto-4-methyl coumarin in DMF was prepared, and polymer **4.9** was added at a ratio of thiol to crosslinker of 1.05:1. Samples were stirred at room temperature and at 50 °C for 1 hour, and the fluorescence spectrum recorded. Analysis of the fluorescence spectrum demonstrated a clear drop in fluorescence between the sample at room temperature and the sample at 50 °C (Figure 4.21), indicating that the retro-Diels-Alder reaction has occurred, liberating the maleimide from the crosslinker even at 55 °C, confirming the suitability of the Diels-Alder crosslinked polymer for the one-pot polyurethane formulation.

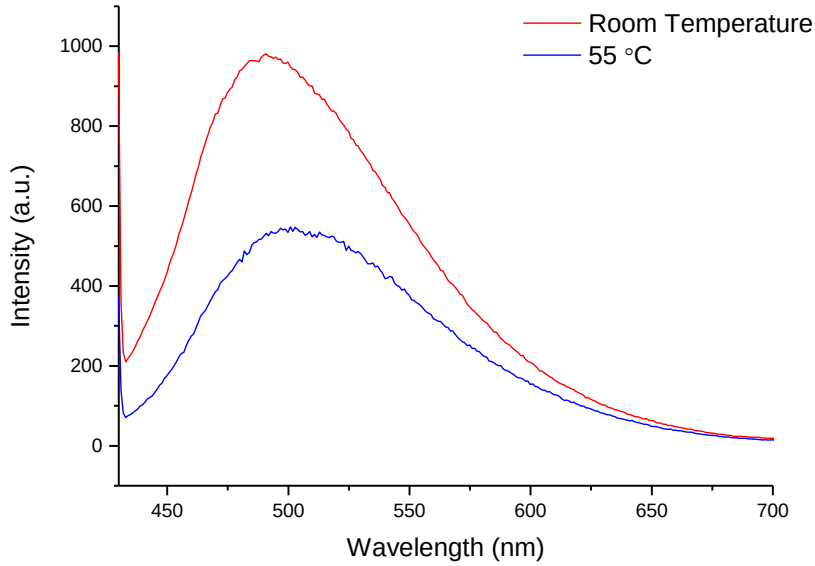

Figure 4.21 Fluorescence spectrua (λ_{ex} = 364 nm) of 7-mercapto-4-methyl coumarin after stirring with polymer 4.9 for 1 hour at room temperature (*red*) and 55 °C (*blue*).

4.3.2.4 Catalysis of the rigid polyurethane foam formulation

As a consequence of the successful confirmation of the responsive behaviour of the polymeric stars at 50 °C, the Diels-Alder crosslinked polymeric stars were evaluated in the rigid polyurethane formation. In addition to polymer **4.9**, a control polymeric catalyst with the non-responsive crosslinker TEGDMA (10% crosslinking density, **4.11**) was evaluated, as well as a catalyst containing 5% Diels-Alder crosslinker and 5% TEGDMA totalling to a 10% crosslinking density (**4.10**). The 5%/5% catalyst was synthesised through the same arm-first methodology as the previous catalysts, through varying the monomer feed to include 10 eq. Diels-Alder crosslinker and 10 eq. TEGDMA, in addition to 200 eq. DMAEMA (Table 4.3).

Table 4.3 Characterisation data for polymers evaluated in the polyurethane foam formulation carried out at 40 °C.

Polymer	Arm DP[a]	Crosslinker[b]	$M_{n,\ theo.}$[c] (kg/mol)	$M_{n,\ SEC}$[d] (kg/mol)	$Đ_M$[d]	%Nitrogen[e]
4.9	180	10% DA	37.6	37.9	1.41	2.20
4.10	170	5% DA 5% TEGDMA	51.7	45.2	1.70	2.92
4.11	170	10% TEGDMA	35.5	41.0	1.27	2.89

[a] determined by ^{1}H NMR spectroscopy (CD_3OD), [b] content based on monomer feed, [c] calculated from conversion, determined by GC analysis, [d] determined by SEC triple-detection analysis (DMF, PMMA standards), [e] determined by elemental analysis.

Following the earlier results using foaming at different temperatures (Figure 4.4), the temperature for foam evaluation was chosen to be 40 °C. It was hypothesised that this temperature would provide a good balance between the rate of reaction and the degree of retro-

Diels-Alder reactions occurring. Indeed, whilst 50 °C would trigger a greater number of retro-Diels-Alder reactions, the rate of rise at this temperature is sufficiently fast that it may be difficult to observe any further increase in rate as a consequence of the responsive polymeric star catalysts. Prior to mixing with the isocyanate, the premixture was heated in an oven at 40 °C for 16 hours, after which the isocyanate was added, the formulation mixed, and poured into the Foamat® vessel for analysis. Foam analysis revealed some difference in overall rise height for the different catalysts (Figure 4.22A), but there was no difference in the foam rise profiles for all the catalysts evaluated (Figure 4.22B). Analysis of the rates of rise further confirmed there was no significant difference between the foam rise rates for the different catalysts (Table 4.4) indicating no increased catalytic effect from the incorporation of the thermoresponsive crosslinker. Moreover, it is further evident that all catalysts had a slower rate of rise and a greater induction period than the current commercial catalyst. Owing to the problems encountered with the reproducibility of the foaming process, discussed in Chapter 2, section 2.3.3.4, and the large mass of polymer required for each individual test (~ 4 g), it was decided that the catalytic activity of the Diels-Alder crosslinked polymeric stars should be investigated using an alternative method, and therefore no further foam testing was carried out.

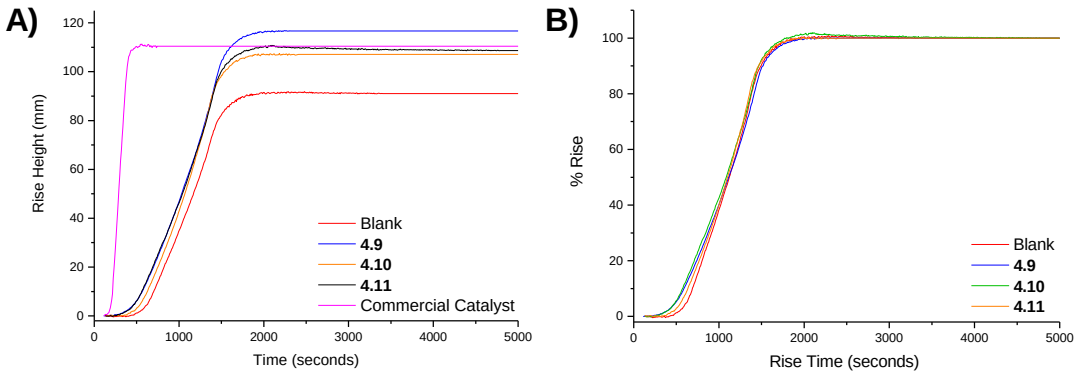

Figure 4.22 Foam rise profiles for the polyurethane foam formulation using Diels-Alder crosslinked polymeric catalysts: (*left*) rise height and (*right*) percentage rise *vs* the blank formulation.

Table 4.4 Rates of rise for the catalysts evaluated in the polyurethane foam formulation at 40 °C.

Catalyst	Rate of rise (mm/sec × 10^{-2})
No Catalyst	8.3
4.9	8.6
4.10	9.6
4.11	9.6

4.3.2.5 Catalysis of the Knoevenagel reaction

It was hypothesised that the tertiary amine within the thermoresponsive catalysts could be used as a catalyst for a different reaction, with catalysis at room temperature and at a raised temperature of 55 °C allowing for differences in catalysis to be observed between the responsive and non-responsive polymers.

The Knoevenagel condensation reaction, a variant on the Aldol condensation reaction, involves the reaction between either a ketone or an aldehyde and an active hydrogen containing compound, producing as α,β-unsaturated compound, and is frequently catalysed by a weakly basic amine.[46-48] Following a modified literature procedure,[47] the reaction between benzaldehyde and ethyl cyanoacetate was carried out in methanol at 55 °C, using 0.05 eq. dimethylbutyl amine as a model catalyst for DMAEMA (Scheme 4.11).

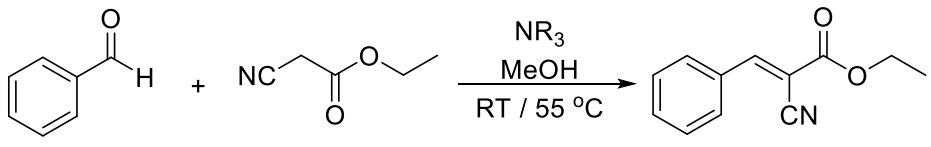

Scheme 4.11 Schematic representation for the Knoevenagel reaction between benzaldehyde and ethyl cyanoacetate, catalysed by tertiary amine.

The catalytic activity of a 10% Diels-Alder crosslinked polymer (**4.12**) and a 10% TEGDMA crosslinked polymer (**4.13**) were evaluated. In addition, to confirm no catalytic activity resulted from the polymeric scaffold, a Knoevenagel reaction was run with the addition of the PHEMA macro-CTA. As evident in Figure 4.23A, the addition of the polymeric catalysts results in an increased conversion of ethyl cyanoacetate in comparison to the catalyst free sample, with no catalytic activity exhibited by the PHEMA arms. At room temperature there is little difference in catalysis between the TEGDMA and the Diels-Alder crosslinked polymers, especially during the initial rate of catalysis, with deviation between the two catalysts only appearing after one hour, with approximately only 10% more conversion for the Diels-Alder crosslinked polymer after 3 hours compared to the TEGDMA crosslinked polymer. Whilst this is

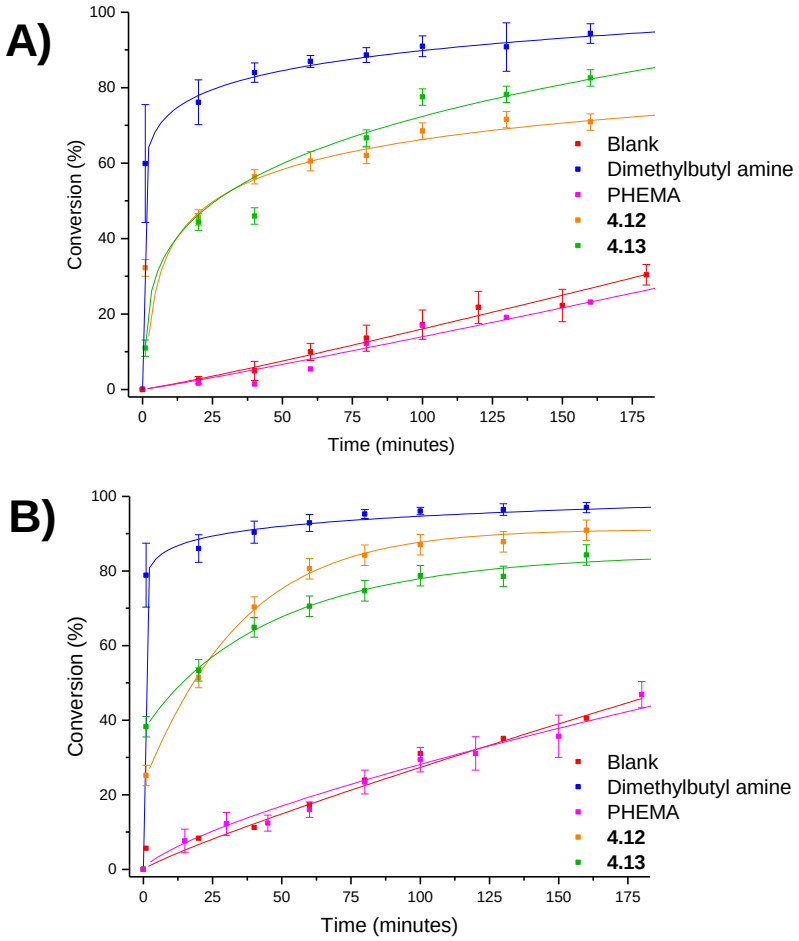

Figure 4.23 Conversion of ethyl cyanoacetate (A) at room temperature and (B) at 55 °C, using polymeric catalysts with a 10% crosslinking density, determined by GC analysis, where 4.12 is the Diels-Alder crosslinked polymer and 4.13 is the TEGDMA crosslinked polymer. Error bars produced from the standard deviation of three repeats.

to be expected at room temperature, as a result of both polymeric stars retaining the crosslinked hyperbranched core, a similar trend is observed at the raised temperature of 55 °C (Figure 4.23B). Here, the Diels-Alder catalyst was found to exhibit only a slightly higher rate of catalysis, with only a 5% faster rate of conversion of ethyl cyanoacetate when compared to the TEGDMA crosslinked polymer, and displaying no difference in the initial rate of catalysis between the two catalysts.

Such minimal difference in catalysis between the two catalysts was speculated to be as a consequence of insufficient crosslinking density which did not prevent diffusion of the reactants to the catalytic amine within the core. Indeed, whilst evaluation in the polyurethane foam formulation indicated that 10% crosslinking density was sufficient at preventing the polyol and the polyisocyanate from reaching the catalytic amine functionality, both the polyol and polyisocyanate are significantly larger than both the benzaldehyde and the ethyl cyanoacetate and therefore it is much more difficult for these to diffuse to the catalyst. Therefore, an increase in crosslinking density may be required to prevent reactant diffusion to the core of the polymeric star.

In order to investigate this theory, a series of both TEGDMA and Diels-Alder crosslinked polymers were synthesised, targeting both 20 and 35% crosslinking density. Polymers were synthesised using chain extension of $PHEMA_{80}$ with DMAEMA (200 eq.) and the crosslinking monomer (20 eq.), with monomer feed varied to target the different crosslinking densities. The successful synthesis of the polymeric stars is evident in the SEC analysis, with a clear shift in the molecular weight from the macro-CTA, in addition to the Mark-Houwink *a* parameters confirming the crosslinked nature of the polymers (Table 4.5).

Table 4.5 Characterisation data for polymers evaluated as catalysts for the Knoevenagel reaction between benzaldehyde and ethyl cyanoacetate.

Polymer	Crosslinker	Crosslinking Density (%)[a]	$M_{n,\ theo.}$[b] (kg/mol)	$M_{n,\ SEC}$[c] (kg/mol)	$Đ_M$[c]	a[c]	D_h[d] (nm)	%N[e]
4.12	D/A	10	31.6	42.1	5.32	0.35	15	3.67
4.13	TEGDMA	10	26.8	39.1	1.71	0.44	8	4.63
4.14	D/A	20	29.1	23.4	1.33	0.25	14	5.07
4.15	TEGDMA	20	33.2	48.6	3.15	0.44	8	4.38
4.16	D/A	35	34.5	29.4	1.61	0.24	16	4.03
4.17	TEGDMA	35	39.4	56.5	2.22	0.45	7	3.59
4.18	D/A	2	25.1	62.1	1.48	0.28	15	4.13
4.19	TEGDMA	2	29.2	65.9	1.22	0.50	7	4.38

[a] content based on monomer feed, [b] calculated from conversion, determined by GC analysis, [c] determined by triple-detection SEC analysis (DMF, PMMA standards), [d] determined by DLS analysis (3 mg/mL in methanol), [e] determined by elemental analysis.

It was predicted that, as the crosslinking density increased, there would be a larger difference in the catalytic activity between the Diels-Alder crosslinker and the TEGDMA crosslinked polymers, as a consequence of the Diels-Alder crosslinked polymer being able to open up upon heating allowing for the amine to come into contact with the reactants. However, evaluation of these polymers revealed little effect of changing the crosslinking density, especially at the raised temperature, with the same ethyl cyanoacetate conversion observed for both the TEGDMA and Diels-Alder crosslinked polymers (Figure 4.24).

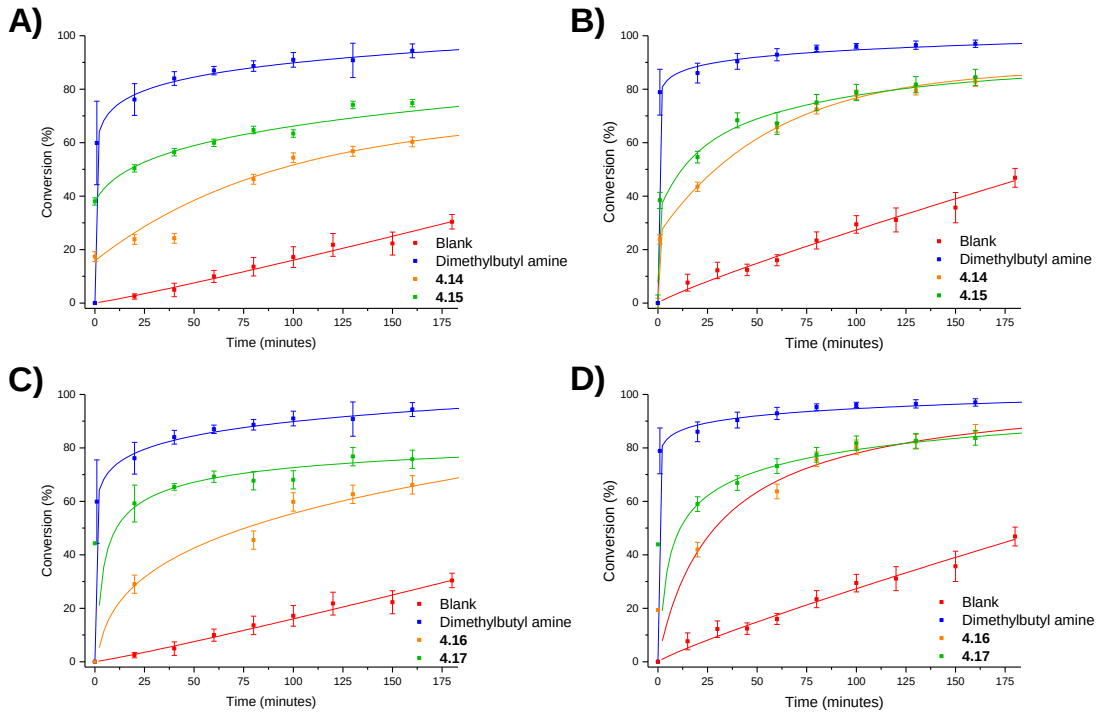

Figure 4.24 Conversion of ethyl cyanoacetate using polymers with a crosslinking density of 20% (A and B, at room temperature and 55 °C respectively), and 35% (C and D, at room temperature and 55 °C respectively), determined by GC analysis, where 4.14 and 4.16 are the Diels-Alder crosslinked polymers and 4.15 and 4.17 are the TEGDMA crosslinked polymers. Error bars produced from the standard deviation of three repeats.

One possible explanation for this, reported by Syrett *et al.*,[37] relates to the proximity of the crosslinking monomers. Should the retro-Diels-Alder reaction occur within the core, the cleaved furan/maleimide groups are spatially close to one another, which favours the reformation of the crosslinker through the Diels-Alder reaction. As a consequence, the polymeric star will not fall apart at the raised temperature, which would result in no observable difference in the catalytic activity compared to the TEGDMA crosslinked polymer. In order to test this, polymeric stars were prepared with a 2% crosslinking density (Table 4.5), with the lower crosslinking density hypothesised to result in less spatially close crosslinking units. Evaluation of the catalytic activity, however, still indicated no difference between the responsive and non-responsive crosslinkers, indicating that spatial separation was potentially insufficient at preventing the recombination of the Diels-Alder crosslinker after the retro-Diels-Alder reaction (Figure 4.25).

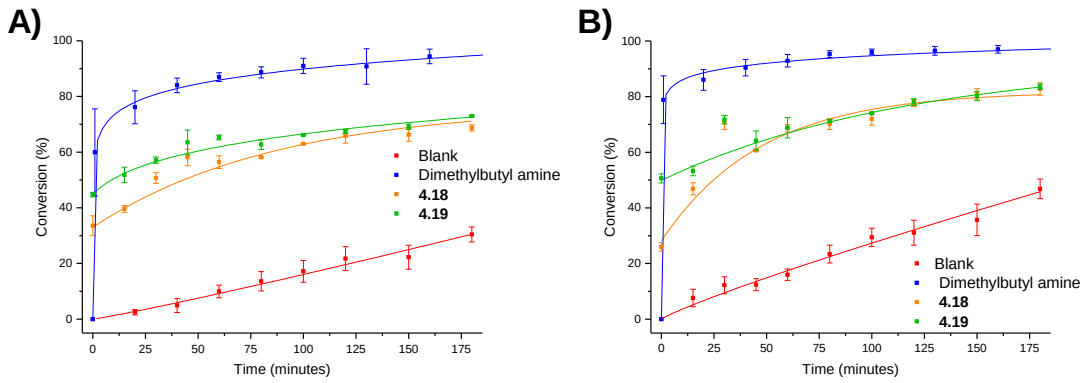

Figure 4.25 Conversion of ethyl cyanoacetate (A) at room temperature and (B) at 55 °C, using polymeric catalysts with a 2% crosslinking density, determined by GC analysis, where 4.18 is the Diels-Alder crosslinked polymer and 4.19 is the TEGDMA crosslinked polymer. Error bars produced from the standard deviation of three repeats.

As a consequence of spatial separation potentially not preventing crosslinker recombination, it was postulated that that addition of a small molecule quencher, in this instance furan, would prevent the Diels-Alder reaction between the two ends of the crosslinker. In order to investigate this, catalysis was repeated with the addition of furan in a 1:1.05 ratio of crosslinker to furan, using the 35% crosslinking density polymers, at 55 °C. In addition to testing the effect of furan to the catalysts, furan was added to the blank formulation to ensure no adverse reactions during the catalysis. Whilst there was no effect of adding furan to the reaction, with the profile mirroring that of a blank reaction without furan, again there was no difference between the two polymeric catalysts at raised temperatures (Figure 4.26).

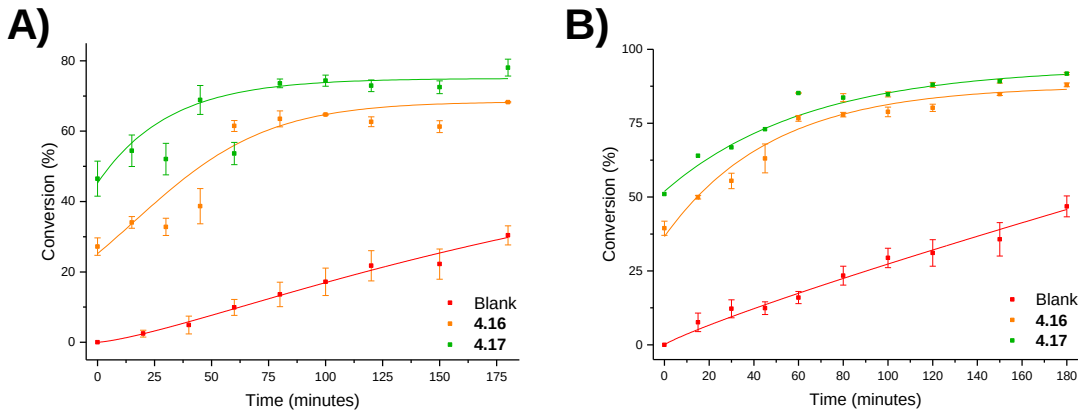

Figure 4.26 Conversion of ethyl cyanoacetate (A) at room temperature and (B) at 55 °C, using polymeric catalysts with a 35% crosslinking density with added small molecule furan as a retro-Diels-Alder quencher, determined by GC analysis, where 4.16 is the Diels-Alder crosslinked polymer and 4.17 is the TEGDMA crosslinked polymer. Error bars produced from the standard deviation of three repeats.

An alternative explanation to crosslinker recombination, the temperature of reaction may be the cause of no catalytic difference between the two crosslinkers. It was hypothesised that there was no difference in catalysis as a consequence of the temperature being insufficiently high enough to trigger a significant amount of retro-Diels-Alder reaction and therefore the Diels-Alder crosslinked polymers are not opening. In order to investigate this, catalysis was carried out at 60 and 70 °C using the 20% crosslinking density polymers. Owing to the rapid rate of catalysis using the small molecule catalysts at 55 °C, the dimethylbutyl amine was not tested at the raised temperatures. It was found that increasing the temperature again had no effect on the catalysis of the two polymeric catalysts, with similar rates of ethyl cyanoacetate conversion observed for both the catalysts (Figure 4.27). This behaviour may be attributable to the kinetics of the reaction at the raised temperatures, with an increase in temperature potentially resulting in a significantly increase rate of reaction, which may make it more difficult to begin to see an additional catalytic effect from the polymeric catalysts.

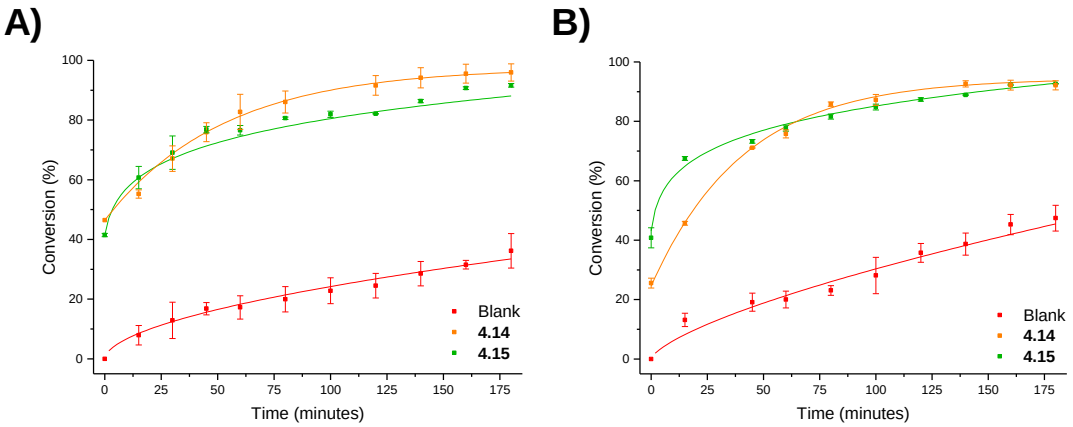

Figure 4.27 Conversion of ethyl cyanoacetate (A) at 60 °C and (B) at 70°C, using polymeric catalysts with a 20% crosslinking density, determined by GC analysis, where 4.14 is the Diels-Alder crosslinked polymer and 4.15 is the TEGDMA crosslinked polymer. Error bars produced from the standard deviation of three repeats.

What was noted throughout the experiments was that, at room temperature, the initial rate of catalysis for the TEGDMA crosslinked polymers tends to be faster than that of the Diels-Alder crosslinked polymers. This may indicate that the more hydrophilic environment generated within the polymeric star core attributable to the TEGDMA crosslinker, in contrast to the more

hydrophobic Diels-Alder crosslinker, is more suited to the benzaldehyde and ethyl cyanoacetate. At a raised temperature this difference in initial rates is less pronounced, which may indicate that there has been some retro-Diels-Alder reaction allowing for a faster rate of catalysis. To confirm this theory, catalysis was repeated using a hydrophobic, sterically bulky pentamethyl benzaldehyde, which should both prevent diffusion into the core of the star, in addition to favouring the more hydrophobic core of the Diels-Alder crosslinked polymer. Catalysis was repeated with the 35% crosslinking density based polymers, and with quenching furan added, with these conditions hypothesised to most likely display a difference between the two polymeric catalysts. At room temperature, the pentamethyl benzaldehyde was found to only be sparingly soluble in solution, yet what is evident is the much reduced rate for the all reactions, including the blank, with both catalysts having approximately the same conversion for ethyl cyanoacetate (Figure 4.28A). At raised temperatures both catalysts were found to catalyse the reaction, with increased conversion for both polymers *vs* the blank. However, the Diels-Alder crosslinked polymer has a noticeably higher conversion than the TEGDMA crosslinked polymeric catalysts, indicating that the crosslinker has undergone the retro-Diels-Alder reaction and resulted in the opening up of the catalyst (Figure 4.28B).

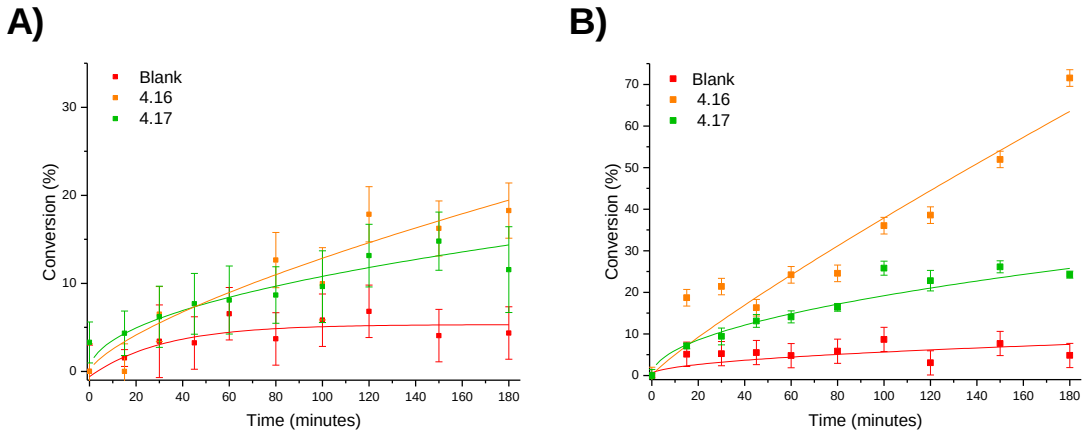

Figure 4.28 Conversion of ethyl cyanoacetate (A) at room temperature and (B) at 55 °C, using the sterically bulky hydrophobic pentamethyl benzaldehyde, and quenching furan, with 35% crosslinked polymeric catalysts, determined by GC analysis, where 4.16 is the Diels-Alder crosslinked polymer and 4.17 is the TEGDMA crosslinked polymer. Error bars produced from the standard deviation of three repeats.

4.3.3 Incorporation of other crosslinkers

4.3.3.1 Disulfide crosslinked polymeric stars

Whilst Diels-Alder chemistry offers one way of incorporating responsive character to the polymeric stars, the application of other stimuli responsive chemistries can also impart responsive character. One such chemistry is the use of disulfides, exploiting redox chemistry to break the disulfide bond and form two thiol species. Consequently disulfide crosslinked polymeric stars were synthesised through the chain extension of $PHEMA_{80}$ with DMAEMA and the commercially available disulfide crosslinker bis(2-methacryloyl) oxyethyl disulfide (DSDMA) (Scheme 4.12).

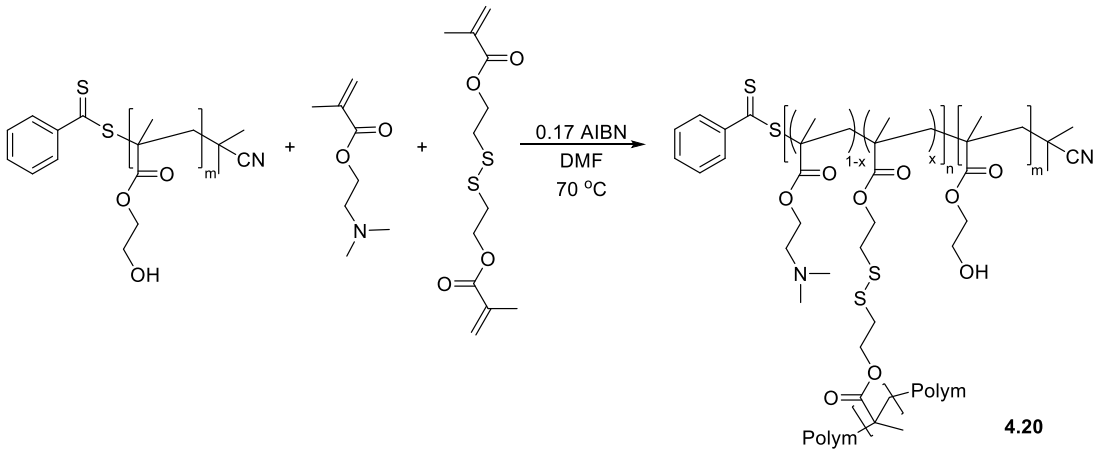

Scheme 4.12 Schematic representation of the synthesis of amine-functionalised polymeric stars (4.20) *via* an arm-first approach using RAFT polymerisation chain extension of PHEMA arms with DMAEMA and the disulfide crosslinker DSDMA.

Analysis of the polymer (**4.20**) using SEC confirmed the successful production of polymeric stars, with a clear shift to higher molecular weights, producing a number-average molecular weight by SEC analysis ($M_{n,\,SEC}$) of 68.1 kg/mol, with a dispersity of 1.54 (Figure 4.29).

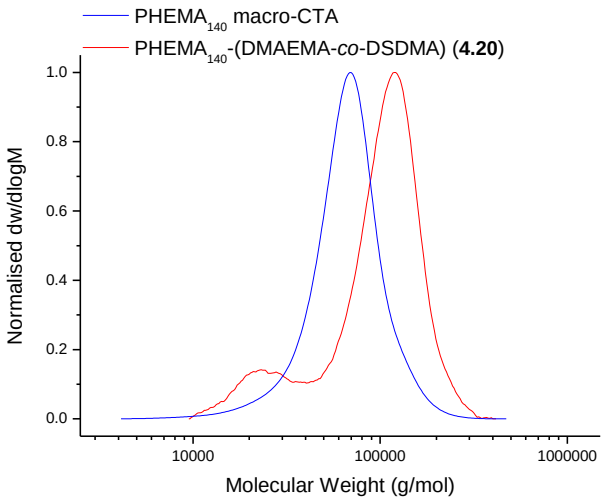

Figure 4.29 Normalised molecular weight distributions for PHEMA$_{140}$-*b*-(DMAEMA-*co*-DSDMA) (4.20), and the PHEMA$_{140}$ macro-CTA (DMF, PMMA standards).

Analysis of the polymer by ^{1}H NMR spectroscopy in deuterated methanol proved unsuccessful, with the polymer only found to swell and not dissolve. Particle size analysis, as determined by DLS in DMF, afforded a hydrodynamic diameter of 14 nm ± 1 nm (PD = 0.40), slightly larger than the TEGDMA crosslinked polymers (Figure 4.30). This size difference is attributed to the larger size of the sulfur atoms requiring more space to fit within the core of the polymer in comparison to the oxygen based TEGDMA crosslinker.

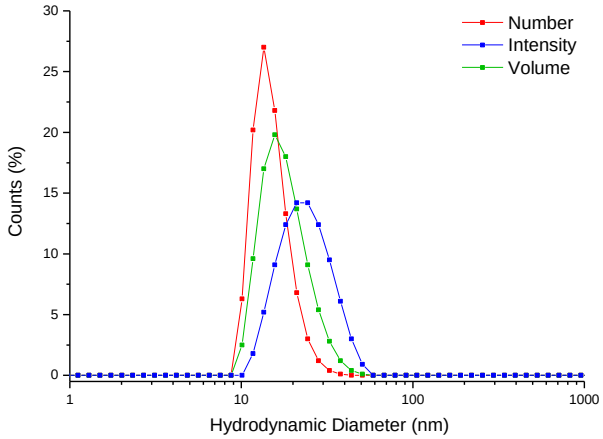

Figure 4.30 Size distribution of 4.20, determined by DLS analysis (2 mg/mL in DMF).

Examination of the responsive behaviour of the disulfide crosslinked polymeric catalysts was carried out through evaluation in the polyurethane formulation. In order to trigger the reduction of the disulfide, dithiothreitol (DTT) was added in a 1:1.05 ratio of crosslinker:DTT, with a blank formulation containing DTT run as a control. Results indicated that there was an increase in catalytic activity between the non-reduced "closed" catalyst and the reduced "open" catalyst (Figure 4.31), with rates of rise of 3.06 mm/sec × 10^{-2} for the "closed" polymeric star and 6.10 mm/sec × 10^{-2} for the "open" polymeric star, double the rate of the non-reduced catalyst, and significantly faster than the blank formulation with a rate of 3.14 mm/sec × 10^{-2}. It should be noted, however, that the DTT was found to be catalytically active itself with a rate of rise of 4.53 mm/sec × 10^{-2}, likely as a consequence of the OH groups on the molecule, and therefore the rate of rise for the "open" catalyst is a combination of the catalytic effect of the "open" catalyst in addition to that exhibited by DTT. This evaluation of the disulfide crosslinked polymeric stars confirms the feasibility of a one-pot formulation, whereby a stimuli responsive catalyst remains dormant within a formulation, producing the same rise profile as a catalyst free formulation, yet upon stimulation is able to result in the opening of the catalyst exposing the catalytically active amines to the formulation, resulting in catalysis of the formation of polyurethane foam.

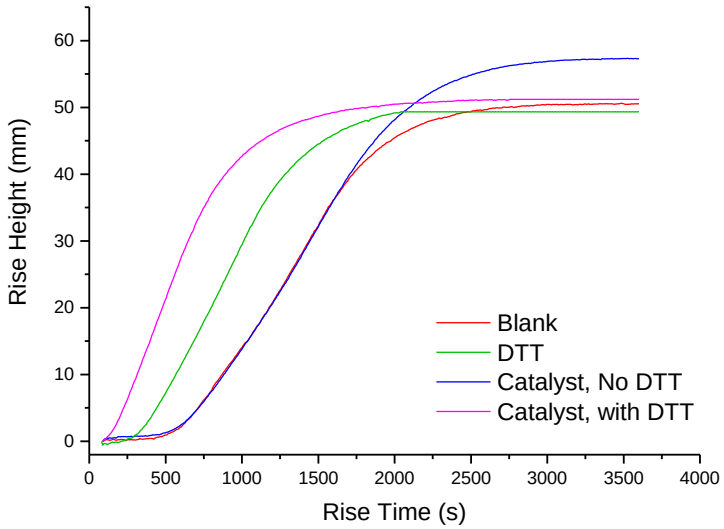

Figure 4.31 Foam rise profile for a polyurethane foam formulation catalysed using the disulfide crosslinked polymer 4.20.

4.4 Conclusion

A furan-maleimide based Diels-Alder crosslinker has been successfully synthesised and incorporated into amine-functionalised polymeric stars using an arm-first RAFT methodology, with the incorporation of the crosslinker confirmed by ^{1}H NMR spectroscopy and SEC analysis. The retro-Diels-Alder reaction temperature was spectroscopically determined, and found occur just above the desired temperature range at 70 °C. Evaluation of the Diels-Alder crosslinked polymers in the polyurethane formulation was found to be unsuccessful, with no difference in catalysis observed for the responsive and non-responsive crosslinkers. Moreover, evaluation of the catalytic activity in the Knoevenagel reaction between benzaldehyde and ethyl cyanoacetate failed to elucidate any difference in catalysis between the non-responsive and responsive crosslinkers, except when reaction conditions were skewed in favour of the Diels-Alder crosslinked polymer. Incorporation of a redox active disulfide crosslinker produced proof-of-principle for a one-pot formulation through evaluation in the polyurethane foam set-up, with non-stimulated polymeric stars matching the rise profile of the catalyst free formulation, yet exhibiting and increased catalytic activity upon addition of the reducing agent. Whilst these disulfide crosslinked particles do provide proof-of-principle for the catalyst, the addition of DTT as a stimulus negates the one-pot idea; if an additional substance needs to be added to trigger catalysis, it negates the idea of a one-pot formulation. Therefore, further work is needed to enable the development of a thermoresponsive catalyst system in which no small molecule needs to be added, only heat applied.

4.5 Experimental

4.5.1 Materials

The following monomers were used as received: 2-hydroxyethyl methacrylate (HEMA, Sigma-Aldrich, 97%), *N,N'*-(dimethylamino) ethyl methacrylate (DMAEMA, Sigma-Aldrich,

98%), tri(ethylene glycol) dimethacrylate (TEGDMA, Sigma-Aldrich, 99%) and bis(2-methacryolyl)oxyethyl disulfide (DSDMA, Sigma-Aldrich). Inhibitor was removed by passing through a plug of basic alumina. 2-cyano-2-propyl benzodithioate (CPBD) was synthesised according to the procedure reported in Chapter 2. The following reagents were used as received: furan (Sigma-Aldrich, 99%), maleimide (Sigma-Aldrich, 99%), ethanolamine (Sigma-Aldrich, 99.5%), triethylamine, (TEA, Fisher Scientific, reagent grade), furfuryl alcohol (Sigma-Aldrich, 98%), methacryloyl chloride (Sigma-Aldrich, 97%), ammonium chloride (Fisher Scientific, 99.5%), furfuryl methacrylate (Sigma-Aldrich, 97%), 7-mercapto-4-methyl coumarin (Sigma-Aldrich, 97%), benzaldehyde (Alfa Aesar, 99%), ethyl cyanoacetate (Sigma-Aldrich, 98%), *N,N*-dimethylbutyl amine (Sigma-Aldrich, 99%), pentamethyl benzaldehyde (Sigma-Aldrich, 97%), dithiothreitol (DTT, Sigma-Aldrich, 97%), 1,2,4-trimethoxy benzene (TMB, Sigma-Aldrich, 97%). The following solvents were used as received: dimethyl formamide (DMF, Fisher Scientific, Laboratory grade and Sigma-Aldrich, spectroscopy grade), methanol (CH_3OH, Fisher Scientific, LT grade), petroleum ether 40-60 °C (pet. ether, Fisher Scientific, LT grade), ethyl acetate (EtOAc, Fisher Scientific, LT grade), anhydrous ethylene glycol (Sigma-Aldrich, 99.8%), toluene (Sigma-Aldrich, reagent grade), 2-propanol (IPA, Fisher Scientific, LT grade), benzene (Sigma-Aldrich, reagent grade), dichloromethane (CH_2Cl_2, Sigma-Aldrich, reagent grade) and diethyl ether (Et_2O, Sigma-Aldrich, AR grade). 2,2'-Azobis(isobutyronitrile) (AIBN) was received from Molekula, recrystallized from methanol and stored at 4 °C. Deuterated solvents (CD_3OD, DMSO-d_6, $CDCl_3$, and DMF-d_7) and silica gel (40-63 μM) were received from Apollo Scientific. Dry solvents were obtained using an Innovative Technology solvent purification system utilising activated alumina.

4.5.2 Instrumentation

In addition to the instrumentation introduced in section 2.5.2, and with the omission of small-angle X-ray scattering, particle size analysis and transmission electron microscopy, the following instrumentation was used in this Chapter: Thermal analysis (Differential Scanning Calorimetry, DSC) was carried out using a Mettler Toledo DSC1 in aluminium pans, with a heating rate of 10 °C/min. unless otherwise stated. Fluorescence spectra were recorded using an Agilent Cary Eclipse Fluorescence spectrophotometer, at a voltage of 850 V.

4.5.3 Synthetic Methods and Procedures

Typical procedure for PHEMA macro-CTA synthesis:

CPBD (1 eq., 350 mg) and HEMA (135 eq.) were dissolved in DMF (90 mL) with radical initiator AIBN (0.12 eq.). Following degassing by purging with nitrogen, the solution was heated to 70 °C for 24 hours (87% conversion). The reaction was quenched in liquid nitrogen and purified by dialysis in 1:1 CH_3OH:H_2O, followed by dialysis in H_2O and subsequent concentration of polymer solution under vacuum. Precipitation into Et_2O afforded a pink-orange solid. (19.6 g, 76%). ^{1}H NMR (400 MHz, CD_3OD): δ (ppm) 7.89 (br s, 2H, *ortho*-Ar*H)*, 7.59 (br s, 1H, *para*-Ar*H*), 7.43 (br s, 2H, *meta*-Ar*H*), 4.05 (br s, O*C*H_2CH_2), 3.79 (br s, OCH_2*C*H_2), 2.03-0.94 (m, CH_2CH_3 backbone). ^{13}C NMR (100 MHz, CD_3OD): δ (ppm) 178.3 (*C*=O), 66.4 (O*C*CO), 59.4 (OC*C*O), 46.9 (C(CH$_3$)*C*H$_2$), 18.5 (C(*C*H$_3$)). IR (neat) max/cm^{-1}: 3435 (υ_{OH}), 2960 (υ_{C-H}), 1723 ($\upsilon_{C=O}$), 1157 (υ_{C-O}). $M_{w,\,SEC}$ = 29.8 kg/mol, $M_{n,\,SEC}$ = 25.9 kg/mol, $Đ_M$ = 1.15.

*Typical procedure for the chain extension of PHEMA with DMAEMA and TEGDMA (**4.1**, **4.10**, **4.13**, **4.15**, **4.17** and **4.19**):*

PHEMA macro-CTA (1 eq., 19.5 g), DMAEMA (200 eq.), and TEGDMA (20 eq.) were dissolved in DMF (120 mL) together with the radical initiator AIBN (0.17 eq.) and the GC

standard TMB. The solution was degassed by purging with nitrogen and the mixture heated for 16 hours (66% conversion). The reaction was quenched by immersion in liquid nitrogen and purified by precipitation into Et_2O three times, affording an orange-pink solid. ^{1}H NMR (400 MHz, CD_3OD): δ (ppm) 7.91 (br s, 2H, *ortho*-Ar*H)*, 7.54 (br s, 1H, *para*-Ar*H*), 7.47 (br s, 2H, *meta*-Ar*H*), 4.31-4.07 (m, C(O)OCH_2CH$_2$, CH_2CH$_2$N, CH_2CH$_2$OH), 3.80-3.67 (m, C(O)OCH$_2$CH_2, OCH$_2$CH$_2$OCH_2CH_2O, CH$_2$CH_2OH), 2.66 (br s, CH$_2$CH_2N), 2.40 (br s, N(CH_3)$_2$), 2.18-0.96 (m, CH_2CH_3 backbone). ^{13}C NMR (100 MHz, CD_3OD): δ (ppm) 178.3 (*C*=O), 66.3 (O*C*CO), 62.1 (O*C*CN), 59.4 (OC*C*O), 56.7 (OC*C*N), 45.0 (C(CH$_3$)*C*H$_2$), 44.5 (N(*C*H$_3$)$_2$), 18.4 (C(*C*H$_3$)). IR (neat) max/cm^{-1}: 3450 (υ_{OH}), 2961 ($\upsilon_{C\text{-}H}$), 2779 ($\upsilon_{N\text{-}CH_3}$), 1725 ($\upsilon_{C=O}$), 1156 ($\upsilon_{C\text{-}O}$). $M_{w,\,SEC}$ = 106.2 kg/mol, $M_{w,\,SEC}$ = 57.3 kg/mol, $M_{n,\,SEC}$ = 37.7 kg/mol, $Đ_M$ = 1.52. D_h = 8 nm ± 1 nm (PD= 0.26). Anal. Calcd. For PHEMA-*b*-(DMAEMA-*co*-TEGDMA): C 56.46; H 8.33; N 3.97%. Found: C 56.36; H 8.36; N 3.95%.

*Typical procedure for the chain extension of PHEMA with DMAEMA and the Diels-Alder crosslinker (**4.8**, **4.9**):*

PHEMA macro-CTA (1 eq., 10.0 g), DMAEMA (200 eq.), and TEGDMA (20 eq.) were dissolved in DMF (230 mL) together with the radical initiator AIBN (0.17 eq.) and the GC standard TMB. The solution was degassed by purging with nitrogen and the mixture heated at 50 °C for 16 hours (30% conversion). The reaction was quenched by immersion in liquid nitrogen and purified by precipitation into Et_2O three times, affording an orange-pink solid. ^{13}C NMR (100 MHz, CD_3OD): δ (ppm) 177.6 (*C*=O), 66.6 (O*C*CO), 62.9 (O*C*CN), 59.4 (OC*C*O), 57.2 (OC*C*N), 45.1 (C(CH$_3$)*C*H$_2$), 44.7 (N(*C*H$_3$)$_2$), 16.6 (C(*C*H$_3$)). IR (neat) max/cm^{-1}: 3659 (υ_{OH}), 2964 ($\upsilon_{C\text{-}H}$), 2824 ($\upsilon_{N\text{-}CH_3}$), 1722 ($\upsilon_{C=O}$), 1451 (υ_{CH}), 1270 ($\upsilon_{C\text{-}O}$), 1147 ($\upsilon_{C\text{-}O}$), 1067 (υ_{CH_3}). $M_{w,\,SEC}$ = 53.4 kg/mol, $M_{n,\,SEC}$ = 37.9 kg/mol, $Đ_M$ = 1.41. D_h = 7 nm ± 1 nm (PD = 0.24).

*Procedure for the chain extension of PHEMA with DMAEMA, TEGDMA and the Diels-Alder crosslinker (**4.11**):*

PHEMA macro-CTA (1 eq., 11.9 g), DMAEMA (200 eq.), Diels-Alder crosslinker (10 eq.) and TEGDMA (10 eq.) were dissolved in DMF (240 mL) together with the radical initiator AIBN (0.17 eq.). The solution was degassed by purging with nitrogen and the mixture heated at 50 °C for 16 hours (38% conversion). The reaction was quenched by immersion in liquid nitrogen and purified by precipitation into Et_2O three times, affording an orange-pink solid. ^{1}H NMR (400 MHz, CD_3OD): δ (ppm) 7.91 (br s, 2H, *ortho*-Ar*H)*, 7.59 (br s, 1H, *para*-Ar*H*), 7.46 (br s, 2H, *meta*-Ar*H*), 6.70 (br m, C(=O)C*H*CH), 6.52 (br s, C(=O)C*H*CCH)), 6.37 (br s, *H*C=C*H*), 5.71 (br s, C=CC*H*), 5.51 (br s, C(=O)OCH_2CC=C), 4.97 (br s, CH_2CH_2OH), 4.13-4.07 (br s, C(O)OCH_2CH_2, CH_2CH_2N, CH_2CH_2OH), 3.80 (br s, C(O)OCH_2CH_2, OCH_2CH_2OCH_2CH_2O, CH_2CH_2OH), 2.69 (br s, CH_2CH_2N), 2.37 (br s, N(CH_3)$_2$), 2.04-0.96 (m, CH_2CH_3 backbone). ^{13}C NMR (100 MHz, CD_3OD): δ (ppm) 177.4 (*C*=O), 66.7 (O*C*CO), 62.9 (O*C*CN), 59.4 (OC*C*O), 57.5 (OC*C*N), 45.1 (C(CH_3)*C*H_2), 44.9 (N(*C*H_3)$_2$), 17.4 (C(*C*H_3)). IR (neat) max/cm^{-1}: 3655 (υ_{OH}), 2964 (υ_{C-H}), 2825 (υ_{N-CH_3}), 1724 ($\upsilon_{C=O}$), 1451 (υ_{CH}), 1271 (υ_{C-O}), 1147 (υ_{C-O}), 1067 (υ_{CH_3}). $M_{w,\,SEC}$ = 63.7 kg/mol, $M_{n,\,SEC}$ = 45.2 kg/mol, $Đ_M$ = 1.41. D_h = 8 nm (PD = 0.29). Anal. Calcd. For PHEMA-*b*-(DMAEMA-*co*-TEGDMA): C 55.50; H 8.03; N 3.11%. Found: C 55.51; H 7.96; N 3.09%.

*Procedure for the chain extension of PHEMA with DMAEMA and DSDMA (**4.20**):*

PHEMA macro-CTA (1 eq., 3 g), DMAEMA (200 eq.), and DSDMA (40 eq.) were dissolved in DMF (120 mL) together with the radical initiator AIBN (0.17 eq.) and the GC standard TMB. The solution was degassed by purging with nitrogen and the mixture heated at 70 °C for 150 minutes (87% conversion). The reaction was quenched by immersion in liquid nitrogen and purified by precipitation into Et_2O three times, affording an orange-pink solid. $M_{w,\,SEC}$ =

104.9 kg/mol, $M_{n,\,SEC}$ = 68.1 kg/mol, $Đ_M$ = 1.54. D_h = 14 nm ± 1 nm (PD = 0.40). Nitrogen content = 3.63%

*Synthesis of dioxatricyclodecene dione (**4.2**):*

Maleic anhydride (1 eq., 8 g), and furan (1.01 eq., 5.6 g) were dissolved in toluene (80 mL) and stirred for 24 hours. The product was isolated by filtration, and washed with cold Et_2O, with the resulting solid dried under vacuum, affording a white crystalline solid (10.7 g, 79%). ^{1}H NMR (400 MHz, $CDCl_3$): δ (ppm) 6.85 (s, 2H, C=C*H*), 5.46 (s, 2H, OC*H*), 3.18 (s, 2H, OC(=O)C*H*). ^{13}C NMR (100 MHz, $CDCl_3$): δ (ppm) 169.7 (*C*=O), 136.8 (*C*=*C*), 82.0 (C*C*C=C), 48.5 (OC(=O)*C*). IR (neat) max/cm^{-1}: 3000 ($\upsilon_{=CH}$), 1857 ($\upsilon_{C=O}$), 1752 ($\upsilon_{C=C}$), 1310 (υ_{CH}), 1282 (υ_{CH}), 1145 (υ_{C-O}), 1147 (υ_{C-O}), 1084 (υ_{CH_3}). *m/z* [ESI MS]: 189.0 (M+Na). Anal. Calcd. For $C_8H_6O_4$: C 57.84; H 3.64. Found: C 57.80; H 3.59.

*Synthesis of hydroxyethyloxa-aza-tricyclodecene dione (**4.3**):*

Dioxatricyclodecene dione (1 eq., 10.9 g), was added to a dried three-neck round bottom flask, equipped with a magnetic stirrer bar, a condenser and a dropping funnel, and dissolved in methanol (250 mL). The solution was cooled on ice, and purged with nitrogen for 30 minutes. Triethylamine (1 eq., 9 mL) was added dropwise, followed by the dropwise addition of ethanolamine (1.01 eq., 4 mL). The flask was removed from the ice and the contents were brought to and maintained under reflux for 16 hours, after which a further 10% of ethanolamine was added, (0.1 eq., 0.4 mL), and the reaction was maintained at reflux for a further 2 hours. The resultant solid was isolated by filtration and washed with IPA (3 × 100 mL), affording a white crystalline solid (9.1 g, 66%). ^{1}H NMR (400 MHz, $CDCl_3$): δ (ppm) 6.50 (s, 2H, C=C*H*), 5.26 (s, 2H, OC*H*), 3.76-3.34 (m, 4H, NCH_2CH_2OH), 2.88 (s, 2H, NC(=O)C*H*), 2.35 (t, 1H, CH_2O*H*, $^3J_{H\text{-}H}$ = 5.6 Hz). ^{13}C NMR (100 MHz, $CDCl_3$): δ (ppm) 176.9 (*C*=O), 136.6 (*C*=*C*), 81.1 (C*C*C=C), 60.2 (NCH$_2$*C*H$_2$OH), 47.6 (NC(=O)*C*), 41.8 (N*C*H$_2$CH$_2$OH). IR (neat) max/cm^{-1}:

3474 (υ_{OH}), 2974 (υ_{CH}), 1768 ($\upsilon_{C=C}$), 1684 ($\upsilon_{C=O}$). *m/z* [ESI MS]: 231.7 (M+Na). Anal. Calcd. For $C_{10}H_{11}NO_4$: C 57.41; H 5.30; N 6.70. Found: C 57.31; H 5.24; N 6.66.

*Synthesis of hydroxyethyl pyrrole dione (**4.4**):*

Hydroxyethyloxa-aza-tricyclodecene dione (1 eq., 5.7 g) was added to a dried round bottom flask, and dissolved in toluene (150 mL). The solution was brought to and maintained under reflux for 16 hours, hot filtered and cooled to room temperature. Following precipitation, the solution was filtered and the solid dried under vacuum, affording a white crystalline solid (3.7 g, 95%). ^{1}H NMR (400 MHz, $CDCl_3$): δ (ppm) 6.71 (s, 2H, C=C*H*), 3.73-3.65 (m, 4H, NC*H*$_2$C*H*$_2$OH), 2.61 (br s, CH_2O*H*). ^{13}C NMR (100 MHz, $CDCl_3$): δ (ppm) 171.3 (*C*=O), 134.3 (*C*=*C*), 60.6 (NCH$_2$*C*H$_2$OH), 40.6 (N*C*H$_2$CH$_2$OH). IR (neat) max/cm^{-1}: 3261 (υ_{OH}), 2962 (υ_{CH}), 1710 ($\upsilon_{C=C}$), 1695 ($\upsilon_{C=O}$). *m/z* [ESI MS]: 163.7 (M+Na).

*Synthesis of hydroxyethyloxa-aza-tricyclodecene dione amino ethanol (**4.5**):*

Hydroxyethyl pyrrole dione (1 eq., 3.6 g), and furfuryl alcohol (1 eq., 2.2 mL) were dissolved in benzene and the solution was brought to and maintained under reflux for 16 hours. The flask was cooled to room temperature, and the resultant solid isolated by precipitation, washed with cold diethyl ether and dried under vacuum, affording a white crystalline solid (2.5 g, 41%). ^{1}H NMR (400 MHz, DMSO-d_6): δ (ppm) 7.36 (s, 2H, C=C*H*), 5.07 (br s, 1H, OCH$_2$O*H*), 4.98 (t, 1H, NCH$_2$CH$_2$O*H*, $^3J_{H\text{-}H}$ = 5.7 Hz), 4.80 (t, 1H, C(=C)C*H*, $^3J_{H\text{-}H}$ = 5.6 Hz), 4.03 (dd, 1H, OCC*H*$_2$OH, $^2J_{H\text{-}H}$ = 12.5 Hz, $^3J_{H\text{-}H}$ = 6.0 Hz), 3.68 (dd, 1H, OCC*H*$_2$OH, $^2J_{H\text{-}H}$ = 12.6 Hz, $^3J_{H\text{-}H}$ = 5.5 Hz), 3.45 (br s, 4H NC*H*$_2$C*H*$_2$OH), 3.04 (d, 1H, NC(=O)C*H*, $^3J_{H\text{-}H}$ = 6.5 Hz), 2.87 (d, 1H, NC(=O)C*H*, $^3J_{H\text{-}H}$ = 6.5 Hz).

*Synthesis of methacryloylethyl pyrrole dione (**4.7**)*:

Hydroxyethyl pyrrole dione (1 eq., 8.8 g) was dissolved in anhydrous CH_2Cl_2 and cooled to 0 °C. TEA (3 eq., 26 mL) was added dropwise, followed by the dropwise addition of methacryloyl

chloride (1.05 eq., 6.4 mL). The flask was allowed to warm to room temperature and left stirring for 16 hours. The solution was extracted with basic water, ammonium chloride, water and brine, and the organic phase dried over magnesium sulfate. The solution was filtered and the solvent was removed under vacuum, affording a white crystalline solid (6.0 g, 46%). ^{1}H NMR (400 MHz, $CDCl_3$): δ (ppm) 6.73 (s, 2H, C=C*H*), 6.06 (s, 1H, C=CH_2), 5.56 (s, 1H, C=CH_2), 4.29 (t, 2H, NCH$_2$CH_2, $^{3}J_{H\text{-}H}$ = 4.7 Hz), 3.85 (t, 2H, NCH_2CH$_2$, $^{3}J_{H\text{-}H}$ = 4.9 Hz), 1.90 (s, 3H, CH_3). ^{13}C NMR (100 MHz, $CDCl_3$): δ (ppm) 170.3 (*C*(=O)N), 167.0 (*C*=O), 135.8 (*C*=CH$_2$), 134.3 (*C*(H)=*C*(H)), 126.3 (C=*C*H$_2$), 61.7 (*C*H$_2$O), 37.0 (N*C*H$_2$), 18.2 (*C*H$_3$). IR (neat) max/cm^{-1}: 2961 (υ_{CH}), 1707 ($\upsilon_{C=O}$), 1440, 1404, 1364 (υ_{CH}).

*Synthesis of Diels-Alder Crosslinker (**4.6**):*

*Using **4.5**:*

Hydroxyethyloxa-aza-tricyclodecene dione amino ethanol (1 eq., 4.1 g) was dissolved in anhydrous CH_2Cl_2 (25 mL), cooled to 0 °C, and TEA added dropwise. Following the dropwise addition of methacryloyl chloride (2.15 eq., 1.95 mL) the reaction was allowed to warm to room temperature and stirred for 24 hours. The reaction solution was extracted with ammonium chloride and brine, the organic phase dried over magnesium sulfate and the solvent removed *in vacuo*. The crude solid was purified using column chromatography (silica gel, 2:1 pet. ether/EtOAc), R_f (2:1 pet. ether/EtOAc): 0.16, affording a viscous colourless liquid (10%).

*Using **4.7***

Methacryloylethyl pyrrole dione (1 eq., 8.0 g) was dissolved in anhydrous toluene (70 mL) and furfuryl methacrylate (1.02 eq., 6 mL) was added dropwise. The mixture was left stirring for 24 hours, and the solvent removed *in vacuo*. The crude solid was purified using column chromatography (silica gel, 3:1 pet. ether/ EtOAc), R_f (2:1 pet. ether/EtOAc): 0.22, affording a viscous colourless liquid (10%).

^{1}H NMR (400 MHz, $CDCl_3$): δ (ppm) 6.55 (dd, 1H, C=CH_{endo}, $^{3}J_{H\text{-}H}$ = 5.7 Hz, $^{2}J_{H\text{-}H}$ = 1.3 Hz), 6.44 (d, 1H, C=CH_{endo}, $^{3}J_{H\text{-}H}$ = 5.7 Hz), 6.40 (dd, 1H, C=CH_{exo}, $^{3}J_{H\text{-}H}$ = 5.7 Hz, $^{3}J_{H\text{-}H}$ = 1.2 Hz), 6.29 (d, 1H, C=CH_{exo}, $^{3}J_{H\text{-}H}$ = 5.8 Hz), 6.17 (m, 1H, C=CH_{exo}), 6.12 (m, 2H, C=CH_{exo}, C=CH_{endo}), 6.07 (m, 1H, C=CH_{exo}), 5.62-5.55 (m, 4H, C=CHCO$_{endo}$, C=CHCO$_{exo}$), 5.31 (dd, 1H, C=CCHC$_{exo}$, $^{3}J_{H\text{-}H}$ = 5.6 Hz, $^{3}J_{H\text{-}H}$ = 1.6 Hz), 5.26 (m, 1H, C=CCHC$_{endo}$), 4.99 (d, 1H, C(=O)OCH_2CC=C$_{endo}$, $^{2}J_{H\text{-}H}$ = 12.9 Hz), 4.89 (d, 1H, C(=O)OCH_2CC=C$_{exo}$, $^{2}J_{H\text{-}H}$ = 12.7 Hz), 4.67 (d, 1H, C(=O)OCH_2CC=C$_{exo}$, $^{2}J_{H\text{-}H}$ = 12.7 Hz), 4.51 (d, 1H, C(=O)OCH_2CC=C$_{endo}$, $^{2}J_{H\text{-}H}$ = 12.8 Hz), 4.29 (m, 2H, NCH$_2$CH_2O$_{endo}$), 4.17 (m, 2H, NCH$_2$CH_2O$_{exo}$), 3.81 (m, 2H, NCH_2CH$_2$O$_{endo}$), 3.66 (m, 2H, NCH_2CH$_2$O$_{exo}$ and NC(=O)CH_{exo}) 3.40 (d, 1H, NC(=O)CH_{exo}, $^{3}J_{H\text{-}H}$ = 7.7 Hz), 3.00 (d, 1H, NC(=O)CH_{endo}, $^{3}J_{H\text{-}H}$ = 6.5 Hz), 2.93 (d, 2H, NC(=O)CH_{endo}, $^{3}J_{H\text{-}H}$ = 6.5 Hz), 1.95 (m, 3H, C(CH$_2$)C$H_{3exo\ and\ endo}$), 1.90 (m, 3H, C(CH$_2$)C$H_{3exo\ and\ endo}$).

4.6 Bibliography

1. Bapat, A. P., Ray, J. G., Savin, D. A., Hoff, E. A., Patton, D. L., Sumerlin, B. S., *Polym. Chem.*, **2012**, 3, 3112.
2. Chen, F., Chen, H., Duan, X., Jia, J., Kong, J., *J. Mater. Sci.*, **2016**, 51, 9367.
3. Chen, H., Jia, J., Duan, X., Yang, Z., Kong, J., *J. Polym. Sci., Part A: Polym. Chem.*, **2015**, 53, 2374.
4. Li, L., Wang, X., Yang, J., Ye, X., Wu, C., *Macromolecules*, **2014**, 47, 650.
5. Rosselgong, J., Armes, S. P., *Macromolecules*, **2012**, 45, 2731.
6. Rosselgong, J., Blanazs, A., Chambon, P., Williams, M., Semsarilar, M., Madsen, J., Battaglia, G., Armes, S. P., *ACS Macro Lett.*, **2012**, 1, 1041.
7. Gao, Y., Böhmer, V. I., Zhou, D., Zhao, T., Wang, W., Paulusse, J. M. J., *J. Control. Release*, **2016**, 288, 375.
8. Jackson, A. W., Fulton, D. A., *Polym. Chem.*, **2013**, 4, 31.
9. Canadell, J., Goossens, H., Klumperman, B., *Macromolecules*, **2011**, 44, 2536.
10. Guimard, N. K., Oehlenschlaeger, K. K., Zhou, J., Hilf, S., Schmidt, F. G., Barner-Kowollik, C., *Macromol. Chem. Phys.*, **2012**, 213, 131.
11. Yang, Y., Urban, M. W., *Chem. Soc. Rev.*, **2013**, 42, 7446.
12. Hentschel, J., Kushner, A. M., Ziller, J., Guan, Z., *Angew. Chem.*, **2012**, 124, 10713.
13. Ghosh, S. K., *Self-healing materials: fundamentals, design strategies, and applications*, John Wiley & Sons, **2009**.
14. Burattini, S., Greenland, B. W., Chappell, D., Colquhoun, H. M., Hayes, W., *Chem. Soc. Rev.*, **2010**, 39, 1973.
15. Roberto, M., Alaitz, R., Alaitz Ruiz de, L., Pablo, C., Damien, D., Germán, C., Hans, J. G., Ibon, O., *Smart Mater. Struct.*, **2016**, 25, 084017.
16. Tsarevsky, N. V., Matyjaszewski, K., *Macromolecules*, **2005**, 38, 3087.
17. Pal, S., Hill, M. R., Sumerlin, B. S., *Polym. Chem.*, **2015**, 6, 7871.

18. Yoon, J. A., Kamada, J., Koynov, K., Mohin, J., Nicolaÿ, R., Zhang, Y., Balazs, A. C., Kowalewski, T., Matyjaszewski, K., *Macromolecules*, **2012**, 45, 142.
19. Wei, Z., Yang, J. H., Zhou, J., Xu, F., Zrinyi, M., Dussault, P. H., Osada, Y., Chen, Y. M., *Chem. Soc. Rev.*, **2014**, 43, 8114.
20. An, S. Y., Noh, S. M., Nam, J. H., Oh, J. K., *Macromol. Rapid Commun.*, **2015**, 36, 1255.
21. Pepels, M., Filot, I., Klumperman, B., Goossens, H., *Polym. Chem.*, **2013**, 4, 4955.
22. Tasdelen, M. A., *Polym. Chem.*, **2011**, 2, 2133.
23. Gandini, A., *Prog. Polym. Sci.*, **2013**, 38, 1.
24. Sanyal, A., *Macromol. Chem. Phys.*, **2010**, 211, 1417.
25. Lallana, E., Sousa-Herves, A., Fernandez-Trillo, F., Riguera, R., Fernandez-Megia, E., *Pharm. Res.*, **2012**, 29, 1.
26. Gregoritza, M., Brandl, F. P., *Eur. J. Pharm. Biopharm.*, **2015**, 97, Part B, 438.
27. Park, J. S., Darlington, T., Starr, A. F., Takahashi, K., Riendeau, J., Thomas Hahn, H., *Compos. Sci. Technol.*, **2010**, 70, 2154.
28. Bergman, S. D., Wudl, F., *J. Mater. Chem.*, **2008**, 18, 41.
29. Chen, X., Dam, M. A., Ono, K., Mal, A., Shen, H., Nutt, S. R., Sheran, K., Wudl, F., *Science*, **2002**, 295, 1698.
30. Murphy, E. B., Wudl, F., *Prog. Polym. Sci.*, **2010**, 35, 223.
31. Diels, O., Alder, K., *Liebigs Ann.*, **1928**, 460, 98.
32. Liu, Y.-L., Chuo, T.-W., *Polym. Chem.*, **2013**, 4, 2194.
33. Stille, J. K., Plummer, L., *J. Org. Chem.*, **1961**, 26, 4026.
34. Mantovani, G., Lecolley, F., Tao, L., Haddleton, D. M., Clerx, J., Cornelissen, J. J., Velonia, K., *J. Am. Chem. Soc.*, **2005**, 127, 2966.
35. Durmaz, H., Colakoglu, B., Tunca, U., Hizal, G., *J. Polym. Sci., Part A: Polym. Chem.*, **2006**, 44, 1667.
36. Altinbasak, I., Sanyal, R., Sanyal, A., *RSC Adv.*, **2016**, 6, 74757.
37. Syrett, J. A., Mantovani, G., Barton, W. R. S., Price, D., Haddleton, D. M., *Polym. Chem.*, **2010**, 1, 102.
38. Reutenauer, P., Buhler, E., Boul, P. J., Candau, S. J., Lehn, J. M., *Chem. Eur. J.*, **2009**, 15, 1893.
39. Zhang, Y., Broekhuis, A. A., Picchioni, F., *Macromolecules*, **2009**, 42, 1906.
40. Liu, Y.-L., Hsieh, C.-Y., *J. Polym. Sci., Part A: Polym. Chem.*, **2006**, 44, 905.
41. Kötteritzsch, J., Stumpf, S., Hoeppener, S., Vitz, J., Hager, M. D., Schubert, U. S., *Macromol. Chem. Phys.*, **2013**, 214, 1636.
42. Peterson, A. M., Jensen, R. E., Palmese, G. R., *ACS Appl. Mater. Interfaces*, **2010**, 2, 1141.
43. Froidevaux, V., Borne, M., Laborbe, E., Auvergne, R., Gandini, A., Boutevin, B., *RSC Adv.*, **2015**, 5, 37742.
44. Heo, Y., Sodano, H. A., *Adv. Funct. Mater.*, **2014**, 24, 5261.
45. Ciganek, E., *Organic Reactions*, **1984**.
46. Tanikaga, R., Konya, N., Kaji, A., *Chem. Lett.*, **1985**, 14, 1583.
47. Li, G., Xiao, J., Zhang, W., *Green Chem.*, **2011**, 13, 1828.
48. Jones, G., *Org. React.*, **1967**, 15, 204.

5. The Synthesis of Thermoresponsive Isocyanate Crosslinked Polymeric Stars

5.1 Abstract

This Chapter reports the synthesis of diisocyanate based monomers, through the synthesis of a new monomer, methacryloyl pyrazole, and the reaction of this monomer with diisocyanates to produce divinyl thermoresponsive crosslinkers. Incorporation of the crosslinkers was attempted through both direct polymerisation of the diisocyanate containing monomer, and through polymerisation of the methacryloyl pyrazole to produce a linear precursor which was subsequently reacted with a diisocyanate to produce a hyperbranched-core star polymer. The formation of crosslinked polymeric stars has been characterised using a variety of analytical techniques, including triple-detection Size Exclusion Chromatography and Transmission Electron Microscopy. The thermoresponsive deblocking of the reaction has been evaluated using Size Exclusion Chromatography, where it has been demonstrated that the deblocking temperature, and therefore disassembly of the polymeric stars, can be modified through variance in the diisocyanate used, producing a range of stars able to deblock between 35 °C and 65 °C. Additionally, an aliphatic blocked isocyanate has been synthesised and characterised, and its suitability for the one-pot polyurethane formulation confirmed.

5.2 Introduction

Within the last two decades, significant advances have been made in the field of latent catalysts for polymerisation systems. Such advancements have resulted in the development of latent catalysts for ring-opening metathesis[1-3] and polyacrylate synthesis.[4-6] A latent catalyst can be described as a compound that is completely inert under storage conditions, allowing for all the reaction components to be mixed and stored without the reaction taking place, yet upon activation becomes highly reactive.[7, 8] Activation of the catalysts can be achieved through a range of techniques, including heating, pressure, photo-irradiation and magnetism, with thermal activation found to be the most facile method of stimulation.[9-13]

Industrially, there is a rising demand for polyurethane formulations with a shelf-life as long as possible, in order to reduce waste and to increase process time of the formulation.[14, 15] As a consequence of this demand, methods have been developed to meet these requirements. Many solutions to improving pot-life have been reported, including the use of blocked isocyanates,[16, 17] discussed in Chapter 6, and deactivated isocyanate powders,[15] yet more recently an alternative method has been developed: "curing-on-demand" formulations. Here, latent catalysts have been developed to ensure that the desired reaction catalysis occurs only when triggered, prolonging the pot-life of the formulation.

One such method that has gained attention in recent years is the encapsulation of polyurethane catalysts, ensuring the catalyst remains dormant until released/activated, allowing for an increase in the timeframe of formulation processability. Bijlard *et al.* demonstrated the successful use of this encapsulation method for the production of a thermoset polyurethane, encapsulating the catalytic dimethyltin dineodecanoate within a polymer shell of poly(methyl methacrylate-*co*-butyl methacrylate-*co*-methacrylic acid), crosslinked with 1,4-butanediol dimethacrylate.[15] Isooctane was also encapsulated as a release agent, with a release mechanism

based on the evaporation of isooctane with heating, increasing the internal pressure of the capsule until eventually rupturing, resulting in the release of the catalyst (Figure 5.1).

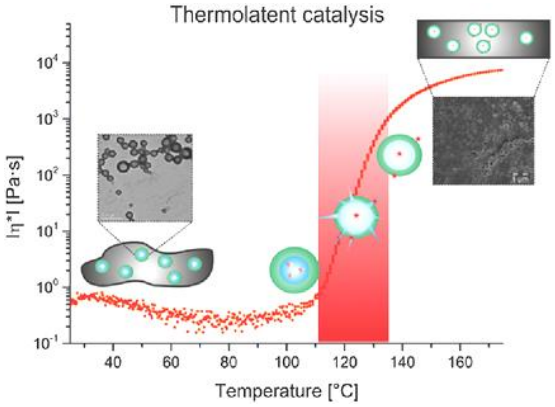

Figure 5.1 Thermolatent catalysis for the production of polyurethane, using a nanocapsule containing a tin catalyst and isooctane as a release agent. Reproduced with permission from Bijlard *et al.*[15]

An alternative to encapsulation is to develop catalysts that remain inert until stimulation. Carroy *et al*. reported the synthesis of photo-latent catalysts consisting of both tin and non-tin compounds for a two-component polyurethane system.[14] It was demonstrated that the latent catalysts both improved pot-life, evidenced in the lower formulation viscosity when compared to the non-latent dibutyltin dilaurate (DBTL) catalyst indicating a significantly reduced production of polyurethane (Figure 5.2A), provided that the formulation is stored away from UV-light, as well as exhibiting a significant catalytic effect on curing of a polyurethane coating after irradiation of the formulation with UV light (Figure 5.2B).

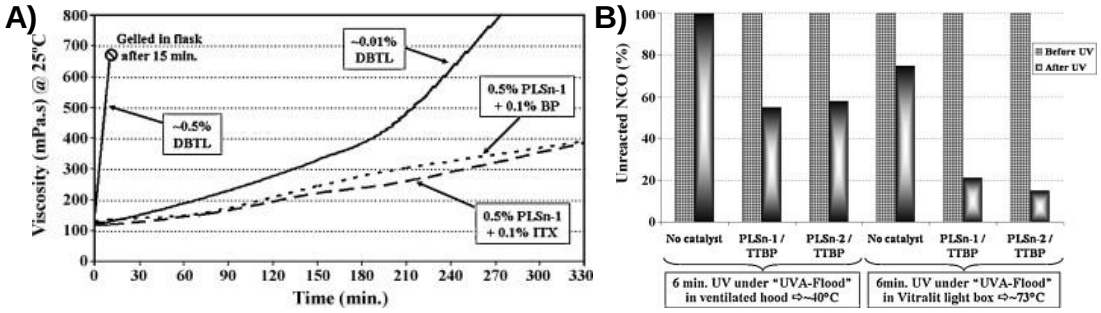

Figure 5.2 The effect of using a photolatent tin catalyst for polyurethane production. (A) influence of the type and level of catalyst on the formulation viscosity, and (B) Catalyst efficiencies under different conditions. Reproduced from Carroy *et al.*[14]

Alsarraf *et al.* reacted different guanidines with a monoisocyanate, analogous to the blocking of isocyanates through reaction with an external blocking agent, to produce a series of delayed-action catalysts which, upon thermal activation, regenerated the catalytic guanidine precursor.[18] Prior to thermal activation, little to no catalytic activity was observed, yet heating of the formulation to 60 °C resulted in a significant increase in conversion (Figure 5.3).

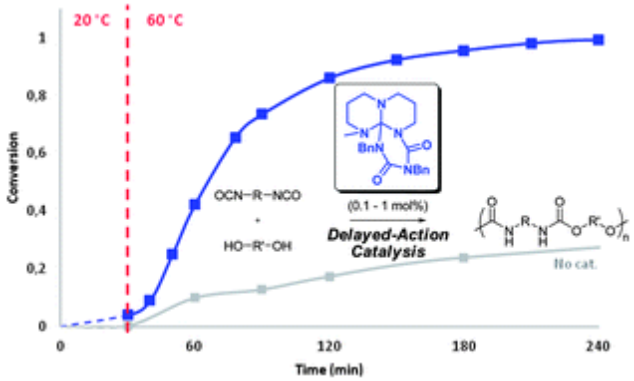

Figure 5.3 The conversion of isophorone diisocyanate and polytetramethylene oxide into polyurethane, catalysed by a thermolatent guanidine based catalyst. Reproduced with permission from Alsarraf *et al*.[18]

However, a large proportion of latent catalysts include the addition of other small molecules to the formulation, for example the release agent isooctane or the ligands of the latent photo-active tin catalysts. Such addition of small molecules to the formulation has been demonstrated to have a marked impact on the final product material. Meier-Westhues reported that, especially in a one-component system, when using a blocked isocyanate method for increasing pot-life, the blocking agent was responsible for increased thermal yellowing, though this could be mitigated through the use of correct stabilisers.[19] Moreover it was noted that residual blocking agents in a paint film affected film quality resulting in lower etch resistance.[19] Other problems associated with the addition of small molecules to polyurethane formulations include their activity as plasticisers,[20] and the formation of bubbles in the final product.

Taking this into account, it was decided that encapsulation of the catalytic tertiary amine within the core of the polymeric star, as demonstrated in previous chapters, would potentially allow for latent catalysis, but to negate the addition of further small molecules, such polymeric

stars would be crosslinked using an isocyanate. Upon heating, it is hypothesised that the blocked isocyanate crosslinker would deblock, releasing an isocyanate (which can be matched to the one used in the formulation), resulting in the destruction of the polymeric stars and exposure of the catalytic tertiary amine to the polyurethane formulation, allowing for catalysis (Figure 2.3).

5.3 Results and Discussion

5.3.1 Synthesis of an isocyanate releasing crosslinker

Following the demonstration of the use of an arm-first Reversible Addition-Fragmentation Chain Transfer (RAFT) polymerisation methodology to successfully synthesise amine-functionalised polymeric stars, it was decided that the same approach would be taken to produce the isocyanate crosslinked polymeric catalysts, with a blocked isocyanate crosslinker replacing the non-responsive tri(ethylene glycol) dimethacrylate crosslinker (TEGDMA). The crosslinker will be synthesised through the reaction of the diisocyanate with a monomer containing an active hydrogen, allowing for the synthesis of a thermally labile blocked isocyanate (Scheme 5.1). The blocking group was chosen to be pyrazole based, as a consequence of the reported deblocking temperature, between 80-110 °C, being close to that required for the one-pot formulation.[21]

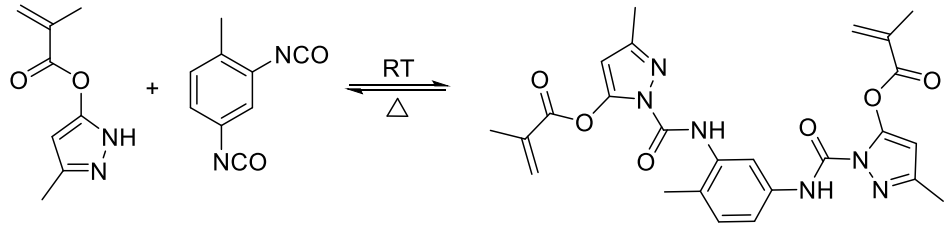

Scheme 5.1 Schematic representation for the synthesis of a thermally labile diisocyanate crosslinker synthesised *via* the reaction of an active hydrogen containing compound and a diisocyanate.

The synthesis of the hydroxy-functionalised pyrazole 3-methyl-1*H*-pyrazol-5-ol (hydroxy pyrazole, **5.1**) was based on a previously reported literature procedure.[22] The reaction between ethyl acetoacetate and hydrazine hydrate was performed for 16 hours in ethanol (Scheme 5.2).

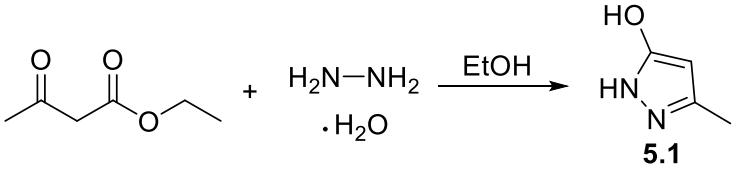

5.1

Scheme 5.2 Schematic representation for the synthesis of hydroxy pyrazole (5.1).

The product was purified by recrystallisation in ethanol, affording a white crystalline solid in an acceptable yield (49%). The successful synthesis was confirmed by ^{1}H and ^{13}C Nuclear Magnetic Resonance (NMR) spectroscopy (Figure 5.4 and Figure 5.5, respectively) and Fourier-Transform Infra-Red (FT-IR) spectroscopy (Figure 5.6), which displayed the characteristic C=O pyrazolinone stretch of the ketone tautomer at υ = 1615 cm^{-1},[23, 24] in addition to NH stretches attributed to 3- substituted pyrazoles at 2990 cm^{-1}. Mass spectral analysis further confirmed synthesis of the hydroxyl pyrazole, with a mass of 98.7 *m/z* (M+H), in addition to elemental analysis and melting point analysis confirming the purity of the product.

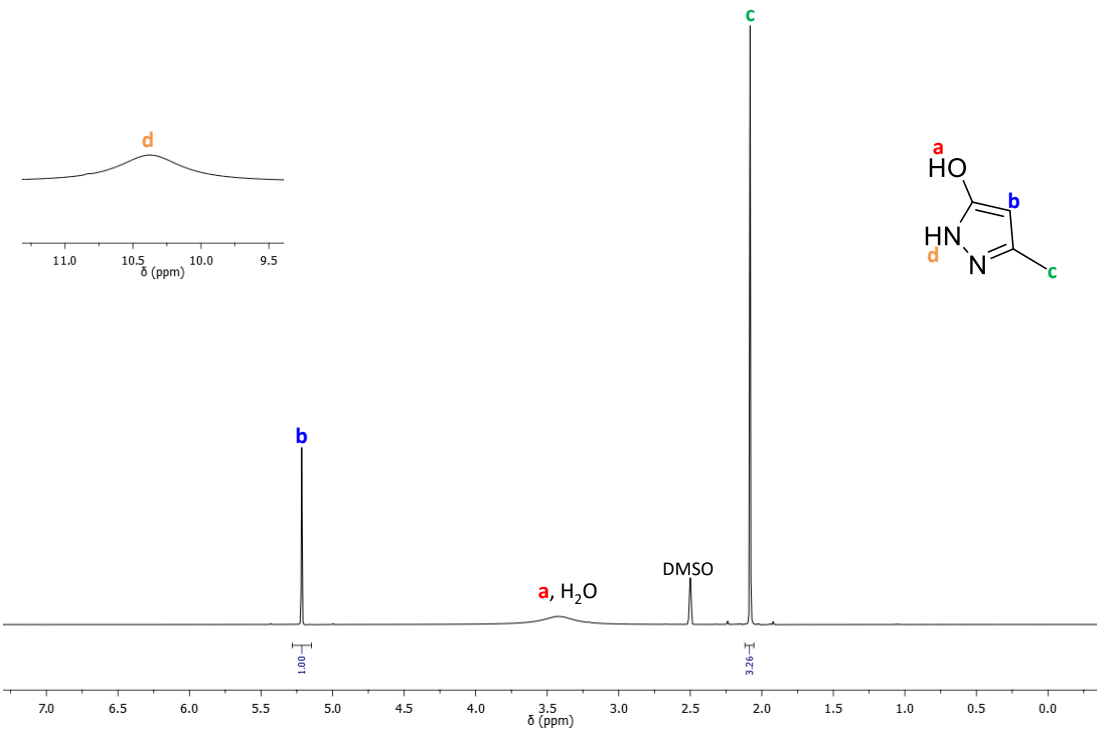

Figure 5.4 ^{1}H NMR spectrum of hydroxy pyrazole, 5.1 (400 MHz, DMSO-d_6).

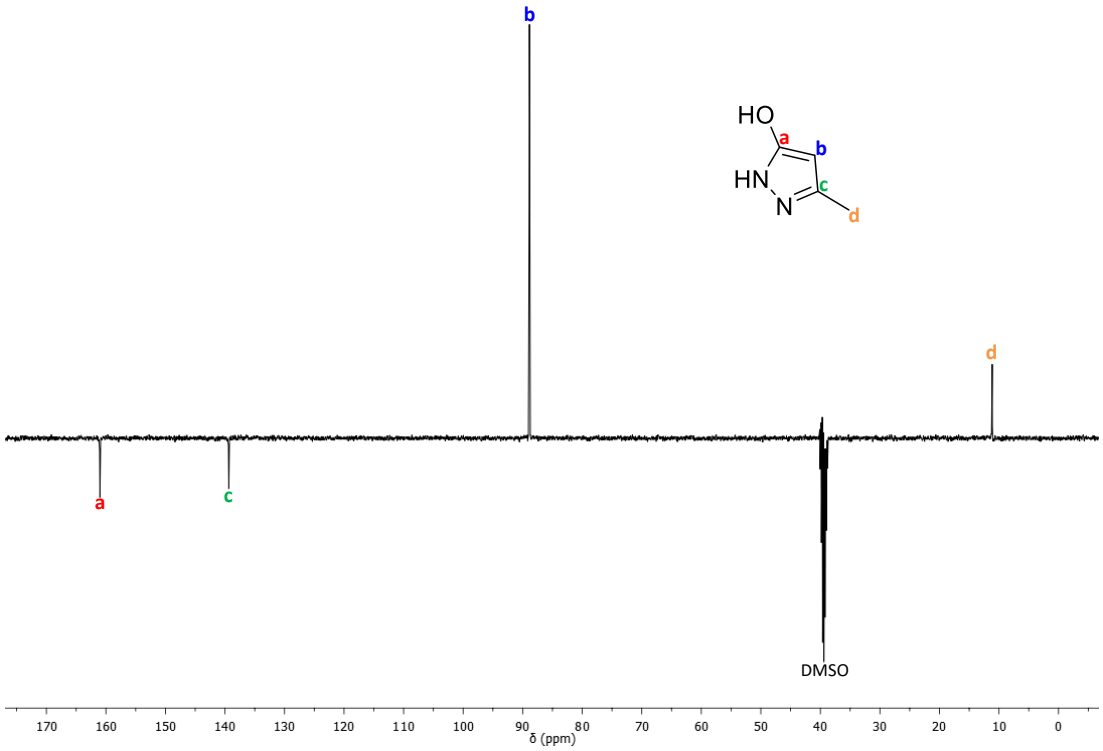

Figure 5.5 ^{13}C NMR spectrum of hydroxy pyrazole, 5.1 (100 MHz, DMSO-d_6).

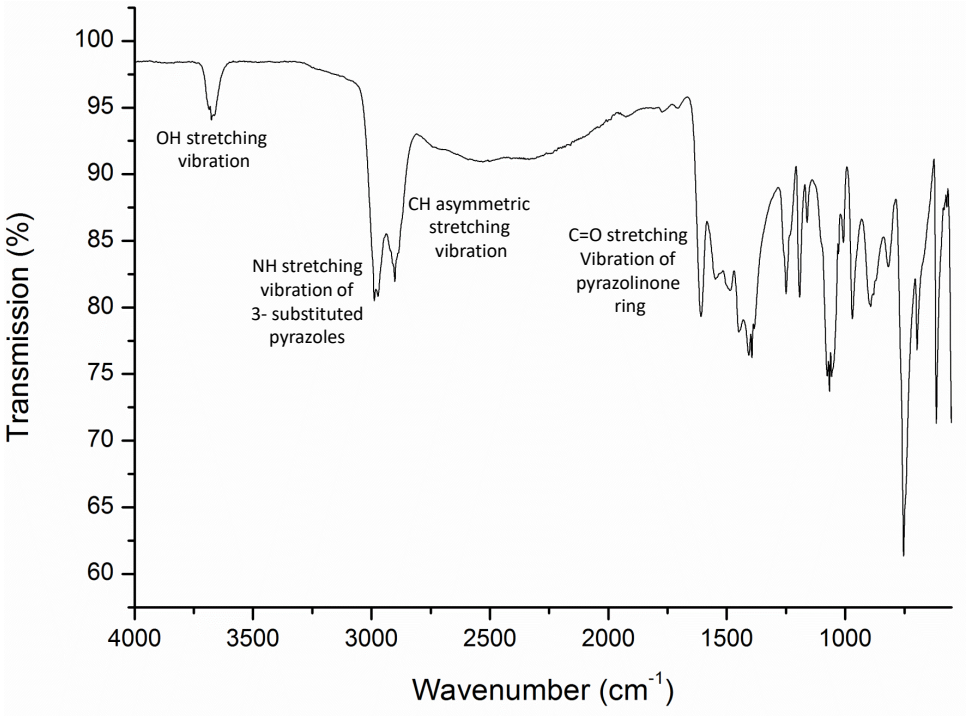

Figure 5.6 FT-IR spectrum of hydroxy pyrazole, 5.1.

In order to produce the pyrazole monomer 3-methacryloyl-5-methyl-2*H*-pyrazole (methacryloyl pyrazole, **5.2**), hydroxy pyrazole was reacted with methacryloyl chloride using a modification of a procedure previously developed in the group for the synthesis of proline-based monomers (Scheme 5.3).[25]

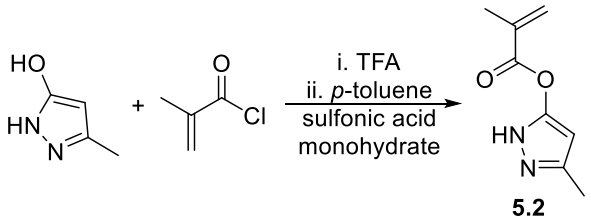

Scheme 5.3 Schematic representation for the synthesis of methacryloyl pyrazole (5.2).

Following precipitation of the monomer in diethyl ether and extraction in dichloromethane with basic water and brine, the monomer was obtained as a white solid in a relatively good yield (66%). A disappearance in the resonance associated with the OH proton in the ^{1}H NMR spectrum (Figure 5.7), in addition to the appearance of the O*C*=O resonance at δ = 164.0 ppm in the ^{13}C NMR spectrum, as well as a loss of the pyrazolinone stretch in the IR spectrum at υ = 1615 cm^{-1} confirmed the successful reaction.

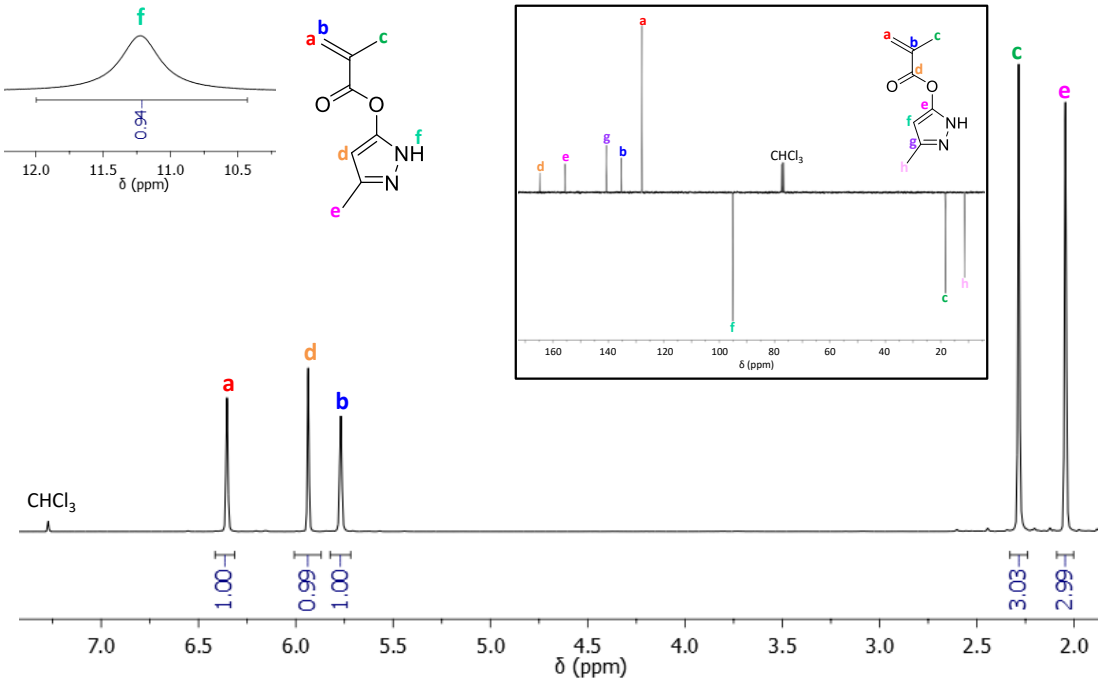

Figure 5.7 NMR spectra of methacryloyl pyrazole, 5.2: (*main*) ^{1}H NMR spectrum (400 MHz, $CDCl_3$) and (*inset*) ^{13}C NMR spectrum (100 MHz, $CDCl_3$).

The diisocyanate monomer was synthesised by stirring the diisocyanate toluene-2,4-diisocyanate (TDI), and methacryloyl pyrazole (**5.2**) in anhydrous acetone for 16 hours. TDI was selected owing to its liquid state at room temperature hypothesised to minimise problems with solubility in comparison to solid diisocyanates, *e.g.* MDI. It was hypothesised that the reaction between the pyrazole secondary amine and the aromatic isocyanate would still proceed without the addition of a catalyst, with catalyst free reactions between secondary amines and isocyanates reported in the literature.[26] The monomer was purified by column chromatography (3:1 dichloromethane/petroleum ether) using silica gel treated with 10% triethylamine to allow for successful separation of the products, affording a white crystalline solid (in a yield of 22%). ^{1}H NMR spectroscopy (Figure 5.8) and IR spectroscopy confirmed the successful synthesis of the TDI crosslinker (**5.3**) through the appearance of resonances associated with urea linkages at δ = 9.02-8.99 ppm and υ = 3363 cm^{-1} respectively (Figure 5.9).

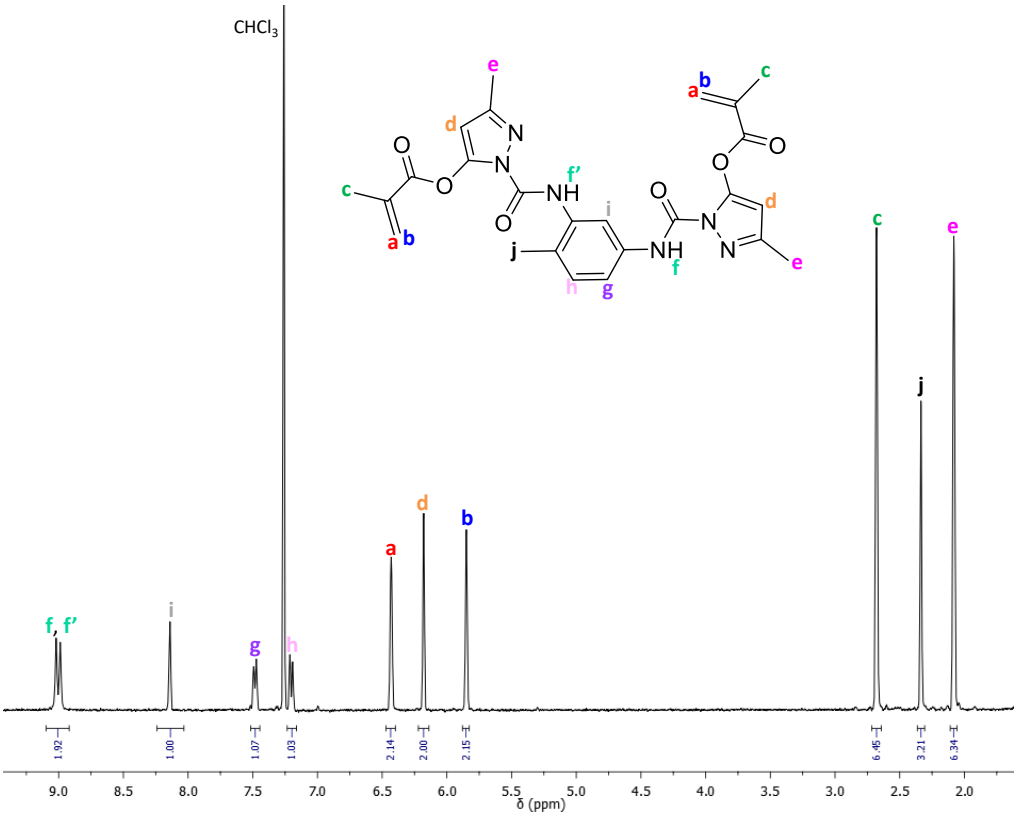

Figure 5.8 ^{1}H NMR spectrum of TDI crosslinker 5.3 (400 MHz, $CDCl_3$).

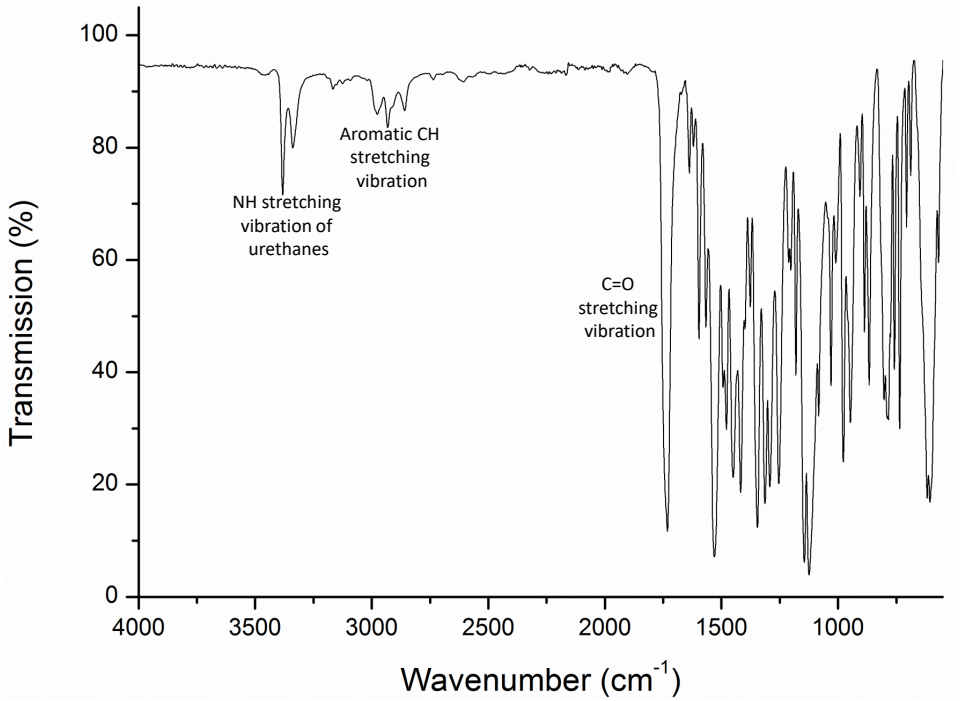

Figure 5.9 FT-IR spectrum of TDI crosslinker 5.3.

5.3.2 Incorporation of isocyanate crosslinker

Incorporation of the isocyanate crosslinker was initially attempted using the arm-first RAFT methodology used in the previous Chapters, through the chain extension of poly(hydroxyethyl methacrylate) arms, $PHEMA_{140}$, with the amino-functionalised monomer *N,N'*-(dimethylamino)ethyl methacrylate (DMAEMA) and the divinyl isocyanate-containing crosslinking monomer **5.3**. However, to minimise the chance of the crosslinker deblocking during polymerisation, the reaction was carried out at 30 °C, and therefore a lower temperature radical initiator (VA-044), with a 10 hour half-life at 44 °C, was used (Scheme 5.4).

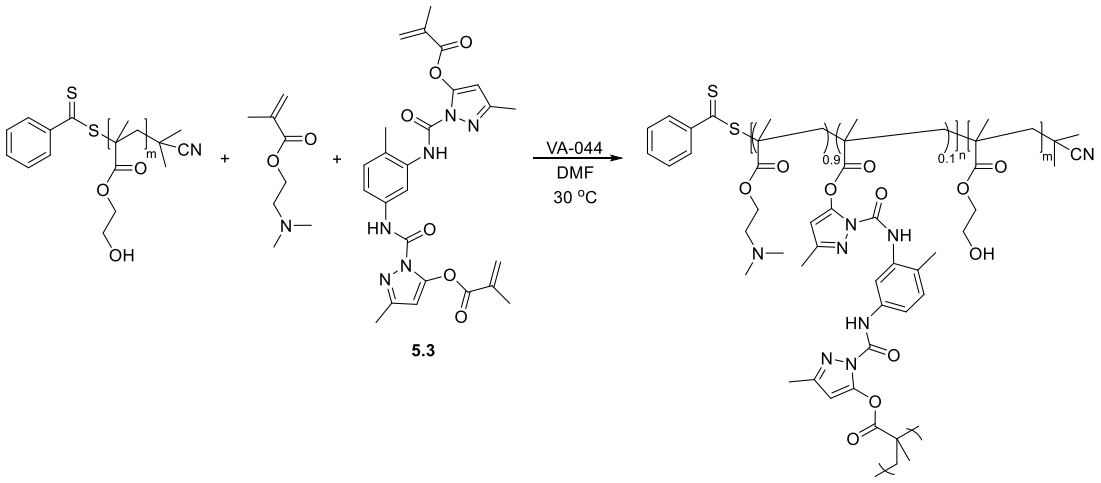

Scheme 5.4 Schematic representation for the RAFT polymerisation of the TDI crosslinker 5.3, *via* chain extension of the PHEMA macro-CTA with DMAEMA and 5.3.

Conversion analysis, as determined by gas chromatograph (GC) analysis, revealed no conversion for any of the monomers, confirmed by the overlapping traces of the PHEMA macro-CTA (chain transfer agent) and the precipitated polymer after the reaction, as determined by Size Exclusion Chromatography (SEC) analysis (Figure 5.10A). It was hypothesised that the low temperature of the reaction may have resulted the generation of too few radicals from the VA-044 initiator. As a consequence of the possibility of deblocking preventing an increase in reaction temperature, the number of initiator equivalents of was increased from 0.17 eq. per macro-CTA to 17 eq., in order to ensure sufficient levels of radicals for the polymerisation to proceed. SEC analysis of the crude reaction mixture indicated that extension, whilst minimal, had occurred, with the appearance of a high molecular weight shoulder in the SEC trace and an in the increase in dispersity ($Đ_M$) from 1.13 to 1.17 (Figure 5.10B).

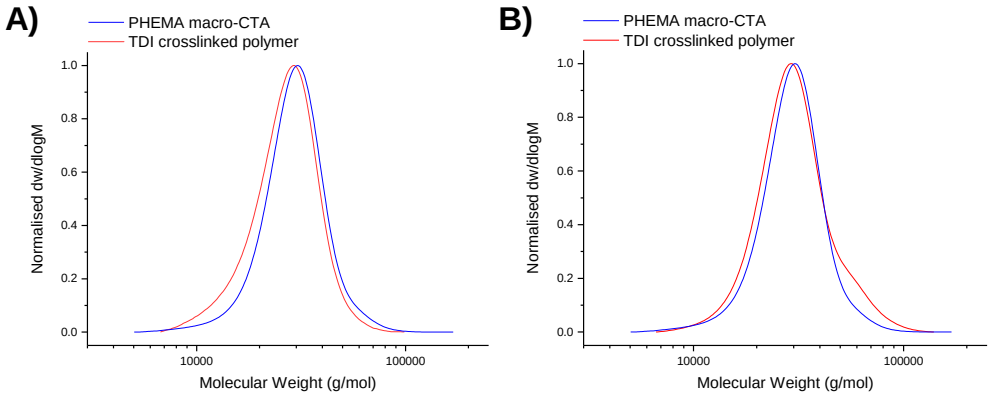

Figure 5.10 Molecular weight distributions, determined by SEC analysis for the chain extension of PHEMA with DMAEMA and TDI crosslinker 5.3 with (A) 0.17 eq. VA-044, and (B) 17 eq. VA0-44 (DMF, PMMA standards).

Whilst ^{1}H NMR spectroscopic analysis indicated the presence of a new signals at δ = 2.68 ppm and δ = 2.36 ppm, attributable to the CH_2CH_2N and $N(CH_3)_2$ from the DMAEMA, respectively (Figure 5.11, protons b and a, respectively), analysis also indicated a large number of resonances attributable to the aromatic signals of the deblocked TDI at δ = 7.50-7.27 ppm (protons d' and e'), in addition to the loss of the urethane signal at δ = 9.00 ppm, suggesting a significant degree of deblocking has occurred during the polymerisation.

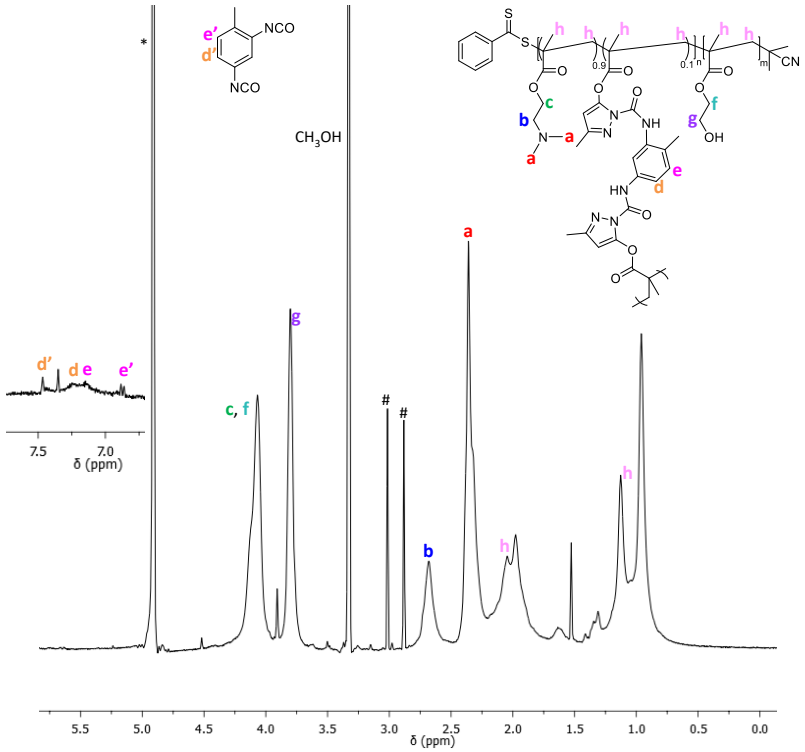

Figure 5.11 ^{1}H NMR spectrum of PHEMA-*b*-(DMAEMA-*co*-TDI crosslinker) indicating chain extension, yet also deblocking of the blocked TDI during polymerisation, * denotes H_2O, # denotes DMF (400 MHz, $CDCl_3$).

Consequently, and in order to determine whether the blocked isocyanate was stable enough to allow for polymerisation, a model compound, a monoisocyanate (phenyl isocyanate) was reacted with methacryloyl pyrazole to produce a mono-functionalised isocyanate monomer. Initial attempts to homopolymerise the monomer using RAFT polymerisation were carried out at 25 °C, with 0.3 eq. of radical initiator VA-044 (Scheme 5.5).

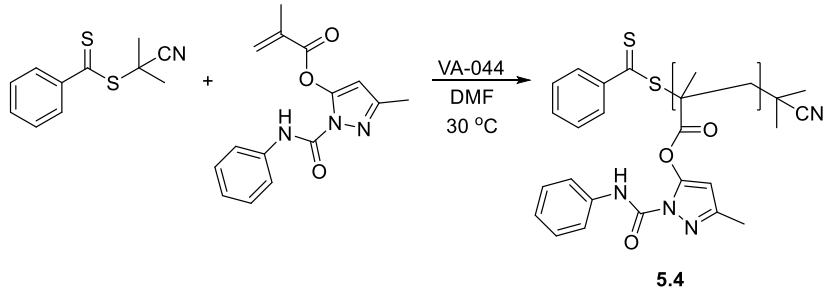

5.4

Scheme 5.5 Schematic representation for the homopolymerisation of methacryloyl pyrazole blocked phenyl isocyanate.

Whilst SEC analysis indicated the production of a polymer (**5.4**) at this low temperature, with a number-average molecular weight by SEC analysis ($M_{n,\,SEC}$) of 15.3 kg/mol and with a relatively low dispersity of 1.43 (Figure 5.12), the crude ^{1}H NMR spectrum indicated a large degree of deblocking of the monomer during polymerisation. In view of the deblocking observed by ^{1}H NMR spectroscopy, further analysis of the polymer was carried out using SEC analysis fitted with a UV-vis detector set at λ = 309 nm, the wavelength attributable to the dithioester functionality of the RAFT CTA. It was hypothesised that, owing to the large degree of deblocking, the polymer produced may be a TDI-based polyurethane generated as a consequence of the deblocked isocyanate reacting with any moisture present, and not a homopolymer of the blocked isocyanate monomer. SEC analysis carried out using a UV-vis detector set at λ = 309 nm revealed the presence of the RAFT end-group on the polymer, indicating that polymerisation had been successful in producing a methacryloyl pyrazole blocked phenyl isocyanate homopolymer (Figure 5.12). In spite of the SEC analysis indicating the successful RAFT polymerisation of methacryloyl pyrazole blocked phenyl isocyanate, ^{1}H NMR analysis clearly indicated a large degree of deblocking for the blocked isocyanate

monomer, with an in-depth stability study, discussed in Chapter 6, concluding that crosslinker was not stable under the RAFT polymerisation conditions.

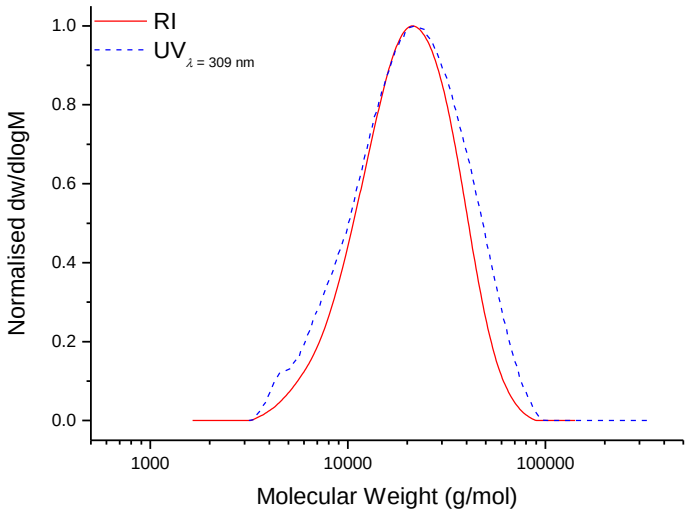

Figure 5.12 Molecular weight distribution of P(pyrazole blocked phenyl isocyanate), 5.4 (DMF, PMMA standards).

As a consequence of the stability problems associated with deblocking of the crosslinker during polymerisation, it was decided that an alternative approach was needed. The synthesis of the crosslinker involved the stirring of the methacryloyl pyrazole with the diisocyanate. It was therefore hypothesised that stirring the isocyanate with an already polymerised methacryloyl pyrazole would also allow for crosslinking of the polymer and produce hyperbranched-core star polymers. In order for this method to be successful, an alternative arm for the polymeric star was chosen, as the OH functionality of the PHEMA block would react with the diisocyanate when added to crosslink the polymers, resulting in the production of a hyperbranched polymer. Poly(ethylene glycol) monomethyl ether methacrylate (PEGMA, M_n = 500 g/mol) was chosen as an alternative to the HEMA as the arms of the star polymers, as it would still ensure solubility in the polyol used in the polyurethane formulation. The length of PEGMA monomer was chosen to overcome any potential problems of thermoresponsive behaviour exhibited by the shorter chain poly(ethylene glycols), which have been shown to precipitate out of solution at raised temperatures.[27] The high internal temperatures of the polyurethane formulation during foaming

may result in polymers containing shorter PEGMAs collapsing during foaming which would prevent the catalytic amine from being exposed to the formulation.

PEGMA was polymerised by RAFT polymerisation, using the RAFT chain-transfer agent 2-cyano-2-propyl benzodithioate (CPBD, Scheme 5.6). Following reaction at 70 °C, and purification by exhaustive dialysis, the product polymer (**5.5**) was isolated by lyophilisation. Control of the polymerisation process was reflected in the agreement between the theoretical number-average molecular weight ($M_{n,\,theo.}$), calculated from conversion determined using ^{1}H NMR spectroscopy (Figure 5.13), and the observed number-average molecular weight ($M_{n,\,obs.}$). The observed number-average molecular weight was determined by comparison of the integrals associated with the aromatic protons in the CPBD RAFT end-group at δ = 7.99 - 7.54 ppm (Figure 5.14, protons a), and the first OCH_2 in the PEGMA brush repeat unit at δ = 4.22 ppm (Figure 5.14, proton b) (54.2 kg/mol and 56.7 kg/mol respectively), generating a degree of polymerisation (DP) of 110 which matched that predicted from conversion analysis.

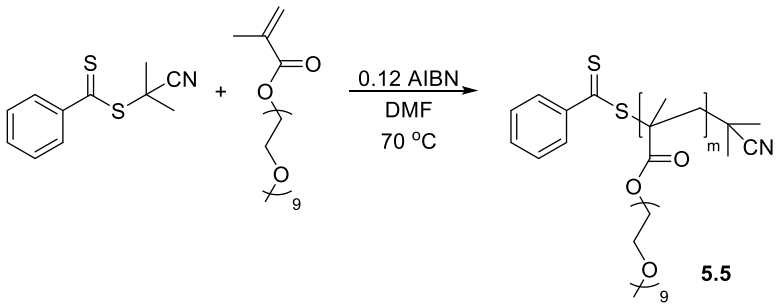

Scheme 5.6 Schematic representation for the RAFT synthesis of the PEGMA homopolymer using the RAFT agent CPBD and the radical initiator AIBN.

$$Conversion = \frac{(1H_{polymer})}{(1H_{monomer} + 1H_{polymer})} = 93\%$$

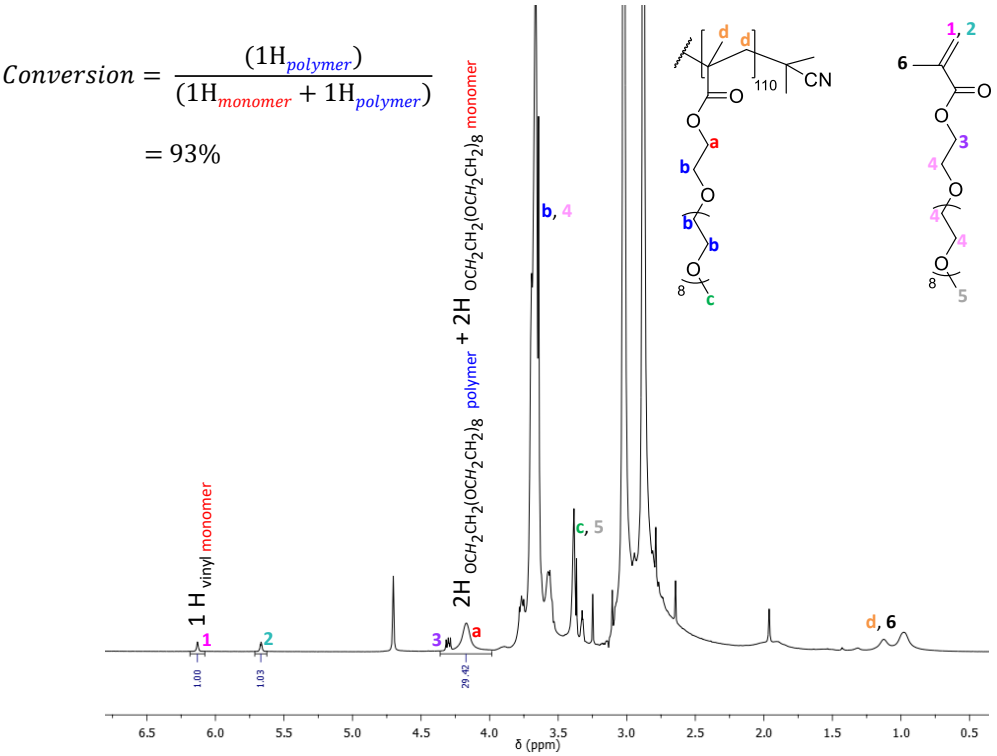

Figure 5.13 ^{1}H NMR spectrum used to calculate conversion for the synthesis of PEGMA homopolymer 5.5. $M_{n,\,theo.}$ calculated by multiplication of the conversion with the equivalents of PEGMA added (400 MHz, D_2O).

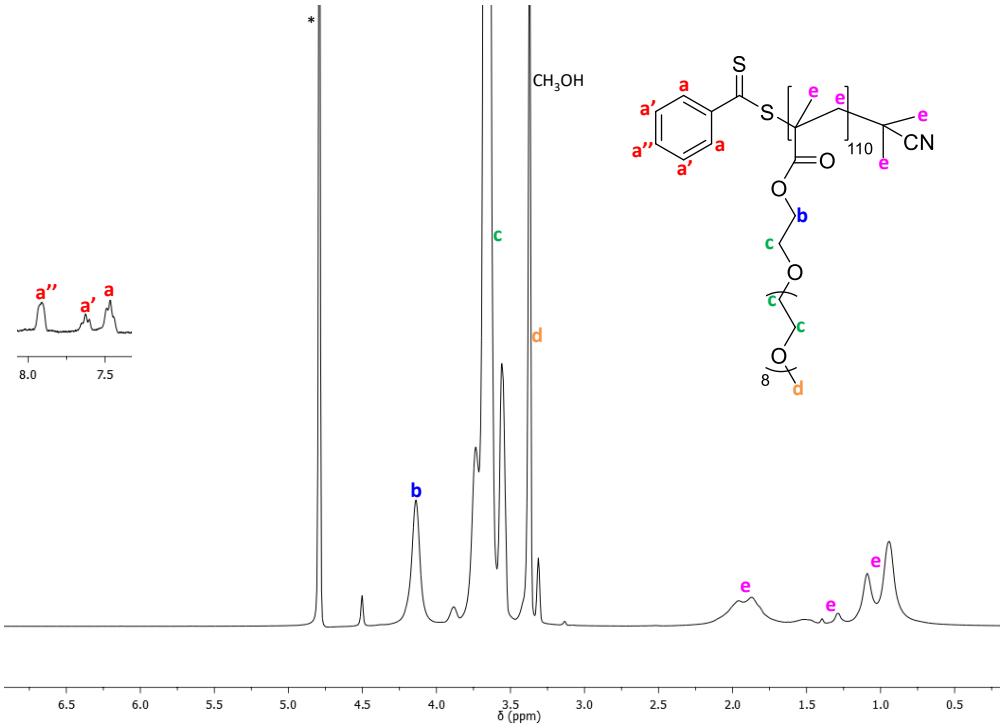

Figure 5.14 ^{1}H NMR spectrum of the PEGMA homopolymer 5.5, * denotes H_2O (400 MHz, CD_3OD).

Moreover, the monomodal peak from refractive index (RI) detector in the SEC analysis, in addition to the low dispersity value of 1.20, further indicate the controlled nature of the process (Figure 5.15). Analysis of the polymer by triple-detection SEC, introduced in Chapter 2 section 2.3.1.1, indicated a Mark-Houwink parameter *a* of 0.52, confirming the linear nature of the polymers.

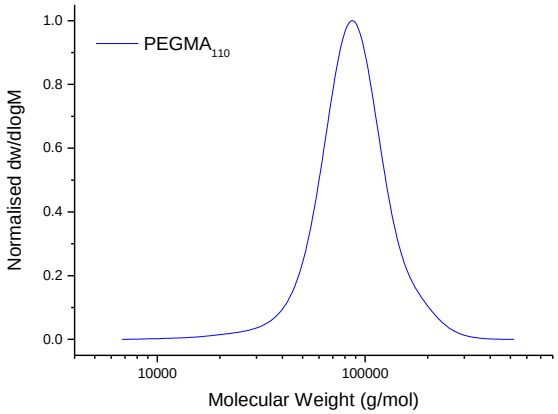

Figure 5.15 Molecular weight distribution for PEGMA homopolymer 5.5, determined by SEC analysis (DMF, PMMA standards).

Following the synthesis of the linear $PEGMA_{110}$ arms, chain extension with the amine-functionalised monomer DMAEMA and methacryloyl pyrazole was carried out to produce the linear star precursor. The reaction was carried out at 70 °C in DMF for 16 hours, with the monomer feed altered to target a 10% incorporation of methacryloyl pyrazole in order to obtain a theoretical crosslinking density of 10% (Scheme 5.7).

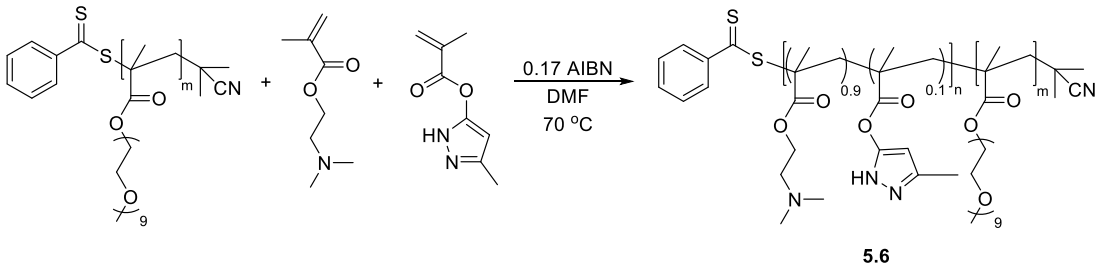

Scheme 5.7 Schematic representation for the RAFT chain extension of the PEGMA macro-CTA (5.5) with DMAEMA and methacryloyl pyrazole (5.2) using the radical initiator AIBN.

Conversion analysis using ^{1}H NMR spectroscopy revealed a DMAEMA conversion of 54% and a methacryloyl pyrazole conversion of 67%, affording $M_{n,\,theo.}$ of 74.1 kg/mol. This theoretical number-average molecular weight was in good agreement with the $M_{n,\,obs.}$ of the resultant polymer (**5.6**), determined by ^{1}H NMR spectroscopy (71.2 kg/mol), which corresponded to a DMAEMA DP of 78 and a pyrazole DP of 13, and was calculated by comparison of the PEGMA ester integrals at δ = 3.40 ppm (Figure 5.16, proton h) with the CH_2CH_2N protons of the DMAEMA at δ = 2.68 ppm (Figure 5.16, proton b), and the C*H* pyrazole proton at δ = 5.82 ppm (Figure 5.16, proton d).

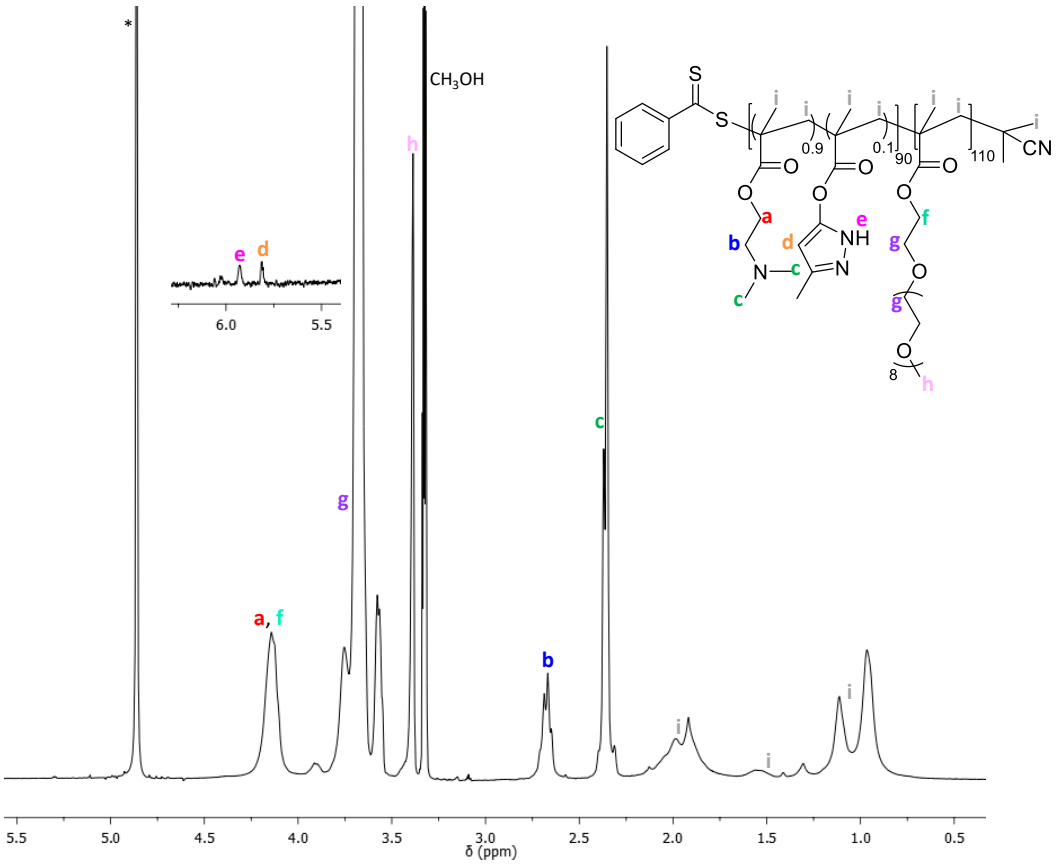

Figure 5.16 ^{1}H NMR spectrum of PEGMA$_{110}$-*b*-(DMAEMA$_{0.9}$-*co*-pyrazole$_{0.1}$)$_{90}$, 5.6,* denotes H_2O (400 MHz, CD_3OD).

Additionally, SEC analysis indicated a low dispersity ($Đ_M$ = 1.16) confirming the controlled nature of the polymerisation, as well as a shift in molecular weight distribution to a higher molecular weight (Figure 5.17). Moreover, SEC analysis with a UV-vis detector at λ = 309 nm confirmed retention of the RAFT end group (Figure 5.17, *inset*). Triple-detection SEC

analysis produced a Mark-Houwink *a* parameter of 0.55, confirming that the polymers remained linear in nature.

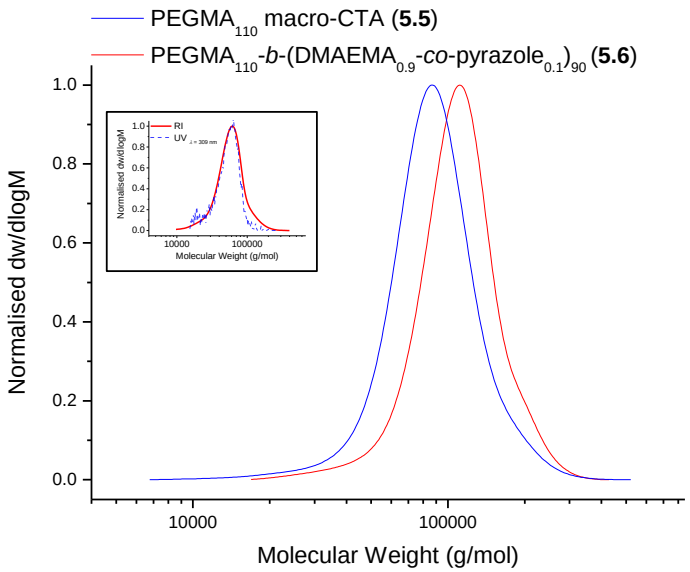

Figure 5.17 Molecular weight distributions, determined by SEC analysis, for 5.6 (*red*) and the macro-CTA 5.5 (*blue*), and (*inset*) overlay of the RI and UV trace at λ = 309 nm (DMF, PMMA standards).

Similar to the synthesis of the monomeric crosslinker, crosslinking of the polymers was achieved *via* stirring of the diisocyanate with linear copolymer **5.6**. To this end, $PEGMA_{110}$-*b*-$(DMAEMA_{0.9}$-*co*-$pyrazole_{0.1})_{90}$ was dissolved in anhydrous acetone and stirred with the diisocyanate, 2,4-toluene diisocyanate (TDI), with the ratio of pyrazole:TDI of 2:1. Following reaction for 48 hours, the resultant polymer (**5.7**) was obtained by precipitation into 4:1 diethyl ether/acetone. ^{1}H NMR spectroscopy was found to be unsuccessful for the characterisation of the resultant polymer, owing to any signals attributable to the TDI being hidden by the RAFT CTA (TDI aromatic signals) or the polymer backbone (TDI methyl group). As such, SEC analysis was used to indicate successful crosslinking of the polymer, with the appearance of a high molecular weight shoulder and an increase in number-average molecular weight from 99.7 kg/mol to 138.3 kg/mol, in addition to an increase in the dispersity from $Đ_M$ = 1.16 to $Đ_M$ = 1.60 (Figure 5.18). Additionally, the Mark-Houwink parameter was found to be *a* = 0.42, less than both the linear $PEGMA_{110}$ and linear $PEGMA_{110}$-*b*-$(DMAEMA_{0.9}$-*co*-$pyrazole_{0.1})_{90}$ (0.52 and

0.55, respectively) and, crucially, below 0.5, which is widely accepted as indicating a polymer with a crosslinked architecture.[28-31]

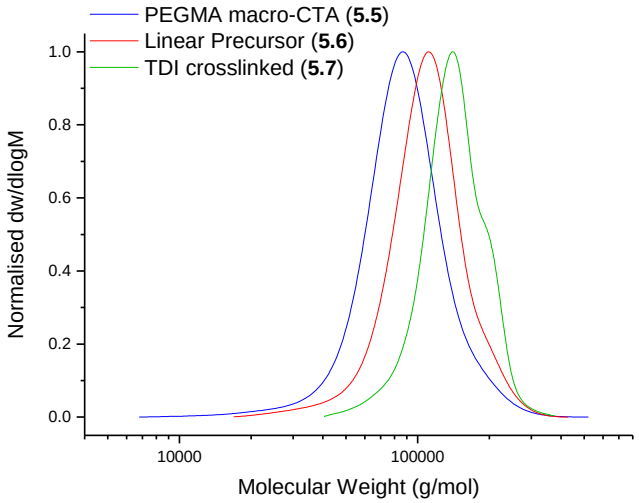

Figure 5.18 Molecular weight distributions, as determine by SEC analysis, of TDI crosslinked polymer 5.7, in addition to the linear precursor (5.6) and the PEGMA macro-CTA (5.5) (DMF, PMMA standards).

The particle size of the polymeric stars was initially probed using Dynamic Light Scattering (DLS) analysis, carried out in methanol at 3 mg/mL. Analysis revealed a hydrodynamic diameter (D_h) of 8 nm ± 1 nm (PD = 0.44) (Figure 5.19).

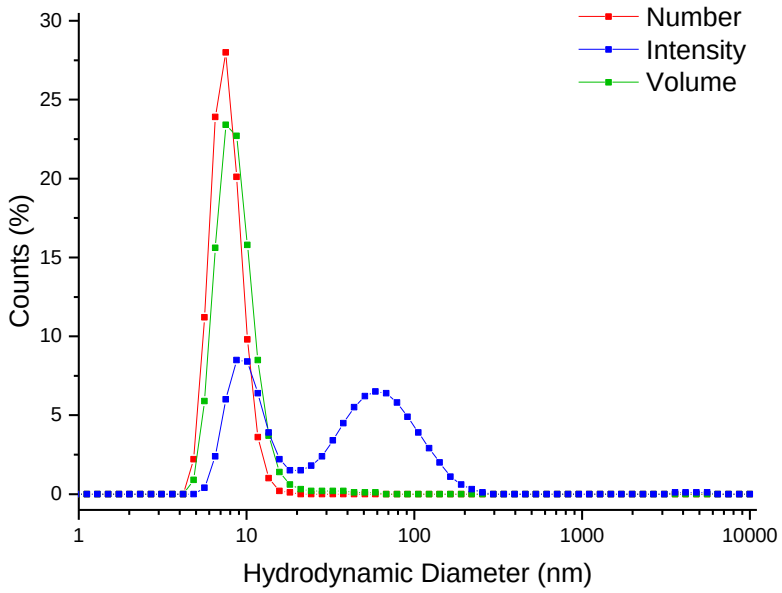

Figure 5.19 Particle size analysis of TDI crosslinked polymer 5.7, determined by DLS analysis (methanol, 3 mg/mL).

The relatively high dispersity value can be attributed to the random nature of the crosslinking, likely to produce polymeric stars of different sizes, as evidenced in the second peak at a larger hydrodynamic diameter in the intensity trace. Indeed, examination of the polymers by Transmission Electron Microscopy (TEM) analysis using graphene oxide (GO) supported TEM grids, found to produce higher contrast images without staining,[32] indicated the presence of a broad distribution of particle sizes, ranging from 3 nm to 26 nm (Figure 5.20).

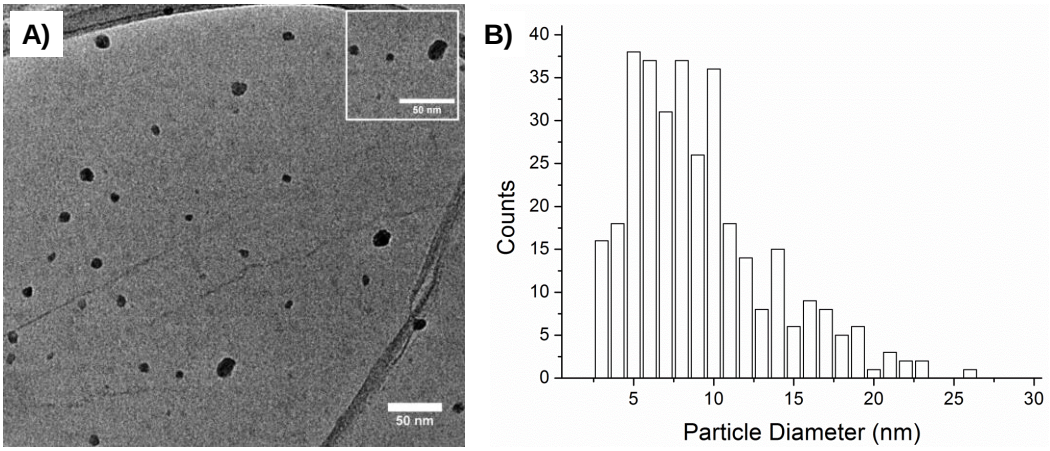

Figure 5.20 Particle size analysis of TDI crosslinked polymer 5.7: (A) representative TEM image (methanol, 3 mg/mL on GO supported TEM grids) and (B) size distribution histogram.

5.3.3 Probing the thermoresponsive behaviour

In order to confirm applicability of the polymeric stars as latent catalysts for polyurethane foam production, the thermoresponsive behaviour of **5.7** was evaluated. Initially, variable temperature ^{1}H NMR (^{1}H VT-NMR) analysis was carried out, with the polymer dissolved in ethylene glycol-d_6, hypothesised to be an appropriate mimic for the polyol used in the polyurethane formulation. Spectroscopic analysis indicated a deblocking temperature of 30-35 °C, with the appearance of a signal at δ = 7.18 ppm at 35 °C, attributed to the NH of the urethane linkage formed from the reaction of the released TDI with the ethylene glycol (Figure 5.21, red region), in addition to a change in the backbone region at δ = 0.78 ppm at 30 °C, as a consequence of the decrease in shielding resulting from the breakdown of the polymer (Figure 5.21, blue region).

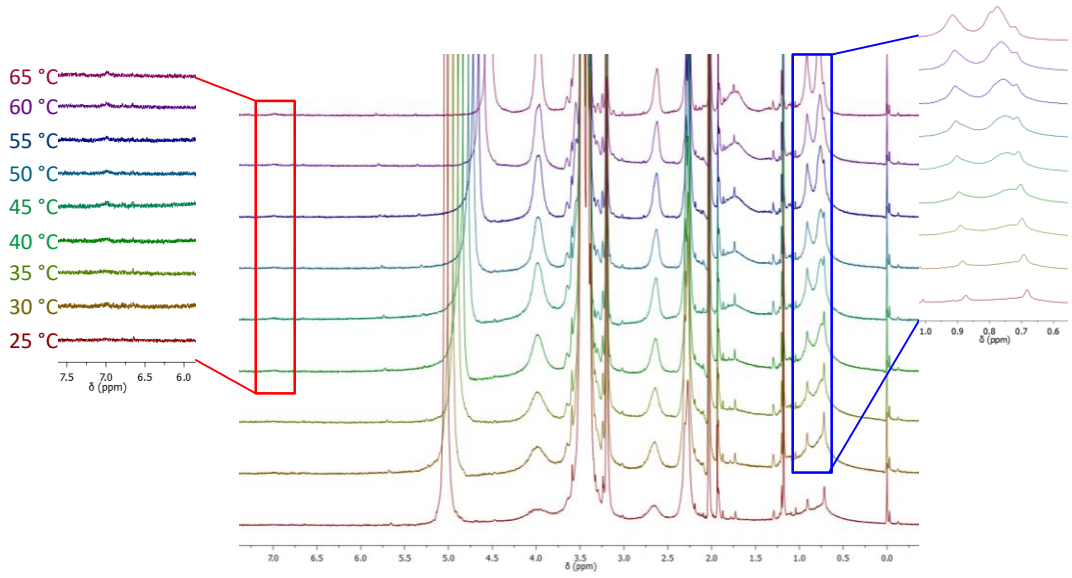

Figure 5.21 Overlaid ^{1}H VT-NMR spectra of 5.7 at 25 °C (*red*), 30 °C (*yellow*), 35 °C (*light green*), 40 °C (*green*), 45 °C (*turquoise*), 50 °C (*light blue*), 55 °C (*blue*), 60 °C (*purple*) and 65 °C (*pink*), showing the evolution of the urethane stretch (*red region*) and the changing polymer backbone (*blue region*) (400 MHz, ethylene glycol-d_6).

One alternative method to probe the thermoresponsive behaviour is to use SEC analysis. Samples of **5.7** were dissolved in the SEC solvent (DMF) and heated at 25-65 °C in 10 °C intervals for 30 minutes. Analysis revealed that the polymers did deblock, with a noticeable shift in the molecular weight trace to a lower molecular weight as the temperature increased, in addition to a decrease in the dispersity, from $Đ_M$ = 1.68 at 25 °C to 1.47 at 55 °C (Figure 5.22).

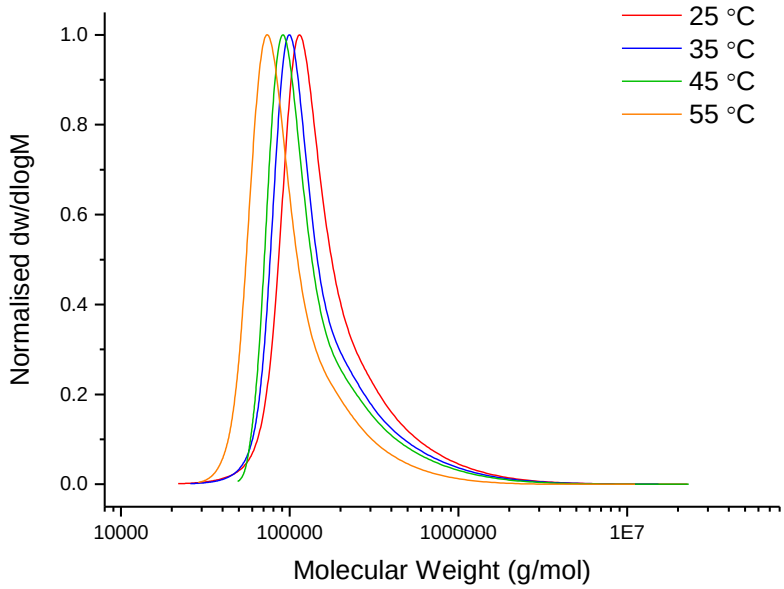

Figure 5.22 Molecular weight distributions, as determined by SEC analysis, for polymer 5.7 heated at different temperatures for 30 minutes (DMF, PMMA standards).

It was further decided that analysis of the viscosity-average molecular weight (M_v), generated by triple-detection SEC, would also provide insight into the responsive behaviour. The viscosity-average molecular weight, calculated according to Equation 5.1, is derived from the number of moles of polymer molecules (N_i) of molar mass M_i, and is dependent on the Mark-Houwink *a* parameter, and therefore proportional to the degree of crosslinking.[33, 34]

$$M_V = \left[\frac{\Sigma M_i^{1+a} N_i}{\Sigma M_i N_i}\right]^{\frac{1}{a}}$$

Equation 5.1 Viscosity-average molecular weight (M_v) and its dependence on the Mark-Houwink parameter *a*.

As the polymer becomes less crosslinked, *a* increases, resulting in the sum of the molecular weights being raised to the power of a smaller number, which results in a net decrease in the M_v. This is indeed what was observed, with an increase in the *a* parameter, from 0.32-0.39, indicating that the polymer is becoming less crosslinked. Moreover, M_v was found to decrease steadily from the sample heated at 35 °C, indicating the polymer is becoming less crosslinked in nature from this point (Figure 5.23), which, combined with the increase in *a* value confirms that the polymeric stars are falling apart. Notably, the deblocking temperature by SEC analysis was in good agreement with that afforded by ^{1}H VT-NMR spectroscopic analysis.

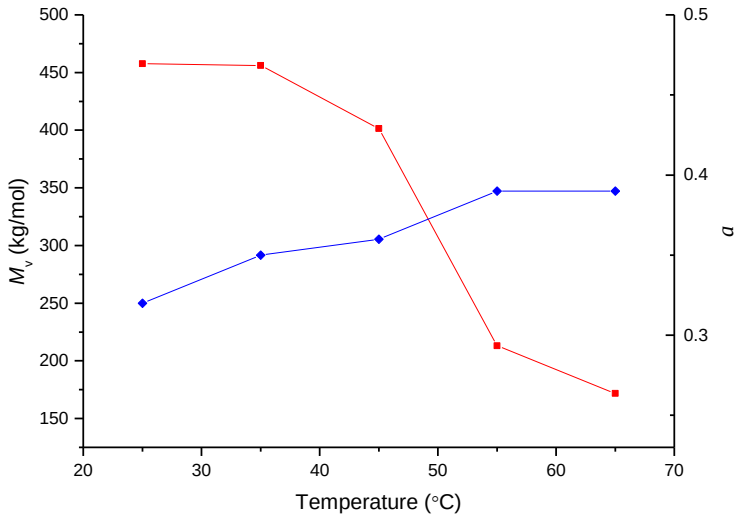

Figure 5.23 SEC analysis of the TDI crosslinked polymer (5.7) when heated for 30 minutes at different temperature (DMF, PMMA standards).

5.3.4 Expansion to other diisocyanates

It was hypothesised that such a synthetic procedure for the synthesis of diisocyanate crosslinked polymers could be expanded, allowing for the production of polymeric stars crosslinked with other diisocyanates. Such polymers have the potential to act as latent catalysts for different polyurethane materials, with, for example, a hexamethylene diisocyanate (HDI) crosslinked polymer able to be applied to a coating based polyurethane material. Moreover, by varying the crosslinking diisocyanate it is hypothesised that different deblocking temperatures, and therefore temperatures at which catalysis would begin, could be targeted, with aliphatic isocyanates widely accepted to deblock at higher temperature than aromatic isocyanates.[35]

Using the same polymeric star precursor (**5.6)** the linear polymer was stirred in anhydrous acetone with either HDI or methylenediphenyl diisocyanate (MDI) (Scheme 5.8).

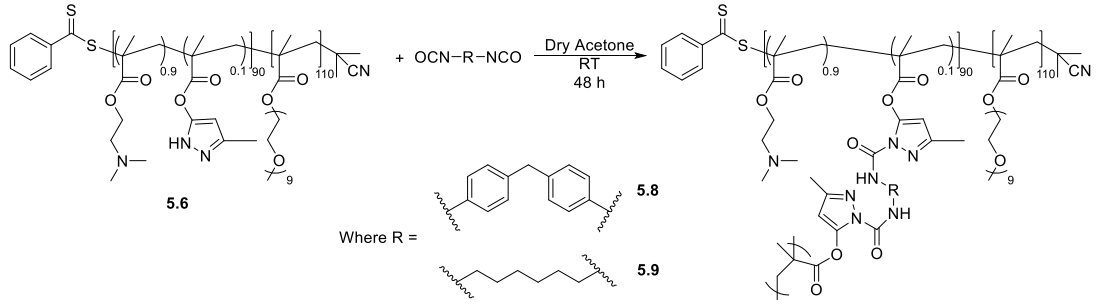

Scheme 5.8 Schematic representation for the synthesis of diisocyanate crosslinked polymers *via* stirring of the linear precursor 5.5 with the diisocyanate.

Polymers were isolated by precipitation into 4:1 diethyl ether/acetone, and analysed using SEC. Analysis revealed a shift to higher molecular weights for both the MDI crosslinked polymeric stars (**5.8**) and the HDI crosslinked polymeric stars (**5.9**) (Figure 5.24). Triple-detection SEC analysis further confirmed the crosslinked nature of the materials, with *a* values of 0.38 and 0.32, respectively. The slight difference in *a* parameter is hypothesised to relate to the steric bulk of the crosslinking isocyanate. Indeed, linear HDI is expected to occupy less space within the core of the star polymer, allowing for higher incorporations and therefore a higher crosslinking density, which is reflected in the lower *a* value. As the steric bulk of the

crosslinking isocyanate increases to the more bulky aromatic isocyanates, it is likely that smaller amounts are incorporated, resulting in a higher *a* value.

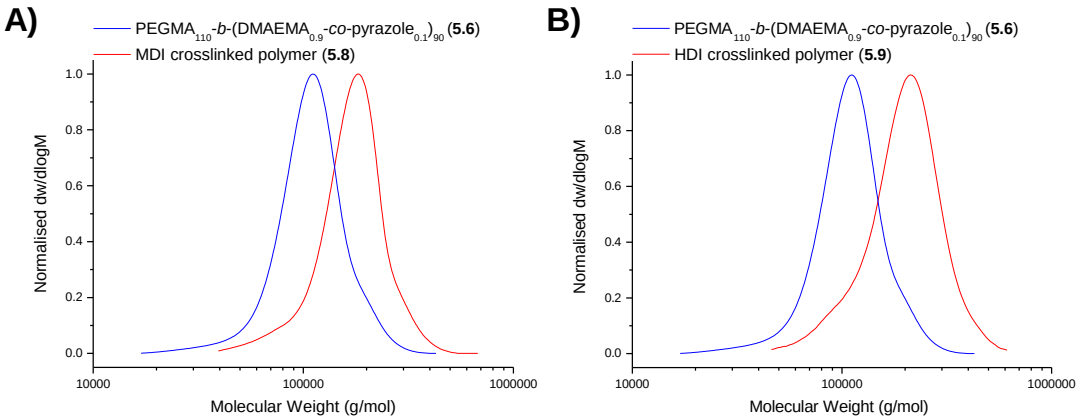

Figure 5.24 Molecular weight distributions for (A) MDI and (B) HDI crosslinked polymers compared with the linear precursor 5.6 (DMF, PMMA standards).

Particle size analysis using DLS (in methanol at 3 mg/mL) revealed the stars to be similar in size to the TDI crosslinked polymers, with the MDI crosslinked polymer found to have a hydrodynamic diameter, determined by number, of 8 nm ± 1 nm (PD = 0.38), with the HDI crosslinked polymer having a diameter of 11 nm ± 1 nm (PD = 0.62) (Figure 5.25).

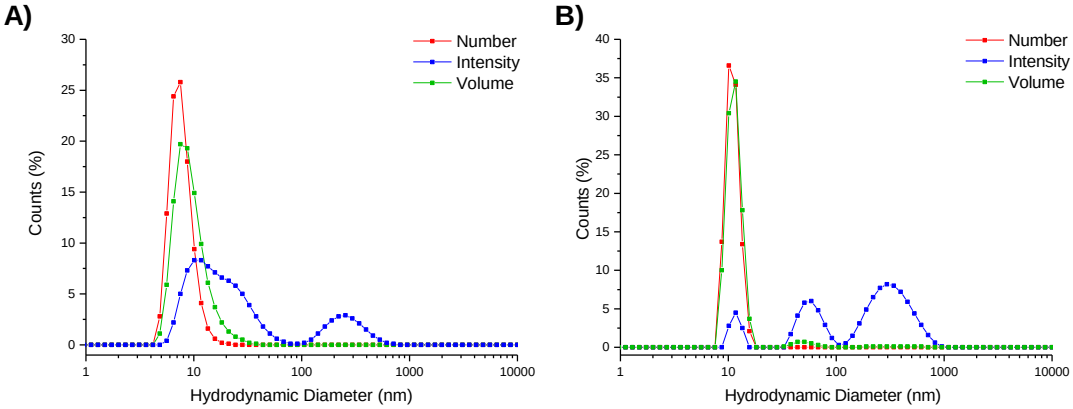

Figure 5.25 Particle size analysis, as determined by DLS analysis in methanol (3 mg/mL) for (A) MDI crosslinked polymer 5.8, and (B) HDI crosslinked polymer 5.9.

Similar to the previously discussed TDI particles, it is hypothesised that the second population in the intensity trace, at approximately 30 nm for the MDI crosslinked polymer **5.8** and at approximately 50 nm for the HDI crosslinked polymer **5.9**, is as a result of larger sized particles, resulting from the random nature of the crosslinking process. Moreover, the third

population identified in the intensity trace is hypothesised to be as a consequence of agglomeration of crosslinking chains during polymerisation, with the agglomeration of polymeric chains using the equivalent acrylate monomer reported in Section 3.3.1.1.

In order to confirm the applicability of these stars as latent catalysts, the polymers were evaluated using the same SEC analysis as previously used for the TDI crosslinked polymeric stars. Evaluation of the crosslinked polymers indicated a deblocking temperature of 50 °C for the MDI crosslinked stars, and 60 °C (based on M_v) or 65 °C (based on a) for the HDI crosslinked stars, with a large decrease in the value of M_v and an increase in the Mark-Houwink parameter a observed in the SEC analysis (Figure 5.26 A and B, respectively).

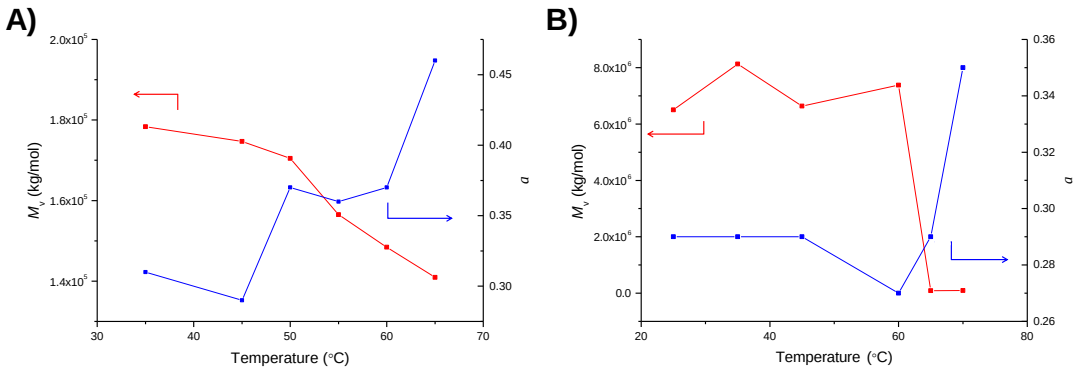

Figure 5.26 SEC analysis of the diisocyanate crosslinked polymers when heated for 30 minutes at different temperatures; (A) MDI crosslinked polymer (5.8), and (B) HDI crosslinked polymer (5.9) (DMF, PMMA standards).

Moreover, analysis of the MDI crosslinked sample heated at 80 °C displayed an SEC trace very similar in shape and molecular weight to the linear star precursor **5.6** (Figure 5.27), indicating complete disintegration of the polymeric stars. The difference in deblocking temperature between the MDI crosslinked polymer (50 °C) and the TDI crosslinked polymers (35 °C) is likely a combination of both electronic and steric effects. Indeed, isocyanate inequivalence, where isocyanates tethered to the same molecule deblock at different temperatures, has been reported.[36] Furthermore, Lee *et al.* reported that TDI was found to deblock before MDI, which were both followed by HDI, yet the two isocyanates on the aromatic

ring of the TDI did not deblock at the same temperature owing to the molecule asymmetry as a consequence of the methyl group bound to the ring.[37] The deblocking temperature of the HDI crosslinked polymer was found to occur at 60 - 65 °C, in agreement with the argument that aliphatic blocked isocyanates deblock at higher temperatures than aromatic blocked isocyanates as a consequence of having no aromatic ring allowing for conjugation of the aromatic π electrons and the N=C=O bond.[35] Moreover, the less sterically hindered nature of the HDI crosslinker is likely to result in a more stable crosslinked core.

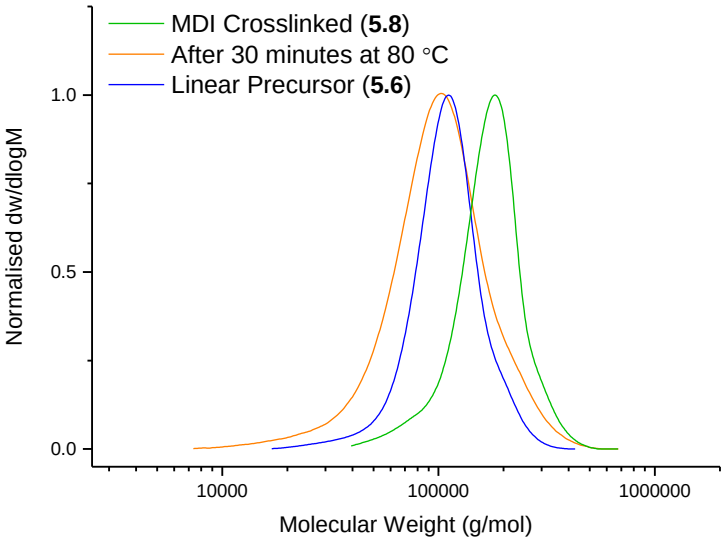

Figure 5.27 Molecular weight distributions for the MDI crosslinked polymer (5.8) before heating (*green*), after heating at 80 °C for 30 minutes (*orange*), compared to the linear precursor 5.6 (*blue*).

5.3.5 One-pot polyurethane formulation

For the one-pot formulation, a blocked isocyanate, in which the isocyanate is rendered inactive through the reaction with an active hydrogen containing compound (introduced in Chapter 1), is mixed with the polyol and the catalyst added. If the catalyst is truly latent, no reaction should occur until activation through heating. Having demonstrated the thermally responsive behaviour of the isocyanate crosslinked polymers, the initial stage of one-pot development was the synthesis of a blocked isocyanate for the formulation. Indeed, the blocked isocyanate used in the formulation would need to have a higher deblocking temperature than of the crosslinked

polymeric catalysts, with the exotherm produced from initial deblocking of the polymeric catalyst, exposure of the catalytic amine and initial polyurethane formation sufficient to trigger further deblocking. As previously reported, aliphatic isocyanates deblock at higher temperature than aromatic isocyanates,[35] and it was hypothesised that by selecting a similar blocking group to the crosslinked polymers, the deblocking temperatures should fall within the desired range. In order to produce a blocked isocyanate with a deblocking temperature of approximately 80-90 °C, a pyrazole blocking agent was again selected and used in conjunction with the aliphatic diisocyanate α,α,α',α'-tetramethyl-1,3-xylylene diisocyanate (TMXDI).

Blocked TMXDI was synthesised through the reaction of TMXDI with 3,5-dimethyl pyrazole, with catalytic dibutyltin dilaurate (DBTL, Scheme 5.8). Following reflux in anhydrous toluene for 16 hours the reaction flask was cooled to room temperature and 5 mL ethanol was added to quench any unreacted isocyanate, with to ensure complete blocking of the isocyanate, which is essential for a successful one-pot formulation.

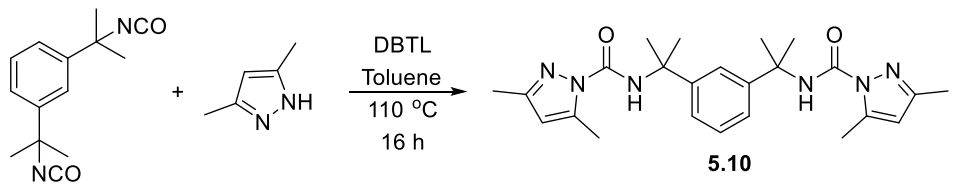

5.10

Scheme 5.9 Schematic representation for the synthesis of 3,5-dimethylpyrazole blocked TMXDI.

The synthesis of 3,5-dimethylpyrazole blocked TMXDI (**5.10**) was confirmed by ^{1}H and ^{13}C NMR spectroscopy (Figure 5.28 and Figure 5.29), with the appearance of the urea signal in the ^{13}C NMR spectrum at δ = 149.9 ppm. The absence of active isocyanate functionality was confirmed by FT-IR spectroscopy, with no peak associated with the isocyanate found at 2275 cm^{-1} (Figure 5.30).

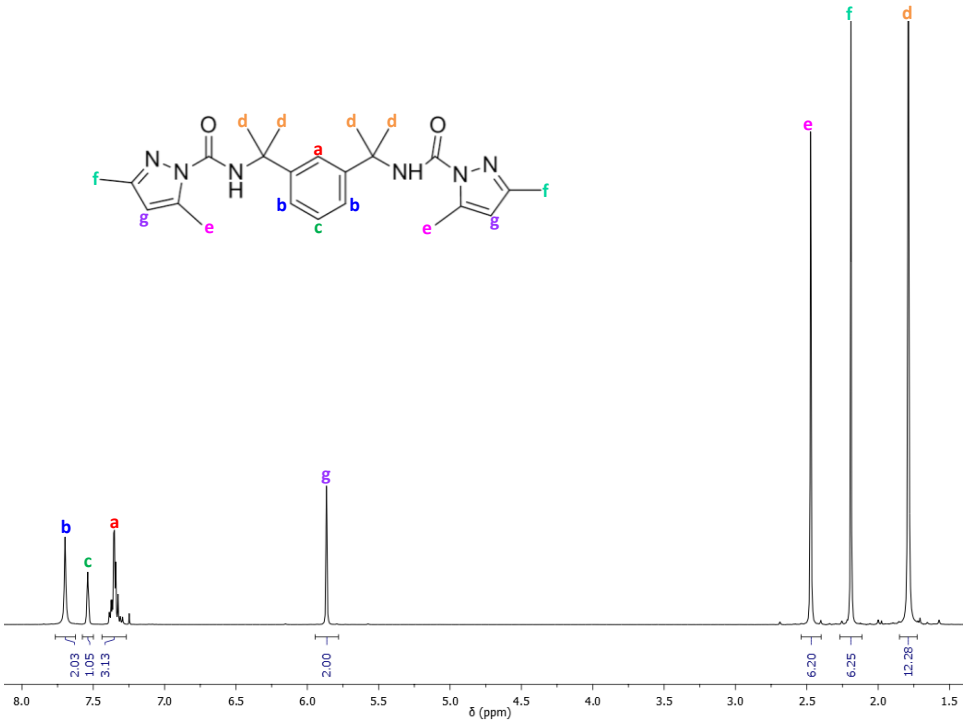

Figure 5.28 ^{1}H NMR spectrum of 3,5-dimethyl pyrazole blocked TMXDI, 5.10 (400 MHz, $CDCl_3$).

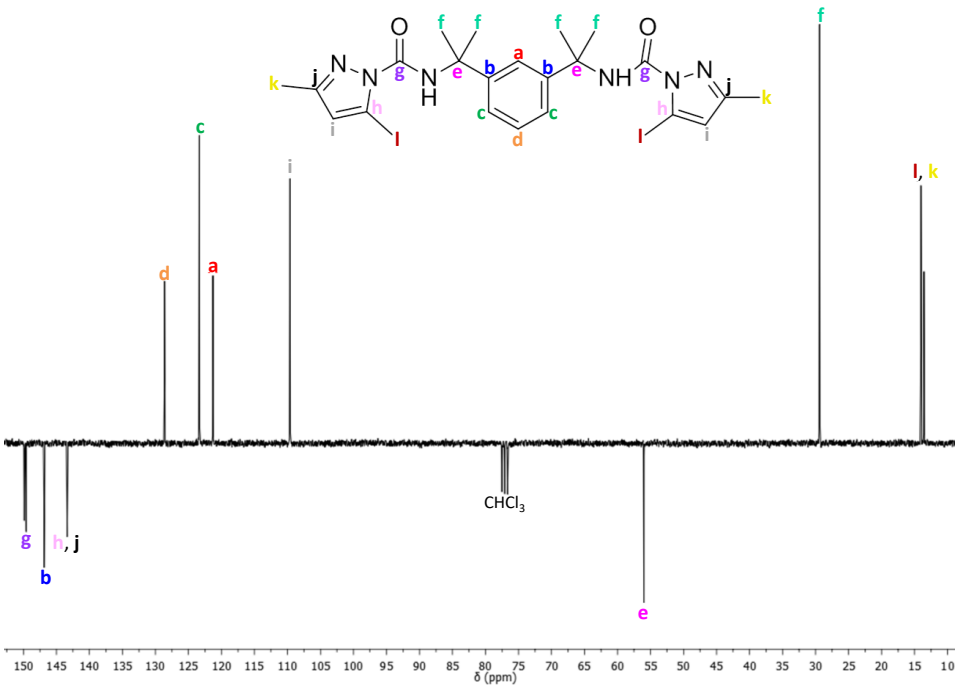

Figure 5.29 ^{13}C NMR spectrum of 3,5-dimethyl pyrazole blocked TMXDI, 5.10 (100 MHz, $CDCl_3$).

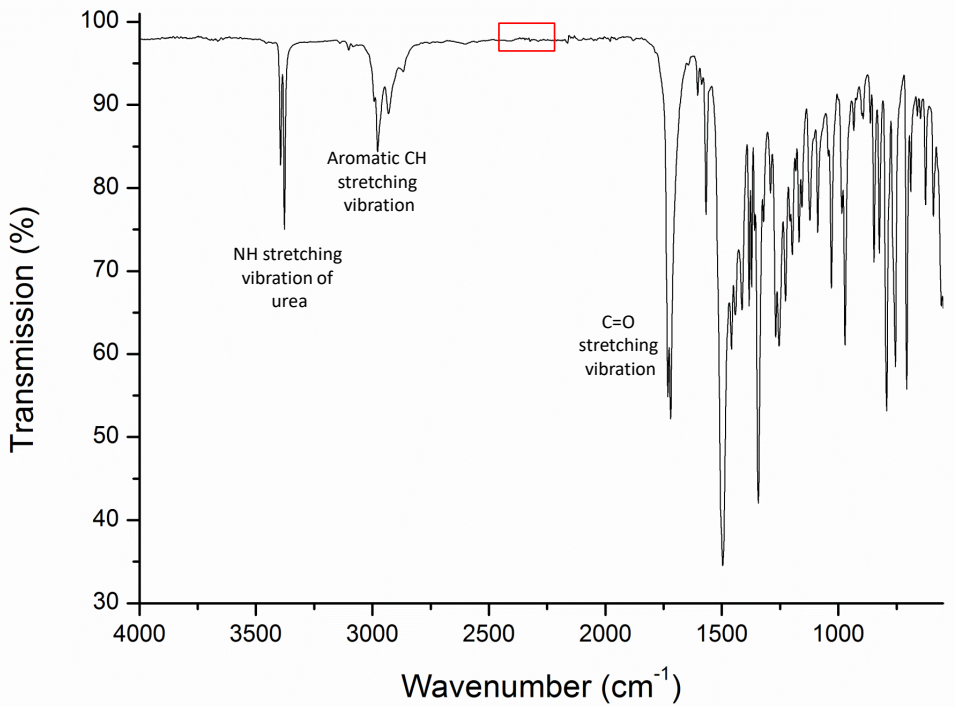

Figure 5.30 IR spectrum of 3,5-dimethylpyrazole blocked TMXDI (5.10), where the red box highlights the wavenumbers where an isocyanate stretch is to be expected.

To ensure its applicability to the one-pot polyurethane formulation, the deblocking behaviour of the blocked TMXDI was investigated. Initial studies on the solid blocked isocyanate using differential scanning calorimetry (DSC) analysis indicated a deblocking temperature of 91 °C (Figure 5.31). It is widely acknowledged that evaluation of a solid state blocked isocyanate produces a higher deblocking temperature than those in the liquid state, either existing in a liquid state or being dissolved in a solvent, with the need to match the method used to probe deblocking temperature to the state of the application.[38] For this reason, DSC analysis of the blocked isocyanate when dissolved in the formulation polyol was carried out (in a 3:1 ratio by weight of isocyanate:polyol), and afforded a slightly lower deblocking temperature of 85 °C, yet still within the desired temperature and, notably, higher than the deblocking temperature for the methacryloyl pyrazole blocked TDI/MDI/HDI.

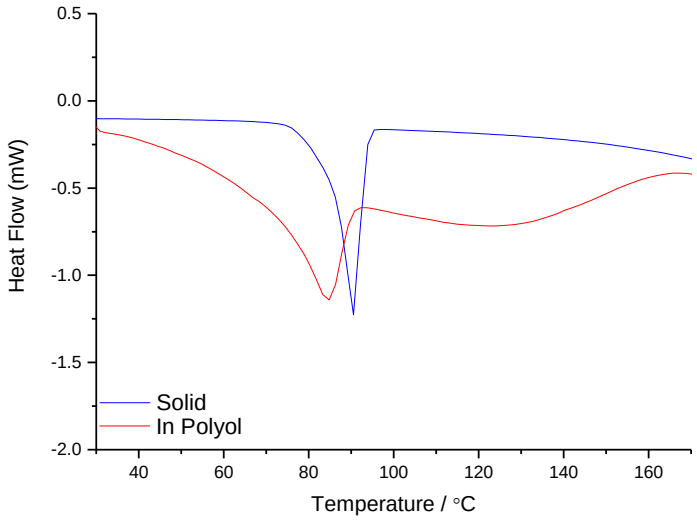

Figure 5.31 DSC thermograms of 5.10 analysed as a solid (*blue*) and dissolved in formulation polyol (*red*). Heating rate = 10 °C/min.

Further testing of the deblocking of the blocked TMXDI was carried out by conducting several small scale polyurethane tests. To this end, a 1:1 ratio of the formulation polyol and the blocked TMXDI were mixed, following incubation of the polyol at a set temperature for 30 minutes. Results from the vial tests indicated a deblocking temperature of between 80-90°C, with the added blocked isocyanate found to fully dissolve, and an increase in the solution viscosity visually observed (Figure 5.32). Moreover, the vial test results were consistent with the temperature determined by DSC results. Analysis of the resultant mixtures using FT-IR spectroscopy further indicated that reaction only occurred at 80-90 °C, with a change in the carbonyl region from two s to a broad single peak (Figure 5.33). Moreover, no visual difference was observed in the samples up until 80-90 °C, therefore confirming the blocked TMXDI as a suitable candidate for the blocked isocyanate for the one-pot formulation. Owing to the promising results from the isocyanate crosslinked polymers and the deblocking of the blocked TMXDI, the materials were sent to AWE for polyurethane formulation evaluation.

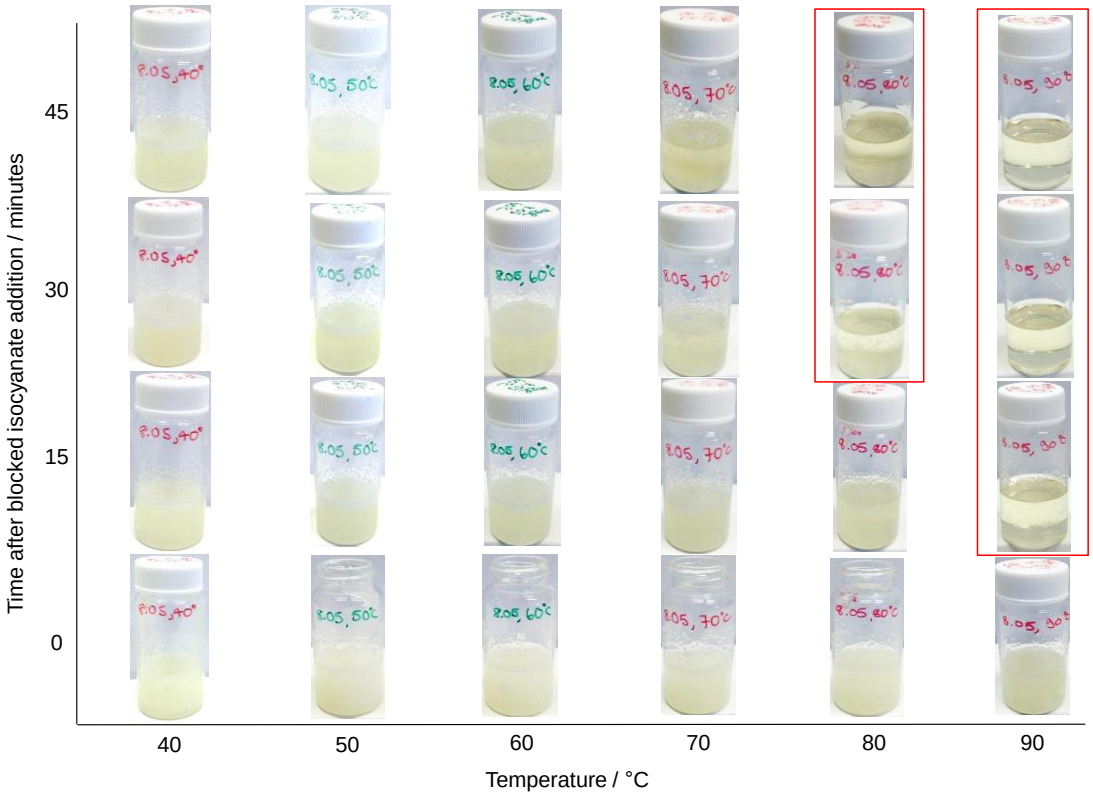

Figure 5.32 Evaluation of the blocked TMXDI (5.10) in formulation polyol incubated at different temperatures.

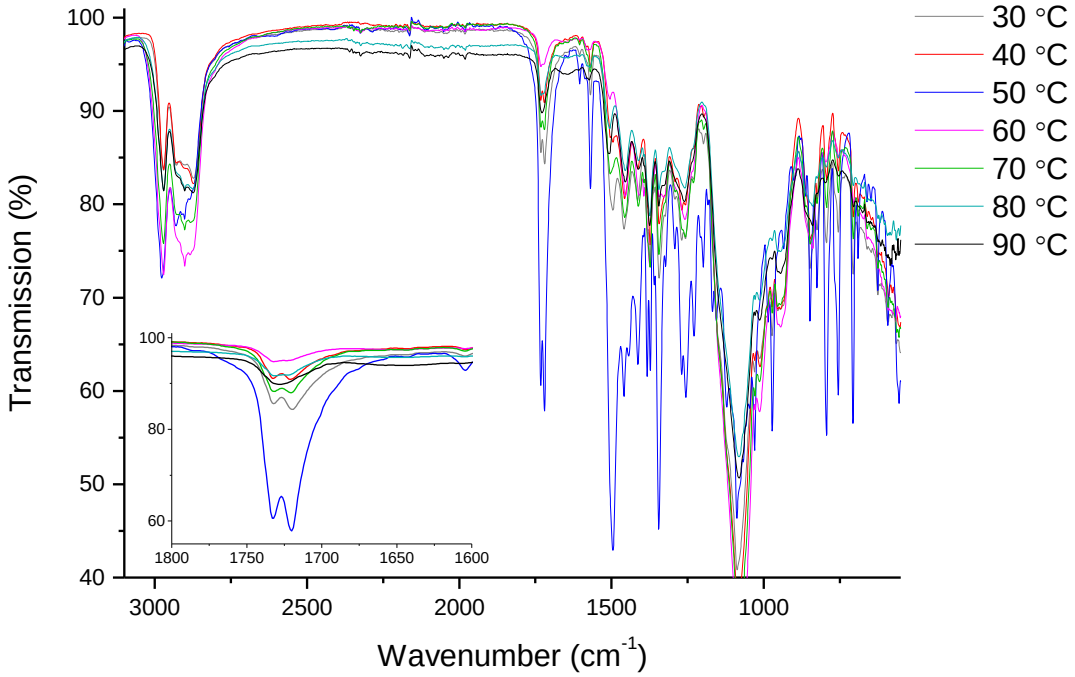

Figure 5.33 Overlaid FT-IR spectra for the polyol and blocked TMXDI mixtures following mixing and reaction for 6 hours.

5.4 Conclusion

A TDI based isocyanate releasing crosslinker has been successfully synthesised through the production of the novel monomer methacryloyl pyrazole and subsequent stirring with TDI. However, the monomeric crosslinker was found to be unsuitable for incorporation into the star polymers using an arm-first RAFT polymerisation method owing to solution instability. To overcome this, an alternative synthetic route *via* the polymerisation of the methacryloyl pyrazole to produce a linear precursor was carried out, and the resultant polymer reacted with the diisocyanate. To understand the thermoresponsive behaviour, ^{1}H VT-NMR spectroscopic analysis, in addition to SEC analysis on samples heated to different temperatures was performed, confirming the deblocking of the crosslinker and disintegration of the polymers. Moreover, the applicability of the synthetic route has been demonstrated to produce polymeric stars crosslinked with other diisocyanates, confirmed to deblock at different temperatures to the TDI crosslinked polymer, and potentially paving the way for their action as latent catalysts in different types of polyurethane formulations. Additionally, the production of 3,5-dimethylpyrazole blocked TMXDI provided a suitable candidate for the formulation blocked isocyanate, with the deblocking temperature confirmed to be different to the crosslinked polymeric catalysts yet within the desired temperature range.

5.5 Experimental

5.5.1 Materials

Silica gel (40-63 μM) and deuterated solvents were received from Apollo Scientific, with deuterated solvents dried over molecular sieves (3 Å, Sigma-Aldrich). The following reagents were used as received: ethyl acetoacetate (Sigma-Aldrich, 98%), hydrazine monohydrate (Fisher Scientific, 99%) trifluoroacetic acid (Sigma-Aldrich, 99%), *p*-toluene sulfonic acid monohydrate (Alfa Aesar, 97%), methacryloyl chloride (Sigma-Aldrich, 97%), triethylamine (TEA, Fisher

Scientific, laboratory grade), toluene diisocyanate (TDI, Sigma-Aldrich, 98%), 4,4'-methylenediphenyl diisocyanate (MDI, Sigma-Aldrich, 98%), 1,6-diisocyanatohexane (HDI, Alfa Aesar, 98%), α,α,α',α'-tetramethyl-1,3-xylylene diisocyanate (TMXDI, Sigma-Aldrich, 97%), 3,5-dimethylpyrazole (Sigma-Aldrich, 99%), and dibutyltin dilaurate (DBTL, Sigma-Aldrich, 95%). The following solvents were used as received: ethanol (EtOH, Fisher Scientific, absolute), diethyl ether (Et_2O, Sigma-Aldrich, AR grade), anhydrous acetone (Sigma-Aldrich, ReagentPlus), dichloromethane (CH_2Cl_2, Sigma-Aldrich, AR grade), hexane (Sigma-Aldrich, ReagentPlus), and petroleum ether 40-60 °C (pet. ether, Fisher Scientific, LT grade). Dry toluene was obtained using an Innovative Technology solvent purification system utilising activated alumina. Dialysis tubing was purchased Spectrum Laboratories. Formulation polyol was provided by AWE.

5.5.2 Instrumentation

In addition to the instrumentation introduced in section 2.5.2, and with the omission of catalyst testing and particle size analysis, small-angle X-ray scattering and gas chromatography, the following instrumentation was used in this Chapter: thermal analysis (Differential Scanning Calorimetry, DSC) was carried out using a Mettler Toledo DSC1 in aluminium pans, with a heating rate of 10 °C/min. unless otherwise stated. Melting points were determined using an Optimelt MPA100 automated melting point apparatus. All TEM images were collected by Miss Maria Inam (O'Reilly Group, University of Warwick).

5.5.3 Synthetic Methods and Procedures

*Synthesis of 5-methyl-2H-pyrazol-3-ol (hydroxy pyrazole, **5.1**):*

The synthesis of the hydroxy-functionalised pyrazole was based on a previously reported literature procedure.[22] To a solution of ethyl acetoacetate (10 g, 1.0 eq.) in ethanol, hydrazine hydrate (8.4 mL, 1.1 eq.) was added, and the solution stirred at room temperature for 16 hours. Following the reaction, the solution was cooled to 0 °C, stirred for 2 hours to ensure all the product had precipitated, filtered and washed with cold ethanol. The solid was recrystallised from ethanol affording a white crystalline solid (7.2 g, 49%). ^{1}H NMR (400 MHz, DMSO-d_6): δ (ppm) 10.46 (br s, 1H, N*H*), 5.22 (s, 1H, C(CH_3)C*H*), 3.50 (br s, 1H, O*H*), 2.08 (s, 3H, CH_3). ^{13}C NMR (100 MHz, DMSO-d_6): δ (ppm) 161.0 (*C*OH), 139.4 (*C*CH_3), 88.9 (C(CH_3)*C*H), 11.1 (*C*H_3). IR (neat) max/cm^{-1}: 3680 (υ_{OH}), 2990 ($\upsilon_{Ar\text{-}CH}$), 1615 ($\upsilon_{C=O,\ pyrazolinone\ ring}$), 1400 ($\upsilon_{C=C}$). *m/z* [ESI MS]: 98.7 (M+Na). Anal. calcd. for $C_4H_6N_2O$: C 49.0; H 6.2; N 28.6%. Found: C 49.0; H 6.1; N 28.9%. m.p. 219-224 °C (Lit:[39] 220-222 °C).

*Synthesis of 3-methacryloyl-5-methyl-2H-pyrazole (methacryloyl pyrazole, **5.2**):*

Synthesis of the methacryloyl pyrazole was based on a modified procedure previously developed in the group.[25] 3-Methyl-1H-pyrazol-5-ol (5 g, 1.0 eq.) was added portion wise to a vigorously stirring solution of trifluoroacetic acid (5 eq.) at 0 °C. Upon addition of *p*-toluene sulfonic acid monohydrate (1.9 g, 0.2 eq.) the resulting solution was stirred at 0 °C for 1 hour. Methacryloyl chloride (10.6 g, 2 eq.) was added dropwise over an hour, allowed to warm to room temperature, and the solution stirred for a further 16 hours. Cold diethyl ether was added dropwise and the resulting precipitate filtered and washed with cold diethyl ether (3 × 50 mL), yielding a pale pink solid. The solid was dissolved in CH_2Cl_2, extracted with basic water and brine, and the organic phase dried over magnesium sulfate. Following filtration, the CH_2Cl_2 was removed *in vacuo*, affording a white solid (5.6 g, 66%). ^{1}H NMR (400 MHz, $CDCl_3$): δ (ppm) 12.99 (br s, 1H, N*H*), 6.47 (s, 1H, CCH_2), 6.34 (s, 1H, C(CH_3)C*H*), 5.89 (s, 1H, CCH_2), 2.49 (s, 3H, CH_3CCH_2), 2.00 (s, 3H, CH_3C=N). ^{13}C NMR (100 MHz, $CDCl_3$): δ (ppm) 164.7 (*C*=O) 155.7 (CH*C*O), 140.7 (N*C*CH_3), 135.3 (CH_2*C*CH_3), 127.9 (*C*H_2), 95.1 (C(CH_3)*C*H), 18.3 (CH_2C*C*H_3),

11.4 (NC*C*H$_3$). IR (neat) max/cm^{-1}: 3150 (υ_{NH}), 2505 (υ_{NH}), 1765 ($\upsilon_{C=O}$), 1600 ($\upsilon_{C=C}$), 1315(υ_{COC}), 1160($\upsilon_{C=N}$). m.p. 237-239 °C.

*Synthesis of TDI containing crosslinker (**5.3**):*

Methacryloyl pyrazole (4.0 g, 1.0 eq.) was dissolved in dry acetone (40 mL) under nitrogen and cooled to 0 °C. TDI was added dropwise, the solution allowed to warm to room temperature and the reaction left for 48 hours. The crude reaction mixture was purified using column chromatography (silica gel treated with a 10% TEA in CH_2Cl_2 solution, 3:1 CH_2Cl_2/ pet. ether), R_f (3:1 CH_2Cl_2/ pet. ether): 0.43, affording a white crystalline solid (40%). ^{1}H NMR (400 MHz, $CDCl_3$): δ (ppm) 9.02 (s, 1H, N*H*), 8.99 (s, 1H, N*H*), 8.15 (s, 1H, Ar*H*), 7.57-7.42 (d, 1H, Ar*H*, $^3J_{H\text{-}H}$ = 8.3 Hz), 7.33-7.23 (d, 1H, Ar*H*, $^3J_{H\text{-}H}$ = 8.3 Hz), 6.43 (s, 2H, CC*H*$_2$), 6.18 (s, 2H, C(CH$_3$)C*H*), 5.85 (s, 2H, CC*H*$_2$), 2.68 (s, 3H, C(CH$_2$)C*H*$_3$), 2.34 (s, 3H, ArC*H*$_3$), 2.09 (s, 3H, N=C(C*H*$_3$)). ^{13}C NMR (100 MHz, $CDCl_3$): δ (ppm) 164.0 (O-*C*=O), 155.2 (C(=O)O*C*), 148.0 (N*C*(CH$_3$)), 145.0 (NH-*C*(=O)-N), 135.4 (CH$_2$*C*CH$_3$), 131.0 (Ar*C*), 128.7 (*C*H$_2$CCH$_3$), 124.3 (Ar*C*), 116.0 (Ar*C*), 112.5(Ar*C*), 102.0 (OC*C*H),18.3(*C*H$_3$CCH$_2$), 14.6 (*C*H$_3$CN). IR (neat) max/cm^{-1}: 3383, 3341 ($\upsilon_{NH\text{-}C(=O)\text{-}NH}$), 1732 ($\upsilon_{C=O}$), 1597 ($\upsilon_{C=C}$).

*Typical procedure for the chain extension of PHEMA with DMAEMA and **5.3**:*

PHEMA$_{140}$ (1eq.), DMAEMA (200 eq.) and TDI crosslinker **5.3** were dissolved in DMF (15 mL), with radical initiator VA-044 (0.17 eq.). Following four freeze-pump cycles, the ampoule was refilled with nitrogen and the mixture heated at 35 °C for 6 hours. The reaction was quenched by immersion in liquid nitrogen and purified by precipitation into 4:1 Et_2O/ acetone, affording a pale pink solid. ^{1}H NMR analysis indicated substantial deblocking and therefore the spectrum was not assigned. $M_{w,\ SEC}$ = 32.1 kg/mol, $M_{n,\ SEC}$ = 27.4 kg/mol, $Đ_M$ = 1.17.

*Procedure for the homopolymerisation of methacryloyl pyrazole blocked phenyl isocyanate (**5.4**):*

2-Cyano-2-proyl benzodithioate (1.0 eq., 10 mg) and methacryloyl pyrazole blocked phenyl isocyanate (100 eq., 900 mg) were dissolved in DMF (3 mL) with radical initiator VA-044 (0.3 eq.). Following removal of oxygen by four freeze-pump-thaw cycles, the ampoule was back-filled with nitrogen and placed in an oil bath at 30 °C for 20 hours. The reaction was quenched by immersion in liquid nitrogen and the polymer isolated by precipitation three times into 4:1 Et_2O/acetone. ^{1}H NMR analysis indicated substantial deblocking and therefore the spectrum was not assigned. $M_{w,\,SEC}$ = 21.9 kg/mol, $M_{n,\,SEC}$ = 15.3 kg/mol, $Đ_M$ = 1.43.

*Procedure for PEGMA macro-CTA synthesis (**5.5**):*

2-Cyano-2-propyl benzodithioate (1.0 eq., 100 mg) and poly(ethylene glycol) monomethyl ether methacrylate (PEGMA, M_n = 500 Da, 110 eq.) were dissolved in DMF (75 mL) with radical initiator AIBN (0.12 eq.). Following removal of oxygen by purging the solution with nitrogen, the mixture was heated to 70 °C for 20 hours (93% conversion). The reaction was quenched by immersion in liquid nitrogen and dialysed extensively against deionised water (MWCO = 8 kg/mol). The solution was lyophilised yielding a viscous pink liquid (18.5 g, 74%). ^{1}H NMR (400 MHz, CD_3OD): δ (ppm) 7.85 (m, 2H, *ortho*-ArH), 7.57 (m, 1H, *para*-ArH), 7.40 (m, 2H, *meta*-Ar*H*), 4.08 (br s, $OCH_2CH_2(OCH_2CH_2)_8$), 4.08-3.50 (m, $O(CH_2CH_2)_8$)), 3.25 (s, CH_2OCH_3), 1.90-0.88 (m, CH_3CH_2 backbone). ^{13}C NMR (100 MHz, $CDCl_3$): δ (ppm) 177.9 (*C*=O), 71.6 ($OCCO(OCCO)_8$), 70.2 ($OCCO(OCCO)_8$), 68.3 ($OCCO(OCCO)_8$), 64.2 ($OCCO(OCCO)_8$), 57.9 (OCH_3), 45.0 ($CCCH_3$), 44.7 ($C(CCH_3)CH_2$), 18.4 ($C(CH_3)$). IR (neat) max/cm^{-1}: 2831, 2777 (υ_{C-H}), 1724 ($\upsilon_{C=O}$), 1454 ($\upsilon_{C-O,\,ester}$). $M_{w,\,SEC}$ = 94.0 kg/mol, $M_{n,\,SEC}$ = 78.3 kg/mol, $Đ_M$ = 1.20.

*Procedure for the chain extension of the $PEGMA_{110}$ macro-CTA with DMAEMA and methacryloyl pyrazole (**5.6**):*

$PEGMA_{110}$ macro-CTA (1 eq., 9.3 g), DMAEMA (200 eq.), and methacryloyl pyrazole (**5.4**, 20 eq.) were dissolved in DMF (150 mL) together with the radical initiator AIBN (0.17 eq.). The solution was degassed by purging with nitrogen and the mixture heated for 16 hours at 70 °C (54% DMAEMA conversion, 67% methacryloyl pyrazole conversion). The reaction was quenched by immersion in liquid nitrogen and purified by precipitation into 4:1 Et_2O/acetone three times, affording a pink-orange solid. ^{1}H NMR (400 MHz, CD_3OD): δ (ppm) 5.92 (s, N*H*), 5.80 (s, NC(CH_3)C*H*), 4.13 (br s, OC$H_2$$CH_2$N and OC$H_2$$CH_2$($OCH_2CH_2$)$_8$), 3.90-3.55 (m, O(C$H_2CH_2$)$_8$)), 3.37 (s, CH_2OCH_3), 2.65 (m, CH_2N), 2.35 (br s, N(CH_3)$_2$), 2.11-0.95 (m, CH_3CH_2 backbone). IR (neat) max/cm^{-1}: 3377 ($\upsilon_{C\text{-}H}$), 2867 ($\upsilon_{C\text{-}H}$), 2752 ($\upsilon_{N\text{-}CH_3}$), 1727 ($\upsilon_{C=O}$), 1453 ($\upsilon_{C\text{-}O,\ ester}$), 1102 ($\upsilon_{C\text{-}O}$). $M_{w,\ SEC}$ = 115.7 kg/mol, $M_{n,\ SEC}$ = 99.7 kg/mol, $Đ_M$ = 1.16.

Typical procedure for the crosslinking of PEGMA-b-(DMAEMA-co-pyrazole):

The linear precursor polymer PEGMA-*b*-(DMAEMA-*co*-pyrazole) (**5.6**) was dissolved in anhydrous acetone and cooled to 0 °C. The diisocyanate was added dropwise, the solution allowed to warm to room temperature and stirred for 48 hours. The polymer was isolated by precipitation into 4:1 Et_2O/acetone three times.

a. TDI crosslinked $PEGMA_{110}$-*b*-($DMAEMA_{0.9}$-*co*-$pyrazole_{0.1}$)$_{90}$ (**5.7**)

^{1}H NMR (400 MHz, CD_3OD): δ (ppm) 7.85 (m, 2H, *ortho*-ArH), 7.57 (m, 1H, *para*-ArH), 7.41 (m, 2H, *meta*-Ar*H*), 5.79 (br s, NC(CH_3)C*H*), 4.14 (br s, OC$H_2$$CH_2$N and OC$H_2$$CH_2$($OCH_2CH_2$)$_8$), 3.76-3.57 (m, O(C$H_2CH_2$)$_8$)), 3.39 (s, CH_2OCH_3), 2.67 (m, CH_2N), 2.35 (br s, N(CH_3)$_2$), 1.98-0.96 (m, CH_3CH_2 backbone and CH_3 TDI).). IR (neat) max/cm^{-1}: 2944 ($\upsilon_{Ar\text{-}H}$), 2869 ($\upsilon_{C\text{-}H}$), 2770 ($\upsilon_{N\text{-}CH_3}$), 1726 ($\upsilon_{C=O}$), 1455 ($\upsilon_{C\text{-}O,\ ester}$), 1100 ($\upsilon_{C\text{-}O}$). $M_{w,\ SEC}$ = 213.0 kg/mol, $M_{n,\ SEC}$ = 133.1 kg/mol, $Đ_M$ = 1.60.

b. MDI crosslinked $PEGMA_{110}$-*b*-($DMAEMA_{0.9}$-*co*-$pyrazole_{0.1}$)$_{90}$ (**5.8**)

^{1}H NMR (400 MHz, CD_3OD): δ (ppm) 7.90-7.12 (m, *ortho*-Ar*H*, *para*-Ar*H*, *meta*-Ar*H*, Ar*H* MDI), 5.79 (br s, NC(CH_3)C*H*), 4.14 (br s, OC$H_2$$CH_2$N and OC$H_2$$CH_2$($OCH_2CH_2$)$_8$), 3.69-3.50 (m, O(C$H_2CH_2$)$_8$), 3.39 (s, CH_2OCH_3), 2.67 (m, CH_2N), 2.37 (br s, N(CH_3)$_2$), 2.170-0.97 (m, CH_3CH_2 backbone). IR (neat) max/cm^{-1}: 2944 ($\upsilon_{Ar\text{-}H}$), 2869 ($\upsilon_{C\text{-}H}$), 2770 ($\upsilon_{N\text{-}CH_3}$), 1726 ($\upsilon_{C=O}$), 1452 ($\upsilon_{C\text{-}O,\ ester}$), 1103($\upsilon_{C\text{-}O}$). $M_{w,\ SEC}$ = 179.3 kg/mol, $M_{n,\ SEC}$ = 155.9 kg/mol, $Đ_M$ = 1.15.

c. HDI crosslinked PEGMA$_{110}$-*b*-(DMAEMA$_{0.9}$-*co*-pyrazole$_{0.1}$)$_{90}$ (**5.9**)

^{1}H NMR (400 MHz, CD_3OD): δ (ppm) 7.90-7.12 (m, *ortho*-Ar*H*, *para*-Ar*H*, *meta*-Ar*H*, Ar*H* MDI), 5.79 (br s, NC(CH_3)C*H*), 4.14 (br s, OC$H_2$$CH_2$N and OC$H_2$$CH_2$($OCH_2CH_2$)$_8$), 3.69-3.50 (m, O(C$H_2CH_2$)$_8$), 3.39 (s, CH_2OCH_3), 2.67 (m, CH_2N), 2.35 (br s, N(CH_3)$_2$), 1.98-0.96 (m, CH_3CH_2 backbone and (CH_2)$_6$ HDI). IR (neat) max/cm^{-1}: 2864 ($\upsilon_{C\text{-}H}$), 2783 ($\upsilon_{N\text{-}CH_3}$), 1730 ($\upsilon_{C=O}$), 1456 ($\upsilon_{C\text{-}O,\ ester}$), 1103 ($\upsilon_{C\text{-}O}$). $M_{w,\ SEC}$ = 212.3 kg/mol, $M_{n,\ SEC}$ = 178.4 kg/mol, $Đ_M$ = 1.19.

*Procedure for the synthesis of 3,5-dimethyl pyrazole blocked TMXDI (**5.10**):*

3,5-Dimethylpyrazole (100 g, 2 eq.) was dissolved in anhydrous toluene, cooled on ice and purged with nitrogen. DBTL (31 μL, 0.0001 eq.) was added, and TMXDI added dropwise (120 mL, 1 eq.). The reaction mixture was allowed to warm to room temperature, and brought to and maintained at reflux for 16 hours. The solution was allowed to cool to room temperature, 5 mL ethanol added and the solution stirred for 30 minutes. The solvent was removed *in vacuo* and the resultant crystalline solid filtered and washed with cold hexane, affording a white crystalline solid (155.5 g, 87%). ^{1}H NMR (400 MHz, $CDCl_3$): δ (ppm) 7.69 (s, 2H, Ar*H*), 7.51 (m, 1H, Ar*H*), 7.35 (m, 1H, Ar*H*), 5.87 (s, 2H, NC(CH_3)C*H*), 2.48 (s, 6H, NC(CH_3)), 2.20 (s, 6H, NC(CH_3)), 1.79 (s, 12H, (CH_3)$_2$). ^{13}C NMR (100 MHz, $CDCl_3$): δ (ppm) 149.9 (*C*=O), 149.6 (*C*=O), 146.9 (Ar*C*), 143.4 (N*C*(CH_3)), 128.6 (Ar*C*), 123.3 (Ar*C*), 121.3 (Ar*C*), 109.6

(NC(CH_3)*C*H), 56.0 (*C*(CH_3)$_2$), 29.4 ((*C*H_3)$_2$), 14.0 (NC(*C*H_3), 13.6 (NC(*C*H_3)). IR (neat) max/ cm^{-1}: 3395, 3378 ($\upsilon_{NH\text{-}C(=O)\text{-}NH}$), 1720 ($\upsilon_{C=O}$).

5.6 Bibliography

1. Neilson, B. M., Bielawski, C. W., *Chem. Commun.,* **2013**, 49, 5453.
2. Coulembier, O., Dove, A. P., Pratt, R. C., Sentman, A. C., Culkin, D. A., Mespouille, L., Dubois, P., Waymouth, R. M., Hedrick, J. L., *Angew. Chem.,* **2005**, 117, 5044.
3. Nimitsiriwat, N., Marshall, E. L., Gibson, V. C., Elsegood, M. R. J., Dale, S. H., *J. Am. Chem. Soc.,* **2004**, 126, 13598.
4. Versace, D.-L., Cerezo Bastida, J., Lorenzini, C., Cachet-Vivier, C., Renard, E., Langlois, V., Malval, J.-P., Fouassier, J.-P., Lalevée, J., *Macromolecules,* **2013**, 46, 8808.
5. Magenau, A. J. D., Strandwitz, N. C., Gennaro, A., Matyjaszewski, K., *Science,* **2011**, 332, 81.
6. Cunningham, A. F., Desobry, V., Dietliker, K., Hüsler, R., Leppard, D. G., *Chimia,* **1994**, 48, 423.
7. Naumann, S., Buchmeiser, M. R., *Macromol. Rapid Commun.,* **2014**, 35, 682.
8. Fink, J. K., *Reactive Polymers Fundamentals and Applications: A Concise Guide to Industrial Polymers*, Elsevier Science, **2013**.
9. Endo, T., Sanda, F., *Macromol. Symp.,* **1996**, 107, 237.
10. Park, S.-J., Seo, M.-K., Lee, J.-R., *J. Polym. Sci., Part A: Polym. Chem.,* **2000**, 38, 2945.
11. Toneri, T., Watanabe, K.-i., Sanda, F., Endo, T., *Macromolecules,* **1999**, 32, 1293.
12. Park, S.-J., Jin, F.-L., Lee, J.-R., Shin, J.-S., *Eur. Polym. J.*, **2005**, 41, 231.
13. Kim, M., Sanda, F., Endo, T., *Macromolecules*, **1999**, 32, 8291.
14. Carroy, A., Hintermann, T., Baudin, G., Bauer, D., Contich, P., Dietliker, K., Faller, M., Kohli Steck, R., Lordelot, C., Misteli, K., *Prog. Org. Coat.*, **2010**, 68, 37.
15. Bijlard, A.-C., Hansen, A., Lieberwirth, I., Landfester, K., Taden, A., *Adv. Mater.*, **2016**, 28, 6372.
16. Wicks, D. A., Wicks Jr, Z. W., *Prog. Org. Coat.,* **2001**, 41, 1.
17. Wicks, Z. W., *Prog. Org. Coat.,* **1981**, 9, 3.
18. Alsarraf, J., Robert, F., Cramail, H., Landais, Y., *Polym. Chem.*, **2013**, 4, 904.
19. Meier-Westhues, U., *Polyurethanes: Coatings, Adhesives and Sealants*, Vincentz Network, **2007**.
20. Carter, J. W., Pappas, S. P., *J. Coat. Technol. Res.*, **1992**, 64, 29.
21. Mühlebach, A., *J. Polym. Sci., Part A: Polym. Chem.,* **1994**, 32, 753.
22. Soleimani, E., Hariri, M., Saei, P., *C. R. Chim.*, **2013**, 16, 773.
23. Amir, M., Javed, S. A., Zaheen Hassan, M., *Med. Chem. Res.*, **2012**, 21, 1261.
24. Khalil, A. K., Hassan, M. A., Mohamed, M. M., El-Sayed, A. B., *Indian J. Chem., Sect. B: Org. Chem. Incl. Med. Chem.*, **2006**, 45B, 2485.
25. Lu, A., Moatsou, D., Longbottom, D. A., O'Reilly, R. K., *Chem. Sci.*, **2013**, 4, 965.
26. Nasar, A. S., Subramani, S., Radhakrishnan, G., *J. Polym. Sci., Part A: Polym. Chem.,* **1999**, 37, 1815.
27. Lutz, J.-F., *J. Polym. Sci., Part A: Polym. Chem.,* **2008**, 46, 3459.
28. Zeng, W., Du, Y., Xue, Y., Frisch, H. L., Mark–Houwink–Staudinger–Sakurada Constants, *Physical Properties of Polymers Handbook*, Springer New York, **2007**.
29. Hiemenz, P. C., Lodge, T. P., *Polymer Chemistry, Second Edition*, Taylor & Francis, **2007**.

30. James, A. B., David, M. H., Becer, C. R., Synthesis and SEC Characterization of Poly(methyl methacrylate) Star Polymers, *Progress in Controlled Radical Polymerization: Materials and Applications*, American Chemical Society, **2012**.
31. Radke, W., Chromatography of Polymers, *Macromolecular Engineering*, Wiley-VCH Verlag GmbH & Co. KGaA, **2007**.
32. Patterson, J. P., Robin, M. P., Chassenieux, C., Colombani, O., O'Reilly, R. K., *Chem. Soc. Rev.*, **2014**, 43, 2412.
33. Young, R. J., Lovell, P. A., *Introduction to Polymers, Third Edition*, Taylor & Francis, **2011**.
34. Elias, H.-G., Bareiss, R., *J. Macromol. Sci., Part A: Pure Appl. Chem.*, **1967**, 1, 1377.
35. Wicks, Z. W., Jones, F. N., Pappas, S. P., Wicks, D. A., *Organic Coatings: Science and Technology*, Wiley-VCH Verlag GmbH & Co. KGaA, **2006**.
36. Muramatsu, I., Tanimoto, Y., Kase, M., Okoshi, N., *Prog. Org. Coat.*, **1993**, 22, 279.
37. Lee, J. M., Subramani, S., Lee, Y. S., Kim, J. H., *Macromol. Res.*, **2005**, 13, 427.
38. Gedan-Smolka, M., Haussler, L., Fischer, D., *Thermochim. Acta*, **2000**, 351, 95.
39. Nasseri, M. A., Salimi, M., Esmaeili, A. A., *RSC Adv.*, **2014**, 4, 61193.

6. The Spectroscopic Determination of Deblocking Temperature for Blocked Isocyanates: A Comparative Study

6.1 Abstract

It is widely accepted in the literature that the determination of the deblocking temperature of blocked isocyanates varies greatly depending on the analytical technique implemented. For this reason, this Chapter emphasises the effect of using different analytical techniques to determine the deblocking temperature for a variety of blocked isocyanates. Emphasis is placed on the effect of varying the spectroscopic technique used to determine the deblocking temperature. The deblocking temperatures were determined for both the blocked isocyanate crosslinkers reported in Chapter 5, as well as an analogous phenyl isocyanate monomer, in addition to looking at other intra- and intermolecularly blocked isocyanates. The deblocking temperature was found to be strongly dependent on the state in which the deblocking temperature is determined, hypothesised to be as a consequence of a mixture of hydrogen bonding effects and solubilising of the blocked isocyanate, with liquid based analyses producing lower deblocking temperatures than solid state techniques, as well as being influenced by instrumental parameters such as the rate of heating of a sample. As such it is noted that the technique used for analysis must be carefully matched to the state of the application to ensure an accurate deblocking temperature. Moreover, addition of small molecule amines was shown to decrease the deblocking temperature, which is highly relevant to a one-pot formulation in which the catalytic amine moieties are in close proximity to the blocked isocyanates and would therefore result in a lower temperature required to trigger the polyurethane formation.

6.2 Introduction

The synthesis of polyurethanes, introduced in Chapter 1.2.1, involves the step-growth polymerisation of a dihydroxyl containing compound, frequently an alcohol or water, and a diisocyanate (Scheme 1.2). Industrially, the high sensitivity of the isocyanate makes prolonged storage isocyanates highly unfeasible. Careful storage of the isocyanate component is required to prevent reaction and subsequent production of an unusable material.[1] In order to overcome this

problem, work has focussed on the development of isocyanate-free polyurethane formulations,[2, 3] for example through the use of carbonylbiscaprolactam,[4, 5] or through the use of "blocked", or "masked" isocyanates, eliminating the problem of isocyanate moisture sensitivity. A blocked isocyanate is an isocyanate analogue that contains no active isocyanate functionality. The isocyanate functional group is masked through the use of a blocking agent, resulting in the formation of a urethane linkage with a relatively labile hydrogen bond on the nitrogen. The blocked isocyanate produced is inert at room temperature yet yields the reactive isocyanate functionality at elevated temperatures.[6] For the majority of blocked isocyanates, the blocking occurs through a reaction with a compound containing an active hydrogen atom (B-H), producing an externally blocked isocyanate (Scheme 1.10). The blocked isocyanate is in equilibrium with its deblocked form, and addition of heat leads to the regeneration of the blocking agent and liberation of the reactive isocyanate functionality at raised temperatures. Further to this, the relative inertness of the blocked isocyanates towards moisture and other nucleophiles, as well as additional free or blocked isocyanates, dramatically increases the shelf life, and advantageously blocked isocyanates have been found to have lower toxicities than free isocyanates.[7, 8] Furthermore, the relative inertness towards a range of conditions has allowed for the development of one-pot polyurethane formulations, as well as a more environmentally friendly and safer synthesis of polyurethanes.

There is a vast range of compounds that have been investigated as external blocking agents for isocyanates, ranging from alcohol-functionalised compounds[9-13] including oximes (of which methylethyl ketone oxime, MEKO, is one of the most reported blocking groups, Scheme 6.1A),[14-17] through to nitrogen containing compounds such as amines and pyrazoles,[14, 18-26] and salts (with sodium bisulfite frequently applied to waterborne coatings).[27-29] Additionally, isocyanates can be blocked internally, for example, forming a dimeric uretdione species (Scheme 6.1B). Whilst selection of different blocking groups enables the tailoring of the deblocking temperature, further alterations of blocking agent substituents (for example the

addition of electron withdrawing groups to an aromatic ring)[30, 31] alongside changes in experimental conditions and the identity of the isocyanate used (aromatic *vs.* aliphatic) allows for further modification in the deblocking temperature.

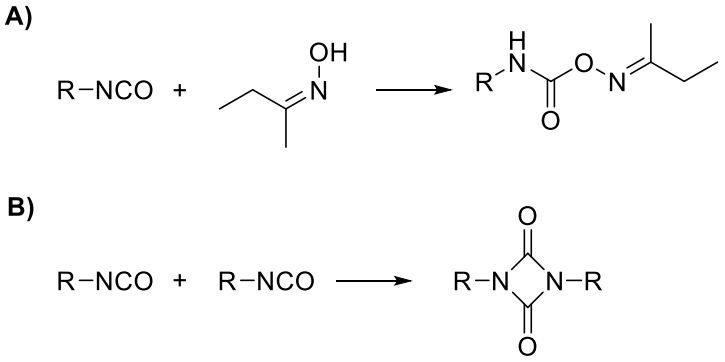

Scheme 6.1 Schematic representation of different types of blocked isocyanates: (A) the blocking of an isocyanate using an external blocking agent, for example MEKO, and (B) the intramolecular blocking of an isocyanate, forming a dimeric uretdione species.

The required temperature at which the isocyanate deblocks is highly dependent on the application of the system, for example heat-cure organic powder coatings tend to require a higher deblocking temperature than isocyanates used in other applications including rigid and flexible polyurethane foams. There is a wealth of information in the literature on methods used to measure and determine the deblocking temperature of an isocyanate, including both isothermal and non-isothermal methods, a summary of which can be found in Table 6.1. It is of great importance at this point to highlight the use of terminology when discussing blocked isocyanates. There is a broad use of the term "deblocking temperature" in the literature but it should be stressed that this term in not quite accurate. The correct term, as highlighted by Delebecq, is "initial deblocking temperature", which describes the temperature at which a feature of deblocking (*e.g.* detection of a free blocking group) can be observed.[32] The exact temperature at which scission of the blocking group and isocyanate occurs would involve the determination of reaction rates and extrapolation back through the Arrhenius equation in order to generate an exact deblocking temperature.

Table 6.1 Common techniques for determining the deblocking temperature of blocked isocyanates.

Technique	Advantages	Disadvantages	Ref.
IR, FTIR Spectroscopy	Immediate result, easy to determine 100% completion of blocking/ deblocking. High resolution instruments allow for ppm detection.	Strongly influenced by heating rate. Sample preparation and evaporation can cause discrepancies in results. Results need to be normalised for analysis.	11, 33-42
DSC Analysis	Relatively high temperature capability (up to 100 °C). No additional sample preparation.	High temperatures may influence baseline and signal: noise ratio.	18, 43-45
TGA Analysis	High temperature capability (up to 1500 °C). Samples require no additional preparation. µg sensitivity.	High temperatures may influence baseline and signal: noise ratio. Boiling point of the blocking group must fall within the probed temperature range.	18, 43-45
UV-Vis Spectroscopy	Determines deblocking temperature within a narrow range. Provides additional information other techniques are not able to provide.	Labour intensive: calculation of multiple molar extinction coefficients required	46-48
NMR Spectroscopy	Highly accurate measurements. Enables all equilibrium species, and therefore kinetics, to be monitored. Small amount of sample (µg) required.	Requires high boiling point solvents. Limited to the temperature range of the instrument probe (typical limit = 160 °C). Significantly lower sensitivity *vs* other techniques (*e.g.* XPS).	32, 39, 49, 50
MS, GC, GC-MS Analysis	Confirmation of starting materials, deblocked product and blocking agent. GC-MS enables the degree of deblocking to be calculated. Highly sensitive (MS limit = ppm, GC limit = ppb).	For degree of deblocking, GC-MS requires calibration to a standard. Limited by the maximum oven operating temperature (typically 300 °C). Samples must be volatilised for analysis.	11, 51, 52
Titration	Only technique to allow for determination of urethane type	Labour intensive, requires additional work-up prior to titration.	14, 53-57
CO_2 Evolution	Immediate result. Produces a single temperature of deblocking.	Requires specialist glassware. Qualitative technique.	58-60
Physical Change	Rheological studies able to produce fairly narrow deblocking temperature.	Highly inaccurate: monitoring of physical change by eye leading to a large source of error.	61, 62
XPS	Highly sensitive technique (ppm detection). Provides elemental surface composition	Samples frequently need to be annealed outside of the instrument preventing real-time analysis. Analysis through comparison to a database.	63, 64

Also frequently reported in the literature are the inconsistencies in quoted deblocking temperatures for the same blocking agents, with different analytical techniques affording different deblocking temperatures.[43] Consequently, this work aims to explore the use of different spectroscopic and analytical techniques to ascertain any trends in factors affecting deblocking temperature. Work will focus on both internally and externally blocked isocyanates, investigating instrumental and chemical parameters in order to determine any trends which may affect the application of blocked isocyanates. Such variables examined include whether ramped or continual heating affords a lower deblocking temperature, applicable, for example, for the curing of polyurethane coatings.

6.3 Results and Discussion

One significant disadvantage of externally blocked isocyanates is what happens to the blocking agent once released. For polyurethane applications, if the free blocking agent remains in the formulation, *i.e.* the boiling point of the agent is too high and therefore the blocking agent doesn't evaporate, the free blocking agent may act as a plasticiser.[65] However, evaporation does not always overcome this problem, with evaporation resulting in the formation of bubbles in the product material, which, for example, is detrimental for coating applications. To this end, initial deblocking investigations were focussed on the internally blocked uretdiones, in which deblocking only releases isocyanates. It should be noted that the deblocking temperatures quoted within this Chapter refer to the appearance of a feature attributed to either the free isocyanate or the free blocking agent.

6.3.1 Internally Blocked Isocyanates

6.3.1.1 Synthesis of Uretdiones

In an initial experiment, internally blocked 1,3-diphenyl-2,4-uretidinedione (diphenyl uretdione, **6.1**) was synthesised according to a previous literature procedure (Scheme 6.2), using tributyl phosphine as catalyst.[66]

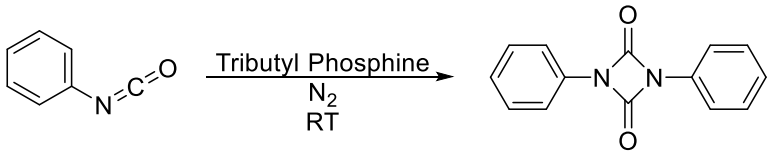

Scheme 6.2 Schematic representation for the synthesis of 1,3-diphenyl-2,4-uretidinedione (diphenyl uretdione).

Successful synthesis was confirmed by ^{13}C Nuclear Magnetic Resonance (NMR) spectroscopy (Figure 6.1), with the appearance of the uretdione ring carbonyl at δ = 150.0 ppm, and the loss of the isocyanate peak at δ = 124.9 ppm.

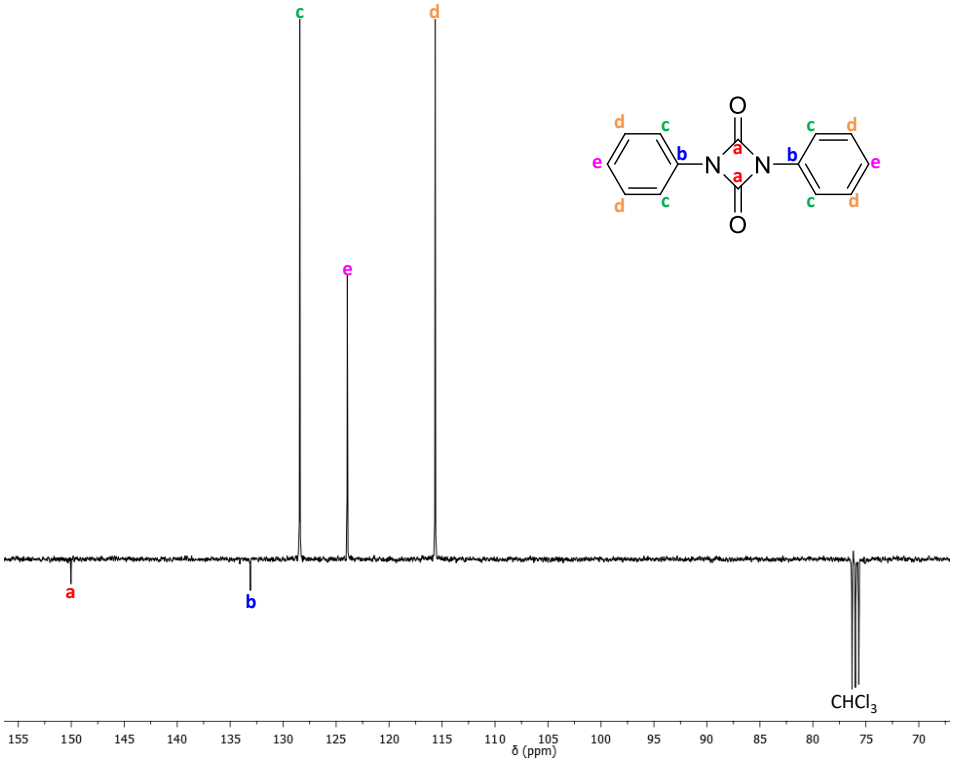

Figure 6.1 ^{13}C NMR spectrum of diphenyl uretdione, 6.1 (100 MHz, $CDCl_3$).

The complete blocking of the isocyanate was confirmed by infra-red (IR) spectroscopy, which clearly indicated the absence of an isocyanate peak at υ = 2275 cm^{-1}, in addition to the appearance of the uretdione peak at υ =1770 cm^{-1} (Figure 6.2).[67, 68]

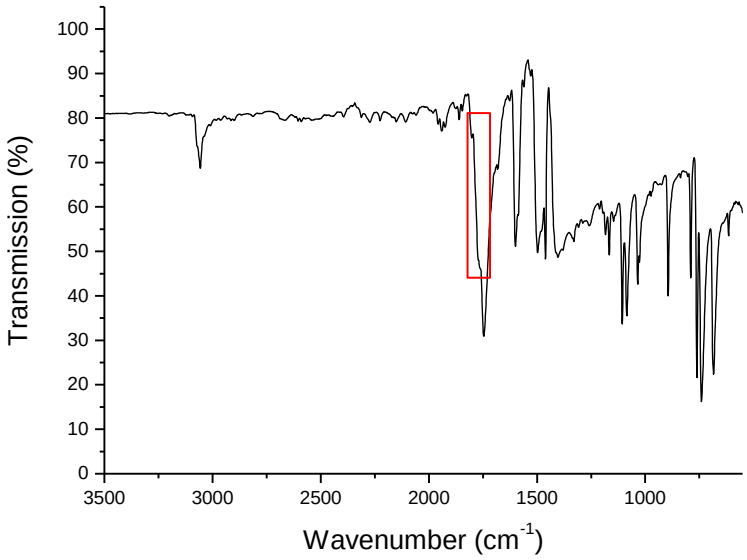

Figure 6.2 IR Spectrum of diphenyl uretdione, 6.1.

Literature indicates that the presence of ring substituents has a strong effect on the deblocking temperature of aromatic based blocked isocyanates.[62] In order to investigate the effect of ring substituents on deblocking temperature, a series of substituted uretdiones were synthesised using different substituted phenyl isocyanates as starting materials. The substituted phenyl isocyanates were selected to investigate both the electronic effects of the substituent (electron withdrawing *vs* electron donating) and the effect of substituent location (*ortho vs meta vs para* location of the ring substituent) (Table 6.2). For all uretdiones, melting point temperature determination is used as one of the only methods of differentiating between the dimeric uretdione species and trimeric isocyanurate species (Figure 1.7), with phenyl isocyanate based uretdione melting at 176-177 °C, and the isocyanurate melting at 283-285 °C.[66] As such, the melting point temperatures were used to confirm the successful synthesis of the dimeric product.[69]

Table 6.2 Diphenyl uretdiones with differing ring substituents and their corresponding deblocking temperature.

Blocked Isocyanate	Ring Substituent	Deblocking Temperature [a] (°C)
6.1	-	197
6.2m	*m*-NO_2	>350
6.2p	*p*-NO_2	296
6.3	*p*-Cl	>350
6.4m	*m*-OMe	220
6.4p	*p*-OMe	224

[a] determined by DSC analysis on the solid material, at a heating rate of 10 °C/min.

6.3.1.2 Evaluation of the deblocking temperature for Uretdiones

Initial investigations focussed on the use of differential scanning calorimetry (DSC) to determine the deblocking temperature. This technique was chosen owing to the high melting point of the uretdiones, and consequently the high deblocking temperature, ruling out the use of variable temperature nuclear magnetic resonance (VT-NMR) spectroscopy owing to the temperature limit of the instrument probe. DSC analysis of the unsubstituted phenyl isocyanate uretdione (**6.1**) indicated a deblocking temperature of 197 °C and a melting temperature of 185 °C (Figure 6.3, second and first exotherm respectively), higher than that determined using the melting point apparatus (161-167 °C), yet only slightly higher than that reported in the literature (176-177 °C).[66]

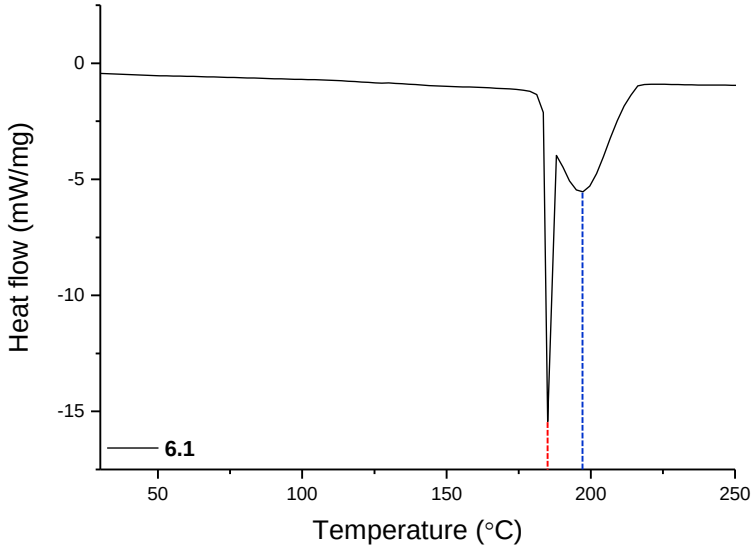

Figure 6.3 DSC thermogram for non-substituted diphenyl uretdione (6.1). Heating rate = 10 °C/min.

It is suggested in the literature that the addition of electron withdrawing groups to phenyl blocked isocyanates reduces the deblocking temperature, therefore the deblocking temperatures of nitro- and chloro-substituted uretdiones (**6.2m**, **6.2p** and **6.3**) were evaluated. As evident in Figure 6.4, varying the ring substituent has a notable effect on the deblocking temperature, though not as anticipated. All three electron withdrawing group substituents, regardless of their ring position, are found to significantly increase the deblocking temperature of the uretdione, with all substituents increasing the deblocking temperature by > 100 °C.

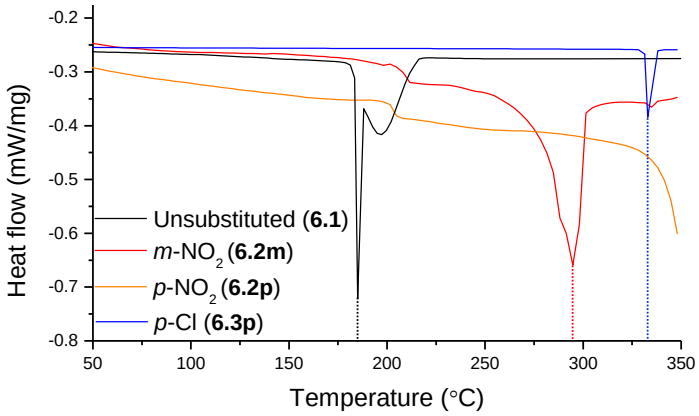

Figure 6.4 DSC thermograms of diphenyl uretdiones with electron-withdrawing ring substituents. Heating rate = 10 °C/min.

This result was rationalised based on the structure of uretdiones *vs* externally blocked aromatic isocyanates (Scheme 6.3). For an externally blocked isocyanate (Scheme 6.3A), there is conjugation between the π electrons of the aromatic ring and the N=C=O bond.[30] These electrons attract the lone pair of the nitrogen resulting in a slightly positive character on the nitrogen atom and increasing repulsion between the nitrogen atom and the attached hydrogen, with the net result of lowering the deblocking temperature. The addition of electron-withdrawing groups amplifies this effect and lowers the deblocking temperature further. In contrast, the uretdione does not have any labile N-H bonds preventing deblocking involving hydrogen abstraction, with deblocking likely proceed *via* a concerted mechanism involving the nitrogen lone pair. As such, addition of electron withdrawing groups to the ring would result in attraction of this lone pair, resulting in the lone pair being less able to undergo the concerted opening of the ring, raising the deblocking temperature. Moreover, the difference in deblocking temperatures for the *meta* substitituted uretdione compared to the *para* substituted uretdione were attributed to the overlap of molecular orbitals for the resonance structures of the substituted uretdiones influencing the nucleophilicity of the nitrogen lone pair resulting in different deblocking temperatures.

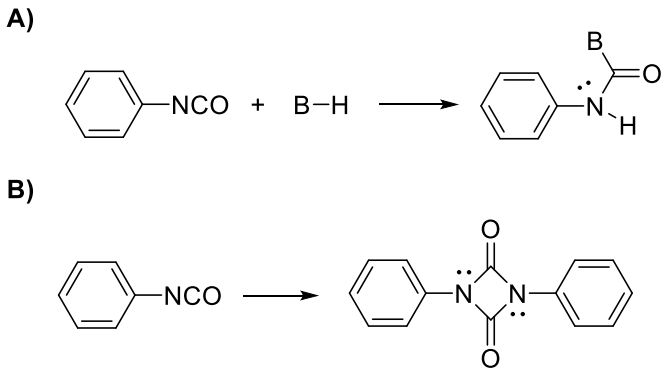

Scheme 6.3 Externally (A) and intramolecular (B) blocked aromatic isocyanates, demonstrating the presence of the labile N-H bond in the externally blocked isocyanates, and its absence in the internally blocked isocyanate.

In addition to the electronic effects, there is a noticeable effect of substituent location on the aromatic ring. The different deblocking temperatures are attributed to the steric strain in the

molecules; the *para* substitution results in a symmetrical molecule (**6.2p**, Figure 6.5A), whereas *meta* substitution results in a more sterically strained molecule (**6.2m,** Figure 6.5B) owing to the proximity of the bulky nitro groups to the central ring. This conformation is therefore likely to favour deblocking to remove this steric strain and results in a lower deblocking temperature. It should be noted, however, that the electronic effects are hypothesised to dominate over the steric effects, with only a slight steric strain in a *meta* substituted uretdione *vs* a *para* substituted uretdione, in comparison to the notably more strained *ortho* substituted product.

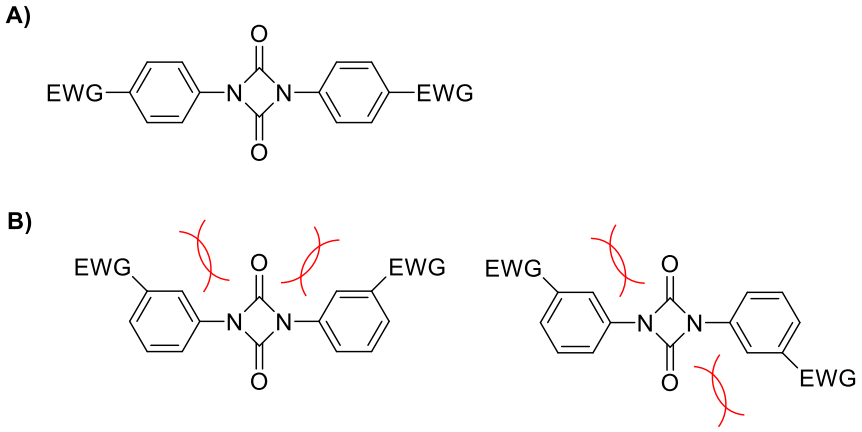

Figure 6.5 Representation of the steric hindrance for substituted uretdiones; (A) no steric hindrance for *p*-substituted uretdiones, and (B) steric hindrance for the two confirmations of *m*-substituted uretdiones.

As a result of the unexpected increase in deblocking temperature upon addition of electron-withdrawing substituents, *p*-methoxy and *m*-methoxy substituted diphenyl uretdiones were prepared to investigate whether the addition of electron-donating groups also had an effect on the deblocking temperature. In agreement with the above hypothesis that disruption of the nitrogen lone pair results in higher deblocking temperatures, with the aforementioned electron withdrawing groups disrupting the nitrogen lone pair through enhancing conjugation with the aromatic ring, both the *meta*- and *para*-methoxy substituted uretdiones were found to have deblocking temperatures higher than the unsubstituted uretdione, but with lower temperatures than the nitro- and chloro-substituted uretdiones (Figure 6.6). Similar to the electron-withdrawing substituted product, the *meta* substituted product was found to have a lower

deblocking temperature than the *para* substituted uretdione, and was similarly attributed to the steric strain generated by the position of the ring substituent in the molecule.

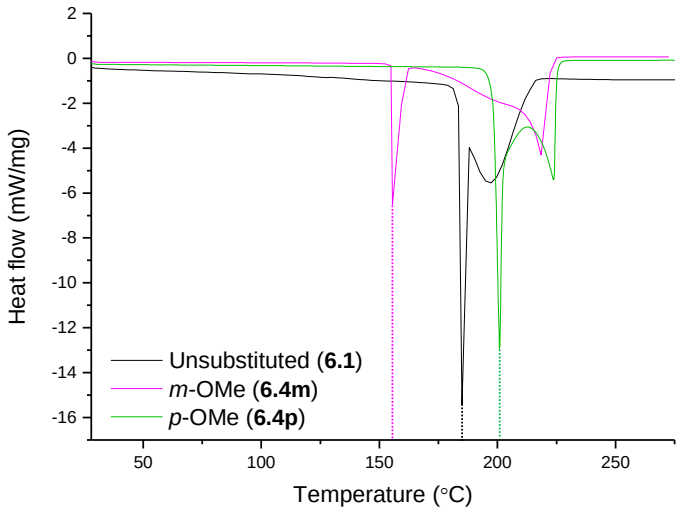

Figure 6.6 DSC thermograms of methoxy substituted diphenyl uretdiones. Heating rate = 10 °C/min.

Whilst the literature has little to no information about the mechanism of deblocking for a uretdione, aside from the uretdione ring undergoing scission,[70] there is a great deal of information available on the mechanism of the reaction between an externally blocked isocyanate and an active hydrogen containing blocking agent, and the effect of nucleophiles on the deblocking temperature.[30, 32, 33] This effect of a nucleophilic species on deblocking is highly relevant, as within a one-pot formulation the blocked isocyanates will come into contact with the catalytic tertiary amine. Therefore, the deblocking temperature of *p*-methoxy diphenyl uretdione, exhibiting the lowest deblocking temperature of the substituted uretdiones studied, was investigated with the addition of different amines to the DSC pan (Figure 6.7). Triethylamine (TEA) was found to exhibit no effect on the deblocking temperature of *p*-methoxy diphenyl uretdione, though the low boiling point of this amine renders it likely to have evaporated prior to reaching the melting point of the uretdione. This hypothesis was confirmed by the presence of an additional peak in the thermogram at 90 °C, the boiling point of TEA. The addition of higher boiling point amines, however, was found to lower the deblocking temperature, with the addition

of *N,N'*-(dimethylamino)ethyl acrylate (DMAEA) found to result in the lowest deblocking temperature (212 °C). Of importance, the methacrylate equivalent, *N,N'*-(dimethylamino)ethyl methacrylate (DMAEMA), present in the polymeric catalysts discussed in previous chapters, was also found to lower the deblocking temperature (216 °C). Interestingly, the addition of ethanolamine was also found to lower the deblocking temperature (215 °C) despite having a boiling point of 170 °C. This would suggest a deblocking mechanism in which the nucleophilic amine species coordinates to the uretdione facilitating deblocking *via* a four-membered transition state, similar to the addition-elimination mechanism proposed for an isocyanate blocked with an active hydrogen containing compound (Scheme 1.10B). Such coordination would potentially prevent the ethanolamine evaporating, which was observed in the lack of an exotherm in the DSC thermogram at around 170 °C. It is hypothesised that the coordination of the amines to the uretdione results in destabilisation of the uretdione ring, lowering the deblocking temperature, though it must be noted that there is little to no discussion in the literature as to the deblocking mechanism of uretdiones. However, studies by Singh and Boivin reported that the addition of triethylamine and other diamines, in addition to heat, produced a product in which the uretdione ring had ruptured, yet there was no discussion of the mechanism.[71]

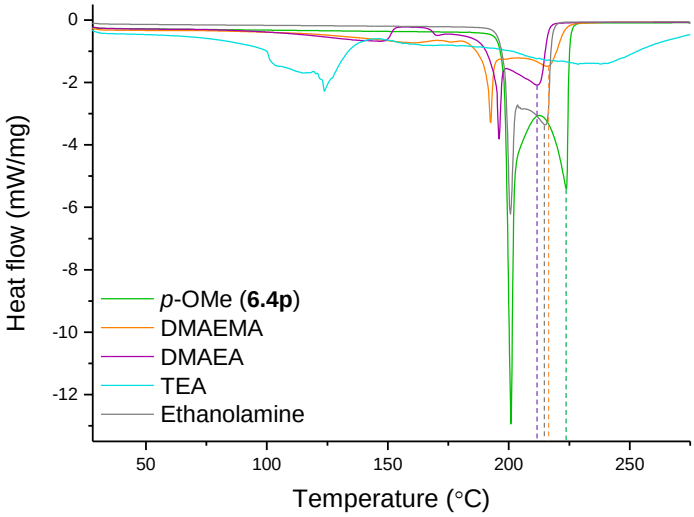

Figure 6.7 DSC thermograms of *p*-methoxy substituted diphenyl uretdione (6.4p) with small molecule amines (10 µL) added to the DSC pans. Heating rate = 10 °C/min.

Whilst the addition of amines was found to lower the deblocking temperature, the lowest uretdione deblocking temperature obtained is still significantly greater than the desired temperature range for triggering the one-pot formulation (around 50-60 °C), and as such, different blocked isocyanates were investigated.

6.3.2 Externally Blocked Isocyanates

Whilst internally blocked isocyanates prevent the addition of contaminants to the product formulation, they are limited in number compared to external blocking groups. Moreover, the range of compounds available as external blocking agents affords a large range of potential deblocking temperatures. To this end, initial investigations were carried out on a commercially available dimethyl pyrazole blocked isocyanate, owing to pyrazole blocked isocyanates being reported as having one of the lowest deblocking temperature, rendering them a suitable candidate for the one-pot formulation thermally initiated within a relatively low temperature range of 50-60 °C.[62]

6.3.2.1 Analysis of Commercially Available Trixene compounds

Trixene BI 7986, purchased from Baxenden Chemicals, is a 3,5-dimethyl pyrazole blocked aliphatic isocyanurate, with a reported deblocking temperature of 120 °C (Scheme 6.4).[72]

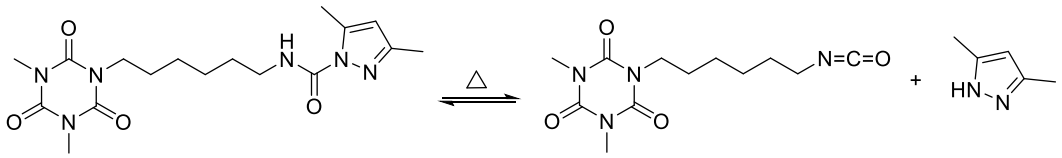

Scheme 6.4 Schematic representation of the deblocking of Trixene BI 7986 (*left*) to produce the free isocyanate and the 3,5-dimethyl pyrazole blocking agent (*right*).

Owing to the formulation of the commercial blocked isocyanate containing water, DSC analysis was found to be no longer suitable for the determination of deblocking owing to the presence of a large exotherm in the temperature region of interest attributed to water evaporation. As such, variable temperature carbon NMR (^{13}C VT-NMR) spectroscopy was

employed, using deuterated dimethyl sulfoxide (DMSO-d_6) as the solvent. It should be noted that, whilst the free isocyanate peak would be observed at approximately δ = 120-130 ppm, this peak may be unsuitable for determining the deblocking temperature as the resultant free isocyanate would immediately react with any moisture present, masking the deblocking and therefore reducing the intensity of the resonance. Therefore the peaks at approximately δ = 12 ppm (Figure 6.8), corresponding to the methyl functionalities in the released blocking agent, were used to determine the deblocking temperature. Additionally, the isocyanate peak may overlap with the signal attributed to the ring carbons of the pyrazole, which are also present in the region δ = 120-130 ppm, rendering the free isocyanate even less suitable for monitoring deblocking. Analysis of the dimethyl pyrazole blocked aliphatic isocyanurate revealed a deblocking temperature of 90°C (Table 6.3). It is likely that the slightly lower temperature compared to that quoted by the manufacturer can be attributed to the detection method employed for determination, with different methods widely acknowledged to produce different temperatures;[33] however, the method of determination is not reported by the company.

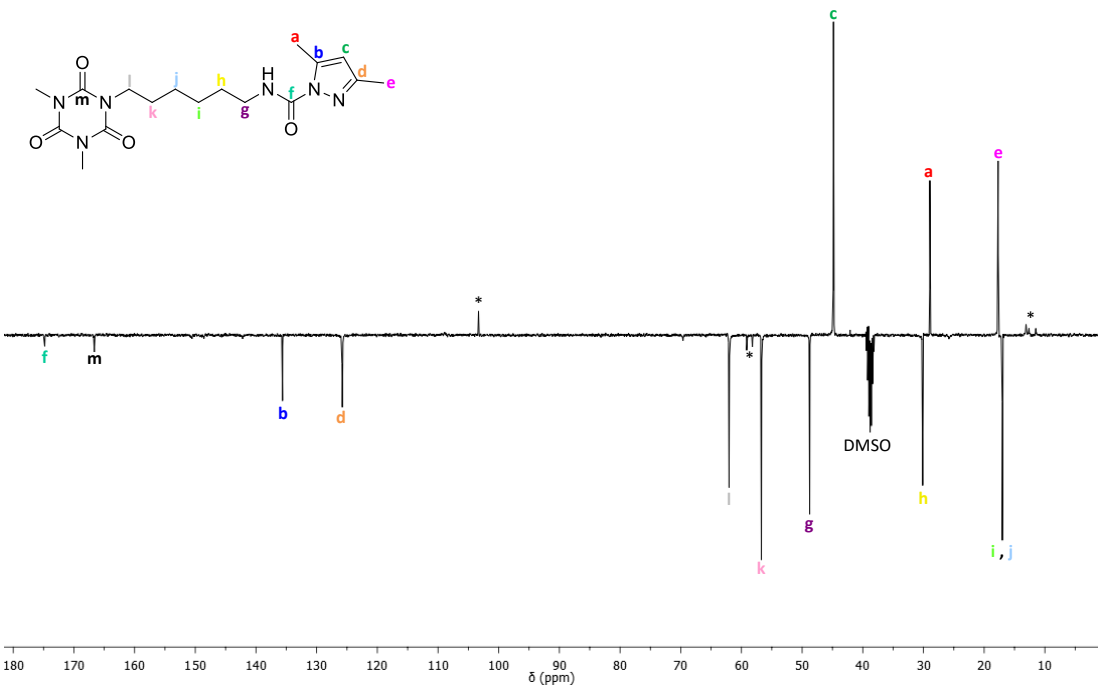

Figure 6.8 ^{13}C NMR spectrum of Trixene BI 7986 at 90 °C. * denotes free 3,5-dimethyl pyrazole (125 MHz, DMSO-d_6).

Table 6.3 Effect of added amines of the deblocking temperature of Trixene BI 7986, as determined using VT-NMR and a sampling method with NMR analysis. [a] reported literature values (in H_2O).

	Deblocking Temperature / °C		
	^{13}C VT-NMR	Sampling Method	pK_a of added amine[a]
Trixene BI 7986	90	>60	-
+ TMPDA	70	60	9.8[73]
+DMAEMA	50	50	8.4[74]
+DMAEA	50	50	8.3[74]
+ TEA	60	50	10.7[75]
+ Ethanolamine	60	55	9.5[76]

Following the earlier results indicating the addition of small molecule amines impacts the deblocking temperature for uretdiones, similar experiments were conducted with the Trixene BI7986. The same small molecule amines (10 wt %) were added to determine whether it is possible to lower the deblocking temperature to within the desired temperature range for the one-pot formulation. Similar to the uretdione experiments, all of the amines were found to lower the deblocking temperature (Table 6.3, Figure 6.9), including triethylamine which previously evaporated in the DSC experiments owing to the higher temperatures used. It is generally accepted that the deblocking temperature is greatly dependent on the presence of highly polar groups capable of deprotonating the urethane bond.[77, 78] As such, it is expected that the higher the pK_a of the amine, the lower the deblocking temperature. However, this was not observed in the ^{13}C VT-NMR spectroscopy analysis. Indeed, whilst TEA did result in a lower deblocking temperature than TMPDA, both DMAEMA and DMAEA were found to produce much lower deblocking temperatures despite their lower pK_a values. It is hypothesised that this much lower

deblocking temperature is as a consequence of the cyclic conformation adopted by the two monomers in solution (Figure 6.10).[74, 79] Within the cyclic confirmation, the free electron pair of the amine nitrogen atom is delocalised by interaction with the carbonyl group. Whilst this renders the amine less available for protonation, it results in an increase in the basicity of the carbonyl oxygen atom therefore increasing its ability to be protonated and consequently producing a lower deblocking temperature. Notably, DMAEMA (the amine investigated as a potential catalyst for a one-pot formulation throughout this thesis) was found to lower the deblocking temperature. This would therefore allow for a dual action of the catalytic DMAEMA particles: first to catalyse the polyurethane production, and secondly to lower the deblocking temperature of the blocked isocyanate resulting in a lower temperature required to trigger the reaction.

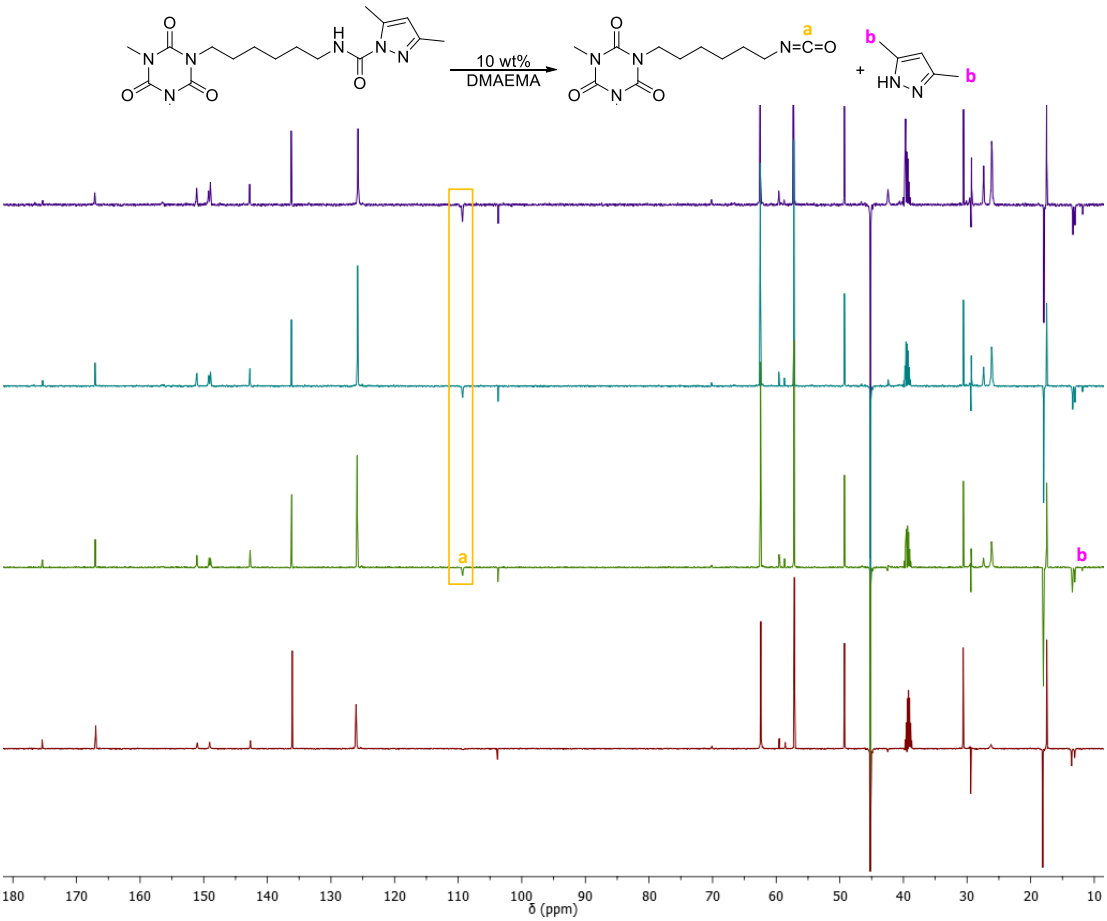

Figure 6.9 Overlaid ^{13}C VT-NMR spectra of Trixene BI 7986 with added DMAEMA (10 wt%) at 25 °C (*red*), 50 °C (*green*), 60 °C (*blue*) and 70 °C (*purple*) showing the evolution of the free isocyanate (a) and released 3,5-dimethyl pyrazole (b), normalised to the methyl group bound to the DMAEMA at δ = 18 ppm (125 MHz, DMSO-d_6).

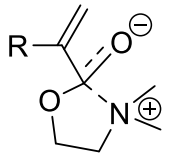

Figure 6.10 Schematic representation of the cyclic confirmation adopted by DMAEMA (R= CH_3) and DMAEA (R = H) when in solution, indicating the delocalisation of the nitrogen atom lone pair. Reproduced from Cotanda *et al*.[79]

Concerns arose about the effect of the ramped heating method used by the NMR instrument, which may lead to an over-estimation of the deblocking temperature as the sample remains at the set temperature for only short periods of time preventing full equilibration of the sample. It was decided that more in depth NMR spectroscopy analysis should be carried out in order to gauge whether the deblocking temperature determined using a ramping method does allow for suitable equilibration time, or whether it provides a superficially high deblocking temperature. To this end, analysis was carried out through continual heating of a sample in a vial, dissolved in DMSO-d_6 and with or without the addition of small molecule amines, at a series of set temperatures. Aliquots for ^{13}C NMR spectroscopic analysis were taken at 0, 60, 90 and 360 minutes. If NMR spectroscopic analysis revealed deblocking, a new blocked isocyanate solution was prepared and heated at a temperature 5°C below the previously tested temperature, with the starting temperature taken as 5°C greater than that recorded by ^{13}C VT-NMR spectroscopy. The process was repeated until NMR spectral resonances attributed to the deblocked isocyanate / free blocking agent were no longer observed. It was hypothesised that this method, compared to a ramped heating method, would present a more accurate deblocking temperature by allowing for sample equilibration at a set temperature. This is indeed what was observed, with most temperatures exhibiting a decrease in deblocking temperature of between 5 and 10 °C (Table 6.3, Figure 6.11). Moreover, similar to the VT-NMR experiments, the addition of small molecule amines resulted in a decrease in the deblocking temperature. Furthermore, the addition of DMAEMA and DMAEA again resulted in the lowest deblocking temperatures, in agreement with the results produced using VT-NMR spectroscopy.

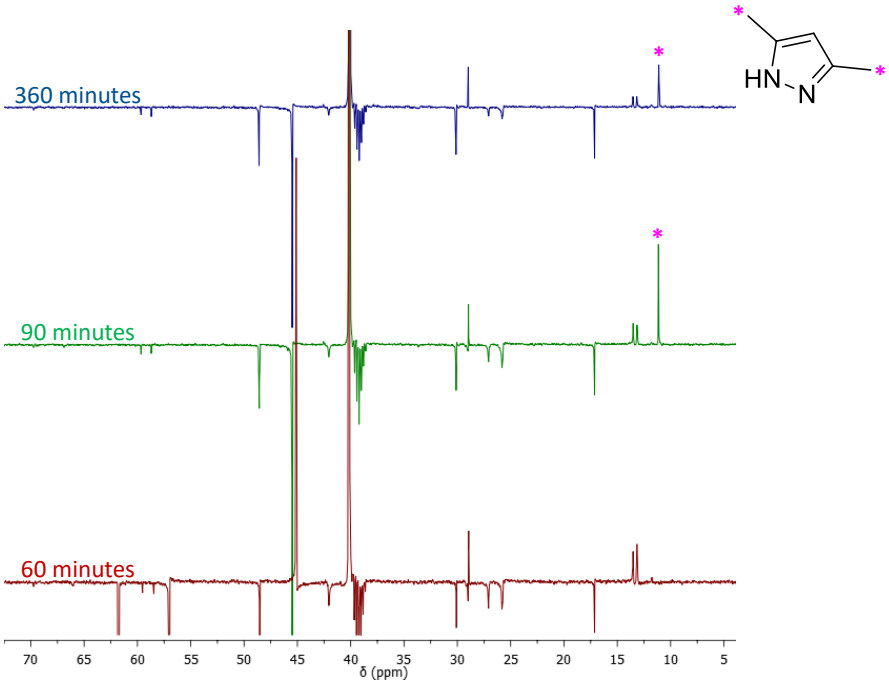

Figure 6.11 Overlaid ^{13}C NMR spectra of Trixene BI 7986 and TEA (10 wt%) at 50 °C, sampled at different time points, normalised to the internal standard TMS (125 MHz, DMSO-d_6).

6.3.2.2 Analysis of methacryloyl pyrazole blocked compounds

Commercially available Trixene has many benefits, including being available on a suitable scale to allow for use in the polyurethane foam evaluations. However, the commercially available blocked isocyanate is likely to contain both known and unknown additives which may prevent the determination of an accurate deblocking temperature for a pyrazole blocked isocyanate, for example, with the added *N*-methyl-2-pyrrolidone likely to impact the deblocking temperature. Moreover, the water rich formulation of Trixene BI 7968 hinders the use of other analytical techniques, *e.g.* DSC, for deblocking determination, with different techniques generally accepted to produce different temperature of deblocking, even for the same compound.[43] As such, and with a view to the development of the one-pot formulation, an in depth study was carried out investigating the determination of deblocking temperature on a methacryloyl pyrazole blocked phenyl isocyanate (**6.5**) and the diisocyanate equivalent methacryloyl pyrazole blocked toluene diisocyanate (**6.6**, one of the crosslinkers introduced in Chapter 5).

As observed in the NMR spectroscopy experiments, different experimental parameters, in this instance the length of time held at a specific temperature to ensure equilibrium is achieved, have an effect on the recorded deblocking temperature. As such, it was decided that NMR analysis of the methacryloyl pyrazole blocked phenyl isocyanate (**6.5**) and methacryloyl pyrazole blocked 2,4-toluene diisocyanate (TDI, **6.6**) should be carried out by both VT-NMR spectrosocpy and with the sampling method. Frequently highlighted in the literature is the importance of tailoring the analytical technique to the application. For example, when applied to coatings, where the blocked isocyanate is likely within a liquid formulation, a solid phase technique such as solid state FTIR would produce a deceptively high deblocking temperature impacting the temperature at which the coating would need to be cured at. With this in mind, NMR spectroscopy analysis of the blocked isocyanates was conducted in both DMSO-d_6 and ethylene glycol-d_6, with the latter a significantly better model for the polyol used in the formulation. VT-^{1}H NMR spectroscopic analysis in DMSO-d_6 indicated a deblocking temperature of 40 °C for both the blocked mono- and diisocyanates (Table 6.4, Figure 6.12), observed through the appearance of the aromatic peaks of the released phenyl isocyanate at δ = 6.42-6.80 ppm, and the released methacryloyl pyrazole methyl group at δ = 1.89 ppm (Figure 6.12, protons a-c and g, respectively). This relatively low temperature of deblocking was as expected, as it is widely reported in the literature that aromatic isocyanates deblock at lower temperature than aliphatic isocyanates (*e.g.*Trixene BI 7986), owing to conjugation of the π electrons of the ring and the N=C=O bond.[30]

Table 6.4 Deblocking temperatures determined using ^{1}H NMR spectroscopy for methacryloyl pyrazole blocked phenyl isocyanate and TDI. (400 MHz)

Technique		Deblocking Temperature / °C	
		Methacryloyl pyrazole blocked phenyl isocyanate **6.5**	Methacryloyl pyrazole blocked 2,4-TDI **6.6**
^{1}H VT-NMR	DMSO-d_6	40	40
	Ethylene glycol-d_6	60	50
	Acetonitrile-d_3	50	50
Sampling ^{1}H NMR	DMSO-d_6	40	25

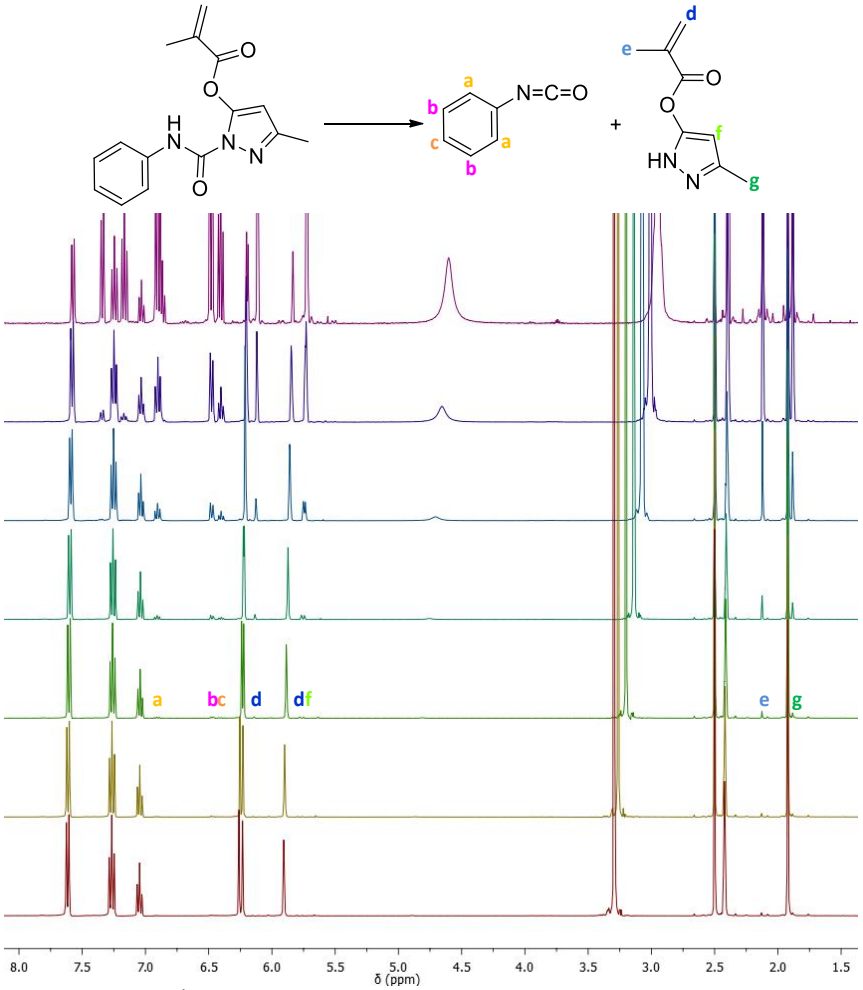

Figure 6.12 Overlaid ^{1}H VT-NMR spectra of 6.5 at 25 °C (*red*), 30 °C (*yellow*), 40 °C (*green*), 50 °C (*turquoise*), 60 °C (*purple*), and 70 °C (*pink*), showing the evolution of the free isocyanate (a, b and c) and released methacryloyl pyrazole (d, e, f and g), normalised to the solvent peak at δ = 2.50 ppm (400 MHz, DMSO-d_6).

Evaluation of the samples in ethylene glycol-d_6 produced a deblocking temperature slightly higher than that observed in the DMSO-d_6. It was expected that ethylene glycol, rich in hydrogen bond donors/acceptors, would lower the deblocking temperature as a consequence of the hydroxyl functionalities being able to hydrogen bond with the hydrogen from the urethane bond, rendering it more labile, and therefore result in more facile deblocking. However, the increase in viscosity when the blocked isocyanate is dissolved in ethylene glycol in comparison to DMSO may in fact hinder the deblocking, as the newly released blocking agent is likely to remain in close proximity to the isocyanate, increasing the possibility of re-blocking owing to the reversible nature of the blocking/deblocking process. One alternative argument for the lower deblocking temperature is that DMSO is markedly more polar than ethylene glycol, with dielectric constants of 47.0 and 37.7, respectively.[80] As mentioned previously, when analysing the effect of added amines, an increase in basicity has been demonstrated to decrease the deblocking temperature.[77] Therefore, a more polar solvent would be expected to result in a lower deblocking temperature. Moreover, with regards to determination of an accurate deblocking temperature, it is important to assess whether there is a solvent effect relating to the hydrogen bonding ability of the solvent, as such an effect would need to be considered when quantifying the deblocking temperature for an application. Therefore, ^{1}H VT-NMR spectroscopy was repeated using anhydrous acetonitrile-d_3 (AcN-d_3), which has a similar relative polarity to DMSO (0.46 and 0.44, respectively),[81] yet is unable to donate or accept hydrogen bonds. ^{1}H NMR spectroscopic analysis indicated a slightly higher deblocking temperature of 50 °C for both blocked isocyanates in AcN-d_3 (Figure 6.13), confirming the impact of hydrogen bonding ability on the lowering of the deblocking temperature.

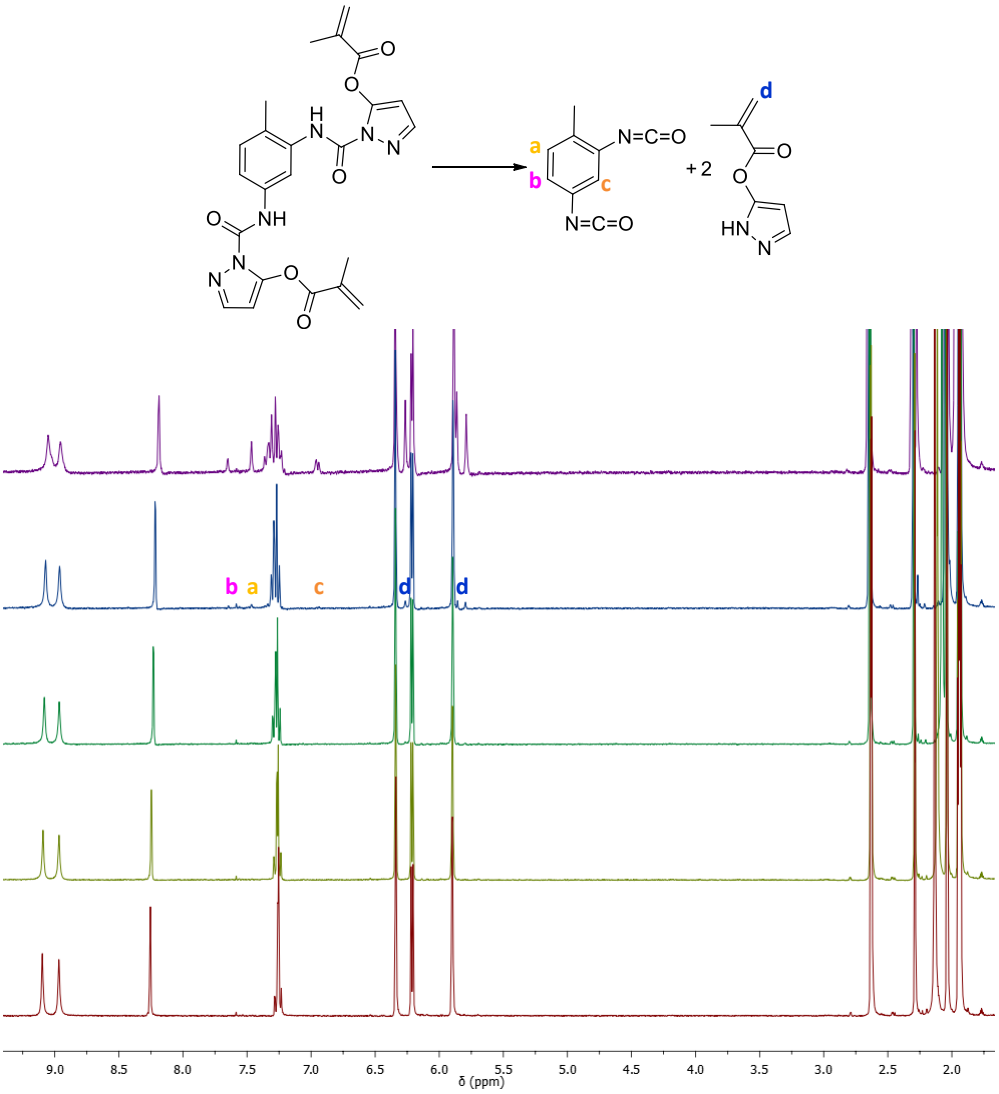

Figure 6.13 Overlaid ^{1}H VT-NMR spectra of 6.6 at 25 °C (*red*), 30 °C (*yellow*), 40 °C (*green*), 50 °C (*blue*), and 60 °C (*purple*), showing the evolution of the free isocyanate (a, b and c) and released methacryloyl pyrazole (d), normalised to the solvent peak at δ = 1.95 ppm (400 MHz, Acetonitrile-d_3).

Similar to previous variable temperature NMR spectroscopic studies, the effect of constant heating *vs* ramped heating was evaluated using the aforementioned method. It should be noted that, with regards to tailoring the analysis method to the application, the majority of applications involve the constant heating of a sample *e.g.* for curing of coatings, and therefore the deblocking temperature produced using this method is more likely accurate for application. It was found that the deblocking temperature of blocked phenyl isocyanate remained unchanged at 40 °C (Figure 6.14). However, the blocked diisocyanate deblocked at 25 °C, 15 °C lower than

with VT-NMR spectroscopic analysis and crucially, for application based purposes, indicates that the crosslinker **6.6** in unstable for prolonged periods in solution.

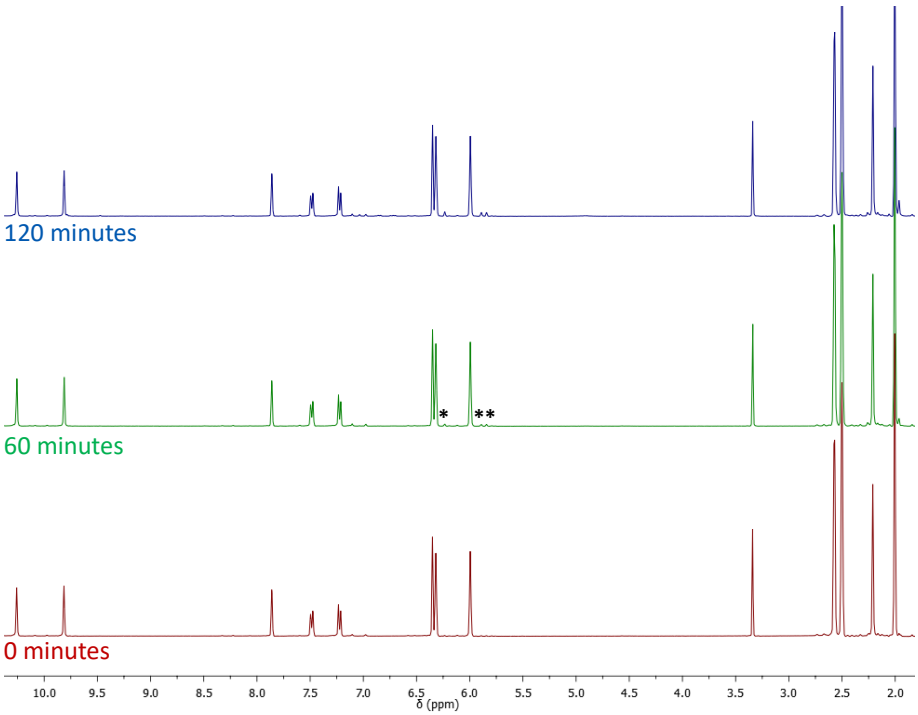

Figure 6.14 Overlaid ^{1}H NMR spectra of 6.5 at 25 °C, sampled at different time points, * indicates free methacryloyl pyrazole, normalised to the internal standard TMS (400 MHz, DMSO-d_6).

The observed lower deblocking temperature of **6.6** compared to the monoisocyanate **6.5** may be as a consequence of having multiple isocyanate groups and the inequivalence of the two isocyanate groups in TDI. Indeed, it has been reported by Bailey *et al*. that phenylene diisocyanates were found to block at a much faster rate than phenyl isocyanate when blocked with alcohols, attributed to the presence of a second isocyanate functionality *para* or *meta* to the first isocyanate.[82] Moreover, the inductive effect of the methyl group in TDI resulted in a slower blocking reaction for the TDI compared to the *m*-phenylene diisocyanate. Additionally, Tassel *et al*. observed that all the isocyanates in isophorone diisocyanate did not block at the same time, with the cyclic isocyanate blocking before the aliphatic isocyanate.[26] It is therefore hypothesised that a combination of having multiple isocyanates and the inductive effect of the methyl group destabilises the blocked TDI more than the phenyl isocyanate and results in a lower deblocking

temperature. This temperature difference is only noticeable in the sampling method owing to the dynamic nature of the blocking/deblocking process and therefore in the ramped NMR experiments there is insufficient time at a set temperature to shift the equilibrium in favour of the deblocking reaction.

Whilst analysis of the isocyanate in the solid state does not directly correlate to the likely state of application, with the majority of industrial applications involving blocked isocyanates dissolved in a solvent or other formulation component *e.g.* a polyol, DSC is a widely applied technique in the literature, and allows for facile changes in the rate of heating, potentially producing a lower deblocking temperature as the slower ramping rate allows for the equilibration of the sample. At a heating rate of 10 °C/minute, analysis of the solid blocked isocyanates indicated deblocking temperatures of 81 °C for the blocked phenyl isocyanates and 88 °C for the blocked TDI (Figure 6.15, Table 6.5), with both temperatures higher than that produced by NMR spectroscopic analysis where the blocked isocyanates are in solution.

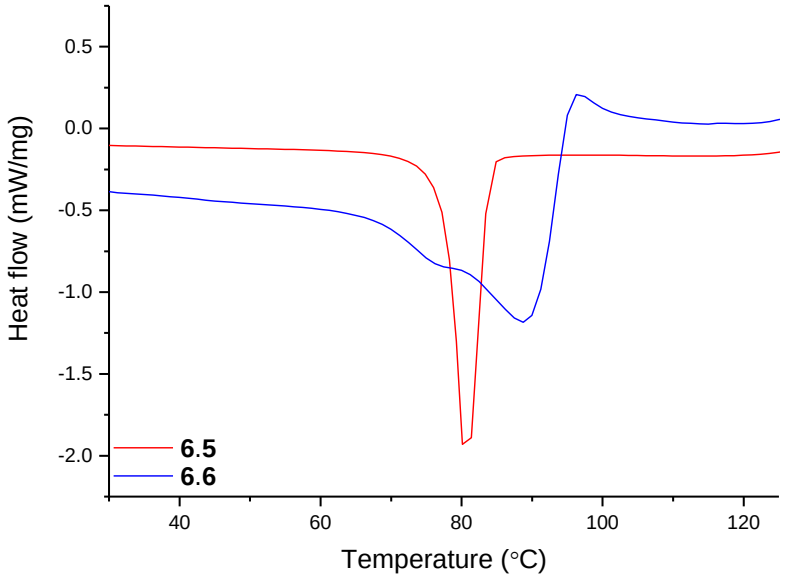

Figure 6.15 DSC thermograms of methacryloyl pyrazole blocked phenyl isocyanate (6.5) and methacryloyl pyrazole blocked TDI (6.6). Heating rate = 10 °C/min.

Table 6.5 Deblocking temperature of methacryloyl pyrazole blocked phenyl isocyanate (6.5) and TDI (6.6) determined by DSC analysis at different ramping rates.

State	Heating Rate (°C/min.)	Deblocking Temperature (°C)	
		6.5	**6.6**
Solid	2	-	64
	10	81	88
In polyol	10	-	76

When heating at the slower rate of 2 °C/minute, the deblocking temperature of the blocked TDI (**6**.6) was found to be 64 °C, 14 °C lower than when the sample was ramped at the higher rate (Table 6.5). This is in good agreement with the hypothesis that the slower heating rate will allow for the deblocking equilibrium to be reached and therefore result in lower deblocking temperatures, similar to the effect of ramping the temperature *versus* holding the temperature at a set value in the NMR spectroscopic analysis. Attempts were made to analyse the deblocking of the blocked diisocyanate when dissolved in the polyol used in the rigid polyurethane foam formulation (Voranol™ 490), with solvent found to strongly impact on deblocking temperature. Analysis indicated that the polyol lowered the deblocking temperature, with the TDI deblocking at 76 °C (Figure 6.16, Table 6.5). This lowering in deblocking temperature is likely to result from a combination of the solid being solubilised in the polyol, resulting in a more labile urethane bond and therefore increasing the likelihood of the urethane bond reacting, in addition to the hydrogen bonding ability of the polyol further destabilising this urethane bond and lowering the deblocking temperature further.

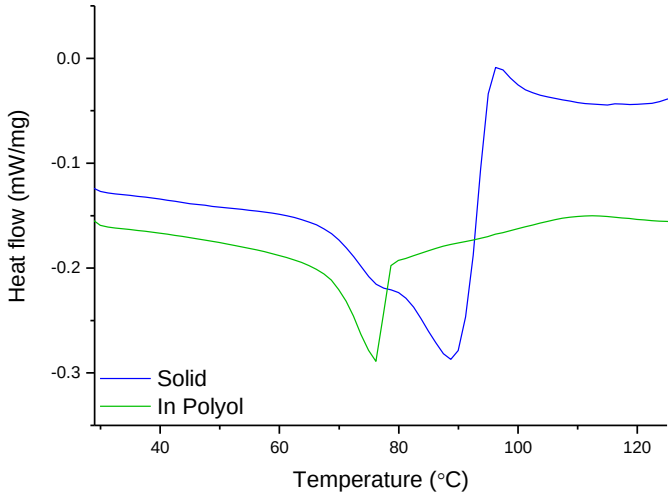

Figure 6.16 DSC thermograms of methacryloyl pyrazole blocked TDI (6.6) as a solid (*blue*) and dissolved in Voranol™ 490 (*green*). Heating rate = 10 °C/min.

Although NMR spectroscopy and DSC allow for determination of the deblocking temperature, the difference in physical states for these techniques produces differing deblocking temperatures. In order to investigate this, samples of the blocked isocyanates were analysed in both a solid state and dissolved in anhydrous acetonitrile using the same technique. Samples were heated at a series of temperatures ranging from 25 – 90 °C, allowing for comparison of state (solid *vs* liquid), and with the constant heating more akin to the method of application, ensuring the deblocking equilibrium is reached. Analysis of these samples was carried out using Fourier-Transform Infra-Red (FT-IR) spectroscopy, in addition to the newly applied technique of X-ray Photoelectron Spectroscopy (XPS), both of which allow for relatively simple determination of the deblocking temperature.

FT-IR spectroscopy is widely used in the literature owing to the facile nature of deblocking determination. The IR spectra exhibit strong bands between ν = 2230 cm^{-1} and ν =2270 cm^{-1} (attributed to free N=C=O), the appearance of which can be compared to the disappearance during deblocking of the bands associated with the blocked isocyanate during deblocking (C=O between ν =1640 cm^{-1} and ν =1720 cm^{-1} and a N-H band at approximately ν =1535 cm^{-1} for the free pyrazole species). As expected, and in agreement with the DSC analysis, the solid heated samples deblocked at 80 and 70 °C for **6.5** and **6.6**, respectively (Table

6.6). FTIR spectroscopic evaluation of the samples heated in acetonitrile revealed lower deblocking temperatures of 50 and 30 °C for **6.5** and **6.6**, respectively (Figure 6.17), in agreement with liquid analysis producing lower deblocking temperatures than solid state analysis, but slightly higher than those obtained using NMR spectroscopy using the sampling method described earlier. This difference can be attributed to the difference in hydrogen bonding ability of the solvents, with DMSO able to accept hydrogen bonds producing lower deblocking temperatures than acetonitrile, with the same effect previously noted in the ramped VT-NMR spectroscopic studies.

Table 6.6 Deblocking temperature of methacryloyl pyrazole blocked phenyl isocyanate (6.5) and TDI (6.6) annealed as a solid or dissolved in acetonitrile, determined by FTIR spectroscopy and XPS analysis.

Analytical Technique	State	Deblocking Temperature (°C)	
		6.5	**6.6**
FTIR	Solid	80	70
	Dissolved in Acetonitrile	50	30
XPS	Solid	70	50
	Dissolved in Acetonitrile	20	50

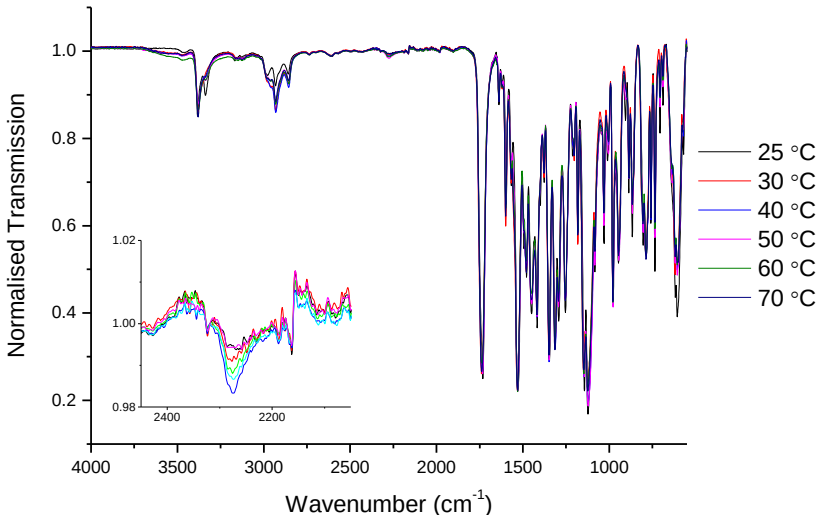

Figure 6.17 Overlaid FTIR spectra of 6.6 heated in acetonitrile at different temperatures, (*inset*) region of FTIR associated with the isocyanate stretch.

XPS analysis allows for the determination of the local bonding environment of various elements, with changes in the carbon, nitrogen and oxygen environments observable as the isocyanates deblock. Analysis of the heated samples by XPS was carried out by monitoring the appearance of a peak in the nitrogen spectra at a bonding energy of 402.37 eV, corresponding to the NH of the unblocked pyrazole ring (Figure 6.18).[83, 84]

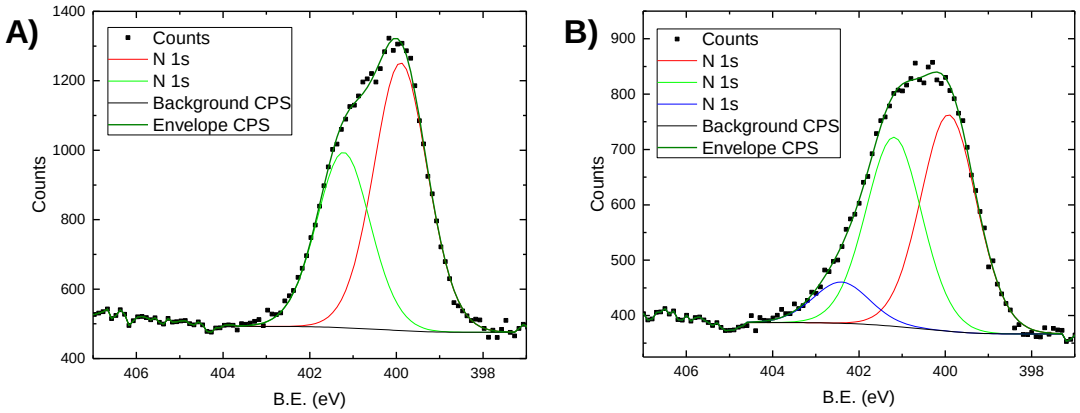

Figure 6.18 Nitrogen (1s) XPS spectra for solid heated 6.5 at 60 °C (*left*) and 70 °C (*right*).

Analysis of the percentage counts in the region (Table 6.7) clearly indicates a shift in the nitrogen environment, attributed to the deblocking of the isocyanate producing a free blocking agent with a distinctive NH functionality, with an increase in the NH content at 402.37 eV once deblocked. Moreover, XPS analysis revealed the same deblocking temperature trends as the previous techniques, with the liquid heated samples yielding lower deblocking temperatures than the solid heated samples, and with **6.6** consistently deblocking at lower temperatures than **6.5** (Table 6.6). Notably, however, XPS analysis produced deblocking temperatures that were nearly all lower than FTIR spectroscopy, despite the samples being identical. Such differences for the deblocking temperatures of the same compound measured using different techniques are readily reported in the literature, with the difference between XPS and FTIR reported by Zhang *et al.* whilst studying sodium bisulfite blocked isocyanates,[63] though no explanation has been provided as to the discrepancy. It is hypothesised that the difference may result from the difference in energy employed in the techniques, with XPS employing ionisation of the material surface

during analysis. This ionisation may shift the equilibrium in favour of deblocking, with Shanmugan and Nasar reporting that deblocking of a blocked isocyanate monomer during ionisation for electron impact mass spectrometry prevented accurate determination of mass.[85] However, it is important to note that assignment of XPS spectra is carried out by comparison with a database of bonding energies and their corresponding functional groups, with multiple groups assigned to the same bonding energy. Therefore XPS should be used as a complimentary technique, as used in this instance, to confirm deblocking results generated using other techniques.

Table 6.7 Relative content of N (1s) of solid samples of 6.5 annealed at different temperatures, determined by XPS analysis.

Bonding Energy (eV)	Relative Content (%)					
	50 °C	60 °C	70 °C	80 °C	90 °C	100 °C
399.83	57.38	60.39	48.42	51.48	44.14	44.97
401.08	42.62	39.61	42.33	41.32	45.83	44.4
402.37			9.55	7.21	10.02	10.64

6.4 Conclusion

Both internally and externally blocked isocyanates have been investigated using a range of analytical techniques to determine their deblocking temperatures. The internally blocked isocyanates (uretdiones) were found to have significantly higher deblocking temperatures than the externally blocked isocyanates, with the addition of both electron donating and withdrawing substituents found to increase the deblocking temperature in comparison with the unsubstituted uretdione. In contrast, externally blocked isocyanates exhibited lower deblocking temperatures, with the methacryloyl pyrazole blocked TDI, used in the polyurethane formulation reported in Chapter 5, deblocking at a lower temperature than the mono isocyanate equivalent. Additionally,

a vast difference in the deblocking temperature is observed when the technique involves solid *vs* liquid samples, with liquid samples exhibiting lower deblocking temperatures. This temperature, however, is more useful from an application based perspective as the blocked isocyanates are more likely to be used in a liquid formulation. Moreover, the analysis of samples produced different deblocking temperatures based on the method of heating, with ramping experiments found to produce higher deblocking temperatures than constant heating at a set temperature, and with different ramping rates further having an impact on the deblocking temperature. The comparative study based on solid and liquid heated samples revealed different deblocking temperatures for identical samples when analysed by FTIR spectroscopy in comparison to XPS. Indeed, this difference in temperatures is frequently alluded to in the literature, and from an application based perspective, care must be taken when choosing the analysis technique to ensure that experimental parameters such as ramping rate and state are matched as close to the application as possible.

6.5 Experimental

6.5.1 Materials

Trixene BI 7986 was purchased from Baxenden Chemicals Ltd. Silica gel (40-63 μM) and deuterated solvents were received from Apollo Scientific, with solvents dried over molecular sieves (3 Å, Sigma-Aldrich). The following reagents were used as received: phenyl isocyanate (Sigma-Aldrich, 98%), 4-chlorophenyl isocyanate (Sigma-Aldrich, 98%), 4-nitrophenyl isocyanate (Fisher Scientific, 99%), 3-nitrophenyl isocyanate (Sigma-Aldrich, 97%), 4-methoxyphenyl isocyanate (Fisher Scientific, 99%), 3-methoxyphenyl isocyanate (Fisher Scientific, 99%), tributyl phosphine (Sigma-Aldrich, 97%), ethyl acetoacetate (Sigma-Aldrich, 98%), hydrazine monohydrate (Fisher Scientific, 99%) trifluoroacetic acid (Sigma-Aldrich, 99%), *p*-toluene sulfonic acid monohydrate (Alfa Aesar, 97%), methacryloyl chloride (Sigma-Aldrich, 97%), triethylamine (Fisher Scientific, laboratory grade), and toluene diisocyanate

(TDI, Sigma-Aldrich, 98%). The following solvents were used as received: ethanol (EtOH, Fisher Scientific, absolute), nitrobenzene (Sigma-Aldrich, 99%), ethyl acetate (EtOAc, Fisher Scientific, LT grade), diethyl ether (Et_2O, Sigma-Aldrich, AR grade), acetone (Sigma-Aldrich, anhydrous, ReagentPlus), dichloromethane (CH_2Cl_2, Sigma-Aldrich, AR grade), toluene (Sigma-Aldrich, AR grade), acetonitrile (AcN, Fisher Scientific, LT grade) and petroleum ether 40-60 °C (pet. ether., Fisher Scientific, LT grade). Dry toluene was obtained using an Innovative Technology solvent purification system utilising activated alumina. Voranol™ 490 was provided by AWE, Aldermaston.

6.5.2 Instrumentation

In addition to the instrumentation introduced in section 2.5.2, and with the omission of gas chromatography, size exclusion chromatography, dynamic light scattering, transmission electron microscopy, small-angle X-ray scattering, particle size analysis and catalysts evaluation, the following instrumentation was used in this Chapter: Thermal analysis was carried out using a Mettler Toledo DSC1 in aluminium pans, with a heating rate of 10 °C/min. unless otherwise stated. The deblocking temperature is taken at the base of the trough. Melting points were determined using an Optimelt MPA100 automated melting point apparatus. The x-ray photoelectron spectroscopy (XPS) measurements were carried out using a Kratos Axis Ultra DLD system, with the samples illuminated by a monochromated beam of Al K_a x-rays ($h\upsilon$ = 1.486.6 eV). Photoelectrons were collected at a take-off angle of 90° (perpendicular to the surface), from an area of approximately 300 μM × 700 μM using a hemispherical analyser and a hybrid electrostatic-magnetic lens system. Survey spectra across the full energy range were recorded at a resolution of 1.75 eV. Experiments were carried out under ultra-high vacuum conditions, with the remaining temperature samples scanned consecutively on another sample holder. The energy range and transmission function of the system were calibrated using clean Ag foil. Data was analysed using the CasaXPS package, employing mixed Gaussian-Lorentzian

(Voigt) line shapes and asymmetry parameters where appropriate. All XPS data was collected by Dr Marc Walker and fitted by Dr Marc Walker and Mr Adam Bennett.

6.5.3 Synthetic Procedures

*Typical procedure for the synthesis of 1,3-bis substituted 1,3-diazetidine-2,4- uretidinediones (diphenyl uretdiones, **6.1**, **6.2**, **6.3** and **6.4**):*

Synthesis of both diphenyl uretdione and substituted uretdiones was based on a modified literature procedure.[66] In a typical experiment, phenyl isocyanate (1.0 eq.) was dissolved in dry toluene under nitrogen. Tributyl phosphine (0.04 eq.) was added dropwise and the solution stirred for 48 hours. The solution was filtered, washed with copious amounts of cold ethanol, and the resultant product purified by recrystallisation, affording a crystalline solid.

a) 1,3-diazetidine-2,4-dione (**6.1**)

   Recrystallisation from hot toluene yielded a crystalline white solid (1.79 g, 20%). m.p.: 161-167 °C. ^{1}H NMR (400 MHz, $CDCl_3$): δ (ppm) 7.18 (t, 4H, *m*-Ar*H*, $^{3}J_{H\text{-}H}$ = 7.5 Hz), 7.40 (t, 2H, *p*-Ar*H*, $^{3}J_{H\text{-}H}$ = 8.4 Hz), 7.56 (d, 4H, *o*-Ar*H*, $^{3}J_{H\text{-}H}$ = 8.6 Hz). ^{13}C NMR (100 MHz, $CDCl_3$): δ (ppm) 150.0 (C=O), 133.1 (Ar*C*-N), 128.4 (Ar*C*), 124.0 (Ar*C*), 115.7 (Ar*C*). IR (neat) max/cm^{-1}: 3060 ($\upsilon_{Ar\text{-}CH}$), 1770 ($\upsilon_{N\text{-}C(=O)\text{-}N}$). Anal. Calcd. For $C_{14}H_{10}N_2O_2$: C 70.6; H 4.2; N 11.8%. Found: C 70.6; H 4.3; N 11.8%.

b) 1,3-bis(4-nitrophenyl)-1,3-diazetidine-2,4-dione (**6.2p**)

   Recrystallisation from hot nitrobenzene yielded a crystalline pale yellow solid (0.3 g, 51%). m.p.: 201-209 °C. ^{1}H NMR (400 MHz, $CDCl_3$): δ (ppm) 8.44-8.41 (d, 4H, Ar*H*, $^{3}J_{H\text{-}H}$ = 8.9 Hz), 7.79-7.76 (d, 4H, Ar*H*, $^{3}J_{H\text{-}H}$ = 8.9 Hz). ^{13}C NMR (100 MHz, $CDCl_3$) δ (ppm) 148.0 (*C*=O), 147.6 (Ar*C*-NO_2), 139.6 (Ar*C*-N), 130.4 (Ar*C*), 124.5 (Ar*C*). IR (neat) max/cm^{-1}: 3080 ($\upsilon_{Ar\text{-}CH}$), 1780 ($\upsilon_{N\text{-}C(=O)\text{-}N}$), 1350 ($\upsilon_{NO_2}$).

c) 1,3-bis(3-nitrophenyl)-1,3-diazetidine-2,4-dione (**6.2m**)

Recrystallisation from hot nitrobenzene yielded a crystalline pale yellow solid (2.1 g, 42%). m.p.: 205-213 °C. ^{1}H NMR (400 MHz, DMSO-d_6): δ (ppm) 8.43 (s, 2H, Ar*H*), 8.39-8.36 (d, 2H, Ar*H*, $^{3}J_{H\text{-}H}$ = 8.1 Hz), 7.98-7.95 (d, 2H, Ar*H*, $^{3}J_{H\text{-}H}$ = 8.2 Hz), 7.91-7.85 (t, 2H, Ar*H*, $^{3}J_{H\text{-}H}$ = 8.0 Hz, 8.1 Hz). ^{13}C NMR (100 MHz, DMSO-d_6) δ (ppm) 148.4 (*C*=O), 148.1 (Ar*C*-NO_2), 135.7 (Ar*C*-N), 135.0 (Ar*C*), 130.8 (Ar*C*), 124.7 (Ar*C*), 124.2 (Ar*C*). IR (neat) max/cm^{-1}: 3060 ($\upsilon_{Ar\text{-}CH}$), 1770 ($\upsilon_{N\text{-}C(=O)\text{-}N}$), 1350 ($\upsilon_{NO_2}$).

d) 1,3-bis(4-chlorophenyl)-1,3-diazetidine-2,4-dione (**6.3**)

Recrystallisation from hot EtOAc yielded a crystalline white solid (1.2 g, 40%). m.p.: 225-233 °C. ^{1}H NMR (400 MHz, DMSO-d_6): δ (ppm) 7.49-7.46 (d, 4H, Ar*H*, $^{3}J_{H\text{-}H}$ = 8.9 Hz), 7.34-7.31 (d, 4H, Ar*H*, $^{3}J_{H\text{-}H}$ = 8.9 Hz). ^{13}C NMR (100 MHz, DMSO-d_6) δ (ppm) 152.3 (*C*=O), 137.9 (Ar*C*-Cl), 128.2 (Ar*C*-N), 126.1 (Ar*C*), 119.4 (Ar*C*). IR (neat) max/cm^{-1}: 3030 ($\upsilon_{Ar\text{-}CH}$), 1755 ($\upsilon_{N\text{-}C(=O)\text{-}N}$).

e) 1,3-bis(4-methoxyphenyl)-1,3-diazetidine-2,4-dione (**6.4p**)

Recrystallisation from hot EtOAc yielded a crystalline white solid (0.80 g, 27%). m.p.: 182-185 °C. ^{1}H NMR (400 MHz, $CDCl_3$): δ (ppm) 7.27-7.24 (d, 4H, Ar*H*, $^{3}J_{H\text{-}H}$ = 9.0 Hz), 6.76-6.73 (d, 4H, Ar*H*, $^{3}J_{H\text{-}H}$ = 9.0 Hz), 3.63 (s, 6H, O*C*H_3). ^{13}C NMR (100 MHz, $CDCl_3$) δ (ppm) 156.3 (*C*=O), 151.3 (Ar*C*-OCH_3), 126.6 (Ar*C*-N), 118.2 (Ar*C*), 114.1 (Ar*C*), 54.9 (*C*H_3). IR (neat) max/cm^{-1}: 3015 ($\upsilon_{Ar\text{-}CH}$), 1770 ($\upsilon_{N\text{-}C(=O)\text{-}N}$). Anal. Calcd. For $C_{14}H_{14}N_2O_4$: C 64.4; H 4.7; N 9.4%. Found: C 64.2; H 4.7; N 9.3%.

f) 1,3-bis(4-methoxyphenyl)-1,3-diazetidine-2,4-dione (**6.4m**)

Recrystallisation from hot EtOAc yielded a crystalline white solid (1.32 g, 42%). m.p.: 152-155 °C. ^{1}H NMR (400 MHz, $CDCl_3$): δ (ppm) 7.29-7.24 (t, 2H, Ar*H*, $^{3}J_{H\text{-}H}$ = 8.1 Hz, 8.1 Hz), 7.11-7.07 (dt, 2H, Ar*H*, $^{3}J_{H\text{-}H}$ = 8.9 Hz, $^{4}J_{H\text{-}H}$ = 2.5 Hz), 6.81 (s, 2H, Ar*H*), 6.71-6.68 (dd, 2H, Ar*H*, $^{3}J_{H\text{-}H}$ = 8.2 Hz, $^{4}J_{H\text{-}H}$ = 1.7 Hz), 3.81 (3, 6H, O*C*H_3). ^{13}C NMR (100 MHz, $CDCl_3$) δ (ppm) 159.7 (*C*=O), 150.3 (Ar*C*-OCH_3), 134.5 (Ar*C*-N), 129.8 (Ar*C*), 110.2 (Ar*C*), 108.2 (Ar*C*), 101.8 (Ar*C*), 54.8 (*C*H_3). IR (neat) max/cm^{-1}: 3015

($\upsilon_{Ar\text{-}CH}$), 1770 ($\upsilon_{N\text{-}C(=O)\text{-}N}$). Anal. Calcd. For $C_{14}H_{14}N_2O_4$: C 64.4; H 4.7; N 9.4%. Found: C 64.3; H 4.7; N 9.3%.

Synthesis of 5-methyl-2H-pyrazol-3-ol:

The synthesis of the hydroxy-functionalised pyrazole was based on a previously reported literature procedure.[86] To a solution of ethyl acetoacetate (10 g, 1.0 eq.) in ethanol, hydrazine hydrate (8.4 ml, 1.1 eq.) was added, and the solution stirred at room temperature for 16 hours. Following the reaction, the solution was cooled to 0 °C, stirred for 2 hours to ensure all the product had precipitated, filtered and washed with cold ethanol. The solid was recrystallised from ethanol affording a white crystalline solid (7.2 g, 49%). ^{1}H NMR (400 MHz, DMSO-d_6): δ (ppm) 10.46 (br s, 1H, N*H*), 5.22 (s, 1H, C(CH_3)C*H*), 3.50 (br s, 1H, O*H*), 2.08 (s, 3H, CH_3). ^{13}C NMR (100 MHz, DMSO-d_6): δ (ppm) 161.0 (*C*OH), 139.4 (*C*CH_3), 88.9 (C(CH_3)*C*H), 11.1 (*C*H_3). IR (neat) max/ cm^{-1}: 3680 (υ_{OH}), 2990 ($\upsilon_{Ar\text{-}CH}$), 1615 ($\upsilon_{C=O,\ pyrazolinone}$ ring), 1400($\upsilon_{C=C}$). *m/z* [ESI MS]: 98.7 (M+Na). Anal. Calcd. for $C_4H_6N_2O$: C 49.0; H 6.2; N 28.6%. Found: C 49.0; H 6.1; N 28.9%. m.p. 219-224 °C (Lit:[87] 220-222 °C).

Synthesis of 3-methacryloyl-5-methyl-2H-pyrazole:

Synthesis of the methacryloyl pyrazole was based on a modified procedure previously developed in the group.[88] 3-Methyl-1*H*-pyrazol-5-ol (5 g, 1.0 eq.) was added portion wise to a vigorously stirring solution of trifluoroacetic acid (5 eq.) at 0 °C. Upon addition of *p*-toluene sulfonic acid monohydrate (1.9 g, 0.2 eq.) the resulting solution was stirred at 0 °C for 1 hour. Methacryloyl chloride (10.6 g, 2 eq.) was added dropwise over an hour and the solution stirred for a further 16 hours. Cold diethyl ether was added dropwise and the resulting precipitate filtered and washed with copious amounts of cold diethyl ether (3 × 50 mL), yielding a pale pink solid. The solid was dissolved in CH_2Cl_2, extracted with basic water and brine, and the organic phase dried over magnesium sulfate. Following filtration, the CH_2Cl_2 was removed *in vacuo*, affording a white solid (5.6 g, 66%). ^{1}H NMR (400 MHz, $CDCl_3$): δ (ppm) 12.99 (br s, 1H, N*H*), 6.47 (s, 1H,

CC*H*$_2$), 6.34 (s, 1H, C(CH$_3$)C*H*), 5.89 (s, 1H, CC*H*$_2$), 2.49 (s, 3H, C*H*$_3$CCH$_2$), 2.00 (s, 3H, C*H*$_3$C=N). ^{13}C NMR (100 MHz, CDCl$_3$): δ (ppm) 164.7 (*C*=O) 155.7 (CH*C*O), 140.7 (N*C*CH$_3$), 135.3 (CH$_2$*C*CH$_3$), 127.9 (*C*H$_2$), 95.1 (C(CH$_3$)*C*H), 18.3 (CH$_2$C*C*H$_3$), 11.4 (NC*C*H$_3$). IR (neat) max/ cm^{-1}: 3150 (υ_{NH}), 2505 (υ_{NH}), 1765 ($\upsilon_{C=O}$), 1600 ($\upsilon_{C=C}$), 1315(υ_{COC}), 1160($\upsilon_{C=N}$). m.p. 237-239 °C.

*Typical procedure for the blocking of isocyanates with 3-methacryloyl-5-methyl-2H-pyrazole (**6.5**, **6.6**):*

In a typical experiment, 3-methacryloyl-5-methyl-2*H*-pyrazole (4.0 g, 1.0 eq.) was dissolved in dry acetone (40 mL) under nitrogen and cooled to 0 °C. The isocyanate was added dropwise, the solution allowed to warm to room temperature and the reaction left for 48 hours.

a) Methacryloyl pyrazole blocked phenyl isocyanate (**6.5**)

The crude reaction mixture was purified using column chromatography (silica gel treated with a 10% TEA in CH_2Cl_2 solution, 2:1 CH_2Cl_2/ pet. ether), R_f (2:1 CH_2Cl_2/ pet. ether): 0.51, affording a white crystalline solid (22%). ^{1}H NMR (400 MHz, CDCl$_3$): δ (ppm) 8.97 (s, 1H, N*H*), 7.56 (d, 2H Ar*H*, $^3J_{H\text{-}H}$ = 7.9 Hz), 7.37 (t, 2H, Ar*H*, $^3J_{H\text{-}H}$ = 7.6 Hz), 7.15 (t, 2H, Ar*H*, $^3J_{H\text{-}H}$ = 7.3 Hz), 6.42 (s, 1H, CC*H*$_2$), 6.17 (s, 1H, C(CH$_3$)C*H*), 5.85 (s, 1H, CC*H*$_2$), 2.68 (s, 3H, C(CH$_2$)C*H*$_3$), 2.08 (s, 3H, N=C(C*H*$_3$). ^{13}C NMR (100 MHz, CDCl$_3$): δ (ppm) 164.0 (O-*C*=O), 155.2 (C(=O)O*C*), 148.0 (N*C*(CH$_3$)), 145.2 (NH-*C*(=O)-N), 136.7 (CH$_2$*C*CH$_3$), 134.9 (Ar*C*-NH), 129.1 (Ar*C*), 128.8 (*C*H$_2$CCH$_3$), 124.6 (Ar*C*), 120.0 (Ar*C*), 101.9 (OC*C*H), 18.3 (*C*H$_3$CCH$_2$), 14.7 (*C*H$_3$CN). IR (neat) max/ cm^{-1}: 3363 ($\upsilon_{NH\text{-}C(=O)\text{-}NH}$), 1735 ($\upsilon_{C=O}$), 1595 ($\upsilon_{C=C}$).

b) Methacryloyl pyrazole blocked TDI (**6.6**)

The crude reaction mixture was purified using column chromatography (silica gel treated with a 10% TEA in CH_2Cl_2 solution, 3:1 CH_2Cl_2/ pet. ether), R_f (3:1 CH_2Cl_2/

pet. ether): 0.43, affording a white crystalline solid (40%). ^{1}H NMR (400 MHz, $CDCl_3$): δ (ppm) 9.02 (s, 1H, N*H*), 8.99 (s, 1H, N*H*), 8.15 (s, 1H, Ar*H*), 7.57-7.42 (d, 1H, Ar*H*, $^{3}J_{H\text{-}H}$ = 8.3 Hz), 7.33-7.23 (d, 1H, Ar*H*, $^{3}J_{H\text{-}H}$ = 8.3 Hz), 6.43 (s, 2H, CCH_2), 6.18 (s, 2H, C(CH_3)C*H*), 5.85 (s, 2H, CCH_2), 2.68 (s, 3H, C(CH_2)CH_3), 2.34 (s, 3H, ArCH_3), 2.09 (s, 3H, N=C(CH_3)). ^{13}C NMR (100 MHz, $CDCl_3$): δ (ppm) 164.0 (O-*C*=O), 155.2 (C(=O)O*C*), 148.0 (N*C*(CH_3)), 145.0 (NH-*C*(=O)-N), 135.4 (CH_2*C*CH_3), 131.0 (Ar*C*), 128.7 (*C*H_2CCH_3), 124.3 (Ar*C*), 116.0 (Ar*C*), 112.5(Ar*C*), 102.0 (OC*C*H),18.3(*C*H_3CCH_2), 14.6 (*C*H_3CN). IR (neat) max/ cm^{-1}: 3383, 3341 ($\upsilon_{NH\text{-}C(=O)\text{-}NH}$), 1732 ($\upsilon_{C=O}$), 1597 ($\upsilon_{C=C}$).

6.6 Bibliography

1. Sompuram, S. R., Vani, K., Wei, L., Ramanathan, H., Olken, S., Bogen, S. A., *Anal. Biochem.*, **2004**, 326, 55.
2. Kathalewar, M. S., Joshi, P. B., Sabnis, A. S., Malshe, V. C., *RSC Adv.*, **2013**, 3, 4110.
3. Maisonneuve, L., Lamarzelle, O., Rix, E., Grau, E., Cramail, H., *Chem. Rev.*, **2015**, 115, 12407.
4. Maier, S., Loontjens, T., Scholtens, B., Mülhaupt, R., *Angew. Chem., Int. Ed.*, **2003**, 42, 5094.
5. Maier, S., Loontjens, T., Scholtens, B., Mülhaupt, R., *Macromolecules*, **2003**, 36, 4727.
6. Eaves, D., *Handbook of Polymer Foams*, Rapra Technology, **2004**.
7. Barceló, D., *Emerging Organic Pollutants in Waste Waters and Sludge*, Springer Berlin Heidelberg, **2004**.
8. Subramani, S., Sultan Nasar, A., Philip Gnanarajan, T., Padmanabha Iyer, N., Radhakrishnan, G., *Polym. Int.*, **2000**, 49, 546.
9. Wicks Jr, Z. W., *Prog. Org. Coat.*, **1975**, 3, 73.
10. Chang, W.-H., Scriven, R. L., Peffer, J. R., Porter, S., *Ind. Eng. Chem. Prod. Res. Dev.*, **1973**, 12, 278.
11. Gedan-Smolka, M., Haussler, L., Fischer, D., *Thermochim. Acta*, **2000**, 351, 95.
12. Wen, X., Mi, R., Huang, Y., Cheng, J., Pi, P., Yang, Z., *J. Coat. Technol. Res.*, **2010**, 7, 373.
13. Subrayan, R. P., Zhang, S., Jones, F. N., Swarup, V., Yezrielev, A. I., *J. Appl. Polym. Sci.*, **2000**, 77, 2212.
14. Muramatsu, I., Tanimoto, Y., Kase, M., Okoshi, N., *Prog. Org. Coat.*, **1993**, 22, 279.
15. Engonga, P. E., Marchetti, V., Gérardin, P., Tekely, P., Loubinoux, B., *J. Fluorine Chem.*, **2000**, 101, 19.
16. Subramani, S., Lee, J. M., Kim, J. H., Cheong, I. W., *Macromol. Res.*, **2005**, 13, 418.
17. Subramani, S., Park, Y.-J., Cheong, I.-W., Kim, J.-H., *Polym. Int.*, **2004**, 53, 1145.
18. Subramani, S., Park, Y.-J., Lee, Y.-S., Kim, J.-H., *Prog. Org. Coat.*, **2003**, 48, 71.
19. Camberlin, Y., Michaud, P., Pesando, C., Pascault, J. P., *Makromol. Chem., Macromol. Symp.*, **1989**, 25, 91.
20. Premkumar, S., Karikal Chozhan, C., Alagar, M., *Polym. Eng. Sci.*, **2009**, 49, 747.

21. Wei, W.-J., Guo, Z.-R., Zhang, Y.-F., Pan, E.-L., *J. Appl. Polym. Sci.*, **2002**, 84, 1346.
22. Sankar, G., Yan, N., *J. Macromol. Sci., Part A: Pure Appl. Chem.*, **2015**, 52, 47.
23. Nasar, A. S., Subramani, S., Radhakrishnan, G., *Polym. Int.*, **1999**, 48, 614.
24. Gertzmann, R., Gürtler, C., *Tetrahedron Lett.*, **2005**, 46, 6659.
25. Wong, S. W., Damusis, A., Frisch, K. C., Jacobs, R. L., Long, J. W., *J. Elastom. Plast.*, **1979**, 11, 15.
26. Tassel, X., Barbry, D., Tighzert, L., *Eur. Polym. J.*, **2000**, 36, 1745.
27. Viganò, M., Suriano, R., Levi, M., Turri, S., Chiari, M., Damin, F., *Surf. Sci.*, **2007**, 601, 1365.
28. Vorlop, K.-D., Muscat, A., Beyersdorf, J., *Biotechnol. Tech.*, 6, 483.
29. Zhang, Y., Gu, J., Jiang, X., Zhu, L., Tan, H., *Pigm. Resin Technol.*, **2011**, 40, 379.
30. Wicks, Z. W., Jones, F. N., Pappas, S. P., Wicks, D. A., *Organic Coatings: Science and Technology*, Wiley-VCH Verlag GmbH & Co. KGaA, **2006**.
31. Entelis, S. G., Nesterov, O. V., *Russ. Chem. Rev.*, **1966**, 35, 917.
32. Delebecq, E., Pascault, J.-P., Boutevin, B., Ganachaud, F., *Chem. Rev.*, **2013**, 113, 80.
33. Wicks, D. A., Wicks, Z. W., *Prog. Org. Coat.*, **1999**, 36, 148.
34. Johnson, J. F., Gill, P. S., Analytical Calorimetry: Volume 5, *Analytical Calorimetry: Volume 5*, Springer US, **1984**.
35. Gironès, J., Pimenta, M. T. B., Vilaseca, F., de Carvalho, A. J. F., Mutjé, P., Curvelo, A. A. S., *Carbohydr. Polym.*, **2007**, 68, 537.
36. Decker, C., Masson, F., Schwalm, R., *Macromol. Mater. Eng.*, **2003**, 288, 17.
37. Lonikar, S. V., Rungsimuntakul, N., Gilbert, R. D., Fornes, R. E., *J. Polym. Sci., Part A: Polym. Chem.*, **1990**, 28, 759.
38. Johnson, J. F., Gill, P. S., *Analytical Calorimetry*, Springer US, **2012**.
39. Sankar, G., Nasar, A. S., *J. Polym. Sci., Part A: Polym. Chem.*, **2007**, 45, 1557.
40. Sankar, G., Nasar, A. S., *J. Appl. Polym. Sci.*, **2008**, 109, 1168.
41. Yang, P. F., De Han, Y., Li, J. Y., Li, T. D., *Int. J. Polym. Anal. Charact.*, **2011**, 16, 251.
42. Ranjbar, Z., Montazeri, S., Nayini, M. M. R., Jannesari, A., *Prog. Org. Coat.*, **2010**, 69, 426.
43. Lee, J. M., Subramani, S., Lee, Y. S., Kim, J. H., *Macromol. Res.*, **2005**, 13, 427.
44. Kothandaraman, H., Thangavel, R., *J. Appl. Polym. Sci.*, **1993**, 47, 1791.
45. Lu, Q.-W., Hoye, T. R., Macosko, C. W., *J. Polym. Sci., Part A: Polym. Chem.*, **2002**, 40, 2310.
46. Tarasov, D. N., Tiger, R. P., Chirkov, Y. N., Entelis, S. G., Tondeur, J. J., *Kinet. Catal.*, **2000**, 41, 355.
47. Kiguchi, T., Aota, H., Matsumoto, A., *J. Polym. Sci., Part A: Polym. Chem.*, **2003**, 41, 606.
48. Mao, H., Yang, F., Wang, C., Wang, Y., Yao, D., Yin, Y., *RSC Adv.*, **2015**, 5, 30631.
49. Cholli, A., Koenig, J., Sun, T., Zhou, H., *J. Appl. Polym. Sci.*, **1983**, 28, 3497.
50. Ying, H., Zhang, Y., Cheng, J., *Nat. Commun.*, **2014**, 5, 3218.
51. Nasar, A. S., Subramani, S., Radhakrishnan, G., *J. Polym. Sci., Part A: Polym. Chem.*, **1999**, 37, 1815.
52. Nagy, T., Antal, B., Czifrák, K., Papp, I., Karger-Kocsis, J., Zsuga, M., Kéki, S., *J. Appl. Polym. Sci.*, **2015**, 132, 42127.
53. Lou, C., Gu, J., Di, M., Ma, L., Wang, Y., Liu, X., *Iran. Polym. J.*, **2011**, 20, 247.
54. Li, A., Fan, G., Chen, H., Zhao, Q., *Res. Chem. Intermed.*, **2012**, 39, 3565.
55. Pilch-Pitera, B., *J. Appl. Polym. Sci.*, **2012**, 124, 3302.
56. Furukawa, M., Yokoyama, T., *J. Polym. Sci., Part C: Polym. Lett.*, **1979**, 17, 175.
57. Davis, A., *Makromol. Chem.*, **1963**, 66, 196.
58. Griffin, G. R., Willwerth, L. J., *Ind. Eng. Chem. Res.*, **1962**, 1, 265.
59. Kothandaraman, H., Nasar, A. S., Lakshmi, R. K., *J. Appl. Polym. Sci.*, **1994**, 53, 31.

60. Kothandaraman, H., Nasar, A. S., *Polymer,* **1993**, 34, 610.
61. Katsamberis, D., Pappas, S. P., *J. Appl. Polym. Sci.,* **1990**, 41, 2059.
62. Mühlebach, A., *J. Polym. Sci., Part A: Polym. Chem.,* **1994**, 32, 753.
63. Zhang, Y., Cao, J., Tan, H., Gu, J., *Pigm. Resin Technol.,* **2014**, 43, 194.
64. Zuo, Y., Gu, J., Zhang, Y., Tan, H., Li, P., Di, M., *J. Adhes. Sci. Technol.*, **2012**, 26, 1685.
65. Carter, J. W., Pappas, S. P., *J. Coat. Technol. Res.,* **1992**, 64, 29.
66. Buckles, R. E., McGrew, L. A., *J. Am. Chem. Soc.*, **1966**, 88, 3582.
67. Birsa, M. L., Braverman, S., Charalambides, Y., Cherkinsky, M., Diaper, C., *Science of Synthesis: Houben-Weyl Methods of Molecular Transformations Vol. 18: Four Carbon-Heteroatom Bonds*, Thieme, **2014**.
68. Possart, W., *Adhesion: Current Research and Applications*, Wiley-VCH Verlag GmbH & Co. KGaA, **2006**.
69. Raiford, L. C., Freyermuth, H. B., *J. Org. Chem.,* **1943**, 08, 230.
70. Kricheldorf, H. R., *Handbook of Polymer Synthesis*, Taylor & Francis, **1991**.
71. Singh, P., Boivin, J. L., *Can. J. Chem.*, **1962**, 40, 935.
72. Urethane Surface Coatings- Blocked Isocyanates, Baxenden Chemicals, http://www.baxchem.co.uk/files/documents/Baxenden_BlockedISO.pdf.pdf 2012.
73. Sandler, S. R., Karo, W., Blomquist, A. T., *Organic Functional Group Preparations*, Elsevier Science, **2013**.
74. van de Wetering, P., Zuidam, N. J., van Steenbergen, M. J., van der Houwen, O. A. G. J., Underberg, W. J. M., Hennink, W. E., *Macromolecules*, **1998**, 31, 8063.
75. R. Crampton, M., A. Robotham, I., *J. Chem. Res., Synop.,* **1997**, 22.
76. Hall, H. K., *J. Am. Chem. Soc.*, **1957**, 79, 5441.
77. Nasar, A. S., Raghavan, A., Kumar, V. S., *J. Macromol. Sci., Part A: Pure Appl. Chem.,* **2005**, 42, 309.
78. Gnanarajan, T. P., Nasar, A. S., Iyer, N. P., Radhakrishnan, G., *J. Polym. Sci., Part A: Polym. Chem.,* **2000**, 38, 4032.
79. Cotanda, P., Wright, D. B., Tyler, M., O'Reilly, R. K., *J. Polym. Sci., Part A: Polym. Chem.*, **2013**, 51, 3333.
80. Furniss, B. S., Vogel, A. I., *Vogel's Textbook of Practical Organic Chemistry Including Qualitative Organic Analysis. 4.ed. Revised by B.S.Furniss A.o: Textbook of Practical Organic Chemistry. 4.ed*, Longman XXXV, **1978**.
81. Reichardt, C., Solvent Effects on the Position of Homogeneous Chemical Equilibria, *Solvents and Solvent Effects in Organic Chemistry*, Wiley-VCH Verlag GmbH & Co. KGaA, **2004**.
82. Bailey, M. E., Kirss, V., Spaunburgh, R. G., *Ind. Eng. Chem.*, **1956**, 48, 794.
83. Dai, Q., Zhang, J., Ma, M., *Appl. Surf. Sci.,* **1993**, 72, 67.
84. Singhbabu, Y. N., Kumari, P., Parida, S., Sahu, R. K., *Carbon,* **2014**, 74, 32.
85. Shanmugam, T., Nasar, A. S., *Macromol. Chem. Phys.,* **2008**, 209, 651.
86. Soleimani, E., Hariri, M., Saei, P., *C. R. Chim.,* **2013**, 16, 773.
87. Nasseri, M. A., Salimi, M., Esmaeili, A. A., *RSC Adv.*, **2014**, 4, 61193.
88. Lu, A., Moatsou, D., Longbottom, D. A., O'Reilly, R. K., *Chem. Sci.*, **2013**, 4, 965.

7. Conclusions and Future Work

7.1 Conclusion

In this Thesis, the development of amine-functionalised polymeric stars synthesised using an arm-first Reversible Addition-Fragmentation Chain Transfer (RAFT) polymerisation method have been reported. Initially, an alcohol functionalised monomer 2-hydroxyethyl methacrylate (HEMA), selected for its potential to enable the dissolution of the catalyst within the formulation polyol, was polymerised to produce polymeric arms of PHEMA with degrees of polymerisation (DPs) ranging from 100 - 240. Subsequent chain extension of these arms with the amine-functionalised monomer, *N,N'*-(dimethyl amino)ethyl methacrylate (DMAEMA) and the non-responsive crosslinker tri(ethylene glycol) dimethacrylate (TEGDMA) was conducted to produce polymeric stars with different arm lengths (short *vs.* long), crosslinking density (from 10% to 20%), and amine content. Optimisation of the polymerisation conditions enabled production of well-defined polymeric stars with relatively narrow dispersities, even when scaled to produced 30 g of polymeric stars ($Đ_M$ = ~ 1.50). Production of stars on this scale allowed for evaluation of the polymers within the polyurethane foam formulation. Foam testing evaluation of these polymeric stars, conducted to investigate the protection afforded to the amine when tethered to the core domain of the star polymer of these non-responsive polymeric stars, revealed that none of the structural parameters investigated appeared to have a significant impact on the protection of the amine. Indeed, similar foam rise profiles were recorded when the crosslinking density was increased from 10, 15 and 20%, in addition to changing the arms from short to longer DPs. Moreover, regardless of the structure of the stars, the rate of rise in the formulation containing the polymeric stars was either the same, or less than that of the blank formulation, indicating complete shielding of the amine from the formulation. However, while development of such polymeric stars for polyurethane foam can be seen as a promising approach, caution must be taken when analysing the foam data, as the method of analysis

normalises the data to the blank profile which investigations revealed to be highly irreproducible.

Owing to the large quantity of material required for foam testing, further investigations were later conducted with analogous acrylate-based polymeric star. Indeed, the acrylate equivalent of the amine functionalised monomer, *N,N'*-(dimethylamino)ethyl acrylate, is highly susceptible to hydrolysis, with hydrolytic behaviour easily monitored using ^{1}H Nuclear Magnetic Resonance (NMR) spectroscopy, and with results validated using an enzymatic assay. The same arm-first methodology allowed for the production of acrylate-based polymeric stars, extensively characterised to confirm their crosslinked nature and that all stars had approximately the same number of arms (12 – 16), and with different structural parameters such as arm length, arm composition and crosslinking density. Hydrolysis of these polymeric stars was found to be strongly dependent on temperature, with significantly faster hydrolysis at 50 °C compared to 25 °C, and with both longer arm length and higher crosslinking densities offering greater protection to the amine within the star core. However, the different arm composition found to have negligible impact on amine protection. Such little impact from the effect of arm composition suggests that amine tethered within other architectures consisting of different corona monomers would be expected to exhibit similar hydrolytic behaviour.

The catalysis using amine-functionalised polymeric stars was further expanded through the introduction of responsive crosslinkers, hypothesised to allow for the production of an "on-demand" catalyst for polyurethane. The synthesis of a furan-maleimide based Diels-Alder crosslinker, and subsequent chain extension of PHEMA with this crosslinker and DMAEMA afforded thermoresponsive polymeric stars, with the successful retro-Diels-Alder reaction confirmed by fluorescence spectroscopy and thermal analysis. Despite this, evaluation as catalysts for both polyurethane foam production and the Knoevenagel reaction

between an aldehyde and an active hydrogen containing compound proved unsuccessful. Indeed foam evaluation indicated no difference between the blank formulation and that containing the responsive crosslinker. Moreover, for the Knoevenagel reaction, an increase in catalytic rate *vs.* the non-responsive polymeric stars was only observed when conditions were heavily skewed to favour the responsive Diels-Alder crosslinked polymeric stars. While this Thesis demonstrates the potential to impart responsive character to the polymeric stars, it would benefit from studies into different responsive chemistries. For example, incorporation of a photosensitive crosslinker, potentially thymine-based, would allow for development of a system that can be crosslinked, un-crosslinked and re-crosslinked by addition of irradiation.

Work focussing on the other one-pot component, blocked isocyanates, confirmed the frequently reported observation that different analytical techniques afford different deblocking temperatures for the same compound. Indeed, for the analysis of methacryloyl pyrazole blocked phenyl isocyanate, different analytical techniques produced a deblocking temperature range of 20 - 81 °C. It was further noted that the monoisocyanate was found to deblock at higher temperatures than diisocyanates, in addition to solid samples deblocking a higher temperature than liquid samples. Moreover samples heated at a constant temperature were found to deblock at lower temperatures than those generated using a ramped technique, observed in the drop in deblocking temperature for methacryloyl pyrazole blocked 2,4-toluene diisocyanate (TDI) of 15 °C when changing from a ramped technique to one involving continual heating. This is particular interest from an application point of view, with the method of continual heating most likely to represent the method applied in application *e.g.* in the heating of a polyurethane coating to allow for curing. Similarly, ramping rate was found to influence the deblocking temperature, with a decrease from 10 °C/min to 2 °C/min when using Dynamic Scanning Calorimetry resulting in a decrease in deblocking temperature of 24 °C. Interestingly, evaluation of the internally blocked diphenyl

uretdiones indicated variance in structural parameter (*i.e.* the addition of both electron-donating and electron-withdrawing groups) increased the deblocking temperature, in contrast to externally blocked isocyanates where this technique is used as a relatively facile method for tailoring the deblocking temperature. Furthermore, for both the internally and externally blocked isocyanates, the addition of amines, including DMAEMA, was found to lower the deblocking temperature.

Combining blocked isocyanates and the production of responsive amine functionalised polymeric stars, latent catalysts based on a blocked isocyanate crosslinker have been reported, and supposed to allow for minimal contamination of the polyurethane formulation through addition of other chemical functionalities. Whilst the direct RAFT polymerisation of the blocked isocyanate monomer was found to be unsuitable for the incorporation of the crosslinker, polymerisation of the blocking group, methacryloyl pyrazole, allowed for the production of a linear polymeric star precursor, which was able to be crosslinked by reaction with the diisocyanate. Furthermore, the degradation of the polymeric stars was confirmed by both variable temperature ^{1}H NMR spectroscopy and Size Exclusion Chromatography, with the latter indicating complete degradation of the polymeric stars into the linear precursor polymers. Application of the synthetic methodology enabled the synthesis of polymeric stars crosslinked with different diisocyanates thus allowing for the production of stars with different deblocking temperatures and hence their degradation.

In summary, this thesis investigated of a range of responsive and non-responsive amine functionalised polymeric stars and with a view towards polyurethane applications. Combining these polymers with work focussing on blocked isocyanates has allowed for the development of thermoresponsive amine functionalised polymeric stars crosslinked with a diisocyanate, which have been demonstrated to both catalyse the production of polyurethane, in addition to lower the deblocking temperatures of blocked isocyanates, imparting on to

them a dual catalytic nature. These results indicate a significant improvement on responsive star polymers obtained using Diels-Alder chemistry, and are the first example of using blocked isocyanates to crosslink polymeric stars.

7.2 Future Work

With the procedure for the synthesis of both responsive and non-responsive amine-functionalised polymeric stars established within this Thesis, there are potentially other opportunities to further explore these polymeric stars. Indeed, as reported in Chapter 5, the catalytic ability of the blocked isocyanate crosslinked polymeric catalysts needs to be evaluated in a polyurethane formulation to assess their suitability to act as latent catalysts for polyurethane. Moreover, with the crosslinking diisocyanate so easily altered, catalysis of other non-foam based polyurethanes could be targeted, for example using hexamethylene diisocyanate as a crosslinker for a polyurethane coating application.

Furthermore, the different deblocking temperatures of the catalysts could also be exploited in a cascade catalysis, in which the TDI crosslinked polymer could encapsulate a reactant which, upon heating at 35 °C, would be released into solution. Here it could react with a compound released from a second polymeric star crosslinked with methylenediphenyl diisocyanate subsequently heated at 50 °C. Other catalysis options utilising the tertiary amine catalyst, for example the Morita-Baylis-Hillman reaction, are available for the TEGDMA crosslinked polymers, owing to their swelling at increased temperature, with the maintenance of star integrity affording a facile method of catalyst removal by precipitation out of the polymeric catalyst.

Moreover, application of the RAFT methodology using the novel pyrazole monomer could produce a linear block copolymer bearing a pyrazole functionalised block. Such a

copolymer could be used as a metal scavenger owing to the application of pyrazoles as metal ligands, for example with copper, which would crosslink the polymer and produce polymeric stars, which could easily be isolated form the system *via* precipitation. Additionally, polymerisation of the novel pyrazole monomer with other hydrophilic monomers could be used to produce hydrogels, crosslinked using the chelation of metal ions, able to undergo a sol-gel transition when triggered chemically or physically. Indeed, whilst metal ion crosslinked hydrogels have already been shown to demonstrate stimuli responsive behaviour using thermal, chemical and physical stimulation, frequently these metal crosslinked hydrogels rely on having ligands at the end of the polymer chain. Polymerisation of the pyrazole could allow for a greater number of metal ligands to be incorporated per polymer chain potentially allowing for greater metal chelation. Such increased metal chelation could expand the range of properties available for hydrogel structures.